

Cartilage Tissue Engineering:

*instructing cell-based tissue repair
through scaffold design*

Members of the committee:

Chairman:	Prof. Dr. A. Blik	(University of Twente)
Promoter:	Prof. Dr. Clemens A. van Blitterswijk	(University of Twente)
Assistant promoter:	Dr. Jens Riesle	(IsoTis Orthobiologics)
Members:	Prof. Dr. Jan Feijen	(University of Twente)
	Prof. Dr. Wiebe Kruijer	(University of Twente)
	Prof. Dr. Klaas de Groot	(University of Leiden)
	Prof. Dr. Ernst Hunziker	(University Hospital, Bern, Switzerland)
	Dr. Daniël Saris	(University Medical Centre, Utrecht)
	Dr. Joost de Wijn	(IsoTis Orthobiologics)

Tim B.F. Woodfield

Cartilage Tissue Engineering:

instructing cell-based tissue repair through scaffold design

PhD Thesis, University of Twente, Enschede, The Netherlands
Copyright © T.B.F. Woodfield, Bilthoven, The Netherlands, 2004. Neither this book nor its parts may be reproduced without written permission of the author.

ISBN: 90-365-2057-6

The research described in this thesis was financially supported by the European Commission (FP5 project "SCAFCART" G5RD-CT-1999-00050).

This publication was sponsored by IsoTis Orthobiologics (Bilthoven, NL), Scanco Medical AG (Bassersdorf, CH), EnvisionTec GmbH (Marl, DE), PoroGen B.V. and Anna Fonds (Leiden, NL), as well as contributions from individual SCAFCART partners.

ISOTIS
OrthoBiologics™

SCANCOMEDICAL

 **PoroGen**

 **envisionTEC.**
Computer Aided Modeling Devices®

Printed by: Febodruk B.V., Enschede, The Netherlands.

Cover art: Tim Woodfield and María de los Milagros Baylac.

Front cover art combines an abstract cross-section of articular cartilage containing chondrocytes, extra-cellular matrix and collagen fibres with scanning electron microscopy images illustrating the development of cartilage from a single cell to a three-dimensional tissue. Rear cover illustration shows the South Island of New Zealand from space, courtesy of Earth Sciences and Image Analysis Laboratory, NASA Johnson Space Centre, ISS006-E-40113, <http://eol.jsc.nasa.gov>.

CARTILAGE TISSUE ENGINEERING:
INSTRUCTING CELL-BASED TISSUE REPAIR
THROUGH SCAFFOLD DESIGN

DISSERTATION

to obtain
the doctor's degree at the University of Twente,
on the authority of the rector magnificus,
prof. dr. F.A. van Vught,
on account of the decision of the graduation committee,
to be publicly defended
on Friday July 2nd, 2004 at 16.45

by

Timothy Bryan Francis Woodfield
born on February 8th, 1975
in Dunedin, New Zealand

Promoter: Prof. Dr. Clemens A. van Blitterswijk

Assistant promoter: Dr. Jens Riesle

List of Publications

This thesis was based on the following publications:

Peer reviewed papers

Woodfield T.B.F., Bezemer J.M., Pieper J.S., van Blitterswijk C.A., Riesle J. Scaffolds for Tissue Engineering of Cartilage. *Critical Reviews in Eukaryotic Gene Expression* **2002**; **12**(3): 209-236.

Woodfield T.B.F., Malda J., de Wijn J., Péters F., Riesle J., van Blitterswijk C.A. Design of Porous Scaffolds for Cartilage Tissue Engineering Using a 3-Dimensional Fibre Deposition Technique. *Biomaterials* **2004**; **25**(18): 4149-4161

Malda J., **Woodfield T.B.F.**, van der Vloodt F., Wilson C., Martens D.E., Tramper J., van Blitterswijk C.A., Riesle J. The Effect of Porous PEGT/PBT Scaffold Architecture on the Composition of Tissue Engineered Cartilage. *Biomaterials* **2004**; in press.

Malda J., **Woodfield T.B.F.**, van der Vloodt F., Kooy F.K., Martens D.E., Tramper J., van Blitterswijk C.A., Riesle J. The Effect of PEGT/PBT Scaffold Architecture on Oxygen Gradients in Tissue Engineered Cartilaginous Constructs. *Biomaterials* **2004**; in press.

Woodfield T.B.F.¹, Miot S.¹, Daniels A.U., Suetterlin R., Peterschmitt I., Heberer M., van Blitterswijk C.A., Riesle J., Martin I. The Effect of Scaffold Composition and Architecture on Human Nasal Chondrocyte Re-differentiation and Cartilaginous Matrix Deposition. *Biomaterials*; accepted.

Woodfield T.B.F., van Blitterswijk C.A., de Wijn J., Sims T., Hollander A., Riesle J. Polymer Scaffolds Fabricated with Organised Pore-size Gradient Structures as a Model for Studying Zonal Organisation within Tissue Engineered Cartilage Constructs. *Tissue Engineering*; submitted.

Woodfield T.B.F., van Blitterswijk C.A., Miot S., Martin I., Riesle J. Gas Plasma Treatment and PEGT/PBT Substrate Composition Regulate Human Chondrocyte Adhesion and Re-differentiation Capacity. *Experimental Cell Research*; submitted.

Woodfield T.B.F., Wedler V., Schneller M., Riesle J., van Blitterswijk C.A. Towards Anatomically-Shaped Tissue-Engineered Implants for Reconstruction of Small Articulating Joints - A Preliminary *in vitro* and *in vivo* Study in Rabbits. *Arthritis Rheumatism*; submitted.

¹ combined first authorship

Selected abstracts

Woodfield, T.B.F., Wedler, V., Schneller, M., Riesle, J., van Blitterswijk, C.A. (2004). Towards Customised Tissue Engineered Implants for Reconstruction of Small Articular Joints. *Proc. World Biomat. Conf.*, Sydney, Australia; 1589.

Woodfield, T.B.F., Miot, S., Martin, I., van Blitterswijk, C.A., Riesle, J. (2004). Gas Plasma Treatment and PEGT/PBT Substrate Composition Regulate Human Chondrocyte Adhesion and Re-differentiation Capacity. *Proc. World Biomat. Conf.*, Sydney, Australia; 1591.

Woodfield, T.B.F., de Wijn, J., Sims, T., Hollander, A., van Blitterswijk, C.A., Riesle, J. (2004). Polymer Scaffolds Fabricated with Organised Pore-size Gradient Structures as a Model for Studying the Zonal Organisation within Tissue Engineered Cartilage Constructs. *Proc. World Biomat. Conf.*, Sydney, Australia; 1590.

Woodfield, T.B.F., Miot, S., van Blitterswijk, C.A., Riesle, J., Martin, I. (2004). Human Chondrocyte Re-differentiation and Cartilaginous Matrix Deposition are Controlled by 3D Scaffold Composition and Architecture. *Proc. World Biomat. Conf.*, Sydney, Australia; 1592.

Woodfield T.B.F., Wedler V., Schneller M., van Blitterswijk C.A., Riesle J. (2003). Rapid Prototyped Scaffolds for the Resurfacing of Small Articular Joints. *Proc. Europ. Tissue Eng. Soc.*, Genoa, Italy; in *Tissue Engineering*, **9**(4): 816.

Woodfield T.B.F., Malda J., Riesle J. and van Blitterswijk C.A. (2002) Fabrication of PEGT/PBT Scaffolds Containing an Organized Pore-Size Gradient Structure. *Proc. Int. Cart. Repair Soc.*, Toronto, Canada; **4**: 108.

Woodfield T.B.F., Malda J., de Wijn J., Riesle J., and van Blitterswijk C.A. (2002). PEGT/ PBT Scaffolds Fabricated with Organized Pore-Size Gradient Structures for Cartilage Tissue Engineering Applications. *Proc. Europ. Soc. Biomat.*, Barcelona, Spain; **17**: 64.

Woodfield T.B.F., Mahmood T., Riesle J., and van Blitterswijk C.A. (2002). Enhanced Cell Attachment and Onset of Chondrogenesis on Gas Plasma Treated 2D and 3D PEGT/PBT Scaffolds. *Trans. Orthop. Res. Soc.*, Dallas, USA; **27**: 473.

Woodfield T.B.F., Malda J., de Wijn J., Riesle J., van Blitterswijk C.A. (2002). Porous PEGT/PBT Scaffolds for Cartilage Tissue Engineering Fabricated Using a 3D-Deposition Technique. *Workshop on Rapid Prototyping for Biomedical Applications*, Freiburg, Germany.

Woodfield T.B.F., de Wijn J., Riesle J., and van Blitterswijk C.A. (2001). *In Vitro* Cartilage Tissue Formation on Porous PEGT/PBT Scaffolds Fabricated Using a 3D-Deposition Technique. *Proc. Europ. Soc. Biomat.*, London, UK; **16**: 93.

"My heroes were a mixture of cowboys, philosophers, musicians, sportsmen, academics, explorers, scientists; just anyone who was doing something exciting. Some of their skills I couldn't understand and some I knew I didn't have the patience to acquire. But they all had one thing in common. They were all people who had not forgotten their childhood dreams and were living life for all it was worth. I was not alone."

[Gary Ball, Mountaineer, 1953-1993]

To my parents
and my sister

Table of Contents

General Introduction	1
<i>Chapter 1</i>	
General Introduction and Aims.....	3
<i>Chapter 2</i>	
Scaffolds for Tissue Engineering of Cartilage: A Review	17
I. Designed Scaffolds: Rapid Prototyping for Cartilage Tissue Engineering.....	43
<i>Chapter 3</i>	
Design of Porous Scaffolds for Cartilage Tissue Engineering Using a 3D Fibre- Deposition Technique.....	45
II. Instructive Scaffolds: Pore Architecture and Chondrocyte Differentiation	63
<i>Chapter 4</i>	
The Effect of PEGT/PBT Scaffold Architecture on the Composition of Tissue Engineered Cartilage.....	65
<i>Chapter 5</i>	
The Effect of PEGT/PBT Scaffold Architecture on Oxygen Gradients in Tissue Engineered Cartilaginous Constructs	79
<i>Chapter 6</i>	
Polymer Scaffolds Fabricated with Organised Pore-size Gradient Structures as a Model for Studying Zonal Organisation within Tissue Engineered Cartilage Constructs	91
III. Instructive Scaffolds: Composition, Pore Architecture and Chondrocyte Re-differentiation	109
<i>Chapter 7</i>	
Gas Plasma Treatment and Substrate Composition Affect Expanded Human Chondrocyte Adhesion and Re-differentiation Capacity	111
<i>Chapter 8</i>	
The Effect of Scaffold Composition and Architecture on Human Nasal Chondrocyte Re-differentiation and Cartilaginous Matrix Deposition Capacity	125
IV. Instructive Anatomically-Shaped Scaffolds: Tissue-Engineered Implants for Joint Reconstruction.....	139
<i>Chapter 9</i>	
Towards Anatomically-Shaped Tissue-Engineered Implants for Reconstruction of Small Articulating Joints - A Preliminary in vitro and in vivo Study in Rabbits	141
Discussion and Conclusions	159
<i>Chapter 10</i>	
Discussion and Conclusions	161
Appendix	169
Appendix A:.....	171
Appendix B:	175
Summary.....	177
Samenvatting	179
References.....	181
Acknowledgements	203
Curriculum Vitae	205
Selected Colour Figures	207

List of Abbreviations

2D	two-dimensional	MPa	megapascal ($\times 10^6$ Pascal)
3D	three-dimensional	MRI	magnetic resonance imaging
3DF	3D fibre deposition	MSC	mesenchymal stem cell
CAD	computer aided design	MW	molecular weight
CAM	computer aided machining	OA	osteoarthritis
CaP	calcium phosphate	PBT	poly(butylene terephthalate)
CNC	computer numerical control	PDGF	platelet-derived growth factor
CM	compression moulding/particle leaching	PEG	poly(ethylene glycol)
CT	computed tomography	PEGT	poly(ethylene glycol)- terephthalate
DMMB	dimethyl methylene blue	PG	proteoglycan
DXF	"drawing" file format	RP	rapid prototyping
ECM	extra cellular matrix	SEM	scanning electron microscopy
FDM	fused deposition modelling	SFF	solid free form fabrication
FGF	fibroblast growth factor	STL	"stereolithography" file format
GAG	glycosaminoglycan	TGF-β	transforming growth factor beta
GP	gas plasma	vol%	volume percent
HA	hydroxyapatite	wt%	weight percent
HYA	hyaluronic acid		

List of Definitions as Used in This Thesis

Accessible pore volume:	The volume within a scaffold representing pores that are interconnecting (see <i>interconnectivity</i>) and entirely accessible to a sphere of given diameter infiltrating the scaffold from the outside surface.
Allogenic:	Denoting cells or a graft derived from a donor of the same species as the recipient.
Anisotropic:	Not having the same physical properties in all directions.
Arthroplasty:	Surgical repair or replacement of a joint.
Articular:	Of or relating to the joint.
Autologous:	Denoting cells or a graft derived from the recipient of the graft.
Cartilage:	Connective tissue dominated by extra-cellular matrix containing collagen type II and large amounts of proteoglycans.
Chondral defect:	A defect confined purely within articular cartilage alone.
Chondrocyte:	A cartilage-forming cell.
Chondrogenesis:	Development of cartilage.
Computed tomography:	Radiological examination using a narrow radiation beam revolving about the sample, aimed at a predetermined axis, in which measured amounts of exit radiation are translated by computer into segmental images.
Condyle:	A rounded projection at the end of a bone.
Distal:	Remote, farther from any point of reference.
Dynamic stiffness:	The frequency dependent, apparent stiffness of a linear elastic member under cyclic or shock loading.
Ectopic:	Occurrence of something in an unnatural location.
Endothelial:	Pertaining to or made up of endothelium.
Femoral:	Of, or relating to, the femur.
Femur:	The long bone between the hip and knee joint.
Hyaline:	Clear, transparent, granule free.
Hydrophilic:	The ability of a surface or volume to attract a liquid.

Hydrophobic:	The ability of a surface or volume to repel a liquid.
Hyperoxia:	High oxygen conditions.
Hypoxia:	Low oxygen conditions.
Bone Induction:	The ability of a biomaterial implant to induce bone formation in an ectopic site e.g. in muscle.
Innervation:	The nerve supply to an area or organ of the body.
Interconnectivity:	The degree to which a single phase within a medium is joined to form continuous paths (see also <i>accessible pore volume</i>).
Instructive scaffold:	Scaffolds containing inherent qualities, such as designed pore architectures and/or biomaterial composition, for regulating specific cellular functions and guiding tissue formation.
Lacunae:	A space or cavity among cells.
Lateral:	Relating to or situated at the side of an organ or the body.
Medial:	Relating to or situated in the central region of an organ or the body.
Mesenchymal stem cell:	Pluripotent cell, derived from mesenchyme, capable of multiple differentiation pathways.
Meniscus:	A crescent shaped structure, such as the fibro-cartilaginous disc that divides the cavity of a synovial joint.
Osteoarthritis:	A disease of the joint cartilage associated with secondary changes in the underlying bone, which may ultimately cause pain and impair the function of the joint.
Osteochondral defect:	A defect which penetrates both the chondral and underlying vascularized subchondral bone.
Osteotomy:	A surgical operation to cut the a bone in two parts, followed by realignment of the ends to allow healing.
Pascal:	The unit measure of stress.
Pericellular:	Peripheral region around a cell.
Periosteum:	The dense layer of fibrous connective tissue that covers the surface of a bone (except that at the articular surfaces).
Perichondrium:	The dense layer of fibrous connective tissue that covers the surface of cartilage.
Pore:	A void or empty space in a material.
Porogen:	A physical object or gas which, when removed, creates a pore in a material.
Porosity:	The collection of pores making up the void space within a porous material.
Proximal:	Nearest or closer to a point of reference.
Subchondral:	Located beneath cartilage.
Synovial joint:	Diarthrosis or freely moving joint. The ends of the adjoining bones are covered with a thin layer of cartilage and the bones are linked by a ligament lined with synovial membrane, secreting the joints lubricant, synovium.
Synovia:	Synovial fluid, a thick colourless lubricating fluid that surrounds a joint and is secreted by the synovial membrane.
Tibia:	The larger, medial bone of the lower leg.
Vascular:	Pertaining to blood vessels or indicative of a copious blood supply.
Viscosity:	The inability for a fluid to flow freely.
Wettability:	The ability of a surface to attract a liquid. Typically measured by water contact angle.



General Introduction

Chapter 1

General Introduction and Aims

Chapter 2

Scaffolds for Tissue Engineering of Cartilage: A Review

“What I want is for everything to be round without, so to speak, a beginning or end of the figure anywhere, so that it makes one, lifelike harmonious whole”

“Wat ik wil is dat alles rond is en er als 't ware begin noch eind ergens aan de vorm is, doch die één harmonisch levend geheel uitmaakt”

[Vincent Van Gogh]

5 μm

Exp

WD

Det

Magn

Spot

Acc.V

Chapter 1

General Introduction and Aims

General:

It has been suggested that the earliest forms of cartilage evolved as part of the embryonic skeleton in vertebrates approximately 300 million years ago [478]. Throughout subsequent stages of human evolution, Nature has dictated that the regenerative capacity of damaged articular cartilage was to remain limited compared with other musculoskeletal tissues such as bone and muscle [313]. As early as 1743, Hunter [202] stated "from Hippocrates to the present age it is universally allowed that ulcerated cartilage is troublesome, and that when once destroyed, it is not repaired." Nature has developed a truly remarkable material both structurally and functionally [67, 169, 392], and as a consequence, Nature perhaps calculated incorrectly that humans, as hunter-gatherers, typically would not outlive the functional lifetime of cartilage present within their synovial joints, thus forgoing the need for complete regenerative capacity. Indeed the calculation may have been correct, however, the rate at which evolution was able to keep pace with the relatively rapid increase in life expectancy throughout the ages perhaps is lacking.

Today, the number of patients worldwide experiencing joint pain and loss of mobility through trauma or degenerative cartilage conditions is considerable, and yet, few approaches employed clinically are capable of restoring long-term function to damaged articular cartilage.

In the last two decades, with the combined advancement of biological sciences and materials engineering, the new field of "tissue engineering" has evolved. Tissues have complex three-dimensional (3D) geometries and highly organised internal architectures which cannot be simply emulated by cells maintained in two-dimensions [1]. Porous scaffolds are central to tissue engineering strategies because they provide a 3D framework for delivering reparative cells or regenerative factors in an organised manner to repair or regenerate damaged tissues. While these tissue engineering strategies have shown promising results, a number of challenges need to be overcome before these strategies are widely accepted clinically. One of the challenges in cartilage tissue engineering is the design and fabrication of 3D scaffolds which are capable of instructing, or guiding, cellular functions in order to obtain functional repair tissue.

This thesis critically reviews and discusses previously published data and explores model systems for studying the effect of scaffold architecture and biomaterial substrate composition on cartilage tissue formation *in vitro* and *in vivo*. In this chapter (**Chapter 1**), a brief introduction to articular cartilage, tissue-engineering and porous scaffolds is provided, as well as the aims and outlines of this thesis. The reader should note, however, that many of the critical topics discussed in this thesis are more thoroughly introduced in **Chapter 2** entitled "Scaffolds for Tissue Engineering of Cartilage: A Review."

Articular Cartilage & Tissue Engineering:

Articular cartilage is a remarkably resilient, load bearing tissue that provides a smooth, near frictionless articulating surface to synovial joints [61]. The unique composition and architecture of articular cartilage give it specific biomechanical attributes for repetitive gliding motion as well as absorption and transfer of mechanical shock loads to underlying subchondral bone. Notably, no synthetic material performs as well as articular cartilage as a joint surface [314].

Regardless of the various causes, joint pain and loss of mobility resulting from damage to articular cartilage and associated secondary effects are among the most common causes of impairment in middle-aged and elderly populations [62]. Nine percent of the US population aged 30 and older has clinical osteoarthritis (OA) of the hip or knee, with total direct costs estimated at \$28.6 billion per annum [123].

A range of clinical options exists for the repair of focal lesions and damage to the articular surface, yet they have only been met with partial success (see Chapter 2). These approaches may reduce pain and increase mobility, but typically only to a limited extent and over a short-term period [40, 63, 332, 472].

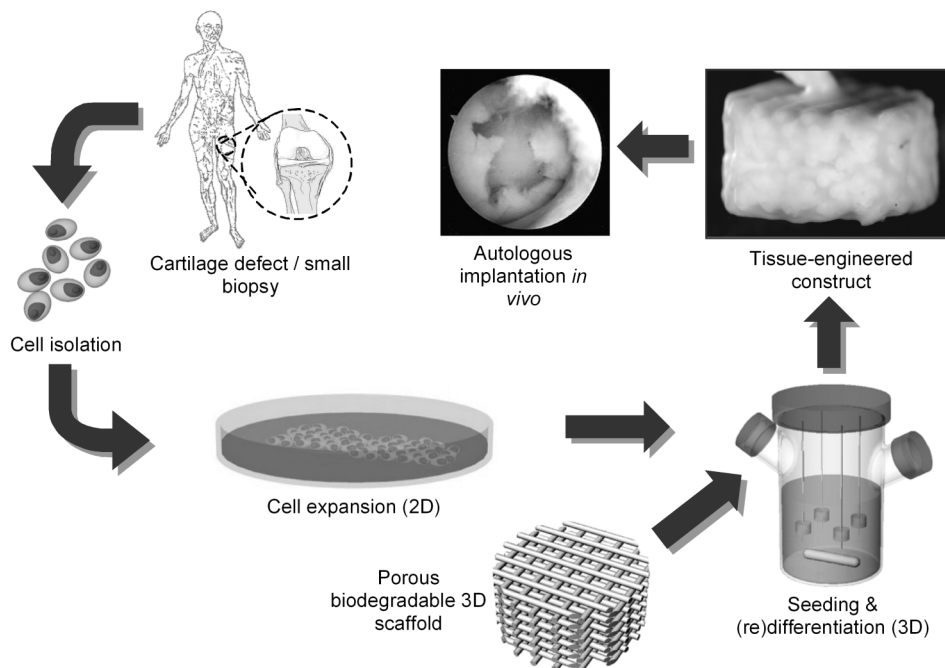


Figure 1 - Diagram representing an autologous tissue engineering approach for articular cartilage repair. Chondrocytes or chondroprogenitor cells are first isolated from the patient and then expanded in order to obtain sufficient numbers. Porous biodegradable scaffolds are seeded with expanded cells and cultured *in vitro*. The final tissue-engineered constructs can be implanted back into the patient.

As a result, there have been significant research efforts in the past decade to develop tissue engineering therapies for cartilage repair. Tissue engineering may be defined as "the application of the principles and methods of engineering and the life sciences toward the fundamental understanding of structure-function relationships in normal and pathological mammalian tissues and the development of biological substitutes that restore, maintain or improve tissue function" [357]. More simply, "tissue engineering pertains to the science of persuading the body to regenerate or repair tissues that fail to regenerate or heal spontaneously" [4]. The modern concept of tissue engineering draws on multiple areas of expertise, from cellular and molecular biology to biomaterials science, chemical and mechanical engineering to orthopaedic surgery [257]. With the recent rapid developments in these converging fields, the potential market worldwide for tissue-engineered products is estimated at nearly €100 billion per year [292].

Although extremely challenging, the general cartilage tissue engineering paradigm states that successful repair or replacement of articular cartilage will require grown tissue possessing the functional properties of the native tissue as well as graft-to-host tissue integration [204, 517]. A viable approach being to elaborate constructs *in vitro* which achieve biochemical compositions and mechanical properties that match those of native tissue, prior to implantation [200]. The various tissue engineering strategies investigated for repairing articular cartilage are reviewed and discussed in detail in Chapter 2.

An example of the general autologous tissue engineering approach for articular cartilage repair is illustrated in Figure 1. Chondrocytes or chondroprogenitor cells are first isolated via biopsy from the patient and then expanded in 2D in order to obtain sufficient numbers. Cartilage has a complex 3D geometry and highly organised internal architecture which chondrocytes maintained in 2D cannot emulate [1]. Accordingly, isolated cells are reintroduced to a 3D environment by transferring or "seeding" them in biodegradable 3D scaffolds. The cell-seeded 3D scaffolds and/or *in vitro* culture environment guide cells to produce the necessary cartilage extra cellular matrix (ECM) proteins. The final tissue-engineered construct can then be implanted into the patient.

Porous 3D Scaffolds:

In a tissue engineering sense, a scaffold may be adequately defined as, "a 3D conduit for cells, growth factors and/or signalling molecules which promotes infiltration and phenotypic regulation of the desired cell type, with concomitant extracellular matrix formation, resulting in functional repair, or regeneration, of damaged tissue" [517]. As the scaffold provides the basic foundation for cell-based tissue engineering strategies, its various properties need to be carefully designed and optimised. Scaffold design criteria for cartilage tissue engineering are discussed in detail in Chapter 2. This section aims to briefly introduce the basic terminology and aspects in characterising and processing of porous scaffold architectures for tissue engineering applications.

In addition to 3D shape, scaffolds need to be porous. A pore can be defined as a void space within a scaffold, whereas porosity can be considered as a collection of pores. Pore size and porosity are important scaffold parameters. Micro-pores (*i.e.* $<20\ \mu\text{m}$) are of a scale to influence cell function (*e.g.* cell attachment), whereas macro-pores (*i.e.* $>50\ \mu\text{m}$) are of a

scale to influence tissue function, for example, pores 50-400 μm in size are typically suggested for bone in-growth in relation to vascularity [391]. However, there is often a compromise between porosity and scaffold mechanical properties. High porosity (e.g. 90%) may provide a greater pore volume for cell infiltration and ECM formation, but conversely decreases mechanical properties in accordance to a power-law relationship [95, 534].

Pore interconnectivity is a critical factor and is often overlooked in scaffold design and characterisation. A scaffold may contain pores making it porous, but unless the pores are interconnecting (i.e. voids linking one pore to another), they serve no purpose and become superfluous in a scaffold for tissue engineering. The size of interconnections between pores should be suitably large to support ECM infiltration of desired tissue and, therefore, is more critical than pore size. It is preferable that scaffolds for tissue engineering have 100% interconnecting pore volume, thereby also maximizing the diffusion and exchange of nutrients (e.g. oxygen) throughout the entire scaffold pore volume [209, 288].

As a measure of pore interconnectivity, the accessible pore volume, or permeability, of a scaffold can be measured. Accessible pore volume can be defined as the total volume of pores which can be infiltrated from all peripheral borders to the interior of the scaffold. Scaffold permeability can be measured by determining the flow rate of fluid flow through interconnecting pores [271]. However, this technique is not suitable in scaffolds with large, 100% interconnected pore volumes as the scaffold provides no resistance to fluid flow. Alternatively, accessible pore volume, as well as vol% porosity, pore size distribution and scaffold surface area to volume ratio (volume fraction) can be characterised using techniques such as mercury intrusion porosimetry [35, 193, 370], micro computed tomography (μCT) [252, 348, 366, 419] or image analysis [35, 500]. Mercury porosimetry is a popular technique which is based on the principle that the pressure required to force a non-wetting liquid such as mercury into pores, against the resistance of liquid surface tension, is indicative of the pore size, assuming the pores are cylindrical in shape [2, 141]. However, the resolution of the technique is severely limited in scaffolds with large pore sizes ($>500 \mu\text{m}$) where low mercury intrusion pressures are necessary, and it has limitations when applied to materials that have irregular pore geometries [2]. Alternative techniques such as μCT , which utilise 3D CT imaging to generate computer models of porous materials, have been developed for analysing bone architecture [252, 348, 366, 419] and more recently scaffold architecture [427, 535]. Using 3D μCT techniques, considerably greater information can be obtained to characterise pore architectures without the physical limitations associated with mercury porosimetry.

Table 1 – Overview of techniques to prepare porous scaffolds for tissue engineering (adapted from Claese [94]).

Technique	Porosity (%)	Pore size (μm)	Comments	Ref
- Foaming using blowing agents	-	20-1000	Non porous outer layer (skin).	[385]
	<80	<350	Pore interconnectivity >99%.	[274]
- Foaming using CaCO_3	<81	100-1000	Difficult control.	[89]
- Foaming using NH_4HCO_3	<94	100-500	Interconnected pores.	[352]
Non-woven fibre	<97	100-500	Insufficient mechanical properties.	[265, 328, 339]
Woven fabrics	-	-	Insufficient mechanical properties.	[442, 515]
	81	-	Described process only possible for PGA-PLLA combination.	[328]
Fibre bonding	-	-	Coating of fibre mesh with another polymer.	[339]
Nanofibre electrospinning	-	-	Interconnected pore structure with a high specific surface area.	[530]
Sintered microspheres	32-39	67-150	Interconnected pores.	[43, 44]
Solvent casting + particulate leaching	20-50	30-425	Spherical pores, salt particles remain in matrix, only thin membranes or small devices.	[340]
	<92	800-1500	Large interconnections (350 μm), irregular pore morphology.	[187]
Coagulation + particulate leaching	<96	250-1180	Wide range of porosities and pore size.	[191]
Solvent merging + particulate leaching	<95	250-500	Good interconnectivity.	[272]
- Fused salt particles + solvent casting + particulate leaching	<97	250-425		[192]
- Fused salt particles + gas foaming + particulate leaching	<94	250-425	Improved interconnectivity compared to solvent casting + particulate leaching.	[349]
Porous membrane lamination	<88	10-400	Irregular pore size, tedious procedure.	[329]
Solvent casting + extrusion	<90	<30	Highly porous; interconnected pores; severe salt breakdown during extrusion.	[512]
Hydrocarbon templating	<88	100-1000	Allows incorporation of proteins.	
	<96	250-420	Control over interconnectivity.	[439]
Solid-liquid phase separation (freeze drying)	<97	<500	1,4-dioxane, phenol, benzene, naphthalene are toxic solvents.	[275, 277, 296, 536, 537]
Emulsion freeze drying	<97	<200	High volume of interconnecting micro-pores.	[509, 510]
Solvent induced phase separation (immersion precipitation)	<95	<10		
	<45	<10	Only possible for films / tubes.	[86]
Thermally induced phase separation (TIPS)	<97	<200	High volume of interconnecting micro-pores.	[431, 536]
	<97	10-500	Only partially interconnected pores; formation of a skin layer.	[338]
Super-critical fluid technology (gas foaming)	10-30	<100	High volume of non-interconnecting micro-pores	[166]
	<97	Micro <50	Low volume of non-interconnecting micro-pores	[509]
		Macro <400	Low volume of interconnecting macro-pores	
<i>Solid free form fabrication (SFF) / Rapid prototyping (RP)</i>				[184, 266, 334, 460, 461, 534]
- 3D Printing with or without particle leaching	<60	45-150	100% interconnected macro-pore structure	[209, 210]
			Irregular pore architecture, limited resolution	[535]
- Fused deposition modelling (FDM)	<80	150-700	100% interconnected macro-pore structure.	[211, 427, 534]
			Only in PCL polymers for bone applications.	
	60		PLA degradation during processing	[522]
- 3D plotting	<75	100-1000	100% interconnected macro-pore structure.	[253, 254, 256]
			Only hydrogel materials investigated.	
- Selective laser sintering (SLS)	-	<50	Low porosity primarily for drug release	[84]
			PEEK/HA composite scaffolds	[468]
- Stereolithography (SLA) / Photopolymerization	<90	>200	100% interconnected macro-pore structure	[100, 448]
			Polymers for bone, heat valve applications	

Scaffold Processing Techniques:

A number of scaffold processing techniques have focused on the development of porous biomaterials for tissue engineering applications, as summarised in Table 1. By far the most common techniques for generating porosity include the various forms of foaming and particle leaching (Fig 2A, 2B). Most of these techniques rely on generating porosity using porogens (e.g. a gas or particulate). While the size and, to a certain extent, the distribution of these porogens can be controlled during processing, their position and orientation to one another are inherently random. Scaffolds based on non-woven fibre meshes or fibre bonding techniques do not require porogens and have been used extensively due to their high porosity and surface to volume ratio (Fig 2C). However, they have extremely limited mechanical properties and also rely on random arrangements of fibres during processing. The control over scaffold architecture using these fabrication techniques are therefore highly process driven, and not design driven. This lack of control in pore structure, particularly with respect to the interconnectivity between pores causes considerable difficulties in designing porous scaffolds whose 3D pore architecture is critical for eliciting specific cell function and subsequent tissue formation.

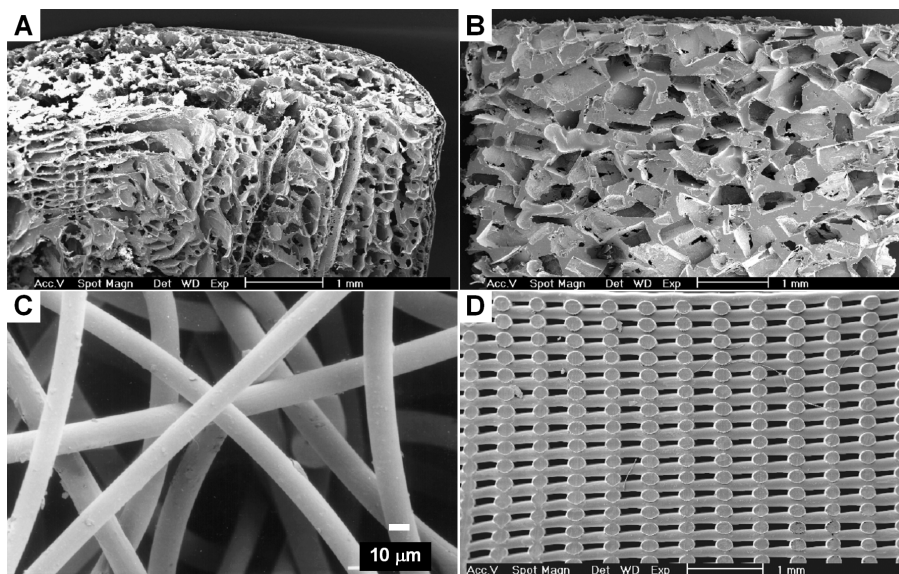


Figure 2 – Scanning electron micrographs showing examples of scaffolds produced using various processing techniques. (A) liquid-solid phase separation and freeze-drying using 1,4-dioxane (PEGT/PBT), (B) compression moulding and particle leaching (PEGT/PBT), (C) non-woven polylactic acid (PLA) mesh with 13 μm fibre diameter, (D) 3D fibre deposition (3DF) of PEGT/PBT scaffold with a 175 μm fibre diameter and an 0.5 mm fibre spacing.

As a result, investigators have recently turned to rapid prototyping (RP) or solid free-form fabrication (SFF) techniques for producing porous scaffolds for tissue engineering applications [195, 209, 211, 253, 266, 460, 514, 526, 534]. RP is a subset of mechanical processing techniques which allows highly complex and reproducible structures to be constructed one

layer at a time via computer-aided design (CAD) models and computer-aided machining (CAM) or tooling processes. These techniques essentially allow researchers to *design-in* desired properties, such as porosity, interconnectivity and pore size, in a number of polymer and ceramic materials [184, 185, 266, 393, 461, 466]. Scaffold RP methodologies studied to date have included stereolithography/photopolymerisation, selective laser sintering, fused deposition modelling and 3D printing [210] using highly specialized polymers and materials designed specifically to meet the processing requirements of each RP system. Application of this technology in combination with modern clinical imaging techniques, such as computed tomography (CT) and magnetic resonance imaging (MRI), has resulted in recent advances in producing customized metallic implants typically for total joint replacement, and more recently in scaffold development [185, 460, 461, 488]. However, the transfer of RP technologies to encompass biocompatible and bioresorbable materials still poses a significant challenge, and few studies have investigated the use of RP techniques in the development of 3D scaffolds for cartilage tissue engineering applications.

PEGT/PBT Co-polymers:

Many natural and synthetic biomaterials are amenable for use as scaffolds for cartilage tissue engineering applications, and are discussed in detail in Chapter 2. As a model substrate for designing scaffolds and investigating structure-function relationships for articular cartilage tissue engineering, we are evaluating a series of amphiphilic, biodegradable poly(ether ester) multiblock co-polymers. The co-polymers are based on hydrophilic poly(ethylene glycol)-terephthalate (PEGT) and hydrophobic poly(butylene terephthalate) (PBT) blocks. The composition is denoted as $a / b / c$, where a represents the poly(ethylene glycol) (PEG) molecular weight (MW g/mol), and b and c represent the weight percentage (wt%) of PEGT and PBT blocks respectively.

A major advantage of these types of co-polymer systems is that, by varying the PEG MW and the weight wt% of PEGT and PBT blocks, an entire family of polymers can be obtained. This offers extensive possibilities in the design of model co-polymer systems with tailor-made properties, such as wettability [371], protein adsorption [299], swelling [111], biodegradation rate [111], and mechanical properties [519]. For example, due to their higher PEG MW and greater wt% of "soft" amorphous PEGT blocks to "hard" crystalline PBT blocks, 1000/70/30 co-polymers have lower mechanical strength and stiffness than 300/55/45 (Fig 4). Tensile testing 1000/70/30 co-polymers resulted in a tensile modulus (E) and tensile strength (σ) of 33.9 ± 1.2 MPa and 5.3 ± 0.3 MPa respectively, while 300/55/45 co-polymers were shown to be 187.5 ± 5.0 MPa and 15.3 ± 0.4 MPa [422].

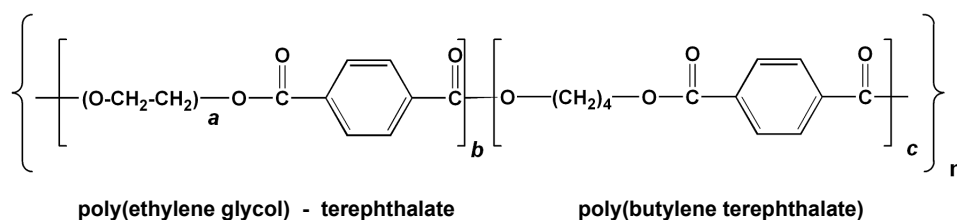


Figure 3 – Chemical structure of PEGT/PBT block co-polymers.

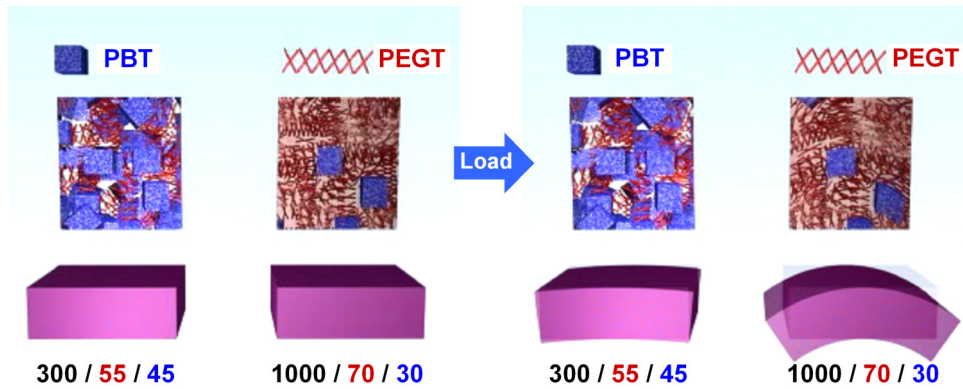


Figure 4 – Schematic representation of the distribution of amorphous PEGT and crystalline PBT blocks within PEGT/PBT biomaterials. By varying the PEG molecular weight, and the wt% ratio of PEGT to PBT, a range of mechanical properties can be achieved. Higher PEG MW and wt% PEGT content (i.e. 1000/70/30) results in a decrease in material stiffness. ► p207.

Various *in vitro* and *in vivo* studies have demonstrated both the biocompatibility and biodegradable nature of PEGT/PBT co-polymers [28, 111, 402, 480] with 1000/70/30, 1000/60/40 and 300/55/45 compositions evaluated for a range of biomedical applications, including tissue engineering of bone and skin [29, 95, 96, 111, 270, 327, 421, 480, 504]. PEGT/PBT co-polymer degradation has been shown to occur via both hydrolysis (cleavage of ester bond linking ester and hydrophilic ether segments) and oxidation (PEG chain scission via free-radical reactions), and in both cases, degradation is more rapid for copolymers with high PEG content (e.g. 1000/70/30) [111]. Controlled release of bioactive factors from these materials has also been demonstrated [30-32].

The attachment, proliferation, morphology and differentiation state of chondrocytes has also been demonstrated on different compositions of 2D PEGT/PBT films [375], and also in porous 3D scaffolds of varying pore size and pore morphology [518]. The control over composition make PEGT/PBT co-polymers excellent model substrates to investigate influences of cell-biomaterial interactions on cell function. Papadaki *et al.* [375] reported that primary bovine chondrocytes seeded on 2D PEGT/PBT films best retained their chondrocytic phenotype when a hydrophilic 1000/70/30 composition was used. More recently, Mahmood *et al.* [299] confirmed that 2D PEGT/PBT films produced from 1000/70/30 compositions better maintained the phenotype of primary adult human articular chondrocytes as compared to 300/55/45 compositions. Other recent studies have demonstrated re-differentiation of microcarrier-expanded human nasal chondrocytes in 3D 300/55/45 scaffold compositions produced by compression moulding and salt leaching [302].

Achieving suitable cell attachment to biomaterial scaffolds is essential. Previous studies have demonstrated that PEGT/PBT co-polymer compositions containing a high PEG content exhibit limited cell attachment characteristics [95, 96, 111]. Surface modification of PEGT/PBT co-polymers using glow-discharge gas plasma (GP) treatment has been studied extensively for bone tissue engineering applications and resulted in enhanced bone progenitor-cell attachment and function in 3D scaffolds [95, 96, 111, 371]. GP surface modification is

commonly used commercially to treat tissue-culture polystyrene (TCPS) surfaces, and has been shown to enhance cell attachment, growth and differentiation [233, 458]. These features are reportedly caused by etching and incorporation of hydroxyl and carboxyl groups in the most superficial layers (*i.e.* at a nano-scale level) of GP treated substrates through a cascade of chemical reactions [83, 371], potentially making it a simple and highly desirable technique for modification of PEGT/PBT scaffolds for cartilage tissue engineering. Little is known about the effects of GP treatment on PEGT/PBT co-polymers in relation to chondrocyte attachment and phenotype expression.

Challenges:

With the recent exponential growth of the field of tissue engineering [293], numerous scaffold materials and designs have been described in literature related to the repair of articular cartilage defects. While considerable progress has been made, the lamentable reality is that tissue engineering of functional cartilage of clinically relevant size still remains largely elusive (see Chapter 2). If the successful repair or replacement of articular cartilage requires grown tissue possessing the functional properties of the native tissue [204, 517], then it appears that we are still very much in the infancy stage of this tissue-engineering paradigm.

Without a clear understanding and characterisation of the influence of the biomaterial and scaffold architecture on cellular function, it is often impossible to make comparisons between studies using various scaffolds as well as make clear distinctions as to which scaffold characteristics are responsible for eliciting observed *in vitro* and/or *in vivo* responses without time consuming trial and error approaches.

One of the challenges in tissue engineering is the design and fabrication of biodegradable scaffolds which are "instructive" for specific cellular functions, and may thus regulate cell adhesion, proliferation, expression of a specific phenotype and extracellular matrix deposition in a predictable and controlled fashion. Cartilage cells are an ideal model for the study of cell-substrate interactions due to the tight relationships which have been established between chondrocyte morphology and function [285]. Mature chondrocytes are well differentiated in their phenotype and are solely responsible for the maintenance of cartilage ECM components, characterised by the synthesis of predominantly type II collagen and the proteoglycan aggrecan [247]. When embedded within their native ECM, healthy chondrocytes exhibit a spherical morphology (Fig 5A). However, when chondrocytes are released from their native ECM and cultured under conditions promoting a spread morphology, such as on 2D substrates (Fig 5B), they progressively lose their original phenotype and display fibroblastic or pre-chondrogenic features, typically characterised by the expression of predominantly type I collagen and the proteoglycan versican [15]. This process is typically described as *de-differentiation* [24, 36], and can have considerable implications for tissue engineering strategies resulting in inferior or no cartilage tissue at all if suitable restoration of a differentiated chondrogenic phenotype cannot be achieved.

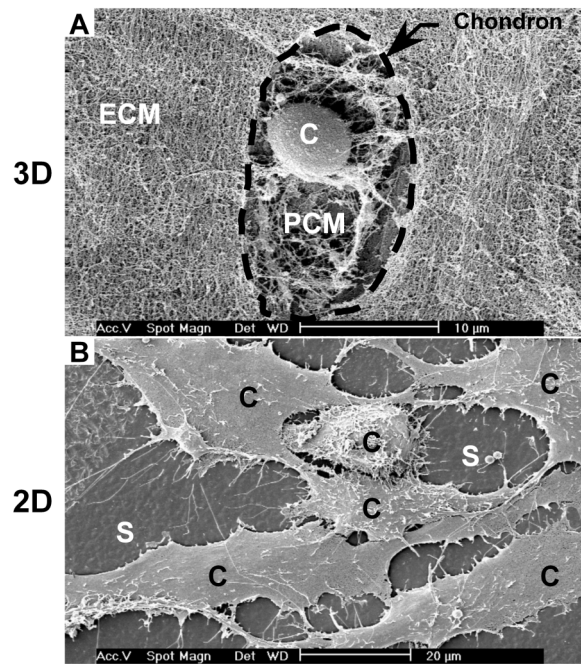


Figure 5 – Scanning electron micrographs of (A) a differentiated articular chondrocyte, and (B) de-differentiated chondrocytes. In (A) the cell (C) has a spherical morphology and is surrounded by pericellular matrix (PCM) making up a chondron (dotted line). The adjacent extra-cellular matrix (ECM) consists predominantly of collagen type II fibrils and negatively charged glycosaminoglycan (GAG) macromolecules. In (B) isolated chondrocytes attached to PEGT/PBT substrate (S) show a spread morphology.

Instructing chondrocyte (re)differentiation:

Chondrocyte *re-differentiation* (i.e. the post-expansion re-expression of chondrocyte phenotype) can be stimulated in a number of ways and are introduced briefly below:

Growth factors/cell expansion: During the expansion phase, culture media supplemented with growth factors, such as transforming growth factor- β (TGF- β), insulin-like growth factor-1 (IGF-1), basic fibroblastic growth factor (bFGF) and platelet derived growth factor (PDGF) have been shown to influence chondrocyte proliferation rate [119], whilst enhancing the ability for subsequent cell re-differentiation [221, 318, 382]. The combination of these growth factors during expansion with other potent re-differentiation factors such as insulin, TGF- β and dexamethasone during 3D culture have been shown to stimulate cartilage tissue formation in scaffolds [226]. Cell expansion on 3D microcarriers has also been demonstrated to influence the re-differentiation potential of chondrocytes [133, 302, 305].

Pellet/mass culture: Culture conditions, such as high-density pellet- or mass-culture techniques, which mimic cell condensation reactions associated with embryonic chondrogenesis or the *in situ* cartilage environment have also been shown to induce re-differentiation related to cell-cell and/or cell-matrix interactions [432, 453, 523]. These culture conditions are often used in combination with growth factor stimulation [38, 524].

Bioreactors/mechanical stimulation: Culture conditions which place tissue-engineered constructs in a dynamic fluid environment such as those present in spinner flask [142, 495] or rotating bioreactor culture [127, 130, 316, 383, 496], or which simulate *in situ* joint loading conditions via dynamic hydrostatic pressure [76-78, 165, 459, 513] or mechanical compression [41, 70, 109, 235, 260, 399], have also been suggested to stimulate chondrocyte re-differentiation [76, 77, 159, 399]. These dynamic culture conditions also aim at optimising nutrient and waste exchange to engineered tissues. This is not only important for maintaining cell viability, but nutrient limitations themselves may also be involved in instructing cell function. For example, a low oxygen environment, comparable to conditions in native cartilage, has been suggested to be an instructive factor in promoting chondrocyte differentiation [303].

Cell-biomaterial interactions: It has long been known that cell behaviour on synthetic polymers is related to both the physical and chemical properties of the substratum [291]. Several properties have been suggested as potential regulators of cell behaviour including wettability, surface chemistry, equilibrium water content and roughness [48, 291, 433]. Furthermore, the specific substrate properties can either directly or indirectly effect cell adhesion, morphology and subsequent cellular activity by controlling adsorption of ions, proteins and other molecules from the culture medium [291, 443]. This is the scenario when seeding and culturing cells on biomaterials in serum-containing media, thereby exposing substrates to potent cell attachment proteins such as fibronectin (FN) and vitronectin (VN). It is this molecularly populated surface that the cells sense and respond to biochemically by means of specific cell receptors such as the integrin family (e.g. $\alpha 5 \beta 1$, $\alpha V \beta 3$) and CD44 [241, 278-280]. Understanding and controlling this substrate-protein milieu plays a large role in the ability of biomaterials scientists to instruct cell function [198].

3D architecture: It is well established that chondrocytes require a 3D environment to maintain their differentiated phenotype and synthesize necessary ECM components such as collagen type II and GAG [24, 153, 288, 318, 517]. The influence of specific surface properties of various biomaterials on chondrocyte behaviour has been so far mostly investigated using 2D films [161, 215, 249, 263, 375]. However, the growing appreciation that cell behaviour in 2D cultures does not necessarily translate into 3D systems [1, 103] prompts for extended studies in 3D scaffolds where the introduction of an additional parameter, the 3D architecture, could modulate the effects of changes in the substrate composition. However, little is known about the specific influence of controlled changes in 3D scaffold architecture on chondrocyte (re)differentiation. It has been suggested that scaffold architecture may control cell function by regulating the diffusion of nutrients (e.g. oxygen) and waste products, as well as influencing cell-cell interactions [535].

In this thesis, we focus specifically on these last two factors. By adopting a less conventional approach to scaffold tissue engineering – instead of starting with a generic scaffold and evaluating tissue formation, we start with the question:

In what ways can we design scaffolds to influence or instruct cell function in 3D ?

Aims and Outline of this Thesis:

The aims of this thesis were to investigate various combinatorial steps involved in developing porous 3D scaffolds which are "instructive" for chondrocyte (re)differentiation and cartilage tissue formation and which ultimately contribute to a functional tissue-engineered implant. In a mechanistic approach to understanding which structure-function relationships are "instructive", a number of *in vitro* and *in vivo* model systems were designed and evaluated based on controlled changes in 3D scaffold architecture and substrate composition. These model systems fall under four separate phases described below. The aims or specific questions for investigation within each phase, were as follows:

I. Designed scaffolds: rapid prototyping for cartilage tissue engineering.

Aim: To apply rapid prototyping (RP) techniques in the development and processing of model PEGT/PBT scaffolds with "designed" pore architectures for cartilage tissue engineering.

II. Instructive scaffolds: pore architecture and chondrocyte differentiation.

Aim: To investigate the influences of controlled changes in 3D PEGT/PBT scaffold architecture on chondrocyte differentiation capacity and zonal organisation within tissue-engineered constructs.

III. Instructive scaffolds: pore architecture, composition and chondrocyte re-differentiation.

Aim: To investigate the influences of controlled changes in PEGT/PBT surface composition and 3D scaffold architecture on human chondrocyte re-differentiation and cartilage tissue formation capacity.

IV. Instructive anatomically-shaped scaffolds: tissue-engineered implants for joint reconstruction.

Aim: To evaluate feasibility and function of anatomically-shaped, tissue-engineered PEGT/PBT implants for joint reconstruction using an autologous rabbit knee model.

Results from experiments describing these model systems from phases I-IV are addressed as chapters in this thesis as outlined below:

General Introduction:

Chapter 2 introduces the reader to a full range of topics relating to articular cartilage structure and function, aetiology, and relative shortcomings in current clinical repair strategies. It highlights pertinent design considerations and limitations related to the development, material selection and processing of scaffolds for articular cartilage tissue engineering. Furthermore, the subsequent impact of current and future aspects of these multidisciplinary scaffold-based approaches related to *in vitro* and *in vivo* cartilage tissue engineering are discussed.

I. Designed scaffolds: rapid prototyping for cartilage tissue engineering:

Chapter 3 focuses around the development, processing and characterisation of model PEGT/PBT scaffolds with "designed" pore architectures using a novel 3D fibre deposition (3DF)

technique. These rapid prototyping (RP) technologies and model scaffolds form a pivotal role in subsequent chapters and are aimed at fulfilling critical scaffold design criteria raised in Chapter 2.

II. Instructive scaffolds: pore architecture and chondrocyte differentiation.

In **Chapter 4** and **Chapter 5**, the effects of controlled changes in PEGT/PBT scaffold architecture, produced using novel 3DF and conventional compression moulding and particle leaching (CM) techniques, on chondrocyte differentiation are evaluated following *in vitro* culture and subcutaneous implantation *in vivo* in nude mice. Mechanical testing and novel micro-computed tomography (μ CT) techniques are described for characterising porous architectures in relation to chondrocyte differentiation capacity. In parallel, **Chapter 5** focuses specifically on the effect of PEGT/PBT scaffold architecture on oxygen gradients measured within tissue-engineered constructs using an oxygen microelectrode.

Chapter 6 describes a model system for studying the zonal organisation within tissue-engineered cartilage constructs using 3DF PEGT/PBT scaffolds designed with organised pore-size gradients. The ability of anisotropic 3DF scaffold architectures to instruct the zonal distribution of chondrocytes and ECM components *in vitro* are evaluated.

III. Instructive scaffolds: composition, pore architecture and chondrocyte re-differentiation.

Chapter 7 and **Chapter 8** describe experiments using clinically relevant cell sources – expanded human chondrocytes. **Chapter 7** describes a 2D model system used to evaluate mechanisms by which PEGT/PBT composition, gas plasma surface modification, and serum-containing/-free media effect human chondrocyte morphology and re-differentiation capacity *in vitro*.

Expanding on themes developed in Chapters 4-7, **Chapter 8** describes a model 3D system evaluating the synergistic effects of controlled changes in both PEGT/PBT scaffold composition and scaffold architecture (CM or 3DF) on human chondrocyte re-differentiation and cartilage tissue formation *in vitro*. Mechanical testing and μ CT techniques are described for characterising porous architectures in relation to chondrocyte re-differentiation capacity.

IV. Instructive anatomically-shaped scaffolds: tissue-engineered implants for joint reconstruction.

Chapter 9 attempts to amalgamate technologies and model systems developed in Chapters 2-8 to describe the feasibility of an entire tissue-engineering concept, from imaging of the defect to a functional, anatomically-shaped tissue-engineered implant for small joint reconstruction. Combinatorial approaches including CT imaging, computer aided design (CAD), two RP techniques (CNC milling and 3D fibre deposition), dynamic seeding and bioreactor culture, were used to engineer cartilagenous implants with varying internal pore architecture (CM or 3DF), but identical external anatomic shape. Constructs were evaluated *in vitro* and following implantation and short-term load bearing in an autologous knee model in rabbits.

Finally, the results of these studies, and suggestions for future directions, are discussed in **Chapter 10**.

Chapter 2

Scaffolds for Tissue Engineering of Cartilage:

A Review

Woodfield T.B.F.^{1,1,2}, Bezemer J.M.², Pieper J.S.², van Blitterswijk C.A.¹, Riesle J.²

¹ Institute for Biomedical Technology, University of Twente, Enschede, The Netherlands

² IsoTis S.A., Bilthoven, The Netherlands

Abstract:

Articular cartilage lesions resulting from trauma or degenerative diseases are commonly encountered clinical problems. It is well established that adult articular cartilage has limited regenerative capacity, and although numerous treatment protocols are currently employed clinically, few approaches exist which are capable of consistently restoring long term function to damaged articular cartilage. Tissue engineering strategies which focus on the use of three-dimensional scaffolds for repairing articular cartilage lesions offer many advantages over current treatment strategies. Appropriate design of biodegradable scaffold conduits (either pre-formed or injectable) allow for the delivery of reparative cells, bioactive factors and/or gene factors to the defect site in an organised manner.

This review seeks to highlight pertinent design considerations and limitations related to the development, material selection and processing of scaffolds for articular cartilage tissue engineering, evidenced over the last decade. In particular, considerations for novel repair strategies which utilise scaffolds in combination with controlled release of bioactive factors or gene therapy are discussed, as well as scaffold criteria related to mechanical stimulation of cell-seeded constructs. Furthermore, the subsequent impact of current and future aspects of these multidisciplinary scaffold-based approaches related to *in vitro* and *in vivo* cartilage tissue engineering are reported herein.

‡ based on: Woodfield TBF, Bezemer JM, Pieper JS, van Blitterswijk CA, Riesle J. Scaffolds for tissue engineering of cartilage. *Crit Rev Eukaryot Gene Expr* **2002**; **12**(3): 209-236.

Introduction:

The main purpose of articular cartilage is to provide a smooth, near frictionless articulating surface and act as a mediator for load transfer to the underlying subchondral bone. However, throughout the steps of human evolution, Nature has dictated that the regenerative capacity of damaged articular cartilage was to remain limited compared with other musculoskeletal tissues such as bone and muscle [313].

Regardless of the various causes, joint pain and loss of mobility resulting from damage to articular cartilage and associated secondary effects are among the most common causes of impairment in middle-aged and elderly populations [62]. Although numerous resources and considerable efforts of surgeons and scientists alike have, for many years, been poured into the study of damaged or lost cartilage, successful repair or regeneration of this complex tissue to date has been limited. Consequently, in the US, approximately 500,000 articular cartilage defects were diagnosed in 2001 and yet less than 5% of these patients were treated with currently available repair techniques [330]. Tissue engineering approaches adopting scaffold conduits for delivery or recruitment of reparative cells, as well as chondrogenic factors, in an organised manner to bridge voids within cartilage defects, offer considerable promise as repair strategies [149, 452]. Therefore, an examination of current developments in scaffolds for cartilage tissue engineering and future perspectives is timely.

Whilst the purpose of this article was not to focus exclusively on articular cartilage applications, they represent, as opposed to repair of fibrocartilagenous tissues and cosmetic cartilage reconstruction, the majority of published literature to date with regard to use of scaffolds for cartilage tissue engineering, and therefore form the basis for subsequent discussion.

Articular Cartilage Structure and Function

Of the connective tissues, cartilage forms a subset containing three different types; hyaline cartilage, fibrocartilage and elastic cartilage. Examples of hyaline cartilage include articular cartilage, which covers the ends of long bones of synovial joints, or nasal septal cartilage. Fibrocartilage is present within the intervertebral disc and menisci, for example, whilst elastic cartilage is found in the ear and epiglottis. In normal articular cartilage, water containing dissolved salts (e.g. Na^+ , K^+ , Ca^{2+} , SO_3^{2-} , HPO_4^-) contributes 70% to 80% of the wet weight, with solid macromolecules contributing the remaining 20% to 30%. The solid phase of the articular cartilage matrix consists predominantly of type II collagen fibrils (along with smaller amounts of type IX and type XI collagens), several types of non-collagenous proteins and a high concentration of high-molecular-weight cartilage proteoglycans [61, 314]. These complex proteoglycan (PG) macromolecules consist of a protein core with multiple covalently-bound, negatively-charged glycosaminoglycan (GAG) chains, 80% to 90% of which are the large, aggregating type called aggrecan. These highly negatively-charged macromolecules bind matrix water generating a swelling pressure. The collagen network resists and balances the swelling pressure generated by proteoglycan-ion interactions, and hence is subjected to tensile stresses, even in the absence of externally applied loads. Thus, an appropriate balance in concentrations of GAG and collagen type II within the extra-cellular matrix (ECM)

is critical for proper biomechanical function of articular cartilage, and provides the tissue with the capacity to resist compressive loads [345].

Whilst solely responsible for the synthesis and maintenance of the articular cartilage, chondrocytes occupy only a small portion of the total volume of adult tissue *i.e.* less than 2% [207]. Mature chondrocytes are well differentiated in their lineage and have a relatively slow turnover rate. The ECM in which they assemble has a highly ordered internal structure [61]. The differences in cell size and shape, collagen fibril diameter and orientation, water concentration, and proteoglycan concentration with depth from the surface can be divided into four zones: the superficial, middle and deep zones, and the zone of calcified cartilage (Fig 1). The superficial zone contains flattened chondrocytes and thin collagen fibrils (20 nm in diameter) that are densely packed and oriented tangentially to the articular surface, thus providing resistance to tensile forces generated by friction between joints. The middle, or transitional, zone contains randomly oriented collagen fibres of larger diameter, and the chondrocytes have a more rounded appearance. The deep, or radial zone, consists of large, spherical chondrocytes aligned in a columnar fashion and thicker collagen fibres (120 nm in diameter) oriented perpendicular to the joint surface. A zone of calcified cartilage follows, whose thickness and intermediate stiffness modulate the transfer of forces through articular cartilage to bone.

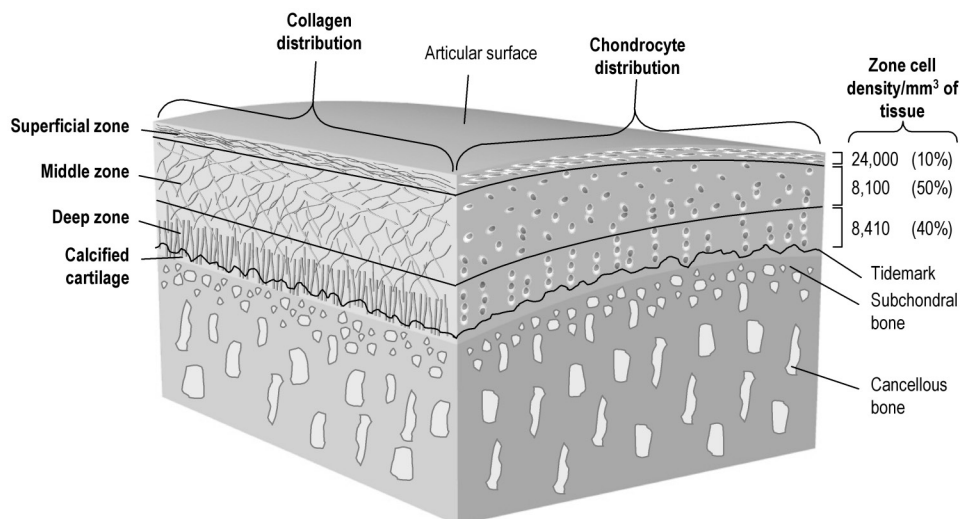


Figure 1 – Anisotropic distribution and orientation of collagen fibres (left face) and chondrocytes (right face) within the superficial (10%), middle (50%) and deep (40%) zones of articular cartilage. Cell density per unit tissue volume data adapted according to Hunziker *et al.*, [207].

Under normal joint loading, cartilage compression causes interstitial fluid exudation from the solid matrix, as well as fluid redistribution within the matrix. Upon load removal, cartilage resorbs the fluid exudate so that it recovers its initial dimensions, as well as creating a natural circulation pattern between the tissue and synovial fluid, crucial for cell nourishment and waste exchange. Internal forces associated with these two deformation processes *i.e.* matrix deformation and interstitial fluid flow, give rise to the observed viscoelastic behaviour of articular cartilage [12].

Cartilage Defects and Repair

In a discussion of articular cartilage repair, it is important to differentiate between two major categories of defects which typically result from traumatic injuries, congenital abnormalities and/or as a consequence of degenerative disease, such as arthritis. The majority of experimental repair strategies investigated to date concern treatment of osteochondral defects *i.e.* full-thickness lesions which extend through the cartilage and calcified cartilage layers into the subchondral bone and underlying vasculature. The second, but more clinically prevalent category of defect, pertains to the treatment of chondral, or partial-thickness lesions, which are characterised by a mechanical disruption of cells and matrix confined to the cartilage layer itself (Fig 2). It is well established that critically sized defects of such nature fail to heal spontaneously [66, 203, 313, 358], whereas in osteochondral defects, a limited spontaneous repair response ensues, due to the ingress of mesenchymal cells and blood vessels from the underlying bone marrow spaces [436]. In the latter case, a fibrocartilagenous repair tissue generally fills the defect site after 6 months to 1 year. However, its matrix composition and structure is highly variable and mechanically inferior compared with normal articular cartilage [436]. As a result, a majority of full-thickness repairs deteriorate [220], and joint function is overcome by accelerated degenerative changes.

A variety of surgical procedures have been developed in an attempt to treat articular cartilage defects, as described in Table 1.

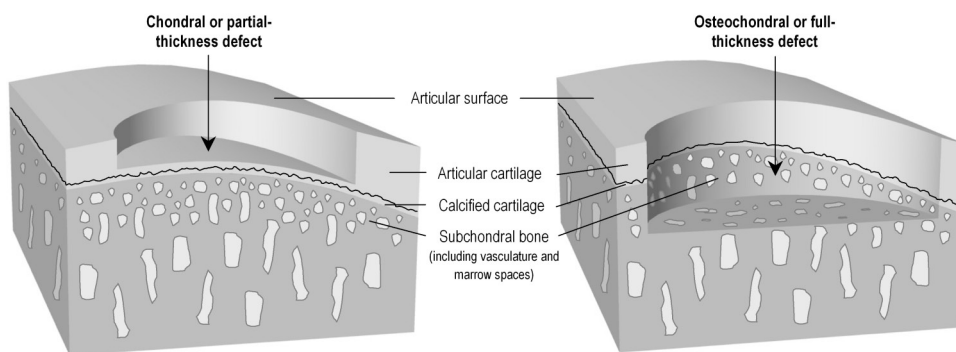


Figure 2 – Articular cartilage lesions are typically chondral (left) or osteochondral (right) in nature. While most experimental scaffold-based repair strategies focus on osteochondral defects, chondral defects are more prevalent clinically.

Table 1 – Overview of conventional and cell-based treatment strategies for articular cartilage repair.

Treatment Strategy	Basis for Treatment	Outcome	Ref
Traditional surgical techniques			
- Lavage	Arthroscopic joint irrigation to remove pain-signalling or pain-mediating molecules.	Short-term pain relief. Limited long-term benefit.	[80, 342]
- Chondral shaving / debridement	Removal of cartilage debris to overcome mechanical impediment.	Short-term symptom relief. Limited long-term benefit.	[26, 167, 196, 245]
- Abrasion arthroplasty/ osteochondral drilling / microfracture	Perforation of subchondral bone to stimulate spontaneous repair response via access to vascular/bone marrow spaces.	Mechanically inferior fibrocartilage repair tissue. Highly variable results and Limited long-term benefit.	[223, 395, 456, 457]
- Osteotomy	Limb realignment to transfer joint load away from damaged cartilage surfaces.	Long-term pain relief. Overloading in joint can exacerbate OA.	[213, 322, 506]
- Osteochondral grafting / mosaicplasty	Transplantation of autologous or allogenic osteochondral plugs (with intact articular cartilage layer) from low weight-bearing area to fill large defects.	Short-term pain relief. Variable long-term benefit. High donor site morbidity. Dead space between plugs.	[6, 14, 21, 39, 104, 135, 162-164]
- Perichondrial / periosteal grafting	Perichondrial/periosteal graft containing stem/chondrogenic cell population placed in defect (cambial layer facing upwards).	Short-term pain relief. Variable and limited long-term benefit. Fixation difficult.	[11, 46, 47, 205, 369]
- Total joint arthroplasty	For severe joint degeneration where replacement with total prosthetic joint (typically metallic alloy) is necessary.	Extensive surgery. Functional relief with 10-15 yr benefit. Limited to elderly patients due to revision surgeries.	[25, 201, 321, 350, 389, 479]
Cell-based / Tissue-Engineering techniques			
- Autologous chondrocyte implantation (ACI)	Regeneration of cartilage tissue using expanded autologous chondrocytes injected under periosteal flap covering defect.	Variable success with equal or better long-term benefit to traditional techniques. Two operations necessary. Costly.	[17, 23, 52, 138, 282, 331, 388].

Despite the poor natural repair response in articular cartilage, interventions which puncture the subchondral bone form the basis for a number of clinical treatments including abrasion arthroplasty, microfracture and osteochondral drilling [219]. Although these treatments are widely accepted and do initiate a healing response, the reparative fibro-cartilage has poor biomechanical properties [40, 63] and, therefore, these approaches only provide relief in the short-term [332]. The long-term efficacy of these treatments remains unpredictable and controversial [367, 456]. Other strategies used clinically to repair cartilage defects include debridement, periosteal or perichondrial grafts, osteochondral autografts and allografts, joint osteotomy and total joint replacement, and have been reviewed elsewhere [64, 65, 137, 172, 203, 204, 358, 368, 472]. While positive temporary outcomes such as reduced pain and increased range of motion have been obtained using these techniques, in general, few of these surgically based protocols have yielded satisfactory clinical and functional results in the long term [205]. Additional concerns with these techniques include the highly invasive surgery, donor site morbidity and possibility of pathogen transfer for allograft procedures. The use of osteochondral autografts or mosaicplasty (Fig 3) provides the advantage of low risk of immunogenic response [105, 230] as well as the absence of disease transfer [68], however, there is only limited low weight-bearing tissue available and the fate of the harvest site is

uncertain. In addition, surgical performance is technically demanding as the grafts must recreate the normal joint contour to be functional [381]. Furthermore, it is not possible to completely fill the defect with cylindrical implants, and consequently, dead space will be present around the grafts (Fig 3). Periosteal and perichondrial grafts offer the benefit of supplying additional progenitor cells and growth factors into the defect which may aid neocartilage formation, although limiting factors include reduced biological activity of grafts from elderly patients [47, 369] and unfavourable long term clinical outcomes [11].



Figure 3 - Open mosaicplasty in a patient with articular cartilage damage to the medial and lateral femoral condyles. Reprinted from Hangody et al. [162] with permission from the author and publisher.

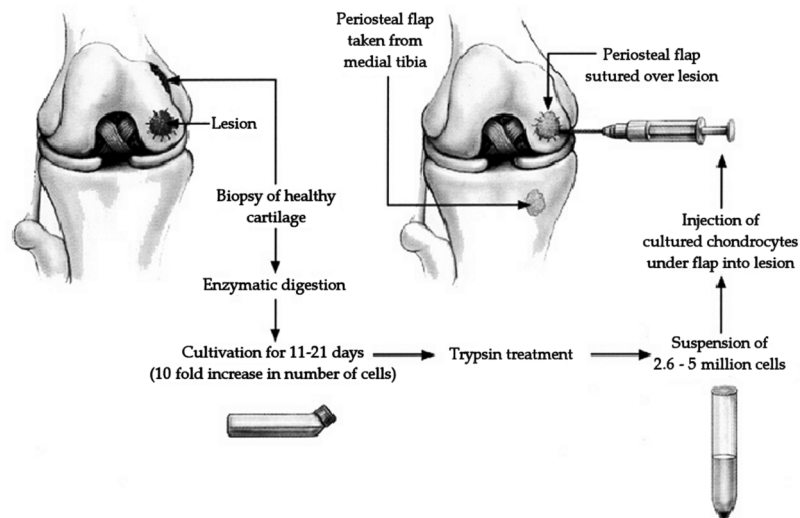


Figure 4 - Autologous chondrocyte implantation (ACI) technique as described by Brittberg et al. [52]. Reproduced with the permission of the author.

Given these facts, the notion that tissue engineering strategies may offer significant advantages over traditional cartilage repair methods stimulated a major effort in orthopaedic research more than a decade ago. Numerous definitions for the field of tissue engineering have been coined, however, a simple and quite elegant definition pertains to the science of persuading the body to regenerate or repair tissues that fail to regenerate or heal spontaneously [4]. It has been regularly stated that articular cartilage is well suited for tissue engineering approaches due to its relatively simple structure based upon a single cell type (*i.e.* the chondrocyte), in addition to factors such as the lack of vascularity and innervation, as well as low oxygen requirements and low cell-to-matrix ratio [139]. Clinical advances using cell-based therapies to treat cartilage lesions have been shown using autologous chondrocyte implantation (ACI) techniques pioneered by Grande *et al.*, [148] and Brittberg *et al.*, [51, 52]. The ACI process involves first harvesting normal articular cartilage from a low load-bearing region of the knee, followed by isolation and *in vitro* expansion of autologous chondrocytes (Fig 4). During a second surgery, the dedifferentiated chondrocyte suspension is injected under a periosteal flap sutured to the defect borders, thus preventing loss of transplanted cells from the defect void. Whilst it is unclear whether neocartilage formation is stimulated from the transplanted chondrocytes, chondroprogenitor populations within the periosteum and local environment, or combinations thereof, repair results have generally been comparable or better in outcome to other surgical interventions described above. While animal studies using the ACI technique have reported the loss of initial hyaline repair tissue, with no significant difference compared to empty defects or periosteum alone after 18 months *in vivo* [50], recent long-term clinical follow-up studies have reported, good to excellent maintenance of stable repair tissue in approximately 80% of cases for single condylar lesions in humans [387]. Disadvantages of the ACI technique, however, include the considerable costs of the procedure, the highly invasive surgery, donor site morbidity, long rehabilitation times, and limited success in patellar defects [54].

Alternative repair approaches which simplify the delivery and retention of cells without the use of a tissue flap include the use of scaffolds, and have received considerable attention. In a tissue engineering sense, a scaffold may be adequately defined as a conduit for cells, growth factors and/or signalling molecules which promotes infiltration and phenotypic regulation of the desired cell type, with concomitant extracellular matrix formation, resulting in functional repair, or regeneration, of damaged tissue. Historically, the concept of combining cells and biomaterial scaffolds for assisting cartilage formation is not novel. In 1977, Green *et al.* [151] seeded decalcified bone samples with isolated chondrocytes with the aim of studying chondrocyte multiplication *in vitro* and cell differentiation following subsequent allografting. Although unsuccessful in forming cartilage, Green *et al.* suggested that improved results might be obtained by adapting the approach using chondrocyte-laden synthetic biocompatible materials. Over a decade later, Cima *et al.* [93] were instrumental in engineering cartilage-like tissue *in vitro* and *in vivo* on basic scaffolds of resorbable and non-resorbable suture materials, and resorbable polyglycolic acid (PGA) non-woven meshes. With the exponential growth of the field of tissue engineering recently [293], there are now a plethora of scaffold materials and designs described in literature related to the repair of cartilagenous defects. While considerable progress has been made, the lamentable reality is that tissue engineering of functional cartilage of clinically relevant size still remains largely elusive.

Finding optimal solutions to repair articular cartilage will likely follow a number of multidisciplinary steps which are highly interrelated in nature. The significance of each of these steps are slowly and pragmatically becoming understood. The ultimate goal is the regeneration of normal articular cartilage, both compositionally and functionally, for a range of chondral and/or osteochondral lesions. This review addresses the three key combinatorial components of tissue engineering, namely, scaffolds and the interrelationship with cells and bioactive factors. Moreover, the current status of scaffold development and material selection and their subsequent impact with respect to tissue engineering of cartilage *in vitro* and *in vivo* are reported herein.

Design Criteria for Scaffold-based Repair Strategies:

Scaffold design should be highly site and function specific, and as a consequence, scaffold requirements are considerably different if successful cartilage repair is to be achieved within a load-bearing or non load-bearing environment. In most cases, scaffolds form a central role in any tissue engineering strategy (Fig 5).

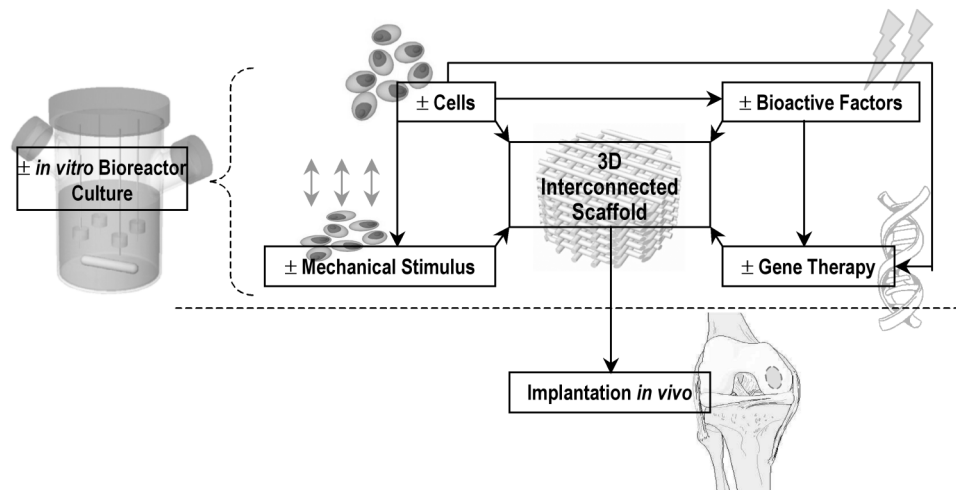


Figure 5 – Scaffolds are central to cartilage tissue engineering strategies. Appropriate design of biodegradable scaffold conduits allow for the delivery of reparative cells and/or chondrogenic factors to the defect site in an organised manner. Chondrocytes or progenitor cells can be introduced *in vitro* and further subjected to mechanical stimuli or genetic enhancement prior to implantation. Alternatively, the scaffold alone can be manipulated with bioactive or gene factors to recruit reparative cells *in vivo* and enhance neo-tissue formation.

Repair Strategies

Tissue engineering approaches for repairing articular cartilage generally adopt two strategies; scaffold with cells, or scaffolds alone. Simply put, scaffolds for cell-based strategies are intended to provide a compatible carrier for viable cells responsible for enhancing restoration of functional ECM and integration with surrounding tissue. In strategies employing scaffolds alone, the scaffold material and geometry are designed to organize and enhance neo-tissue formation from host mesenchymal cells infiltrating the defect. The ability to further stimulate repair quality of cell-seeded scaffolds *in vitro* is possible by manipulating the culture environment via mechanical and/or bioactive stimuli, with accurate control offered via advanced bioreactor culture systems. Alternatively, scaffolds pre-seeded with genetically modified cells, or scaffolds engineered to release bioactive or gene factors can be used to promote desired repair pathways or inhibit undesired processes.

Considering the unique biological environments pertaining to chondral and osteochondral defects serves to further highlight the sources of reparative cells and the form of scaffolds typically used to augment these repair strategies.

Cell types used in cell-scaffold constructs cultured *in vitro* for studying repair of both chondral and osteochondral defects have included committed chondrocytes or progenitor cells from various sources. Articular chondrocytes are a common choice as these cells are responsible for maintenance and synthesis of essential cartilage matrix molecules, type II collagen and GAG. Studies have shown the potential of using the zonal characteristics of cells within cartilage, such as chondrocytes obtained exclusively from deep zone articular cartilage [228, 502], or chondrons [261]. Highly promising alternative cell sources, which limit donor site morbidity associated with harvesting articular cartilage, include hyaline nasal septal cartilage [226, 416, 417, 483], and auricular cartilage [311]. As an alternative to harvesting cartilage to obtain a source of chondrogenic cells, the use of various progenitor, or mesenchymal stem cells (MSCs), have been studied extensively [74, 149, 224, 404, 497, 499]. The advantage of these MSCs is that certain sub-populations have the capacity to differentiate into cartilage or bone depending on local cues provided *in vitro* or *in vivo*, and are thus, instrumental in recapitulating the normal subchondral bone plate [498]. MSCs, isolated from bone marrow aspirates, can be seeded in scaffolds and implanted in chondral or osteochondral defects following prior chondrogenic stimulation *in vitro*, or alternatively, recruited *in vivo* from the underlying subchondral bone spaces in the case of osteochondral lesions. In chondral defects, where the underlying bone is not penetrated, cell recruitment is more difficult. However, it has been reported that synovial tissue contains progenitor cells capable of initiating repair in chondral lesions in the presence of growth factors [208], while other recent studies suggest progenitor cell populations also exist within superficial zone articular cartilage [482].

The type of defect (chondral and osteochondral) may also influence the form of scaffold used. Smaller chondral defects may be more amenable to the use of less invasive injectable materials containing cells and/or growth factors which solidify *in situ*. Conversely, osteochondral defects may require more invasive strategies by implanting pre-formed scaffolds which either support the delivery of *in vitro*-formed repair tissue, or stimulate repair via host MSC infiltration and differentiation *in vivo*.

Scaffold Design

In order to implement these various strategies, there are a number of generic scaffold design requirements which require prudent consideration. These requirements are illustrated in Table 2 and discussed further in no particular order of importance.

Scaffold biocompatibility is critical to the success of any cartilage repair strategy, and relates to the ability of a material to perform with an appropriate host response in a specific application [37]. Therefore, scaffolds designed specifically for cartilage repair should not invoke adverse inflammatory or immune responses in order to optimize contact with surrounding native tissue and ensure continuity and stability of the repair tissue from the onset. Numerous scaffold materials deemed biocompatible have been used for cartilage repair, examples of which are discussed later. When designing new scaffolds, it should be noted that a material considered biocompatible for one application does not guarantee that scaffolds developed from the same material will be biocompatible in a cartilage repair setting [4]. Moreover, biocompatibility issues such as surface chemistry, structure and morphologic features of the scaffold, as well as processing and sterilization should also be considered [288].

Table 2 – Generic scaffold design requirements related to the repair of chondral and osteochondral articular cartilage defects.

Scaffold Requirements:	Biological and material basis:
Biocompatibility	To prevent adverse inflammatory or immune responses.
Cell attachment	To optimize cell seeding for delivery and retention of cells and promote maintenance of chondrogenic phenotype.
Porous 3D environment	Support cell migration, proliferation and ECM production. High surface area to volume ratio optimal.
Interconnected / permeable	Maximize nutrient/waste exchange and limit oxygen gradients.
Biodegradation	Preferably in harmony with desired repair or regeneration process, whereby, by-products are metabolized or excreted from the body without eliciting an inflammatory response.
Bioactivity / gene delivery	Act as a cell carrier or control the release of growth factors, transfection vectors and/or genetically modified cells.
Mechanical integrity and integration	Sufficient to support or match surrounding native tissue at site of implantation, as well as mediate mechanical stimulus to cells during loading.
Structural anisotropy	Promote native anisotropic tissue structure.
Size and Shape	Reproducibly create scaffold of clinically relevant size and shape.
Surgical application	Preferably allow minimally invasive techniques using injectable/flexible scaffold strategies which can be reshaped/resized by surgeon to fit the specific defect. Press-fit solutions require mechanical integrity.

For successful tissue genesis, the scaffold should facilitate cell attachment to promote efficient seeding, or infiltration of cells and also assist in retention, proliferation and organization of reparative cells within the defect. However, conditions that favour rapid increases in cell number (*i.e.* serially passaged monolayer cultures), typically fail to produce hyaline cartilage matrix without additional chondrogenic stimuli, as a result of cell dedifferentiation to a more fibroblastic lineage. Scaffolds should also be designed to promote a differentiated cell phenotype for synthesis of functional cartilage ECM

components such as type II collagen and GAG. For example, studies have shown that chondrocyte proliferation, differentiation and ECM production can be affected by changes of surface chemistry [215, 375, 518] and roughness [48] as well as by providing a three-dimensional (3D) surface geometry [133]. In addition, modulation of cell adhesion via bioactive surface modification techniques can offer significant advantages. Other than indirect recognition of potent, serum-borne cell attachment proteins such as fibronectin, fibrinogen and vitronectin adsorbed to typical scaffold surfaces, cell responses can be activated by incorporation of adhesion promoting oligopeptides [198, 259]. In native cartilage, attachment of chondrocytes to the surrounding ECM is mediated by cell-surface receptors, such as the integrin family [463]. These integrins have been shown to bind to short amino acid sequences, such as Arg-Gly-Asp (RGD) sequences, present in types II and VI collagen within in the ECM. A number of studies incorporating specific peptide sequences into two-dimensional biomaterial surfaces showing improved adhesion with particular cell types have been reported [108, 177, 418], and are now becoming a focus for chondrocyte attachment within 3D scaffolds. In a recent study, RGD peptides were covalently bonded to alginate hydrogels and shown to facilitate integrin-mediated attachment of chondrocytes. The rate and magnitude of cell attachment increased with substrate stiffness, suggesting that chondrocytes can sense substrate mechanics via integrins [136]. It should be noted that, while integrin receptor ligands are the best studied, other chondrocyte receptors such as CD44, a PG receptor which mediates binding to hyaluronan, are also of considerable interest for cartilage adhesion [216]. Surface modification technologies promoting specific cell adhesion may become crucial as researchers move towards using culture conditions which are both serum-free and human- or animal-derived protein deficient, due to the associated health risks and regulatory hurdles for tissue engineered implants. For example, fibroblasts seeded in serum-free medium on PEG diacrylate hydrogels were able to promote spreading only when RGD peptides were incorporated and not in inactive controls [177].

In addition to cell adhesive properties, scaffolds should provide a sufficiently macro-porous, 3D space to further permit cell migration, proliferation and importantly, synthesis of ECM components. Whilst very high scaffold porosity can result in high surface area to volume ratios, it is detrimental to scaffold stiffness and mechanical integrity, and tradeoffs are necessary. Therefore, pore interconnectivity is a pertinent consideration. For example, a fully interconnected scaffold, even if not highly porous, will likely assist in efficient transfer of nutrients and waste products to, and from, cells throughout the scaffold, or, in the case of repair of osteochondral defects, also provide pathways for vascular invasion and concomitant bone formation. For similar reasons, in micro-porous scaffolds such as hydrogels, high material permeability is also necessary for diffusion of nutrients and waste to and from cells embedded within them.

The use of biodegradable scaffolds allows these carriers to perform important temporary functions within the body, however, degradation by-products should be easily metabolized or excreted without compromising biocompatibility or eliciting an inflammatory response. Scaffold degradation rate can be influenced by a number of factors, such as, material composition, scaffold size and morphology, and mechanical loading, to name a few [288]. Degradation rate can have a significant effect on overall mechanical stability of the scaffold due to surface erosion or bulk degradation, and thus, can influence the timing of repair processes [209]. For example, to allow time for synthesis of functional repair tissue capable of

load bearing *in vivo*, scaffold degradation rate and resorption should preferably be concomitant with that of the newly synthesized tissue, and be in the order of days to months. Alternatively, scaffolds whose mechanical properties are comparable to those of the native cartilage, could support earlier implantation of a more immature or neocartilage-like repair tissue, resulting in improved integration and reduced *in vitro* culture time. Here, the scaffold protects the neocartilage from *in vivo* loads, and finally degrades when functional tissue has developed. Furthermore, biomaterials which degrade in response to local cellular information may offer more attractive solutions [198]. For example, Park *et al.* [377] recently reported on the development of a synthetic matrix-metalloproteinase (MMP) sensitive poly-(ethylene glycol) (PEG) based hydrogel for cartilage repair. A MMP-sensitive peptide was used as a cross-linker for gelation of chondrocyte embedded constructs, whereby chondrocyte protease activity was able to locally degrade the hydrogels, thereby allowing scaffold remodelling by cells directly. Such approaches allow the bio-responsive nature of the scaffold to adopt resorption rates which match the matrix deposition rate of cells.

The use of scaffolds for controlled release of bioactive factors or gene therapy are receiving considerable attention (see section 4). Simply put, these strategies allow the delivery of various growth factors which have been shown to stimulate differentiation or maintenance of chondrogenic phenotype and/or modulate cartilage matrix synthesis [49, 221, 317]. Examples of such growth factors include insulin-like growth factor-1 (IGF-1), transforming growth factor beta-1 (TGF- β 1), and platelet-derived growth factor (PDGF).

Mechanical stability of the scaffold carrying cells, genes, or growth factors once deposited within the defect is a key requirement. If the mechanical integrity is compromised, or significant volumetric changes occur, then the scaffold could be in jeopardy of deviating above or below the articulating surface, or even working loose from chondral or osteochondral compartments. As a result, it is becoming more commonly accepted that the mechanical properties of the scaffold should preferably match those of the surrounding tissue [157, 210, 288]. Perhaps, more importantly, such steps may help reduce shear stresses generated by having vastly different properties at the interface between native and repair tissue during loading [5], thus assisting with tissue integration, one of the major topics of concern currently in articular cartilage repair [364]. Sufficient mechanical stiffness will also prevent, or reduce, excessive loading at the border of the defect as modelled by Aeschlimann *et al.*, [3], thus preventing accelerated damage to adjacent native tissue. Yet few materials themselves [445], or *in vitro* cultured cell-scaffold constructs currently evaluated, approach the mechanical stiffness of natural human articular cartilage at the point of implantation. For example, Ma *et al.* [294] showed that cartilage constructs cultured for 7 months in a bioreactor reached 40% of the mechanical properties of natural cartilage, resulting in aggregate compressive modulus of approximately 0.18 MPa. Human articular femoral cartilage, when tested under uniaxial confined compression, yields an aggregate (equilibrium) modulus of 0.6 MPa, and a dynamic stiffness of 4.5 MPa at 0.1 Hz [475]. Under impact loading, cartilage has been known to withstand stresses up to 20 MPa [250], although the onset of chondrocyte apoptosis has been suggested at stresses as low as 6 MPa [98]. The dynamic, rather than static, properties of articular cartilage may provide a more sensitive benchmark with which to emulate into future scaffold designs. For a more detailed review of biomechanical issues related to design of scaffolds for functional cartilage tissue engineering, see Butler *et al.*, [72] and Mow *et al.*, [346].

In general, cell-seeded scaffolds used for tissue engineering-based procedures involve the introduction of a uniform population of cells into the defect in order to repair articular cartilage which is, intrinsically, highly organised in structure. Consequently, advanced scaffold design should also address the anisotropic nature of articular cartilage with respect to cell/GAG distribution and collagen orientation for example. Figure 1 shows the distinct cartilage zones and the respective average cell densities per cubic mm determined from normal human adult femoral condyles, as recently reported by Hunziker *et al.*, [207]. Higher cell densities reside in the superficial zone compared with middle and deep zones, and therefore, the cells control vastly different ECM volume domains with depth. Some studies are beginning to emerge where scaffold geometry and/or seeding methods have assisted in tailoring an anisotropic cell distribution [474], and tissue exhibiting specific superficial zone proteins [239]. By imitating the zonal organization within native tissue, the hope is that the local cell environment will also stimulate synthesis of an organised collagen structure. Furthermore, scaffolds design may incorporate mechanisms for integrating the repair tissue with subchondral bone. Recent studies have sought to address some of these issues by the development of biphasic cartilage-bone scaffold compartments, or introducing cell excluding barriers to prevent the ingress of blood borne mesenchymal cells from the underlying bone into the cartilage repair space [206, 211].

Clinically, the average defect size diagnosed within femoral articular cartilage is approximately 5 cm² [10], which corresponds to a 2.5 cm diameter circular defect. Human articular cartilage thickness has been shown to range between 0.5-7.1 mm at various locations within the knee [237], and therefore, depending on the type of repair strategy (either chondral or osteochondral), overall scaffold thickness could then range between 0.5-25 mm. In comparison, scaffolds used for *in vitro* studies [495] and also *in vivo* animal studies [204] are typically 3-10 mm in diameter and 1-5 mm thick. Tissue-engineered scaffolds optimized at these reduced dimensions will likely behave very differently when applied at clinically relevant sizes, and yet, very little research is focused in this area. Limiting factors such as oxygen and nutrient gradients, pore volume and interconnectivity, mechanical properties and effects of cell seeding density will all be significant in the clinical setting, and will not be solved by simple scaling-up of dimensions. Future design of scaffolds and *in vitro* studies should take into account these size issues. Taking an initial step in this direction, Bryant *et al.*, [58] showed that chondrocytes encapsulated and statically cultured in permeable 8 mm thick photopolymerizable poly(ethylene oxide) hydrogels produced cartilagenous tissue both histologically and biochemically comparable to a 2 mm thick gel, however, the diameter of the gels was only 9 mm. Additional concerns are that, often, the exact defect size and shape is unknown until during surgery, and for large defects, the curvature of the joint surface can also be considerable. Flexible or pre-shaped scaffolds which can be press-fitted into the defect may be desirable, although, minimally invasive, arthroscopic approaches to deliver injectable cartilage repair components are receiving considerable attention.

Novel Scaffold Processing Techniques

Scaffold processing techniques used to date have focused on the development of porous materials via fibre bonding, solvent casting, particulate leaching, membrane lamination, melt moulding, temperature-induced phase separation, and gas foaming [210, 286]. A wide range of scaffold characteristics, such as porosity and pore size, have been reported with such fabrication techniques, however, the control of these scaffold characteristics are highly process, and not design driven.

Investigators have recently turned to rapid prototyping (RP) techniques for producing porous 3D scaffolds for tissue engineering applications [211, 460, 534]. RP is a subset of mechanical processing techniques which allow highly complex, but reproducible structures, to be constructed one layer at a time via computer-aided design models and computer-controlled tooling processes. These techniques essentially allow researchers to design-in desired properties, such as porosity, interconnectivity and pore size, in a number of polymer and ceramic materials. RP methodologies studied to date have included stereolithography, selective laser sintering, ballistic particle manufacturing, and 3D printing [210]. However, the transfer of RP technologies to encompass biocompatible and bioresorbable materials still poses a significant challenge, particularly in developing scaffolds for cartilage tissue engineering applications.

Recently we reported on the fabrication of biodegradable co-polymer scaffolds using a custom designed 3D deposition technique [519]. By controlling fibre deposition geometries, scaffolds with a 100% interconnected pore network have been produced (Fig 6) whose mechanical properties are similar to those of natural articular cartilage. Hutmacher *et al.*, [211] reported the development of various fibrous scaffold designs as well as anisotropic structures containing cell excluding barriers for bone and cartilage tissue engineering applications via fused deposition modelling of polycaprolactone. Landers *et al.*, [255] have reported a 3D plotting system able to accurately dispense hydrogel fibres containing viable cells, thereby allowing fabrication of various interconnected scaffold designs pre-embedded with cells. Such systems could, theoretically, be used to build complex 3D geometries with specifically placed or oriented cells. Alternatively, RP techniques used to create joint-specific moulds are also being investigated to generate entire articulating surfaces from cell-laden agarose gels [323]. While it remains unclear whether scaffolds maintain their joint-specific shape during culture, these approaches aim to solve current problems with tissue integration by resurfacing the whole joint.

Further development of RP technologies offer promising avenues to generate scaffolds which meet a large number of the scaffold requirements explained in Table 2.

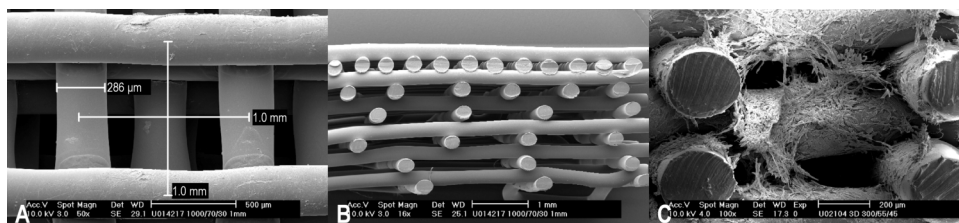


Figure 6 – Scanning electron micrographs of 3D, interconnected PEGT/PBT scaffolds created by successively depositing fibrous layers of molten polymer in a computer controlled 0° - 90° pattern. (a) Top view of scaffold containing a staggered fibre spacing between layers (typical fibre and pore size dimensions labelled); (b) cross-section of anisotropic scaffold containing depth dependant pore-size gradients; (c) cross-section of scaffold with homogeneous fibre spacing showing attachment of expanded human articular chondrocytes throughout exposed surfaces following 3 days dynamic seeding *in vitro*.

Scaffold Materials:

The various biocompatible scaffold materials investigated to date for cartilage repair fall under two categories: either natural or synthetic materials. This review will not discuss all of these materials (for more extensive coverage see [4, 209, 210, 288]), but rather focus on those materials recently reported as having promising chondrogenic and bioactive characteristics for cartilage tissue engineering.

Natural Materials

Natural hydrogel materials evaluated as vehicles for cell delivery, and as temporary scaffolds for the development of cartilaginous tissues have included alginate [73, 171, 486], collagen [486, 497] and agarose [407]. Advantages of such formulations allow an even, 3D distribution of cells to be implanted *in vivo* [379] or injected. Given that the natural scaffold into which cells migrate during spontaneous repair is the fibrin clot, it is not surprising that injectable fibrin based gels or glues have been investigated for cartilage repair [188, 485]. However, *in vivo* studies have shown cell migration and tissue repair using such materials appears to be limited [53]. Alternatively, Chenite *et al.*, [87] reported using thermally sensitive neutral solutions based on chitosan/glycerol-phosphate salt combinations to provide injectable cells as well as bioactive factors. These formulations possess a physiological pH which remain fluid below room temperature during cell and protein encapsulation, but form monolithic gels at body temperature. Therefore, when injected *in vivo*, the liquid formulations turn into gel implants *in situ*. This system was used successfully to deliver biologically active growth factors *in vivo* as well as an encapsulating matrix for living chondrocytes.

Due to the limited mechanical stability of the above materials, the use of insoluble biodegradable materials have also been investigated. Examples include demineralised bone [106, 336], hydroxyapatite composites [484], hyaluronate [57] and collagen. Collagen matrices have been found to contain molecular cues capable of stimulating new collagen production by transplanted cells as compared with other scaffold types [147]. Lyophilized collagen-based scaffolds in particular revealed promising results in this respect due to their

biocompatibility, biodegradability, and appropriate mechanical integrity [132, 231, 355, 390, 487]. Moreover, the use of collagen crosslinking techniques offers the opportunity to modulate the handling properties of collagen, as well as its ability to resorb [390, 487].

Incorporation of chondroitin sulphate to type I collagen scaffolds demonstrated favourable effects with respect to chondrocyte proliferation and GAG retention [487]. Increased proliferation and GAG synthesis has been reported in type II compared to type I collagen gels [398], while increased DNA and GAG contents were also observed after culturing cells in type II collagen-GAG scaffolds compared to type I collagen-GAG scaffolds [347, 354, 355]. However, when collagen type I and II scaffolds, laden with chondrocytes, were implanted in canine chondral defects, reparative tissue formation was enhanced, but it was predominantly fibrocartilagenous in nature. Using different natural materials, but still acknowledging the supportive influence of tissue-specific matrix molecules on the chondrocytic phenotype, Sechriest *et al.*, [434] combined chondroitin sulphate and chitosan, a glycosaminoglycan analogue, which supported stimulation of collagen type II and proteoglycan production, but limited mitosis *in vitro*.

Other natural polymers such as hyaluronic acid (HYA) based carriers have shown promise as scaffold materials [7, 248, 450]. HYA is a hydrophilic proteoglycan matrix component and its interaction with chondrocytes is important for the assembly and maintenance of the cartilage matrix. Studies in osteochondral defects in rabbits using non-woven meshes based on HYA (modified by esterification of the carboxyl groups of the glucuronic acid) and seeded with autologous chondrocytes, resulted in hyaline-like tissue after 6 months implantation [154]. These same scaffolds have also been shown to support *in vitro* growth of human chondrocytes which maintain their original phenotype, evidenced by production of collagen type-II and aggrecan and down-regulation of collagen type-I [153]. Using porous sponges of the same material, other groups showed either greater attachment of rabbit mesenchymal progenitor cells, or more cartilage per unit area, compared with a 3-D calcium phosphate ceramic delivery vehicle without HYA [450]. Recent studies have shown, however, that scaffold HYA content has a significant effect on cartilage formation *in vitro*, whereby small amounts of HYA (2% w/w) in 3-D collagen scaffolds enhanced type-II and aggrecan mRNA, whilst greater amounts (10%w/w) were inhibitory [8].

Although the use of naturally derived polymers have achieved some promising results, concerns regarding batch variations and the potential for pathogen transfer has prompted the development of scaffolds based on synthetic polymers.

Synthetic Materials:

Advantages of biocompatible and biodegradable synthetic polymers, such as their ability to be mass produced as well as tailored to specific applications, has seen their extensive use as scaffold materials for cartilage repair, and have recently been reviewed [131, 209, 288, 471].

Since their first use in the early 1990's, poly(α -hydroxy esters) such as poly(glycolic acid) (PGA), poly(lactic acid) (PLA), and poly(lactide-co-glycolide) (PLGA) co-polymers constitute by far the greatest proportion of studies with respect to cartilage tissue engineering reported in literature [79, 90, 91, 145, 215, 408], particularly non-woven fibrous PGA variations [73, 124, 125, 131, 147, 295, 317, 380, 396, 416, 444, 454]. These polymers are degraded by hydrolysis, with the more hydrophobic, but less crystalline, PLA polymers degrading slower than their

highly crystalline, hydrophilic PGA counterparts. Compared to the homopolymers, amorphous PLGA co-polymers can be tailored to resorb at varying rates by modifying copolymer ratio. As a scaffold for *in vitro* cartilage regeneration, PGA was stated to provide more favourable results in terms of cell density and collagen type II production as compared with fibrin, collagen, PLA and PLGA scaffolds [287]. In *in vivo* studies, Freed *et al.*, [124] implanted non-woven PGA meshes, seeded with or without chondrocytes, into osteochondral defects in adult rabbits. Six month repair was qualitatively better for cell-PGA allografts than for PGA alone, with respect to surface smoothness, columnar alignment of chondrocytes, spatially uniform GAG distribution, reconstitution of the subchondral plate, and bonding of the repair tissue to the underlying bone. PLA scaffolds have been shown to support chondrogenesis *in vivo*, but at a reduced level to that of PGA [125]. PLGA scaffolds, reinforced with PGA fibres to obtain suitable mechanical properties [445], and seeded with autologous chondrocytes, resulted in hyaline-like cartilage and regeneration of underlying bone after 16 weeks implantation in osteochondral defects in goats [360].

At present, we are evaluating a series of amphiphilic, biodegradable poly(ether ester) multiblock copolymers as carrier materials for articular cartilage repair. The copolymers are based on hydrophilic poly(ethylene glycol)-terephthalate (PEGT) and hydrophobic poly(butylene terephthalate) (PBT) blocks. A major advantage of these types of copolymer systems is that by varying the amount and the length of the two building blocks, an entire family of polymers can be obtained. This offers extensive possibilities in the design of systems with tailor-made properties, such as swelling, degradability, mechanical strength and release rate. Various *in vitro* and *in vivo* studies have demonstrated both the biocompatibility and biodegradable nature of PEGT/PBT copolymers [28, 111, 402, 480]. Degradation occurs via both hydrolysis (cleavage of ester bond linking ester and hydrophilic ether segments) and oxidation (PEG chain scission via free-radical reactions), and in both cases, degradation is more rapid for copolymers with high PEG content [111]. The attachment, proliferation, morphology, and differentiation state of chondrocytes has also been demonstrated on different compositions of 2D PEGT/PBT films [375], and also in porous 3D scaffolds of varying pore size, and pore morphology [518]. Using a range of processing techniques, the mechanical properties, such as dynamic compressive stiffness of these scaffolds have been shown to be in the range of those determined for native human articular cartilage [519]. Controlled release of bioactive factors from these materials has also been demonstrated (see section 4).

Polymeric hydrogels are useful for embedding cells but typically, their limited mechanical stability has meant that their use in articular cartilage repair has been limited. However, recent studies have demonstrated that semi-interpenetrating network (IPN) hydrogels, in certain formulations, can have compressive properties comparable to those of adult bovine cartilage tissue [144]. Furthermore, the use of polymeric materials for the development of injectable cartilage repair solutions are becoming more predominant. Particularly attractive approaches are those which are able to polymerize or gel during implantation. A recent preliminary study by Healy *et al.* [175] reported the synthesis of a thermo-responsive hydrogel, poly(N-isopropylacrylamide) [P(NIPAAm)] which is water-soluble at room temperature, but phase separates at approximately 32°C, thus imparting both injectability and *in situ* stabilization. P(NIPAAm-co-AAc) gels seeded with bovine chondrocytes were shown to promote tissue with a cartilage-like appearance and sulphated GAG expression following 28

day culture. Transdermal photopolymerization has also been used to subcutaneously place a mixture of polymer and isolated chondrocytes to regenerate cartilage tissue *in vivo* [121]. In this study, semi-IPN gels containing primary bovine articular chondrocytes and varying proportions of poly(ethylene oxide)-dimethacrylate and poly(ethylene oxide) (PEO) were implanted in athymic mice. Chondrocytes survived implantation and photopolymerization and at 7 weeks, histologic analysis exhibited a tissue structure resembling neocartilage, with positive GAG distribution throughout the hydrogels. Polymers that can be chemically crosslinked *in situ*, rather than polymerized, eliminate the need for light during surgery. In this regard, biodegradable materials based on poly(propylene fumarate) (PPF) have been recently developed as possible injectable materials for orthopaedic applications [174, 288]. In addition, oligo(poly(ethylene glycol) fumarate) (OPF) hydrogel variants have been modified with RGD peptides [222] or formed in multiple layers, each with distinct mechanical properties [470]. While biocompatibility has been demonstrated *in vivo* [386], studies involving cell-laden PPF or OPF materials for cartilage repair have not been reported.

Biphasic Scaffolds

To better control cell location and implant fixation, biphasic scaffolds have also recently been developed for the treatments of osteochondral defects allowing fixation of the new construct within the bony compartment at surgery. In this case, providing optimal materials and/or cells for both subchondral bone and cartilage regeneration may allow rapid remodelling of the growth plate and assist with integration of new cartilage tissue. For strategies involving *in vitro* tissue formation prior to implantation, biphasic scaffold design could incorporate cell exclusion measures which prevent migration of bone-marrow-derived mesenchymal cells into cartilage regions.

Examples of biphasic scaffold designs studied *in vitro* include the use of a natural coralline or calcite material attached via fibrin-cell-solution to a 3D 90:10 PGA:PLLA fleece for the cultivation of bovine chondrocytes. During *in vitro* perfusion culture, new cartilage-like matrix formed and fused with the underlying biomaterial [244]. Other approaches have combined composites based on chondrocyte-seeded PGA non-woven meshes anchored to periosteal-cell-seeded PLGA/PEG porous foams [426]. The two phases, initially cultured separately, were combined after 1 or 4 weeks *in vitro* culture with improved integration between the more immature 1-week constructs.

Composites of cell laden fibrin glue and porous hydroxyapatite have been evaluated *in vivo* in goats, but construct instability resulted in a poor repair response [484]. Alternatively, MSCs exposed to TGF- β 1 were loaded into a sponge composed of a HYA derivative for the construction of the cartilage component, while MSCs exposed to osteogenic supplements were loaded into a porous calcium phosphate ceramic component for bone formation. The two phases were joined together with fibrin glue, and after 6 week subcutaneous implantation in rats, bone was detected in the ceramic component, however, fibrocartilage was observed in the HYA sponge [134]. More promising results were obtained in a short term study by Niederauer *et al.*, [360] whereby, biphasic combinations of PLGA or fibre-reinforced PLGA in addition to bioglass or calcium sulphate materials were implanted in goats with or without cells. Scaffold stiffness of the relative phases was also matched to those on natural bone and articular cartilage. In all combinations investigated, a hyaline-like cartilage repair

was seen with good remodelling of subchondral bone at 16 weeks, with the authors suggesting that scaffold stiffness may be an important variable.

An interesting approach adopted by Kandel and co-workers has been to *in vitro*-form cartilage layers anchored to filter materials [228, 462, 531]. Here isolation and plating of deep-zone chondrocytes resulted in 0.3 mm thick cartilage layers on top of the underlying substrate after 10 weeks static culture. Biphasic cartilage constructs are thus formed *in vitro*, with additional medium supplements (β -glycerophosphate) shown to instigate formation of a calcified cartilage layer characteristic at the tidemark region in normal tissue.

Co-workers have demonstrated the osteoinductive potential of calcium phosphate-based materials with particular geometries [532]. Osteochondral repair constructs composed in part with such materials, loaded with or without cells, may be beneficial in biphasic scaffold design. In addition, it has also been reported that other materials such as demineralised bone matrix can induce chondrocyte differentiation in human dermal fibroblasts [336, 528], while *in vivo* studies suggest certain geometries of BMP-loaded hydroxyapatite particles can induce chondrogenesis and osteogenesis [246].

Some studies have even provided evidence that whole joints may be able to be formed via scaffold and tissue engineering approaches. One study addressed the formation of small phalanges from three types of bovine-cell sources (periosteum, chondrocytes and tenocytes) transplanted onto biodegradable polymer matrices [217]. Whilst the resulting structures had the shape and composition of human phalanges when cultured ectopically, samples were never functionally evaluated in a loaded environment *in vivo*.

Controlled Release of Bioactive Factors:

A critical issue in tissue engineering is local and well-timed delivery of the various cell-signalling molecules that are crucial in tissue development. For cartilage, it has been reported that growth and maturation is supported by growth/differentiation factors including insulin-like growth factor-1 (IGF-1), transforming growth factor beta-1 (TGF- β 1), fibroblast growth factor-2 (FGF-2) [312, 317] and bone morphogenetic proteins (BMP-2 and BMP-3) [181]. Biomaterial scaffolds offer significant opportunities for controlled local delivery of such agents.

Various approaches to combine growth factors and scaffolds have been investigated [264, 423, 464, 511]. Absorption of growth factors into natural polymers e.g. collagen [465], gelatin [525] or synthetic polymers e.g. polylactides and copolymers thereof [335], allows local delivery, but the opportunity to control release is often minimal [464]. Incorporation of proteins into polymers offers a tool to obtain well-controlled release of proteins over prolonged periods [329]. However, the methods used to prepare polymeric scaffolds are often not suitable for incorporation of labile proteins, due to the high temperatures used [277, 328], exposure to organic solvents [277], or the need for removal of the porogens [329].

Recently, Whang *et al.*, [510] developed an emulsion freeze-drying process to overcome some of these drawbacks. The method consists of creating an emulsion from a PLGA solution in methylene chloride and an aqueous protein solution. Subsequently, the emulsion is quenched in liquid nitrogen, and methylene chloride and water are removed by freeze-drying [509]. The large pores in the resulting matrices are formed by the dispersed water phase and since the proteins are also dissolved in the water phase, this implies that the

proteins are located within the large interconnected pores. This may limit the possibilities to obtain slow release of proteins. Furthermore, it appeared that the type of protein influenced the ultimate structure of the pores. In case of bovine serum albumin (BSA) loaded scaffolds, the median pore size was 65 μm , while incorporation of rhBMP-2 resulted in a median pore size of only 9 μm , which is probably too small for optimal tissue in-growth [510].

To eliminate the use of organic solvents and heat, proteins have been incorporated by a gas foaming/salt leaching process [440]. Protein, polymer and salt particles were mixed and compressed into a disk and foamed in a high-pressure vessel using CO_2 . Following foaming, salt was removed by immersion in distilled water. Active growth factor could be released from such scaffolds for periods over one month. However, the entrapment efficiency was poor, and a considerable amount of the growth factor was lost during the salt leaching step. Other researchers have entrapped growth factors into biodegradable microspheres, which were mixed with a cell-suspension and subsequently seeded onto porous sponges to provide local controlled release [45]. Implantation of such constructs in a dynamic environment may result in moving of the particles from the site of implantation.

Most of the research on protein release from biodegradable polymers has been focused on PLGA copolymers, because of their good biocompatibility, non-toxicity and (tunable) biodegradation characteristics [101]. A major disadvantage of using hydrophobic polymers like PLGA for protein delivery systems is the instability of proteins in the polymer matrix [102, 289, 476, 481]. During storage and release, moisture and interactions with the hydrophobic polymer surface may induce aggregation [102]. In addition, polymer matrix degradation may generate a pH drop within the PLGA matrices, which may also cause protein degradation [289, 297]. Furthermore, the release characteristics of PLGA systems are difficult to control, often resulting in a burst release, instead of the generally desired constant release. To overcome these drawbacks, biodegradable hydrogel-based release systems are attracting increasing attention [22]. Among them, hydrophilic/hydrophobic block copolymers are of particular interest .

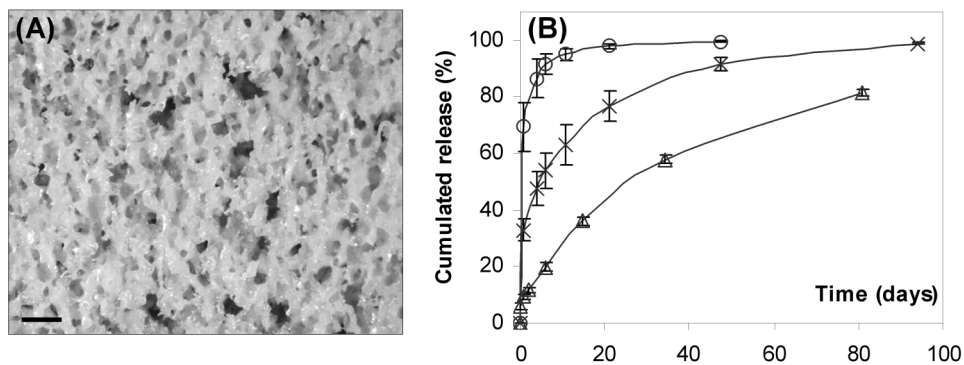


Figure 7 – (a) Light micrograph of lysozyme incorporated PEGT/PBT scaffold, and (b) corresponding lysozyme release from coated scaffolds. Coatings were prepared from emulsions varying in ratio of aqueous protein solution to polymer (O : w/p = 2, x : w/p = 1, Δ : w/p = 0.5; scale bar = 1 mm).

Recently, we evaluated the same series of amphiphilic, biodegradable PEGT/PBT multiblock copolymers introduced previously, also as a matrix for controlled release systems [33]. *In vitro* and *in vivo* experiments showed that a continuous release of a variety of proteins and peptides could be obtained, over long periods, with preservation of the protein activity. To combine macroporous PEGT/PBT scaffolds with proteins, a new approach was developed which involved coating the scaffold pores with a protein-loaded polymeric film. Scaffolds were produced using a compression moulding/salt leaching method, resulting in scaffolds with interconnected pores of approximately 500 μ m diameter (porosity: 78 % v/v). Coated scaffolds were prepared using an emulsion method, whereby an emulsion of a polymer solution and an aqueous protein solution was forced through the scaffold by applying a vacuum. To modulate release rates, the ratio of aqueous protein solution to polymer (w/p, in ml/g) was varied (0.5, 1 and 2 ml/g). Figure 7 plots the release of a model protein, lysozyme, against time for three different w/p ratios. By decreasing the w/p ratios, the release rates could be tailored from 6 days to over three months. No decrease in protein activity was found during the release, indicating that lysozyme was not damaged during the coating process and release period.

The current work on protein delivery from scaffolds is mainly focused on release of single proteins. Tissue formation, however, is a dynamic process, involving a large number of hormones, growth and differentiation factors, acting at different stages in tissue development. An ideal delivery system would allow release of a number of factors, with distinct release kinetics. A first attempt towards such an approach was recently reported by Richardson *et al.* [413] in the context of therapeutic angiogenesis. Scaffolds, containing both vascular endothelial growth factor (VEGF) and platelet-derived growth factor (PDGF), were prepared by a gas foaming/salt leaching technique as described above. To obtain distinct release profiles for the two proteins, particulate polymer and one factor were mixed with microspheres containing a pre-encapsulated second one, before processing into scaffolds. Using an *in vivo* model of therapeutic angiogenesis, the authors claimed a more rapid formation of mature vascular network for the dual delivery system as compared to single factor delivery.

Gene Therapy:

The *ex vivo* transfer of cDNAs encoding certain growth factors such as IGF-1, BMP-2, BMP-7 and TGF- β 1 superfamily members to chondrocytes, periosteal cells, or bone-derived mesenchymal stem cells has received increasing recent attention as an alternative cartilage repair strategy [229, 320, 361]. *Ex vivo* gene therapy involves cell harvesting and expansion, followed by genetic modification with an appropriate vector using either adenoviral or retroviral methods [319, 529], or via recent, more favourable, non-viral techniques [140, 145]. *In vitro* data suggest that the chondrogenic potential of these cells is maintained [310, 361], and by transducing these cells with chondroinductive factors, both bioactive factors and target cells can be delivered directly to the defect site. Appropriate scaffold design and implementation will only but augment this approach by performing the crucial task of mediating the transfer of these genetically enhanced cells or transfection vectors and ensuring they remain within the defect [521]. This is a pertinent consideration given that

repeated local injections of growth modulating substances have not induced healing of partial thickness defects [208], and also suggests that if genetically modified cells are not suitably retained within the defect, similar inferior results can only but ensue. For example, Kang *et al.* (1997) reported a rapid decrease in transgene expression over a 4 week period due to infiltration of donor cells following implantation of a scaffold laden with genetically modified chondrocytes in osteochondral defects in rabbits. Recent direct *in vivo* gene transfer techniques may offer a more elegant approach to *ex vivo* methods currently evaluated which require costly prior surgical harvest and transfection of cells. Palmer *et al.* [374] implanted collagen-GAG scaffolds laden with adenoviral vectors into osteochondral defects in rabbits and reported the ability to directly transfect bone marrow derived cells infiltrating into the scaffold *in situ*.

In vivo studies adopting scaffolds and gene therapy approaches for cartilage repair are limited, and whether such techniques are able to functionally reconstruct the articular cartilage surface remain unclear. However, promising results have been reported recently where BMP-7 gene-enhanced periosteal-derived mesenchymal stem cells, grown in PGA non-woven fibre meshes, were implanted in osteochondral defects in rabbits [319]. After 12 weeks implantation, histological sections revealed near complete subchondral bone and hyaline-like cartilage regeneration, with good integration to surrounding native tissue, and positive immunostaining of predominantly type-II collagen. These results were not replicated in control samples where constructs containing non-genetically modified cells were implanted. Moreover, the authors noted that local environmental signals other than BMP-7 must also play a role given the observation that the transfected MSCs differentiated into distinct bone and cartilage zones, with BMP-7 likely regulating local populations of blood or synovium borne cells. We advocate that scaffold structure and degradation rates will also likely play a key role.

Such studies suggest that combinatorial tissue engineering approaches combining genetically modified cells and scaffolds hold significant promise. In future, transfection of multiple chondrogenative growth factor genes (e.g. IGF-1, BMP-2 and 7, TGF- β 1) and/or chondroprotective cartilage catabolic inhibitor genes (e.g. interleukin-1 receptor antagonist) may be possible, as demonstrated by Nixon *et al.*, [362].

Controlling the Mechanical Environment:

Mechanical cues are crucial for normal skeletal development, growth and maturation [212]. Under joint loading, the chondrocyte microenvironment is exposed to a number of static and/or dynamic stimuli including: hydrostatic and osmotic pressures; compressive, shear and tensile stresses and strains; fluid and ion flows; electrical potentials; and oxygen gradients [337, 346]. Furthermore, since cartilage is avascular, aneural and alymphatic, catabolic and anabolic changes in chondrocyte activity are believed to occur via transduction of mechanical signals into metabolic events and structural adaptations [477], which, ultimately, determine the biomechanical properties of the tissue. As a result, a significant body of work over the last decade has been dedicated to studying the effects of mechanical stimulation on chondrocytes and cartilage explants (see [56, 158, 176, 337, 477] for a more thorough coverage). In general, loading studies to date suggest that static compression suppresses

sulphated GAG synthesis, as opposed to dynamic compression, which inhibits cell division, and promotes sulphated GAG synthesis and overall cartilage production *in vitro*. Furthermore, chondrogenic stimulation is dependant on loading frequency and duration, with reduced stimulation or even inhibition at low frequencies (generally <0.03 Hz), whereas, loading at higher frequencies in the range of 0.1–1 Hz appears stimulatory in a dose dependant manner [120]. In addition to compression, intermediate levels of hydrostatic pressure (2.6-5 MPa) have been shown to increase PG synthesis [378] with intermittent pressures (10 MPa at 1 Hz) stimulating both collagen type II and aggrecan mRNA levels [447].

Results gleaned from such studies are now becoming the focus for *in vitro* conditioning of cell-seeded tissue-engineered scaffolds in order to enhance cartilage structure and composition prior to implantation. Careful scaffold design and selection is, therefore, a key consideration as it will be responsible for mediating the transfer of the desired *in vitro* and/or *in vivo* mechanical stimuli to the cells embedded within it. Scaffolds used for such loading studies have predominantly been performed on cells embedded in agarose [70, 120, 240, 260, 325, 414, 424] or alginate gels [405]. These gels allow a homogeneous 3D distribution of cells which are able to maintain their chondrocytic phenotype during culture. While these gels provide a useful research tool for studying cell deformation, signalling pathways and biosynthesis rates, loss of mechanical stability over time *in vitro* can occur, and therefore, are not likely candidates for subsequent implantation *in vivo*. In fact, most loading studies are performed over time periods of hours to days, rather than weeks, although a few long term loading studies in agarose have been reported [325]. Mechanically stiff scaffolds may be necessary to further determine the effects of long term loading and predict what affects physiological load bearing will have on cell seeded constructs *in vivo*. Combinations of mechanical stimuli are also currently under investigation. For example, when growth factors (TGF- β 1 and IGF-1) were coupled with dynamic loading of chondrocyte seeded agarose gels, a synergistic improvement in aggregate modulus was greater than the sum of the two stimuli applied on their own. Such studies suggest that appropriate administration of chemical and mechanical stimulators of matrix biosynthesis in the right combination can optimize the growth of tissue-engineered articular cartilage constructs [324]. Similar additive effects on chondrocyte proliferation and collagen synthesis have been shown in relation to combining reduced oxygen tension with various intermittent hydrostatic pressures [165].

Compared with static culture conditions, the positive response of chondrocytes to fluid induced shear stresses [446], as well as exposure to uniform mixing of nutrients within culture media [142, 363, 494] have spawned a range of bioreactor designs to both apply and monitor responses to varying mechanical stimuli, as well as control mass transfer conditions. Bioreactor systems reporting various levels of enhanced cell proliferation, GAG and total collagen accumulation, and corresponding increases in mechanical properties for *in vitro* culture of cell-seeded scaffolds have included spinner flasks, rotating-wall bioreactors and perfusion systems. The specific function and comparisons in cartilage tissue formed in such systems have been recently reviewed [118, 129, 337, 472, 494]. Bioreactors which combine mechanical stimuli through dynamic mechanical compression and medium mixing for cell-seeded constructs have also recently been reported [110].

By facilitating maintenance of nutrient levels for high-density cell cultures, bioreactor systems can be further adapted to essentially expand on pellet culture techniques. Here, cells concentrated in perfused culture chambers allow tissue formation to occur within the ECM

scaffold synthesized by the cell mass itself. Chondrocyte constructs, cultured for 3 weeks in such a scaffold-free bioreactor system, have shown promising repair potential following 24 weeks implantation in minipig knees with chondral, superficial osteochondral, and full-thickness articular defects [300].

In vivo Considerations:

The ultimate success of any cartilage repair strategy must be established in animal models prior to clinical application. Such studies serve to highlight some of the existing problems confounding scaffold-based tissue engineering strategies in articular cartilage, as well as reveal some inherent limitations of the animal models themselves.

Integration between host and repair tissue *in vivo* poses considerable problems, particularly with the surrounding cartilage chondral defects [49, 149]. It has been shown that *in vitro* culture time, or in other words, the developmental stage of the repair tissue, can have a significant effect on the integrative interaction between repair and native tissue [114, 364]. Obradovic *et al.*, showed that integration in immature (1 week-old) *in vitro* cultured constructs with articular cartilage explants was enhanced due to cell proliferation and progressive matrix remodelling at the tissue interface, as opposed to mature (8 week-old) constructs. Furthermore, enzyme treatment at the native defect border to partially remove proteoglycans, known to inhibit cell adhesion, improved integration in a synergistic manner, in accordance with studies by Hunziker *et al.*, [208] in chondral defects. Obradovic *et al.*, stated that while integration of immature tissue improved integration, the bulk mechanical properties of the tissue were low compared with mature constructs. This suggests that future scaffold designs which support rapid cartilage ECM synthesis and cell proliferation to enhance integration, but on the other hand, have sufficient mechanical stability to protect this newly-formed tissue from *in vivo* joint loads, could offer significant promise.

Other concerns regarding scaffold-based repair strategies is the lack of knowledge with respect to the location, retention and viability of reparative cells once implanted *in vivo*. The large variation in repair results and limited success of tissue-engineered scaffold constructs to date may be, in part, related to the loss of cell viability and/or the inability to retain a critical number of chondrogenic cells in the proper region of the defect with time. For example, Ostrander *et al.*, [373] seeded rabbit perichondrial cells in PLA constructs into osteochondral defects in rabbits. Repair tissue was harvested at various intervals from 0-28 days after implantation, and the number of donor cells determined by targeting a gender-specific "Y gene", and a control MMP-1 gene promoter. Average cell viability was found to be 87% or more, with donor cells present in repair tissue for 28 days after implantation. However, the number of donor cells declined from approximately 1 million at time zero to approximately 140,000 at day 28. This decline in donor cells was accompanied by a significant influx of host cells into the repair tissue. This is also significant for repair strategies that incorporate MSCs into osteochondral defects, as it cannot be excluded that enhanced tissue repair is derived from host cells recruited to the defect in response to the implant, rather than the repopulation of the tissue by the implanted MSCs. In this regard, Quintavalla *et al.*, [400] recently implanted fluorescently labelled MSC/gelatin constructs into osteochondral defects in goats. The cells retained the dye up to 1 month and were detected by histology and flow cytometry. At

intervals spanning 2 weeks post-implantation, gradual loss of implanted cells in the defect as well as fragments of gelatin sponge containing labelled MSCs in deep marrow spaces. Although longer assessment times are necessary, the authors suggested that by determining the fate of implanted cells in short-term *in vitro* models, scaffold designs could be more rapidly optimized with respect to cell retention needed for successful, long-term cartilage regeneration.

As illustrated in the above examples, numerous animal models have been used to assess scaffold-based repair strategies in load bearing joints, however, most common small and large animal studies are carried out using rabbit and goat models respectively. As outlined recently by Hunziker [204], limitations in anatomical scale between osteochondral components of these animals and humans are considerable, and relate to overall joint size, joint loading and thickness of and cell distribution within the cartilage layer itself. The catabolic joint environment present in advanced degenerative diseases as well as joint loading can also have significant consequences for scaffold-based repair with respect to the fate of implanted neo-tissue and scaffold degradation issues. These events are difficult to assess *in vivo* and should be emulated into *in vitro* models. These inexorable inconsistencies between animal models and the clinical setting make drawing definitive conclusions on various scaffold designs and repair strategies difficult. In addition, with the large variation in scaffold materials, cell types and culture conditions used, comparisons between *in vivo* studies are almost impossible. Standardized evaluation methods are necessary to not only compare different scaffold-based repair strategies, but also compare if such strategies are more favourable than traditional repair strategies, rather than just empty defects. Assessment criteria and histological grading scales such as that established by the International Cartilage Repair Society (ICRS) for example should become commonly adopted [368]. Lamentably, since long-term functional stability of repair tissue *in vivo* is critical, the length of time needed to assess new treatment options, even at the pre-clinical stage, limits rapid innovation and development of repair strategies.

Conclusions and Future Considerations:

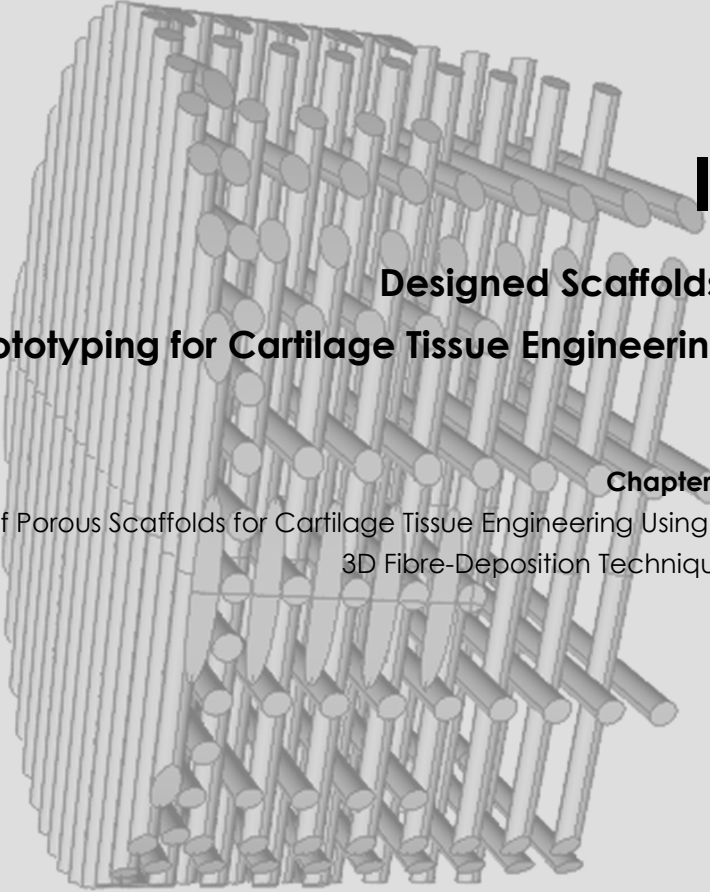
Early research in tissue-engineered constructs for cartilage repair stimulated the concept that placing chondrogenic cells within a scaffold would provide sufficient stimulus to repair damaged articular cartilage lesions. While such simple solutions may yet prove possible, evidence provided over the last ten years points to the contrary.

Combinatorial approaches may be necessary in order to advance current *in vitro* and *in vivo* strategies. Smarter biodegradable materials, designed with specific geometries or multiphasic compositions, need to be developed, not only to provide a 3D environment for cell attachment and guide ECM formation, but to release multiple bioactive factors at varying intervals, as well as transduce mechanical signals to metabolically active cells, whether by *in vitro* or *in vivo* means. The determination of which genes, or which combination of genes that might prove most useful for promoting chondrogenesis for repair of chondral and osteochondral lesions via gene therapy is necessary. Furthermore, the inexorable functional demands necessary in load bearing cartilage may require the repair tissue to closely resemble that of native tissue in terms of composition and architecture for long term success.

Many materials, scaffold designs, processing techniques and *in vitro* culture systems are amenable to scaffold-based tissue engineering approaches for articular cartilage repair. It seems unlikely that a single approach will meet all requirements necessary for repairing various cartilage lesions, whether they be chondral or osteochondral, in healthy or osteoarthritic cartilage, or in young or old patients alike. However, the number of patients worldwide, experiencing joint pain and loss of mobility through trauma or degenerative cartilage conditions are considerable. Therefore, the significance of an imperfect yet functional repair solution perhaps is more than timely.

Acknowledgements:

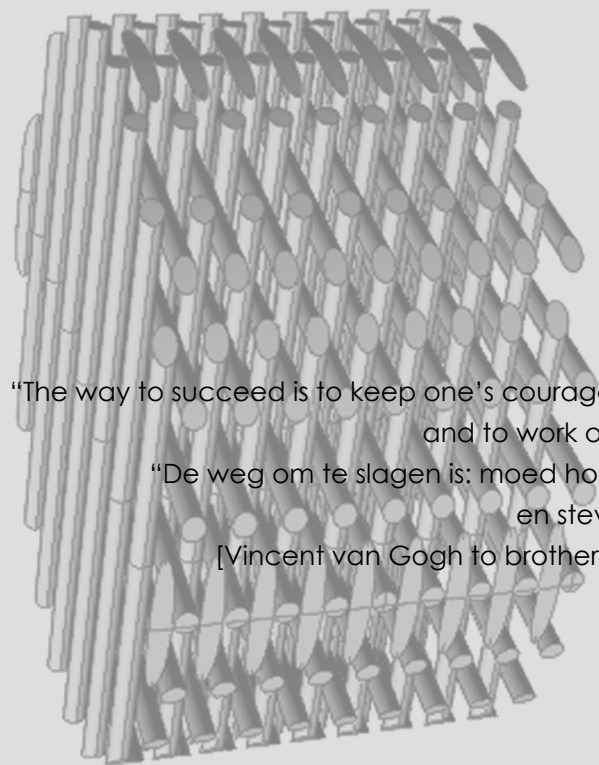
The authors would like to acknowledge the support from the European Commission (FP5 project "Scafcart" G5RD-CT-1999-00050). Discussions with Dr. I. Martin, Dr. G. van Osch and Dr. P. Hatton are gratefully acknowledged.



I.

Designed Scaffolds: Rapid Prototyping for Cartilage Tissue Engineering

Chapter 3
Design of Porous Scaffolds for Cartilage Tissue Engineering Using a
3D Fibre-Deposition Technique



“The way to succeed is to keep one's courage and patience,
and to work on energetically”
“De weg om te slagen is: moed houden en geduld
en stevig doorwerken”
[Vincent van Gogh to brother Theo, Feb 1886]

Chapter 3

Design of Porous Scaffolds for Cartilage Tissue Engineering Using a 3D Fibre-Deposition Technique

Woodfield T.B.F.^{‡1,2}, Malda J.^{1,2}, de Wijn J.², Péters F.², Riesle J.², van Blitterswijk C.A.^{1,2}

¹ Institute for Biomedical Technology, University of Twente, Enschede, The Netherlands

² IsoTis S.A., Bilthoven, The Netherlands

Abstract:

In this study we present and characterize a fibre deposition technique for producing three-dimensional poly(ethylene glycol)-terephthalate - poly(butylene terephthalate) (PEGT/PBT) block co-polymer scaffolds with a 100% interconnecting pore network for engineering of articular cartilage. The technique allowed us to “design-in” desired scaffold characteristics layer-by-layer by accurately controlling the deposition of molten co-polymer fibres from a pressure-driven syringe onto a computer controlled x-y-z table. By varying PEGT/PBT composition, porosity and pore geometry, 3D-deposited scaffolds were produced with a range of mechanical properties. The equilibrium modulus and dynamic stiffness ranged between 0.05 – 2.5 MPa and 0.16 – 4.33 MPa respectively, and were similar to native articular cartilage explants (0.27 MPa and 4.10 MPa respectively).

3D-deposited scaffolds seeded with bovine articular chondrocytes supported a homogeneous cell distribution and subsequent cartilage-like tissue formation following *in vitro* culture as well as subcutaneous implantation in nude mice. This was demonstrated by the presence of articular cartilage extra cellular matrix constituents (glycosaminoglycan and type II collagen) throughout the interconnected pore volume. Similar results were achieved with respect to the attachment of expanded human articular chondrocytes, resulting in a homogenous distribution of viable cells after 5 days dynamic seeding.

The processing methods and model scaffolds developed in this study provide a useful method to further investigate the effects of scaffold composition and pore architecture on articular cartilage tissue formation.

[‡] Woodfield TBF, Malda J, de Wijn J, Péters F, Riesle J, van Blitterswijk CA. Design of porous scaffolds for cartilage tissue engineering using a three-dimensional fibre-deposition technique. *Biomater* **2004**; **25**(18): 4149-4161.

Introduction:

The main function of articular cartilage is to provide a smooth, near frictionless articulating surface while mediating the transfer of load within the joint to the underlying subchondral bone [314]. When damaged, however, the regenerative capacity of articular cartilage remains limited in comparison with other musculoskeletal tissues such as bone and muscle [313]. Although numerous treatment protocols are currently employed clinically, few approaches, if any, exist which are capable of consistently restoring long term function to damaged articular cartilage [203, 205]. Tissue engineering approaches adopting scaffold conduits for delivery or recruitment of reparative cells in an organised manner to bridge voids within cartilage defects, offer considerable promise as repair strategies [149, 452].

Scaffolds designed for use in cell-based therapies to repair damaged articular cartilage should ideally provide the following characteristics: (i) a three-dimensional (3D) and highly porous structure to support cell attachment, proliferation and extra-cellular matrix (ECM) production; (ii) an interconnected/permeable pore network to promote nutrient and waste exchange; (iii) a biocompatible and bioresorbable substrate with controllable degradation rates; (iv) a suitable surface chemistry for cell attachment, proliferation, and differentiation; (v) mechanical properties to support, or match, those of the tissues at the site of implantation; (vi) an architecture which promotes formation of the native anisotropic tissue structure; and (vii) a reproducible architecture of clinically relevant size and shape [205, 209, 288, 517, 526, 527]. Yet most scaffolds reported to date for cartilage repair conform to only a few of these criteria.

Scaffold processing techniques used to date have focused on the development of porous materials via fibre bonding, solvent casting, particulate leaching, membrane lamination, melt moulding, temperature-induced phase separation and gas foaming [210, 286]. The control over scaffold architecture using these fabrication techniques however, are highly process driven, and not design driven. As a result, investigators have recently turned to rapid prototyping (RP) techniques for producing porous scaffolds for tissue engineering applications [195, 209, 211, 460, 534]. RP is a subset of mechanical processing techniques which allows highly complex, but reproducible structures, to be constructed one layer at a time via computer-aided design (CAD) models and computer-controlled tooling processes (CAM). These techniques essentially allow researchers to design-in desired properties, such as porosity, interconnectivity and pore size, in a number of polymer and ceramic materials. RP methodologies studied to date have included stereolithography, selective laser sintering, ballistic particle manufacturing and 3D printing [210], using highly specialized polymers and materials designed specifically to meet the processing requirements of each RP system. However, the transfer of RP technologies to encompass biocompatible and bioresorbable materials still poses a significant challenge, particularly in developing 3D scaffolds for tissue engineering applications.

Hutmacher and co-workers [195, 209-211, 534] have developed scaffolds primarily for bone tissue engineering applications based on fused deposition modelling (FDM) of poly(ϵ -caprolactone) (PCL) polymers. This process uses rollers to feed a pre-formed fibre through a heated nozzle onto a computer controlled table. PCL was chosen due to its relatively low melting temperature ($\sim 60^{\circ}\text{C}$) and thermal stability at high temperatures [534]. Drawbacks of

the FDM technique include the need for pre-formed fibres with specific size and material properties to feed through the rollers and nozzle. As a result, FDM has a narrow processing window [253], and its use with biodegradable polymer systems other than PCL have not been reported. More recently, computer-guided 3D plotting techniques have been developed [253, 254, 256, 491, 492] which use a pressurized syringe to produce scaffolds with complex geometries and a wider range of processing capability, *i.e.* agar, agarose materials at room temperature as well as hot melts from low viscosity polymers.

At present, we are evaluating a series of amphiphilic, biodegradable poly(ether ester) multiblock co-polymers as carrier materials for articular cartilage repair. These thermoplastic elastomers are based on hydrophilic poly(ethylene glycol)-terephthalate (PEGT) and hydrophobic poly(butylene terephthalate) (PBT) blocks. A major advantage of these types of co-polymer systems is that by varying the amount and the length of the two building blocks, an entire family of polymers can be obtained. This offers extensive possibilities in the design of systems with tailor-made properties, such as swelling, degradability and mechanical strength [30, 422, 480]. The addition of 0.2 wt% α -tocopherol as an antioxidant provides stability to the PEGT/PBT co-polymers at elevated temperatures, thus providing suitable viscosities to support a wide range of processing techniques. Various *in vitro* and *in vivo* studies have demonstrated both the biocompatibility and biodegradable nature of PEGT/PBT co-polymers [28, 111, 402, 480] and are currently applied for a range of biomedical applications [29, 299, 375, 403, 517]. Degradation occurs via both hydrolysis (cleavage of ester bond linking ester and hydrophilic ether segments) and oxidation (PEG chain scission via free-radical reactions), and in both cases, degradation is more rapid for copolymers with high PEG content [111]. The attachment, proliferation, morphology, and differentiation state of chondrocytes has also been demonstrated on different compositions of 2D PEGT/PBT films [299, 375]. Controlled release of bioactive factors from these materials has also been demonstrated [32, 517].

Few investigators have produced scaffolds for articular cartilage tissue engineering applications using RP, or evaluated *in vitro* and *in vivo* tissue formation on such scaffolds. Further development of RP technologies offer promising avenues to generate scaffolds which meet a large number of the scaffold requirements explained previously. Therefore, the purpose of this study was to evaluate a model 3D deposition system for producing porous PEGT/PBT scaffolds. The mechanical properties of various scaffolds were assessed for comparison with normal articular cartilage and results following *in vitro* and *in vivo* tissue culture are reported herein.

Materials and Methods:

Materials:

PEGT/PBT co-polymers were obtained from IsoTis S.A. (Bilthoven, The Netherlands) with a composition denoted as $a / b / c$, where a represents the PEG molecular weight (MW), and b and c represent the weight percentage (wt%) of the PEGT and PBT blocks respectively. Co-polymer compositions of hydrophobic 300/55/45 and hydrophilic 1000/70/30 were chosen for use in this study based on previous work indicating their suitability for chondrocyte attachment and tissue formation [205, 299, 375, 517].

The mechanical properties of these co-polymer compositions have been determined previously from dense tensile test specimens [422]. The tensile modulus (E) and tensile strength (σ) for 300/55/45 co-polymer compositions were 187.5 ± 5.0 MPa, 15.3 ± 0.4 MPa respectively, while for 1000/70/30 co-polymers were shown to be 33.95 ± 1.2 MPa and 5.27 ± 0.3 MPa respectively.

3D-Deposition Process:

Porous 3D scaffolds were constructed using a custom designed fibre-deposition device consisting of 5 main components; (1) a thermostatically controlled heating jacket; (2) a molten co-polymer dispensing unit consisting of a syringe and nozzle; (3) a force-controlled plunger to regulate flow of molten co-polymer (4); a stepper motor driven x-y-z table; and (5) a positional control unit consisting of stepper-motor drivers linked to a personal computer containing software for generating fibre deposition paths (Fig 1).

The stainless steel heating jacket contained four thermostatically-controlled heating rods capable of evenly conducting heat (from 0-350°C) to a stainless steel syringe placed within the heating jacket. Co-polymer granules were placed in the syringe purged with nitrogen gas and allowed to melt. A stainless steel plunger with a teflon seal was used to apply pressure to the molten polymer. Pressure was regulated by placing the entire deposition device beneath the crosshead of a standard tension-compression test machine (Hounsfield HTE) in order to control the displacement of the plunger and monitor the resultant force (detected by a 20 kN load cell). Therefore, accurate control over the flow-rate of polymer from the nozzle of the syringe was obtained. The nozzles were custom designed, and constructed by brazing medical grade syringe needles of varying diameter (e.g. 150, 250 and 350 μm inside diameter) onto a threaded, conical stainless steel tip.

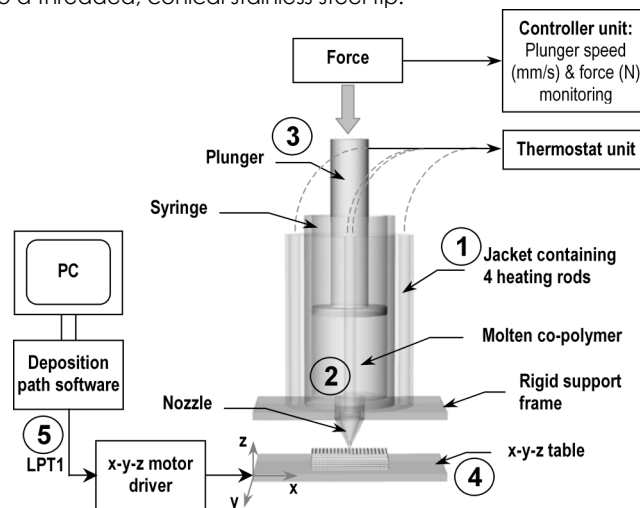


Figure 1 – The 3D deposition device consisted of 5 main components: (1) a thermostatically controlled heating jacket; (2) a molten co-polymer dispensing unit consisting of a syringe and nozzle; (3) a force-controlled plunger to regulate flow of molten co-polymer (4); a stepper motor driven x-y-z table; and (5) a positional control unit consisting of stepper-motor drivers linked to a personal computer containing software for generating fibre deposition paths.

Table 1 – Processing parameters for 3D deposited scaffolds

Sample	Fibre Deposition Temperature (°C)	Nozzle Diameter (µm)	Applied Force (kN)	Crosshead Speed (mm/min)	x-y-z Table Speed (mm/s)	x-y Fibre Spacing (mm)	z Fibre Spacing (mm)
300/55/45 - 1.0 mm	200	250	2.0	0.4	5	1.0	0.2
300/55/45 - 1.0 mm stag	200	250	2.0	0.4	5	1.0	0.2
300/55/45 - 2.0 mm	200	250	2.0	0.4	5	2.0	0.2
1000/70/30 - 0.5 mm	180	250	1.5	0.2	5	0.5	0.2
1000/70/30 - 1.0 mm	180	250	1.5	0.2	5	1.0	0.2
1000/70/30 - 1.0 mm stag	180	250	1.5	0.2	5	1.0	0.2

Stepper motors (Saia-Burgess AG, Switzerland) coordinated speed and translation of the x-y-z table (Proxxon GmbH, Germany), and were controlled by a custom deposition program (designed using Visual Basic, Microsoft Corporation) via the printer port (LPT1). The program required inputs of the overall scaffold dimensions, the spacing between deposited fibres, the number of fibre layers, and the speed at which the x-y-z table translated (Table 1). By lowering the x-y table one layer-step in the z-direction, successive layers of rapidly solidifying fibres were laminated to previous layers in a 0° - 90° pattern creating a consistent pore size and 100% interconnecting pore volume (Fig 2). Fibre layers could be continuously deposited resulting in scaffolds up to 10 mm thick in some cases, however, in general, scaffolds 4 mm thick were created for cell culture experiments. These dimensions were chosen given that 4 mm is approximately the thickness of the cartilage layer present in human articular knee cartilage [92, 237] and also presented challenging dimensions with which to assess *in vitro* cartilage formation.

For cell culture experiments, cylindrical samples were cored from 4 mm thick blocks. Prior to cell seeding, scaffolds were incubated in isopropanol overnight to remove contaminants before being allowed to air-dry, with a further drying step overnight in a vacuum oven at 50°C. Scaffolds were then sterilized by gamma irradiation (minimum dose 25 kGy) in a JS6500 Tote Box Irradiator at Isotron B.V. (Ede, The Netherlands).

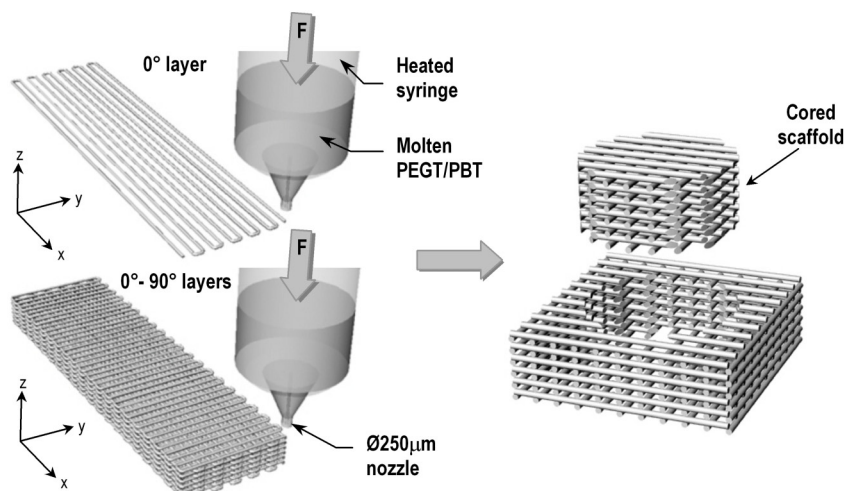


Figure 2 – 3D deposition process where Ø250 µm PEGT/PBT fibres are successively laid down in a computer controlled pattern (0° - 90° orientation shown). Scaffolds are subsequently cored from the deposited bulk material

Characterisation:

Due to the regular pore geometry, determining the interconnecting pore size of the resulting scaffolds was possible using scanning electron microscopy (SEM). The theoretical volume percent (vol%) porosity was calculated for each scaffold using deposition geometries based on a unit cube, whereby the fibre diameter and spacing between layers were equal (*i.e.* no overlap due to the fusion between fibres from one layer to another was assumed).

$$\text{Vol\% porosity}_{\text{theoretical}} = \left(1 - \frac{V_f}{V_c}\right) \times 100\% \quad \text{Eq. (1)}$$

Here, $V_f = \text{scaffold fibre volume (mm}^3) = \frac{\pi \cdot d^2 \cdot L \cdot n_1 \cdot n_2}{4}$

and $V_c = \text{total scaffold cube volume (mm}^3) = L \cdot w \cdot h$

$$\text{Therefore, Vol\% porosity}_{\text{theoretical}} = \left(1 - \frac{\pi \cdot d^2 \cdot n_1 \cdot n_2}{4 \cdot w \cdot h}\right) \times 100\% \quad \text{Eq. (2)}$$

where d , L , w and h refer to the fibre diameter, fibre length, scaffold width, and scaffold height in millimetres respectively. Furthermore, n_1 represents the number of fibres per layer, while n_2 represents the number of layers per scaffold.

Vol% porosity was also measured using mass/volume techniques according to the following relationship:

$$\text{Vol\% porosity}_{\text{measured}} = \left(1 - \frac{V_s}{V_c}\right) \times 100\% \quad \text{Eq. (3)}$$

Here, $V_s = \text{apparent scaffold volume (mm}^3) = \frac{m}{\rho}$

and $V_c = \text{total scaffold cube volume (mm}^3) = L \cdot w \cdot h$

$$\text{Therefore, Vol\% porosity}_{\text{measured}} = \left(1 - \frac{m}{\rho \cdot L \cdot w \cdot h}\right) \times 100\% \quad \text{Eq. (4)}$$

where m represents the mass of the scaffold (g) and ρ represents the co-polymer density (g/mm³), whereby, $\rho_{300/55/45}$ equals 1.25×10^{-3} g/mm³ and $\rho_{1000/70/30}$ equals 1.20×10^{-3} g/mm³.

Due to the amphiphilic nature of the PEGT/PBT co-polymers, the degree of swelling was determined by measuring the percentage change in diameter (mm²) between dry scaffolds and scaffolds incubated at 37°C for 24 hours in a phosphate buffered saline (PBS) solution.

Differential Scanning Calorimetry (DSC):

Differential scanning calorimetry (DSC Pyris 1, Perkin Elmer) was used to determine the thermal response of the co-polymers pre- and post-processing. Samples (7.5-14.0 mg) of 300/55/45 and 1000/70/30 resin and 3D-deposited scaffolds produced after 1 hour of fibre deposition were heated from 80°C to 250°C at a rate of 10°C/min in aluminium pans with nitrogen as a purge gas. The resulting DSC curves were analyzed to determine melting (T_m) and crystallization (T_c) temperatures of the more crystalline PBT component.

Intrinsic Viscosity (IV):

Intrinsic viscosity was measured to give an indication of relative changes in molecular weight (MW) of the co-polymer pre- and post-processing [75]. The intrinsic viscosity (η) of 300/55/45 and 1000/70/30 resins and 3D-deposited scaffolds produced after 1 hour of fibre deposition were determined from a solution of 0.5 g/dl of co-polymer in chloroform (CHCl₃) using a Schott Geräte Ubbelohde viscometer (DIN type 0c) at 25°C.

Mechanical Evaluation:

Scaffolds: Ø4 mm x 4 mm thick cylinders were cored from 3D-deposited blocks and soaked overnight in phosphate buffered saline (PBS, Sigma) to allow for hydration and swelling. Samples were then placed in a PBS bath at room temperature between two compression plates of a Zwick Z050 tension-compression machine. The unconfined equilibrium modulus was determined by applying a step displacement (20% strain) and monitoring compressive force with time until equilibrium was reached (approximately 900 seconds). The ratio of equilibrium force to cross-sectional area was divided by the applied strain to calculate the equilibrium modulus (in MPa). Dynamic stiffness properties were determined by applying unconfined cyclic compression between 5% and 20% strain at a frequency of 0.1 Hz until an equilibrium force amplitude was observed (typically 50 cycles). Dynamic stiffness (in MPa) was calculated by taking the ratio of average force amplitude for the last 10 cycles to cross-sectional area, and dividing by the applied strain.

Articular Cartilage: Osteochondral plugs Ø4 mm were cored from the trochlear groove of 6-month old bovine knee joints. Articular cartilage cylinders, 4 mm thick, were obtained using a custom designed holder that allowed perpendicular sections to be accurately made. Samples were then immediately placed in PBS at room temperature for 3-4 hours to equilibrate. The equilibrium modulus (at 20% strain) and dynamic stiffness (at 0.1 Hz) were determined as above for the scaffolds, however, a greater number of cycles were necessary to reach an equilibrium force amplitude for dynamic stiffness measurements (typically 100 cycles).

Tissue Culture:

Bovine: For seeding and culture of bovine chondrocytes, 3D deposited scaffolds were produced using a 300/55/45 co-polymer composition and a 1 mm fibre spacing (Fig 3A, 3B). Chondrocytes were isolated via collagenase digestion from articular cartilage harvested from medial and lateral condyles of freshly slaughtered 6-month old bovine knee joints. Primary cells were dynamically seeded in spinner flasks (100 mL working volume, 50 rpm) on Ø7 mm by 4 mm thick scaffolds for 3 days at a density of 8×10^6 cells per scaffold. The culture medium contained HEPES (Invitrogen)-buffered DMEM (Invitrogen) supplemented with 10% fetal bovine serum (FBS, Sigma-Aldrich), 0.2 mM ascorbic acid 2-phosphate (Invitrogen), 0.1 mM non-essential amino acids (Sigma-Aldrich), 0.4 mM proline (Sigma-Aldrich), 100 units/ml penicillin (Invitrogen), and 100 µg/ml streptomycin (Invitrogen). The scaffolds were then dynamically cultured in spinner flasks for 21 days in the same medium, which was refreshed every 3-4 days.

To access the ability of scaffolds to support chondrogenesis *in vivo*, smaller Ø4 mm by 4 mm thick scaffolds were seeded dynamically (as described above) for 7 days at a cell density of 3×10^6 cells per scaffold (*i.e.* the same cell density/mm² as the larger *in vitro* scaffolds). Scaffolds were subsequently implanted in subcutaneous pockets of 6-week old nude mice (HdCpb:NMRI-nu, Harlan, The Netherlands). Animals were sacrificed at 21 days after implantation, and constructs were processed histologically as described below.

Human: 3D deposited scaffolds for seeding of expanded human articular chondrocytes were also produced from 300/55/45 co-polymers with a 1 mm fibre spacing, however, the spacing of fibres was staggered between successive layers (Fig 3C). Human articular chondrocytes were isolated via collagenase digestion of biopsies obtained from patients undergoing hip replacement surgery and culture-expanded in monolayer until passage 2. The cells were then trypsinized and dynamically seeded in spinner flasks (as described above) on Ø4 mm by 4 mm thick scaffolds for 5 days at a density of 3×10^6 cells/scaffold using the same above-mentioned culture medium, and without the use of additional growth factors.

Evaluation:

Histology: Samples were fixed overnight in 0.14M cacodylate buffer (pH = 7.2 - 7.4) containing 0.25% glutaraldehyde (Merck). Samples were then dehydrated in sequential ethanol series, plastic embedded in glycol-methacrylate (Merck) and cut using a microtome to yield 5 µm thick sections. Sections were stained with haematoxylin (Sigma-Aldrich) and fast green (Merck) to visualize cells/cell nuclei and counterstained with safranin-O (Sigma-Aldrich) to visualize extracellular glycosaminoglycans (GAG). Mounted slides were examined under a light microscope (Nikon Eclipse E400) and representative images captured using a digital camera (Sony Corporation, Japan) and Matrix Vision software (Matrix Vision GmbH, Germany).

Scanning Electron Microscopy (SEM): Samples were fixed and dehydrated as described above and critical point dried from liquid carbon dioxide using a Balzers CPD 030 Critical Point Dryer. Dried tissue-cultured samples or as-produced scaffolds were then sputter-coated (Cressington) with a thin gold layer and studied using a Philips XL30 Environmental Scanning Electron Microscope (ESEM).

Immunohistochemistry: Constructs were embedded in optimal cutting temperature (OCT) compound (Tissue-Tek) and snap frozen at -60°C. Cryo-sections, 5 µm in thickness, were made (Cryotome, Thermo Shandon) and fixed in acetone for 8 minutes. Collagen type II was immuno-localized using an Animal Research Kit (Dako) in combination with a collagen type II antibody (1:200, II-II6B3, Developmental Studies Hybridoma Bank). In brief, after digestion for 20 minutes with 0.025% trypsin-EDTA (Invitrogen) at room temperature, samples were rinsed with PBS (Invitrogen) and incubated with peroxidase block for 5 minutes. Samples were then incubated with a biotinylated primary antibody for 15 minutes, rinsed with PBS, followed by the application of streptavidin-peroxidase for 15 minutes. After rinsing with PBS, the staining was visualized using DAB-solution for 5 minutes in addition to counter staining with haematoxylin (Sigma). Samples were examined under a light microscope (Nikon Eclipse E400) and representative images captured using a digital camera (Sony Corporation, Japan) and Matrix Vision software (Matrix Vision GmbH, Germany).

Cell Viability: A live/dead assay (Molecular Probes) was used to access cell viability. Ethidium-bromide homodimer was used as a marker for dead cells due to the fact that it binds fragmented deoxyribonucleic acid (DNA) in cells that no longer have an intact plasma membrane, and fluoresces red. Calcein AM is capable of permeating the plasma membrane of viable cells, where it is cleaved by intracellular esterases and fluoresces green [170]. Constructs were harvested and 1 mm thick sections incubated in a PBS solution containing 6 $\mu\text{mol/L}$ ethidium bromide homodimer and 2 $\mu\text{mol/L}$ calcein AM for 30 minutes at 37°C. Sections were examined in an inverted fluorescent microscope (Nikon Eclipse E400) using a FITC Texas Red filter. Representative images were captured using a digital camera (Sony Corporation, Japan) and Matrix Vision software (Matrix Vision GmbH, Germany).

Results & Discussion:

Characterisation:

SEM analysis confirmed that 3D deposited scaffolds consisted of 100% interconnecting pores (Fig 3A-3D, 3F). Only in scaffold designs where the fibre spacing was controlled to deliberately produce completely dense layers (as illustrated in the pore gradient scaffolds in Fig 3E) was interconnectivity compromised. By varying the deposition path (e.g. the fibre spacing) and accurately controlling deposition parameters (e.g. temperature, syringe pressure, x-y-z table velocity), a range of scaffold architectures were produced from 300/55/45 and 1000/70/30 PEGT/PBT co-polymer compositions. Scaffolds contained smooth fibres approximately 250 μm in diameter and, with a fibre spacing ranging between 0.5 mm and 2.0 mm, average interconnecting pore sizes in the x-y plane ranged between ~ 150 μm and ~ 1650 μm respectively, as shown by SEM analysis (Table 2). Average interconnecting pore size in the z-plane was related to the fibre diameter, and ranged between 170-195 μm irrespective of fibre spacing. During deposition, molten PEGT/PBT co-polymers fibres rapidly solidified resulting in a continuous bond with the underlying fibres and, hence, a solid fusion between scaffold layers (Fig 3A-3F).

Due to the higher wt% PBT content and, thus, more hydrophobic nature of 300/55/45 co-polymers, swelling in scaffolds produced using this composition was limited to an increase of approximately 2.0%. Conversely, the more hydrophilic 1000/70/30 co-polymers showed an increase in swelling by approximately 18% (Table 2).

Table 2 – Structural characterisation of deposited scaffolds

Sample	Theoretical Pore Size		Avg. Interconnecting Pore Size		Swelling (%)	Theoretical Vol% Porosity (%)	Measured Vol% Porosity (%)
	x-y plane (μm)	z-plane (μm)	x-y plane (μm)	z-plane (μm)			
300/55/45 - 1.0 mm	750	200	646 \pm 65	185 \pm 52	2.1 \pm 1.2	78.0	70.8 \pm 1.77
300/55/45 - 1.0 mm stag	750	200	610 \pm 20	180 \pm 22	1.8 \pm 0.1	78.0	70.2 \pm 1.16
300/55/45 - 2.0 mm	1750	200	1653 \pm 91	171 \pm 27	2.0 \pm 0.6	87.4	87.4 \pm 0.43
1000/70/30 - 0.5 mm	250	200	150 \pm 38	195 \pm 21	17.7 \pm 2.4	59.2	55.4 \pm 0.93
1000/70/30 - 1.0 mm	750	200	652 \pm 49	188 \pm 30	18.7 \pm 2.6	78.0	71.5 \pm 1.13
1000/70/30 - 1.0 mm stag	750	200	616 \pm 33	177 \pm 46	16.8 \pm 2.0	78.0	71.5 \pm 1.81

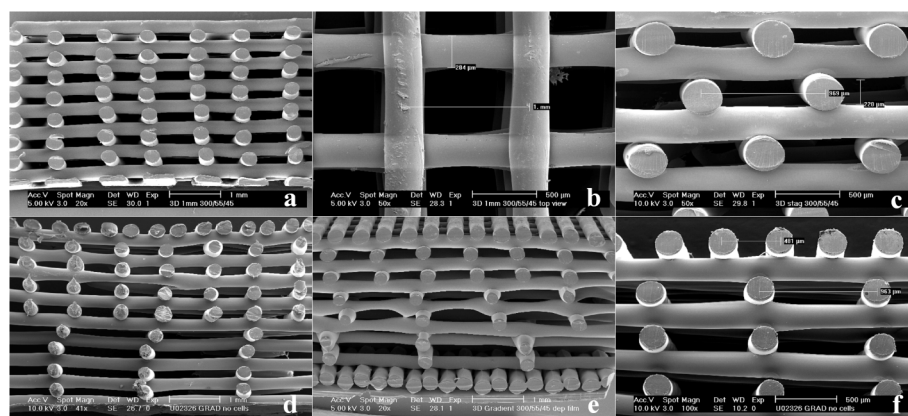


Figure 3 – SEM sections of 3D deposited scaffolds with varying fibre deposition geometries; (A) homogeneous 1 mm fibre spacing showing typical fibre diameters and pore geometries x 20, (B) top view x 50; (C) 1 mm staggered fibre spacing x 50; (D) inhomogeneous pore-size gradient x 20; (E) inhomogeneous pore-size gradient deposited on dense basal layer of fibres x 20; (F) superficial layer of gradient scaffold x 50.

Theoretical volume percent porosity based on deposition paths ranged between 59.0% and 87.4%. However, due to the fusion between fibres and the underlying layers, measured porosity values were somewhat less, as has been shown during 3D dispensing of hydrogel materials [256]. These differences can be further explained by the fact that the theoretical calculations assume a unit cube as opposed to the actual continuous strand of fibre which generated edge effects. Minor deviations in fibre diameter and deposition geometry also likely make a contribution.

Intrinsic Viscosity and Thermal Characterisation:

There was no significant increase in IV of deposited scaffolds compared with co-polymer resin indicating the 3D deposition process did not significantly alter the relative MW of both 300/55/45 and 1000/70/30 co-polymers (Table 3). DSC analysis of thermal properties resulted in a slightly higher melting temperature (T_m), enthalpy of fusion of the more crystalline PBT phase (ΔH_{PBT}), and crystallization temperature (T_c) for deposited scaffolds as compared with resin. This was likely due to differences in thermal history between resin processing and 3D deposition, rather than significant changes in co-polymer crystallinity. These results demonstrate that the processing parameters used did not induce changes in MW due to degradation at elevated temperatures or shear forces during fibre deposition, which in turn could compromise scaffold biocompatibility and/or biodegradation.

Table 3 – Intrinsic viscosity and thermal characterisation of deposition process

Sample	Intrinsic Viscosity η (dl/g)	Melting Temp T_m PBT (°C)	Enthalpy of Fusion ΔH_{PBT} (J/g)	Crystallization Temp T_c PBT (°C)
300/55/45 resin	0.68 ± 0.03	151.4 ± 2.7	19.5 ± 4.4	95.6 ± 3.5
300/55/45 scaffold	0.66 ± 0.01	156.5 ± 3.2	22.8 ± 5.5	103.4 ± 3.6
1000/70/30 resin	0.80 ± 0.01	149.8 ± 3.0	13.2 ± 1.8	106.1 ± 10.3
1000/70/30 scaffold	0.79 ± 0.01	155.8 ± 4.8	12.0 ± 7.0	116.0 ± 12.3

Mechanical Properties:

Under compression, articular cartilage behaves like a poroelastic material, whereby its response to compressive loads are frequency and strain dependent, and is governed by the interrelationship between solid ECM constituents (e.g. collagen type II) and interstitial fluid flow (e.g. water) [115, 267, 269]. To characterize the mechanical properties of scaffolds with varying architecture and co-polymer composition, both static and dynamic compression tests were performed under wet conditions and compared with native articular cartilage tissue.

With respect to co-polymer composition, scaffolds deposited using 300/55/45 yielded higher equilibrium modulus and dynamic stiffness values as compared with 1000/70/30 scaffolds of the same geometry (Fig 4). This was likely due to the lower PEG MW and greater wt% ratio of "hard" PBT blocks to "soft" PEGT blocks present in the 300/55/45 scaffolds, and limited water uptake. Similar mechanical behaviour has been reported in tensile test specimens of PEGT/PBT co-polymers with the same composition [111].

Figure 4 illustrates that by controlling scaffold architecture, the mechanical properties could also be influenced. In general, highly porous structures exhibit limited mechanical properties whereby a power-law exists relating porosity to compressive stiffness [534]. Similar behaviour was seen in this study where scaffolds with reduced fibre spacing (e.g. 0.5 mm) and, thus, low vol% porosity (e.g. 59.0%), resulted in higher equilibrium modulus and dynamic stiffness as compared with scaffolds with larger fibre spacing (e.g. 2 mm) and high vol% porosity (e.g. 87%). It must be noted, however, that by altering the deposition pattern, the bulk mechanical properties of the scaffolds were changed. Therefore, equilibrium modulus and dynamic stiffness could not be directly correlated with scaffold porosity. For example the equilibrium modulus and dynamic stiffness of 1 mm staggered 300/55/45 and 1000/70/30 scaffolds (Fig 3C) were approximately 50% of those values measured for scaffolds with a homogeneous 1 mm fibre spacing, even though they had almost identical vol% porosity (see Table 2). This was due to the fact that, under compression, the homogeneous 1 mm spaced scaffolds with fibres lying directly underneath each other presented stiffer columns of fibres compared with staggered scaffolds where fibres, in any given layer, never lay directly underneath one another.

In natural cartilage tissue, unconfined compression testing of bovine articular cartilage explants resulted in an equilibrium modulus and dynamic stiffness (at 0.1 Hz) of 0.27 MPa and 4.10 MPa respectively. These values compare favourably with previous unconfined compression studies on bovine articular cartilage [225, 242]. Only 300/55/45 scaffolds with a 2 mm fibre spacing and 1000/70/30 scaffolds with both 1 mm and 1 mm staggered spacing had equilibrium modulus values equal-to or less-than bovine articular cartilage. When tested under dynamic compression, 300/55/45 scaffolds with 0.5 and 1.0 mm spacing most closely resembled those of native cartilage compared with scaffolds deposited from 1000/70/30 co-polymers.

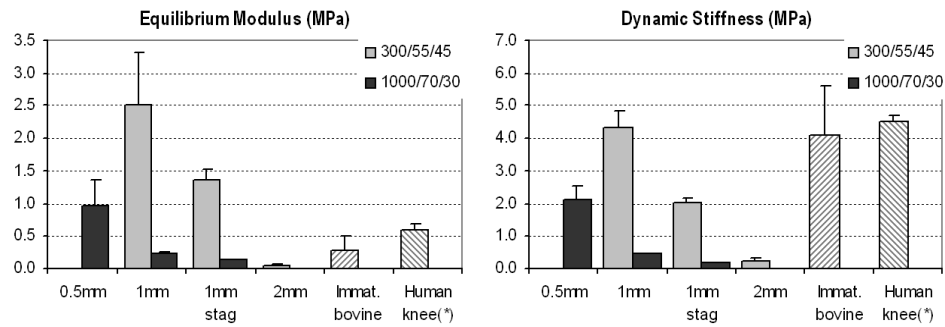


Figure 4 – Equilibrium modulus and dynamic stiffness (0.1 Hz) of hydrated 3D-deposited scaffolds compared with natural articular cartilage (* taken from Treppo et al. [475]).

The equilibrium modulus and dynamic stiffness (at 0.1 Hz) values cited in literature for human articular knee cartilage tested under confined compression are 0.6 MPa and 4.5 MPa respectively [475]. Although unconfined compression tests were performed in this study, which tend to underestimate values measured via confined compression, the mechanical data obtained in this study suggest that it is possible to design 3D deposited PEGT/PBT scaffolds which match the static and dynamic properties of articular cartilage, and thus be capable of supporting *in vivo* loading conditions within the human knee joint. While other investigators have reported the development of scaffolds with similar compressive modulus to articular cartilage [360], the development of scaffolds with similar dynamic stiffness properties to articular cartilage has not been reported previously. Given the frequency dependant response of articular cartilage under compression, we postulate that the dynamic, rather than static, properties of articular cartilage may provide a more appropriate benchmark with which to emulate into scaffolds designed for articular cartilage repair. In future studies, we intend to evaluate in more detail the mechanical response of 3D-deposited scaffolds over and larger range of dynamic frequencies.

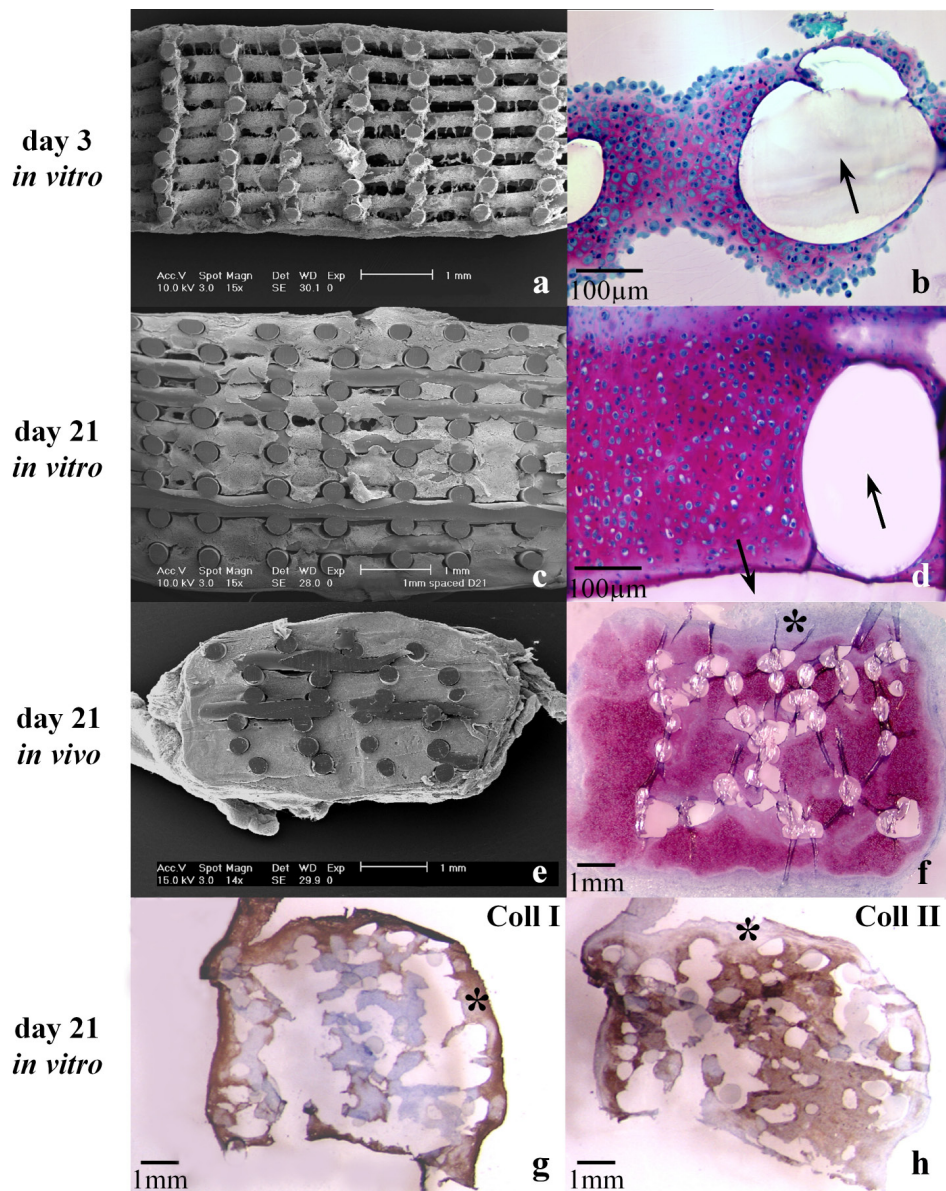


Figure 5 – SEM (A, C, E x 15), safranin-O stained (B, D, F), and collagen type-I and type-II immunohistochemistry sections (G, H) of 3D-deposited 300/55/45 scaffolds following (A, B) 3 days dynamic seeding of bovine articular chondrocytes; (C, D, G, H) 21 days dynamic culture in vitro ; (E, F) 21 days subcutaneous implantation in nude mice; (arrows indicate PEGT/PBT fibre, * indicates fibrous capsule). ► p208.

Tissue Culture:

SEM sections following 3 days dynamic seeding showed rapid cell/cell-aggregate attachment onto, and throughout, the PEGT/PBT scaffolds (Fig 5A). Under these conditions, the early onset of chondrogenesis was promoted as seen in safranin-O sections where newly synthesized ECM stained positively for GAG (Fig 5B). There was near-complete formation of cartilage-like tissue within the interconnecting pores after 21 days dynamic culture (Fig 5C). Again, positive GAG staining was observed throughout, even in ECM synthesized deep within the $\varnothing 7$ mm by 4 mm thick scaffold (Fig 5D). Similar to previous reports studying dynamic culture of cartilagenous constructs *in vitro* [316, 494], a thin capsule of fibroblast-like cells was observed surrounding the periphery of the scaffold. This was highlighted in immuno-sections where the periphery of the constructs positively expressed collagen type I, which is synthesized by cells with a fibroblastic phenotype (Fig 5G). In contrast, collagen type II, which is synthesized by cells with a chondrocytic phenotype, was predominantly expressed throughout the interior of the constructs (Fig 5H), and was in accordance with the GAG staining observed in safranin-O sections.

Subcutaneous implantation of $\varnothing 4$ mm by 4 mm thick scaffolds, dynamically cultured for 7 days, resulted in greater tissue formation than *in vitro* samples, as observed qualitatively from SEM and safranin-O sections (Fig 5E, 5F). ECM exhibiting a cartilage-like morphology was observed throughout the scaffold and stained positively for GAG even beyond the border of the scaffold fibres. Again, at the very periphery of the construct, a fibrous capsule was present.

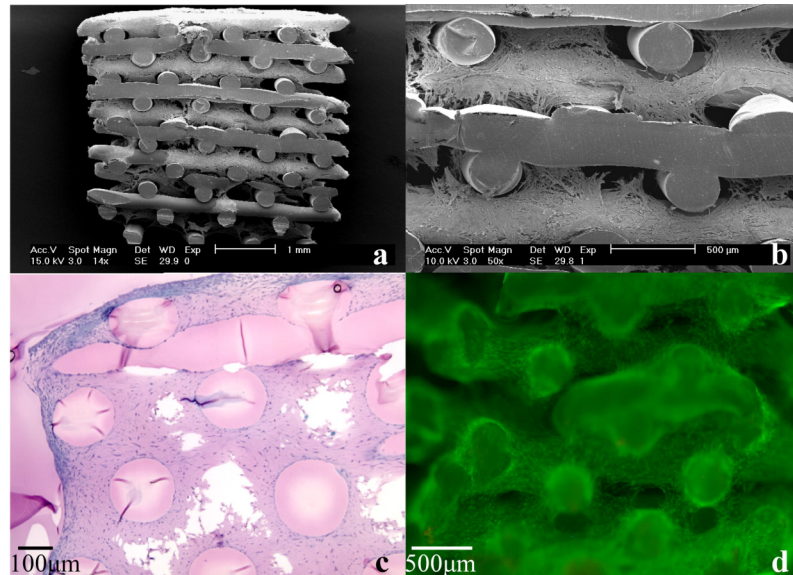


Figure 6 – SEM (A $\times 15$, B $\times 50$), safranin-O (C), and live/dead (D) sections showing attachment, proliferation and high percentage of live (green) expanded human articular chondrocytes throughout interconnecting pores on 3D-deposited 300/55/45 scaffolds following 5 days dynamic seeding. ► p209.

Although bovine chondrocytes, which typically exhibit a higher metabolic activity as compared to human chondrocytes [226], were used in this evaluation study, the rapid chondrogenesis observed may further be attributed to the large number of cell-cell interactions as well as enhanced nutrient exchange provided by the highly accessible and interconnecting pore structure in addition to the dynamic flow conditions [129, 306, 307, 496]. A preferable cell source for scaffold-based strategies to repair clinically-sized articular cartilage defects are human articular chondrocytes, which are typically culture expanded in monolayer to yield sufficient quantities for seeding [517]. In this study, seeding of expanded (passage 2) human articular chondrocytes resulted in rapid cell attachment and proliferation as indicated by multiple layers of elongated cells observed in SEM and safranin-O sections at day 5 (Fig 6A, 6B, 6C). Furthermore, tissue was beginning to bridge the interconnecting pores between the staggered fibres (Fig 6C), and contained a high percentage of living cells as observed in fluorescent live/dead stained sections (Fig 6D).

3D-Deposition Process:

While the intent was that the 3D deposition device be adapted to a RP system in the future, thus allowing complex 3D geometries to be developed from CAD/CAM design and control of fibre deposition, our initial goal was the development of simple geometries with controlled and repeatable pore architectures in order to study tissue formation. In the development of 3D-deposited scaffolds, it is important to discuss the critical processing parameters.

If we assume the molten co-polymer to be a viscous Newtonian fluid (*i.e.* non-compressible) with a parabolic flow profile (*i.e.* when nozzle length = 6x nozzle diameter), the flow rate from the nozzle can be expressed according to the Hagen-Poiseuille equation [491]:

$$Q = \frac{\pi \cdot \Delta P}{128 \cdot L \cdot \eta} \cdot d^4 \quad \text{Eq. (5)}$$

As shown in Equation 5, the flow rate (Q) of the co-polymer is directly proportional to both the pressure differential (ΔP) across the syringe and nozzle tip, and the nozzle diameter (d), while both Q and ΔP are inversely proportional to nozzle length (L) and co-polymer viscosity (η). Controlling co-polymer flow rate is critical as a high Q resulted in over-deposition of the fibre, causing draping between fibres and reducing porosity, whereas a low Q will reduce the fibre diameter, thus compromising contact between the underlying fibres and overall scaffold integrity. Changes in Q could be buffered by controlling x-y-z table velocity, thus adjusting the take-off speed of fibre from the nozzle. Furthermore, minor decreases in nozzle diameter will dramatically decrease flow rate and require considerably greater pressures to deposit suitable fibres, as will an increase in nozzle length to a lesser extent. For very small nozzle diameters (*i.e.* <100 μm), the pressures required to achieve a suitable flow rate can be beyond those practically possible, necessitating changes in viscosity. Addition of solvents, such as chloroform [491, 492], or increasing the syringe temperature to reduce the co-polymer viscosity would assist deposition of fibres at small nozzle diameters. However, incomplete removal of solvents post-processing and exposure of polymers to excessive oxidation at elevated temperatures can be detrimental to scaffold biocompatibility [209, 254]. On a macroscopic level, a reduced fibre diameter would allow a higher scaffold

resolution but would also result in a reduced pore size in the z-direction as well as increasing the processing time of thick scaffolds. One solution would be to deposit two layers of fibres in an identical pattern, directly on top of one other, thereby doubling the interconnecting pore size in the z-direction.

The 3D deposition device presented here was designed to eliminate these concerns by using a solvent-free processing technique and thermally stable co-polymers operating under a non-oxidizing nitrogen environment. As shown by IV and DSC analysis, PEGT/PBT co-polymer MW was not affected by the deposition process (Table 3). Furthermore, there was no shrinkage of scaffolds during processing, and hydrophilic scaffold compositions (*i.e.* 1000/70/30) also allowed for swelling during subsequent culture. In addition to varying scaffold fibre spacing, nozzles and/or syringes could be interchanged during processing in the future in order to deposit fibres of different diameter, or co-polymers of different composition. This would allow considerable freedom with respect to the structural organization of scaffolds. For example, interconnecting pore size, fibre surface area, surface chemistry, degradation behaviour and mechanical properties could be controlled from one layer to another. We already demonstrated in this study the ability to create anisotropic scaffolds containing pore-size gradients ranging from very small pores ($\sim 150\mu\text{m}$) to very large pores ($\sim 1650\mu\text{m}$) throughout the depth of the construct (Fig 3D-3F).

Conclusions:

We have presented and characterised a fibre deposition technique for producing 3D scaffolds with a well-defined, and 100% interconnecting, pore network for engineering of articular cartilage. The 3D deposition technique allowed us to "design-in" desired scaffold characteristics, such as porosity, pore size and mechanical properties using computer controlled tooling processes. Using two PEGT/PBT co-polymer compositions, and by changing the spacing between deposited fibres from one layer to another, a range of scaffold geometries were created, including scaffolds with a staggered fibre spacing; scaffolds with pore size gradients with height; and scaffolds with complete dense layers (Fig 3).

Fibre-based scaffolds were generated from two different PEGT/PBT co-polymers compositions, a hydrophobic 300/55/45 and hydrophilic 1000/70/30, with varying swelling capabilities ranging between 2% and 18% respectively. Static and dynamic mechanical compression showed differences in equilibrium modulus and dynamic stiffness ranging from 0.05 – 2.5 MPa and 0.16 – 4.33 MPa respectively, based on co-polymer composition and scaffold porosity. Furthermore, by maintaining a consistent vol% porosity, mechanical properties could be influenced by manipulating scaffold geometry (*e.g.* a homogenous fibre spacing as compared to a staggered fibre spacing between layers). Scaffolds constructed from 300/55/45 co-polymer fibres with a 1 mm spacing and porosity of 71% resulted in a similar dynamic stiffness values compared with bovine and human articular cartilage tested at a frequency of 0.1 Hz. Thermal characterisation (DSC and IV analysis) showed that relative co-polymer MW was not significantly altered during processing compared with PEGT/PBT resin.

3D-deposited scaffolds supported rapid attachment of bovine chondrocytes and tissue formation following dynamic culture *in vitro* and subcutaneous implantation in nude mice as demonstrated by the presence articular cartilage ECM constituents, GAG and type II

collagen, throughout the interconnected interior pore volume. Similar results were achieved with respect to the attachment of expanded human articular chondrocytes, resulting in a homogenous distribution of viable cells after 5 days dynamic seeding.

The processing methods and model scaffolds developed in this study provide an elegant method to further investigate the effects of scaffold composition and pore architecture on cartilage tissue formation *in vitro* or under load bearing conditions *in vivo*.

Acknowledgements:

The authors would like to acknowledge funding from the European Commission (FP5 project "Scafcart" G5RD-CT-1999-00050).

The background of the slide is a grayscale scanning electron micrograph (SEM) showing a porous, interconnected scaffold structure. The pores are roughly spherical and vary in size, creating a complex, three-dimensional network. The walls of the pores are composed of thin, interconnected fibers or layers of material.

II.

Instructive Scaffolds: Pore Architecture and Chondrocyte Differentiation

Chapter 4

The Effect of PEGT/PBT Scaffold Architecture on the Composition of Tissue Engineered Cartilage.

Chapter 5

The Effect of PEGT/PBT Scaffold Architecture on Oxygen Gradients in Tissue Engineered Cartilaginous Constructs.

Chapter 6

Polymer Scaffolds Fabricated with Organised Pore-Size Gradient Structures as a Model for Studying the Zonal Organisation Within Tissue Engineered Cartilage Constructs.

"Nothing is a waste of time if you use the experience wisely."

[Auguste Rodin, 1840-1917]

50 μ m

Exp

WD Det

Spot Magn Acc.V

Chapter 4

The Effect of PEGT/PBT Scaffold Architecture on the Composition of Tissue Engineered Cartilage.

Malda J.^{1,2,3}, Woodfield T.B.F.^{‡1,2}, van der Vloodt F.³, Wilson C.⁴, Martens D.E.³, Tramper J.³, van Blitterswijk C.A.^{1,2}, Riesle J.²

¹ Institute for Biomedical Technology, University of Twente, Enschede, The Netherlands

² IsoTis S.A., Bilthoven, The Netherlands

³ Food and Bioprocess Engineering Group, Wageningen University, Wageningen, The Netherlands

⁴ Department of Orthopaedics, University Medical Centre, Utrecht, The Netherlands

Abstract:

A highly interconnecting and accessible pore network has been suggested as one of a number of prerequisites in the design of scaffolds for tissue engineering.

In the present study, two processing techniques, compression-moulding / particulate-leaching (CM), and 3D fibre deposition (3DF), were used to develop porous scaffolds from biodegradable poly(ethylene glycol)-terephthalate / poly(butylene terephthalate) (PEGT/PBT) co-polymers with varying pore architectures. Three-dimensional micro-computed tomography (μ CT) was used to characterize scaffold architectures and scaffolds were seeded with articular chondrocytes to evaluate tissue formation.

Scaffold porosity ranged between 75 and 80%. Average pore size of tortuous CM scaffolds (182 μ m) was lower than those of organised 3DF scaffolds (525 μ m).

The weight ratio of glycosaminoglycans(GAG)/DNA, as a measure of cartilage-like tissue formation, did not change after 14 days of culture whereas, following subcutaneous implantation, GAG/DNA increased significantly and was significantly higher in 3DF constructs than in CM constructs, whilst collagen type II was present within both constructs.

In conclusion, 3DF PEGT/PBT scaffolds create an environment *in vitro* that enhances cartilaginous matrix deposition and hold particular promise for treatment of articular cartilage defects.

[‡] Malda J, Woodfield TBF, van der Vloodt F, Wilson C, Martens DE, Tramper J, van Blitterswijk CA, Riesle J. The Effect of PEGT/PBT Scaffold Architecture on the Composition of Tissue Engineered Cartilage. *Biomater*, 2004 (in press).

Introduction:

Tissue engineering holds promise for revolutionary advances in health care and considerable efforts have been directed towards the development of autologous substitutes to regenerate, maintain, or improve tissue and organ function. None more so than articular cartilage, a connective tissue which, when damaged, exhibits limited intrinsic regenerative capacity [62]. In general, tissue-engineered constructs require a highly porous artificial extracellular matrix (ECM) or scaffold material to accommodate mammalian cells and to organize tissue regeneration in a three-dimensional (3D) environment. Nevertheless, limitation in the diffusion of nutrients has been suggested as a cause for the inhomogeneous neo-cartilage distribution observed in larger tissue-engineered cartilaginous constructs, whereby, the onset of chondrogenesis occurs solely within the peripheral boundaries [127, 155, 304, 365]. Indeed, it has been demonstrated that nutrient gradients, such as oxygen in particular [232, 304], can be measured and do occur within these tissue-engineered constructs. Therefore, in an effort to improve nutrient transport to cells, there has been considerable interest in the development of bioreactors in which medium flow is applied [258, 383, 493], or which mimic the periodic compressive stresses within articulating joints [143, 325]. Although these dynamic culture conditions typically result in an improved quality of the neo-cartilage tissue formed, the 3D pore architecture present within scaffolds used for cartilage tissue engineering also likely has a large influence on tissue formation. While several investigators [35, 276, 354] have evaluated the effect of scaffold pore size on cartilage tissue formation, to the best of our knowledge, pore architecture was not investigated systematically. In characterizing porous materials it is common practice to quote an average pore size or a pore-size distribution [354]. While these are important characteristics, particularly for controlling mechanical properties, pore accessibility and the pore tortuosity are, next to the porosity, of great significance for minimizing diffusional constraints and ultimately for successful tissue-engineering applications [209, 271, 349, 517, 534].

In this study we wanted to more closely evaluate the effect of a pore architecture, and more specifically, pore accessibility, on the composition of tissue-engineered cartilage. Therefore, careful design and characterisation of porous scaffolds was necessary. The two most commonly used scaffold architectures reported in the literature for cartilage repair are porous sponges and non-woven fibre meshes [397]. At present, we are evaluating a series of amphiphilic, biodegradable poly(ether ester) multiblock copolymers as carrier materials for articular cartilage repair. The co-polymers are based on hydrophilic poly(ethylene glycol)-terephthalate (PEGT) and hydrophobic poly(butylene terephthalate) (PBT) blocks. Varying the amount and the length of the PEGT and PBT blocks offers extensive possibilities in the design of polymer systems with tailor-made properties, such as swelling, degradability and mechanical strength, as reported previously [30, 111, 422, 480].

Two porous PEGT/PBT scaffold architectures were evaluated herein; a compression-moulded / particle-leached sponge (CM), and a novel 3D-deposited fibre (3DF) scaffold. By accurately controlling the two processing techniques, the aim was to produce scaffolds with the same bulk composition and overall porosity, but different pore geometries. Scaffold architecture was then comprehensively characterised and cartilage tissue formation was evaluated on cell-seeded constructs maintained *in vitro* and *in vivo*.

Materials and Methods:

Scaffold Preparation

PEGT/PBT co-polymers were obtained from IsoTis S.A. (Bilthoven, The Netherlands). Two scaffolds with different architecture were produced from PEGT/PBT resin with a PEG molecular weight of 300 g/mol and a PEGT: PBT weight percentage ratio of 55:45.

CM scaffolds (Fig 1A, 1C) were prepared using a compression moulding and particle-leaching method as previously described [116]. Porous 3DF scaffolds (Fig 1B, 1D) were produced using a novel 3D fibre deposition technique also described previously [519]. Previous thermal analysis studies have demonstrated that the compression moulding and 3D fibre deposition processing techniques described here do not result in changes of PEG molecular weight or PEGT/PBT composition [519] and, therefore, any differences seen between scaffolds in this study could not be related to differences in scaffold composition.

Cylindrical scaffolds $\varnothing 4 \times 4$ mm, were cored from the bulk porous CM and 3DF blocks and placed on surgical needles in 250 ml spinner flasks before being steam-sterilized (15 minutes, 121°C). Sterilized samples were incubated for at least 3 hours in culture medium at 37°C to allow for scaffold hydration and serum protein adsorption prior to cell seeding.

Scaffold Characterisation

Micro-computed tomography (μ CT) - Scaffolds were scanned using a desktop MicroCT machine (μ CT-40, Scanco Medical, Bassersdorf, Switzerland) at a resolution of 12 μ m in all three spatial dimensions (X-Ray voltage 45 kVp). Two hundred 2D slices (2048x2048 pixels) were scanned of every sample covering a height of 2.4 mm. The resulting grey-scale images were segmented and a threshold applied to extract the polymer architecture and then inverted to extract the pore volume architecture. This allowed 3D reconstruction (see Fig 1C, 1D) of the total object volume (OV), scaffold volume (SV) and pore volume (PV) ($OV = SV + PV$) from stacked 2D images, which in turn could be analyzed to give information on porosity, surface area and pore size using algorithms previously developed for analyzing bone architecture [251, 348, 419, 535]. Using a surface meshing technique [284], specific scaffold surface area was calculated (total surface area/ SV). The pore size distribution was obtained by direct 3D measurement using a distance transformation technique [180], whereby the number of voxels within the total PV that could be filled by a sphere of a given diameter D_{pore} were measured (Fig 2B). The average pore diameter was obtained by taking the mean over all sphere diameters.

To characterize the scaffold accessibility, an algorithm was designed (Scanco Medical, Bassersdorf, Switzerland) to mimic mercury intrusion porosimetry [2]. In other words, by starting at the periphery of the scaffold and working inwards, at a given sphere diameter, D_{int} , the amount of accessible pore volume was measured. Using a distance transformation [180], the local diameter, D , at every point within the PV was determined. Following a thresholding operation, the volume of pores with a local sphere diameter smaller than D_{int} were suppressed. All components of this thresholded structure not connected to the 'outside air' were then discarded using a component labelling operation. The volume of the resulting

pore structure was determined and then plotted to produce a graph of the accessible pore volume versus interconnecting pore diameter D_{int} (Fig 2A).

In addition to μ CT, scaffold porosity was also determined using mass/volume techniques according to the following relationship:

$$\text{Vol\% porosity}_{\text{measured}} = (1 - V_s/V_T) \times 100\%$$

V_s (mm^3) is the apparent scaffold volume (= polymer volume) given by m/ρ , where m and ρ equal the mass of the dry scaffold (g) and the polymer density ($\rho_{300/55/45} = 1.25 \times 10^{-3} \text{ g/cm}^3$), respectively. The total scaffold volume V_T (mm^3) was given by $\pi \cdot d^2 \cdot h/4$, where d and h equal the scaffold diameter (mm) and scaffold height (mm), respectively.

Mechanical characterisation - to characterize the mechanical properties of scaffolds with varying architecture dynamic compression tests were carried out under wet conditions and compared with native articular cartilage tissue, as explained previously [519].

Cell Isolation and Culture

Chondrocytes were isolated from articular cartilage of the femoral condyles of 6-months-old bovine calves as previously described [305]. Isolated chondrocytes were seeded (3 million per scaffold) on the cylindrical ($\varnothing 4 \times 4 \text{ mm}$) scaffolds and culture in HEPES (Invitrogen)-buffered DMEM (Invitrogen) culture medium supplemented with 10% FBS (Sigma-Aldrich), 0.2 mM ascorbic acid 2-phosphate (Invitrogen), 0.1 mM non-essential amino acids (Sigma-Aldrich), 0.4 mM proline (Sigma-Aldrich), 100 units/ml penicillin (Invitrogen), and 100 $\mu\text{g/ml}$ streptomycin (Invitrogen). Cell seeding and tissue culture were carried out in spinner flasks (Bellco Glass) stirred at 60 rpm, and contained at 37°C in a humidified 5% CO_2 incubator for up to 42 days. Culture medium was replaced every 2-3 days. This study reports the evaluation of a total of 230 scaffolds (excluding controls containing no cells), divided over two independent experiments.

In vivo Implantation

Constructs cultured for 14 days as described above, were implanted in subcutaneous pockets of 6-week old nude mice (HdCpb:NMRI-nu, Harlan, The Netherlands). Animals were sacrificed at 7, 14, 21 and 28 days after implantation (i.e. 21, 28, 35 and 42 days after seeding), and constructs were processed histologically and biochemically, as described below.

Histology

Samples ($n=3$ per time point) were taken after 3, 7, 14, 21 and 35 days after seeding and fixed overnight in 0.14 M cacodylate buffer (pH = 7.2 - 7.4) containing 0.25% glutaraldehyde (Merck) and subsequently dehydrated in a graded ethanol series. Samples were then embedded in glycol methacrylate (Merck) and cut using a microtome to yield 5 μm thick sections. Sections were stained with haematoxylin (Sigma-Aldrich) and fast green (Merck) for cells and with safranin-O (Sigma-Aldrich) for glycosaminoglycans (GAG)

Scanning Electron Microscopy (SEM)

Samples ($n=3$ per time point) were taken after 3 days *in vitro* and after 14 days *in vitro* and an additional 21 days *in vivo*. Constructs were fixed and dehydrated as described above and critical point dried from liquid carbon dioxide using a Balzers CPD 030 Critical Point Dryer. Dried tissue-cultured samples or as-produced scaffolds were then sputter-coated (Cressington) with a thin gold layer and studied in a Philips XL 30 Environmental Scanning Electron Microscope (ESEM).

Immunohistochemistry

Constructs ($n=3$ per time point) were taken after 14 days *in vitro* and an additional 21 days *in vivo*. Samples were embedded in an optimal cutting temperature (O.C.T.) compound (Tissue-Tek) and cryo-sectioned to yield 5 μm thick sections, which were fixed in acetone for 8 minutes. Collagen type II was immunolocalized using an Animal Research Kit (Dako) in combination with a collagen type II antibody (1:200, II-II6B3, Developmental Studies Hybridoma Bank). After digestion for 20 minutes with 0.025% trypsin-EDTA (Invitrogen) at room temperature, samples were rinsed with PBS (Invitrogen) and incubated with peroxidase block for 5 minutes. Subsequently, the biotinylated primary antibody was applied for 15 minutes and rinsed with PBS. Streptavidin-peroxidase was then applied for 15 minutes. After rinsing with PBS, the staining was visualized using DAB-solution for 5 minutes. Counter staining was performed with haematoxylin (Sigma-Aldrich).

Biochemical Assays

Constructs ($n=3$ per time point) were taken after 3, 14, 21, 28, 35 or 42 days and digested overnight at 56°C in a solution containing proteinase K, pepstatin A and iodoacetamide (Sigma-Aldrich). Quantification of total DNA was done by Cyquant dye kit (Molecular Probes) using a spectrofluorometer (Perkin Elmer). The amount of glycosaminoglycans was determined spectrophotometrically after reaction with dimethylmethylene blue dye (DMMB, Sigma-Aldrich) [122]. Intensity of colour change was quantified immediately in a microplate reader (EL 312e Bio-TEK Instruments) by measuring absorbance at 520 nm. The amount of GAG was calculated using a standard of chondroitin sulphate B (Sigma-Aldrich). Total collagen was determined by measuring the amount of hydroxyproline present in each construct. Aliquots of proteinase K digest to be evaluated for hydroxyproline were hydrolyzed in 6N HCl at 110°C for 16 hours. The hydrolyzate was assayed for hydroxyproline using methods that have been described in detail elsewhere [341].

Statistics

Statistical significance was assessed by one-way analysis of variance (ANOVA) followed by a Student-Newman-Kuels posthoc test using Sigma Stat software (Jandal Corp.) with $p < 0.05$ as the criteria for statistical significance.

Results and Discussion:

Scaffold Characterisation

The two processing techniques used in this study, compression moulding / particle leaching and 3D fibre deposition, enabled fabrication of porous polymer scaffolds (Fig 1A, 1B, 1C, 1D) with reproducible and comparable porosities. The volume % porosity based on mass-volume techniques was in the same range as the values obtained by 3D micro-computed tomography (μ CT) analysis (Table 1). The specific scaffold surface area, was 10.0 mm^{-1} and 3.3 mm^{-1} for CM and 3DF scaffolds, respectively. Both CM and 3DF scaffolds were $\sim 100\%$ interconnected, however CM scaffolds had a considerably lower cut-off value (*i.e.* a pore size at which accessibility dropped below 90%) of $\sim 120 \mu\text{m}$ compared with a $\sim 680 \mu\text{m}$ cut-off value in 3DF scaffolds (Fig 2A). The average pore size for CM scaffolds was $182 \mu\text{m}$, but was substantially higher for 3DF scaffolds, namely $525 \mu\text{m}$ (Fig 2B). For the CM scaffold the pore sizes approximated a Poisson distribution around an average of $182 \mu\text{m}$, whilst, due to the layered organizational structure, two separate peaks were observed for the 3DF scaffolds (Fig 2B). This was related to the fibre diameter dependent pore size in the z-direction ($\sim 200 \mu\text{m}$) compared with pores generated in the x-y plane based on a 1 mm fibre spacing (*i.e.* $\sim 700 \mu\text{m}$ pore size).

Table 1 - Structural and mechanical characterisation of PEGT/PBT scaffold architecture and articular cartilage (AC).

Sample	Measured Vol% Porosity		Surface Area/Unit Vol	Avg. Pore Size (D_{pore})	Dynamic Stiffness @ 0.1Hz (MPa)
	m/V (%)	μ CT (%)	μ CT (mm^{-1})	μ CT (μm)	
CM	75.6 ± 1.9	81.8	10.0	182	1.72 ± 0.33
3DF	70.2 ± 1.8	77.6	3.3	525	4.33 ± 0.52
Bovine AC [519]					4.10 ± 1.57
Human AC (0.1 Hz) [475]					4.50

The pore volume of 3DF scaffolds could be considered as a collection of continuous straight channels, unlike tortuous path of channels in CM scaffolds, which contained dead ends and narrow interconnections. Due to the tortuous pore structure and the lower average pore size in CM scaffolds, pores could be easily be blocked with cells during seeding ("filtration effect"), thus preventing further cell access to the inner regions. Within the organised pore volume of 3DF scaffolds, the filtration effect would be less likely to occur and the diffusion distance would also be reduced.

It has been demonstrated that the effective diffusion coefficient within a scaffold is proportional to the porosity and inversely proportional to the tortuosity of the route through the pores that the substrate encounters [508]. Therefore, given that CM and 3DF scaffolds have similar porosity but different tortuosity, the effective diffusion coefficient of constructs based on 3DF scaffolds would be higher and nutrient transport would thus be enhanced in comparison to constructs based on CM scaffolds.

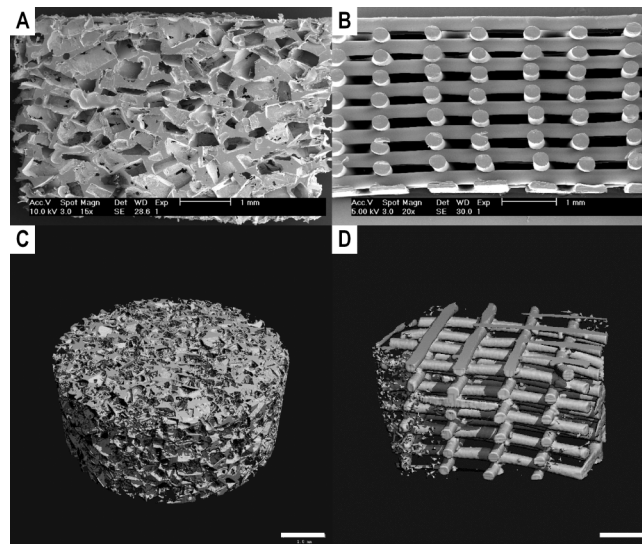


Figure 1 - Electron micrographs of CM (A) and 3DF (B) scaffolds. Three dimensional reconstruction of CM (C) and 3DF (D) scaffolds from micro computed tomography (μ CT) scans. Scale bar represents 1 mm.

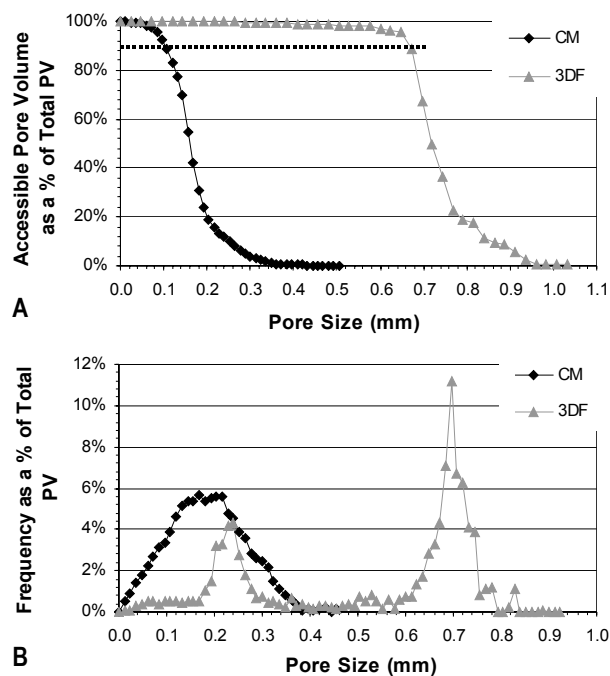


Figure 2 - Accessible pore volume distribution (A) and pore size distribution (B) for CM and 3DF scaffolds represented as a percentage of total pore volume (PV) as was assessed based on micro computed tomography scans.

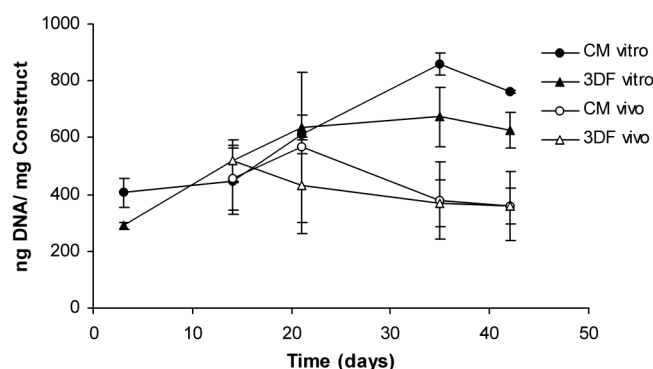


Figure 3 - DNA content of CM and 3DF constructs cultured *in vitro* and *in vivo* as assessed by Cyquant dye kit.

Cell Density of TE Constructs

After 3 days, DNA content per mg construct (proportional to the number of cells per wet weight) was slightly but significantly higher for the CM constructs (Fig 3). This was likely related to their higher surface area per unit volume available for cell attachment compared with 3DF scaffolds (Table 1). Furthermore, the filtration effect within the tortuous pore structure was a plausible cause for the higher cell numbers observed on the outside of CM constructs (not shown). At the time of implantation at 14 days, however, there were no significant differences in overall cell number between CM and 3DF scaffolds. After 35 and 42 days, DNA/mg construct was significantly lower in *in vivo* cultures and was likely due to increased cartilaginous matrix deposition compared with *in vitro* cultures.

In addition, cell numbers in CM constructs after 35 and 42 days *in vitro* culture was slightly but significantly higher in comparison to 3DF constructs, possibly due to the higher surface area per unit volume available for cell proliferation within CM constructs. No differences in cell density between scaffold architectures were observed *in vivo*.

Glycosaminoglycan (GAG) Content

After 3 days of culture in spinner flasks, cells were distributed throughout both scaffolds (Fig 4A, 4B), however, particularly for CM scaffolds, more cells were present at the periphery (not shown). Safranin-O staining demonstrated that GAG, as a measure of cartilaginous tissue formation, was already present at this early time point. During the first 14 days of culture, tissue developed within the scaffolds and staining for GAG increased in both constructs (Fig 4C, 4D). Meanwhile, a layer of spindle shaped cells developed at the periphery of the constructs. This dense layer of cells, exhibiting a more fibroblast-like morphology than a differentiated chondrocyte morphology, could possibly have hampered nutrient transport into the construct. Prolonged dynamic culture *in vitro* did not result in further increase of cartilaginous tissue (Fig 4E, 4F), and no difference in staining for GAG was observed between the two scaffold types. However, subcutaneous implantation in pockets on the back of nude mice yielded more intense staining for GAG within 3DF constructs 7 days after implantation (14+7

days) (Fig 4H). Even more neo-cartilage tissue had developed after 21 days implantation (14+21 days), displaying a distinct chondrocytic morphology (Fig 4J). In contrast, no additional production of GAG was observed within CM constructs following subcutaneous implantation (Fig 4G, 4I), demonstrating that within 3DF scaffolds implanted *in vivo*, a more favourable environment for cartilaginous matrix deposition was created.

While explants containing cultured chondrocytes appeared non-vascular, scaffolds implanted without cultured chondrocytes did not stain for GAG and were highly vascularized (inset Fig 4I, 4J).

The changes in GAG content as observed by histological evaluation using safranin-O were confirmed by the dimethylmethylene blue (DMMB) assay (Fig 5A, 5B). Again, no differences between scaffold architectures were observed for the amount of GAG produced per cell, or per mg construct, during the first 14 days *in vitro* (Fig 5A, 5B). GAG content for both constructs increased from approximately 3 μg per mg construct on day 3, to 7 μg per mg construct on day 14, *i.e.* from about 8 to 14 mg GAG per mg DNA. Prolonged dynamic culture *in vitro* resulted in a slight decrease of GAG content, which was likely due to a low production rate in combination with diffusion of GAG into the culture medium as was previously reported in other studies [363]. After subcutaneous implantation, GAG content increased, resulting in significantly higher GAG per cell values after 35 and 42 days compared with *in vitro* samples (Fig 5A, 5B). Moreover, 3DF constructs contained significantly greater amounts of GAG (15.5 μg per mg construct, or 41 mg per mg DNA) compared with CM constructs (8 μg per mg construct, or 21 mg per mg DNA, respectively). Similarly, Freed *et al.* [125] demonstrated that neo-tissue formed on fibrous PGA scaffolds had a higher GAG content compared to spongy PLLA scaffolds. However, that experiment did not clarify if the enhanced GAG formation was attributed to the scaffold architecture or the composition.

Previous studies *in vitro* using PGA-based constructs exhibited a higher GAG content (7-11 μg GAG per mg construct [125, 127, 142]) in comparison to those reported in this study for PEGT/PBT-based constructs (3-8.5 μg GAG per mg construct). In addition, upon implantation of these constructs in subcutaneous pockets in nude mice about 20 μg per mg construct was produced within 6 weeks, whereas in the present study we observed 15.5 μg GAG per mg 3DF-based construct. It should be noted, however, that in contrast to PGA, PEGT/PBT copolymers have a much slower degradation [112]. Consequently, a considerable volume of the construct will still be taken up by the biomaterial after 6 weeks and the formed neo-tissue will have an actual higher GAG content if normalized to tissue volume.

Although extensive cartilaginous tissue deposition was observed within 3DF scaffolds *in vivo*, considerably less cartilaginous tissue formed *in vitro* and no difference between the two architectures was observed. Thus, *in vitro*, further cell re-differentiation and concomitant ECM formation was limited by factors other than scaffold architecture. The conditions, which favoured cartilage formation *in vivo*, were likely related to the presence of specific host-derived growth factors [308, 467] and the absence of the dense fibrous cell layer present at the periphery of *in vitro* cultured constructs.

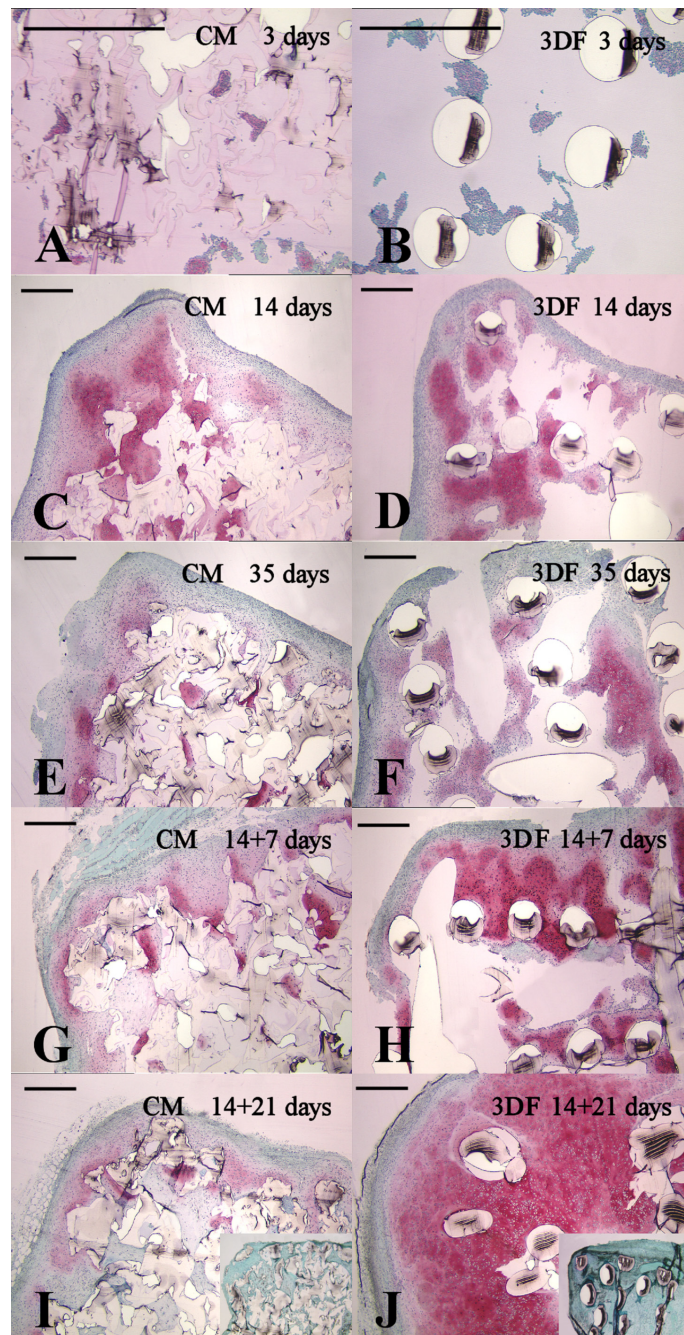


Figure 4 - Photomicrographs of safranin-O stained sections of CM (A, C, E, G, I) and 3DF (B, D, F, H, J) constructs cultured for 3 (A, B), 14 (C, D), 35 (E, F) days *in vitro* and 14 days *in vitro* and subsequently 7 (G, H) and 21 (I, J) days *in vivo*. Inset of I and J shows non-seeded controls. Scale bar represents 500 μm. ► p210.

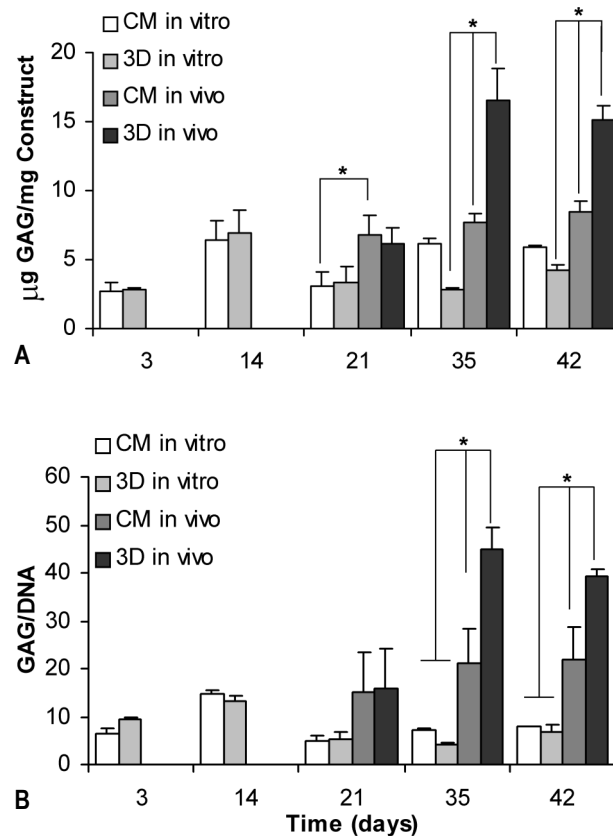


Figure 5 - Glycosaminoglycan (GAG) content per wet weight (A) and mg GAG content per mg DNA (B) of CM and 3DF constructs cultured in vitro and in vivo ($\mu\text{g GAG per mg construct}$). * = significant difference ($p < 0.05$) as assessed by DMMB staining.

Scanning Electron Microscopy (SEM)

Scanning electron microscopy confirmed histological observations that cells had attached and spread on the PEGT/PBT constructs (Fig 6A, 6B) after 3 days. CM constructs cultured for 14 days in particular exhibited pores filled with fibroblast-like cells (Fig 6C), whereas, following subcutaneous implantation, sparsely distributed round cells embedded in a ECM, a typical feature of hyaline cartilage tissue, were observed in both scaffolds as shown for the 3DF scaffold (Fig 6D). Filamentous secretions, similar to those observed on hyaluronic acid-based fibrous scaffolds [153], were present on both scaffold types. However, in accordance with histology, 3DF constructs exhibited homogeneous formation of dense ECM throughout the internal pores, whereas more areas with spindle shaped fibroblast-like cells were observed in CM constructs. In addition, few internal pores within CM constructs were completely filled with ECM. SEM analysis confirmed that cartilaginous tissue formation *in vivo* was enhanced on 3DF scaffolds.

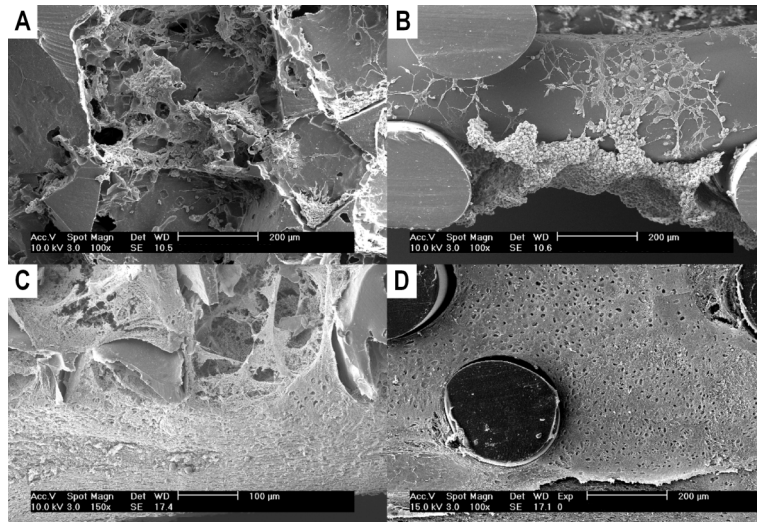


Figure 6 - Electron photomicrographs of CM (A, C) and 3DF (B, D) constructs after 3 days of *in vitro* culture (A, B) and 14 days of culture (C) and 14 days of *in vitro* culture and, subsequently, 21 days *in vivo* (D).

Collagen Content

Total collagen content was assessed using the hydroxyproline assay. Collagen content did not change after 14 days of *in vitro* culture, whereas a significant increase was observed following *in vitro* implantation (Fig 7). Although significantly more collagen per mg construct was produced *in vitro* in comparison to *in vivo*, no significant differences were observed between the two scaffold types at any of the time points assessed. Furthermore, total collagen production by bovine chondrocytes on fibrous PGA scaffolds cultured in spinner flasks for 6 weeks was reported to be approximately 3 times higher than for PEGT/PBT scaffolds used in this study [127, 142].

Given that the hydroxyproline assay cannot discriminate between collagen types (*i.e.* type I and II), qualitative immunohistochemical assay was performed on samples maintained *in vitro* for 14 days and subsequently implanted for 21 days *in vivo*. Staining for collagen type II, a specific component of the hyaline cartilage extra cellular matrix, could be demonstrated in both constructs, however, expression was never present at the peripheral edges of the constructs (Fig 8A, 8B), but distributed homogeneously throughout the inner matrix (Fig 8C, 8D).

Although differences in collagen type II content may be present between CM and 3DF constructs, using the qualitative immunohistochemical staining, we did not observe an effect of scaffold architecture on the formation of collagen type II within the present study. Similarly, Li Vecchi *et al.* [276] demonstrated that the amount of type II collagen was not influenced by the pore size (ranging between 117 μm and 334 μm) of porous hydrophilic and hydrophobic high density polyethylene (HDPE) matrices.

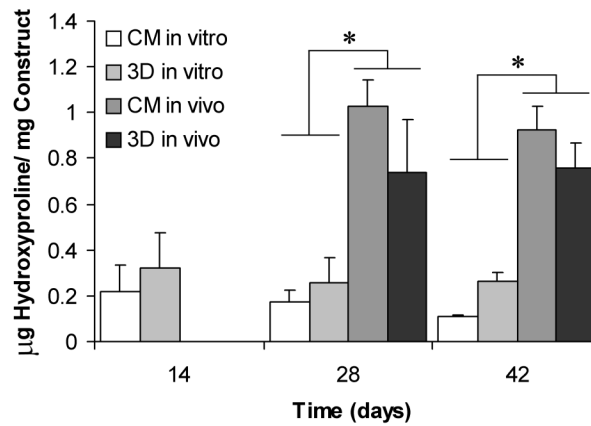


Figure 7 - Hydroxyproline content (as a measure of total collagen) per wet weight of CM and 3DF constructs cultured in vitro and in vivo.

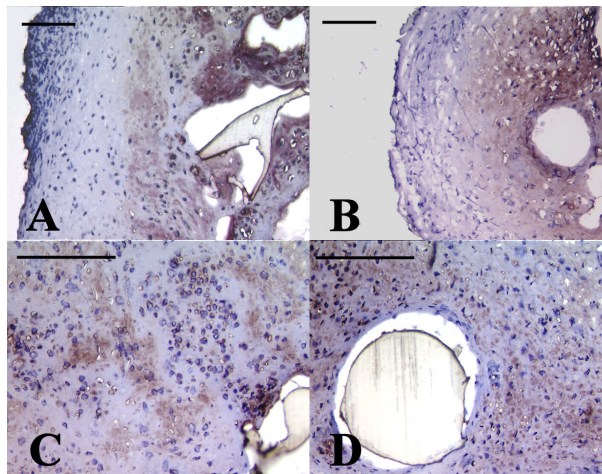


Figure 8 - Immunolocalization of collagen type II in the periphery (A, B) and centre (C, D) of CM (A, C) and 3DF (B, D) constructs cultured 14 days in vitro and, additionally, 21 days in vivo. Scale bar represents 150 µm. Collagen type II was localized mainly within the centre of the constructs. ► p211.

Mechanical Characterisation

Dynamic compression tests were performed under wet conditions in order to characterize the mechanical stability of hydrated CM and 3DF architectures compared with native articular cartilage tissue. The dynamic stiffness (0.1 Hz) of 3DF scaffolds (4.33 MPa) was higher than for CM scaffolds (1.72 MPa) even though overall porosity was similar and pore size was significantly higher in 3DF scaffolds (Table 1). This was likely due to the organised fibre structure present within 3DF scaffolds compared with the irregular tortuous pores generated by particulates in CM scaffolds. 3DF scaffolds compared favourably with dynamic stiffness

values measured for bovine articular cartilage [519] and human knee articular cartilage values obtained from literature [475] (Table 1).

Mechanical properties of fibrous PGA scaffolds were reported to be considerably lower than those of natural cartilage [295]. Although it has been shown in hyaluronic acid-based scaffolds, for example [7], that the presence of cells and deposited ECM can enhance the stability, the mechanical properties of constructs with cells will not be within the same range of those for native tissue. Due to the stability of PEGT/PBT scaffolds under dynamic mechanical compression scaffolds based on these architectures examined in this study would be suitable candidates for further *in vivo* assessment in a load bearing joint model. Moreover, it has been demonstrated that integration of immature *in vitro* cultured constructs to the surrounding articular cartilage was enhanced as opposed to mature constructs [364], and this may be particularly relevant in articular cartilage repair strategies that involve early implantation of cell-seeded scaffolds. Under this environment, these constructs could support *in vivo* loading conditions whilst simultaneously exposing cells and neo-tissue to specific stimuli present in the *in vivo* environment.

Conclusions:

To the best of our knowledge, no data has been reported in the literature that specifically demonstrates the effect of pore architecture, in particular pore accessibility and pore tortuosity, on the formation of neo-cartilage tissue. In the present study we evaluated two ~100% interconnected porous PEGT/PBT scaffolds, a compression-moulded / particle-leached sponge (CM), and a novel 3D-deposited fibre (3DF) scaffold.

In vivo significantly more cartilaginous tissue was formed within 3DF constructs compared to CM constructs and collagen type II was found present regardless of scaffold type. *In vitro*, however, culture conditions did not support extensive cartilaginous tissue formation and consequently no differences were observed between the two scaffold architectures. Although GAG and total collagen content for was reported higher for fibrous PGA-based constructs, these will not, in contrast to PEGT/PBT-based constructs, possess mechanical properties in the range of natural cartilage.

In conclusion, within 3DF PEGT/PBT scaffolds with a less tortuous and more accessible pore volume, an environment is created *in vivo* that enhances matrix deposition. Therefore, tissue-engineered constructs based on these scaffolds hold particular promise for treatment of articular cartilage defects.

Acknowledgments:

The authors gratefully acknowledge Dr. I. Martin for his comments regarding this manuscript, Dr. Andres Laib (Scanco Medical AG, Bassersdorf, Switzerland) for assistance with micro-computed tomography analysis as well as funding from the European Commission (FP5 project "Scafcart" G5RD-CT-1999-00050). The collagen type II monoclonal antibody (developed by T.F. Linsenmayer) was obtained from the Developmental Studies Hybridoma Bank developed under the auspices of the NICHD and maintained by The University of Iowa, Department of Biological Science, Iowa City, IA 52242.

Chapter 5

The Effect of PEGT/PBT Scaffold Architecture on Oxygen Gradients in Tissue Engineered Cartilaginous Constructs

Malda J.^{1,2,3}, Woodfield T.B.F.^{1,2}, van der Vloodt F.³, Kooy F.K.³, Martens D.E.³, Tramper J.³, van Blitterswijk C.A.^{1,2}, Riesle J.²

¹ Institute for Biomedical Technology, University of Twente, Enschede, The Netherlands

² IsoTis S.A., Bilthoven, The Netherlands

³ Food and Bioprocess Engineering Group, Wageningen University, Wageningen, The Netherlands

Abstract:

Repair of articular cartilage defects using tissue engineered constructs composed of a scaffold and cultured autologous cells holds promise for future treatments. However, nutrient limitation (e.g. oxygen) has been suggested as a cause of the onset of chondrogenesis solely within the peripheral boundaries of larger constructs.

In the present study, oxygen gradients were evaluated by microelectrode measurements in two porous poly(ethylene glycol)-terephthalate poly(butylene terephthalate) (PEGT/PBT) scaffold architectures, a compression-moulded and particle-leached sponge (CM) and a 3D-deposited fibre (3DF) scaffold. During the first 14 days *in vitro*, gradients intensified, after which a gradual decrease of the gradients was observed *in vitro*. *In vivo*, however, gradients changed instantly and became less pronounced. Although similar gradients were observed regardless of scaffold type, significantly more cells were present in the centre of 3DF constructs after two weeks of *in vivo* culture.

Our results stress the importance of a rationally designed scaffold for tissue-engineering applications. Organised structures, such as the 3DF PEGT/PBT polymer scaffolds, offer possibilities for regulation of nutrient supply and, therefore, hold promise for clinical approaches for cartilage repair.

‡ Malda J, Woodfield TBF, van der Vloodt F, Kooy FK, Martens DE, Tramper J, van Blitterswijk CA, Riesle J. The Effect of PEGT/PBT Scaffold Architecture on Oxygen Gradients in Tissue Engineered Cartilaginous Constructs. *Biomater* **2004** (in press).

Introduction:

Implantation of a tissue-engineered polymer-cartilage construct may be a potential treatment for articular cartilage defects. However, the creation of constructs of clinically relevant dimensions, homogeneously filled with neo-cartilage tissue still poses a challenge. High-density cell cultures are often limited by inadequate supply of nutrients [69]. More specifically, the supply of oxygen already becomes limiting for the culture of tissues thicker than 100-200 μm [99, 273]. Previous investigations tried to overcome diffusion limitations within cartilage tissue-engineered constructs by bioreactor culture [126, 363, 380, 382, 520] for example. A bioreactor provides control over the hydrodynamic factors around the construct, and hence, external diffusion limitations can be minimized. Furthermore, mechanical loading of constructs [71, 325, 420] has proven to be an effective tool to increase histological and biochemical properties of tissue engineered constructs, partly by decreasing the internal diffusion constraints. Despite the fact that external and internal mass transfer within the previously described dynamic systems is increased, considerable gradients (e.g. of oxygen [232, 304]) will still be present inside tissue engineered constructs, due to the required size and the high cell density. Consequently, for the mitigation of these gradients there is still need for better understanding of the internal diffusion constraints. Although the presence of interconnecting channels is commonly stated as one of the prerequisites that a proper tissue-engineering scaffold should fulfil [209], its direct effect on the supply of nutrients to the cells has not been described. Within the present study we used porous biodegradable segmented-block-copolymer scaffolds. The biocompatibility of this material, which is composed of poly(ethylene glycol)-terephthalate (PEGT) and poly(butylene terephthalate) (PBT) segments, has been demonstrated in several studies [18, 29, 156, 326, 401, 480]. By varying the ratio of the alternating soft (PEGT) and hard (PBT) segments the mechanical properties of this material can be tailored to match the mechanical properties of cartilage [422, 517]. In addition, formation of cartilage-like tissue on PEGT/PBT scaffolds has been demonstrated *in vitro* and *in vivo* [302].

The experiments described within this communication are part of a series of studies that included the production [519] of these scaffold types as well as the characterisation and evaluation of the effect of scaffold architecture on cartilaginous matrix formation [307]. The aim of the present study was to evaluate the effect of scaffold architecture on the resulting oxygen gradient during *in vitro* and *in vivo* cartilaginous tissue formation. We employed two porous PEGT/PBT scaffold architectures, a compression-moulded / particle-leached sponge (CM), and a 3D-deposited fibre (3DF) scaffold (Fig 1). By controlling the two processing techniques, scaffolds with the same bulk composition and overall porosity, but different pore sizes and pore tortuosity could be produced. The average pore size of the CM scaffold was 182 μm , as opposed to 525 μm of the 3DF scaffolds [307]. We hypothesized that the organised pores of the 3DF scaffold, with its less tortuous and more open structure, would result in a less pronounced oxygen gradient within the constructs during *in vitro* and *in vivo* culture. To verify this hypothesis, constructs were cultured in spinner flasks and implanted subcutaneously in nude mice. Oxygen gradients were measured using a microelectrode, whilst spatial cell distribution was monitored by means of safranin-O staining, DNA quantification and image analysis.

Materials and Methods:

Scaffold Preparation

PEGT/PBT co-polymers were obtained from IsoTis S.A. (Bilthoven, The Netherlands) with a composition denoted as a PEGT b PBT c , where a represents PEG molecular weight (MW, g/mol), and b and c represent the weight percentage (wt%) of the PEGT and PBT blocks respectively. Two model scaffold types (~80% porous) with different architecture were produced from 300PEGT55PBT45 resin. Porous CM scaffolds were prepared using a compression moulding and particle leaching method [116] and porous 3DF scaffolds were produced using a 3D fibre deposition technique [519].

Cylindrical scaffolds (4 x 4 mm), were cored from the bulk porous CM and 3DF blocks and placed on surgical needles in 250 ml spinner flasks (Bellco, Vineland, NY) before being steam-sterilized (15 minutes, 121°C). Prior to cell seeding, samples were incubated for at least 3 hours in culture medium containing HEPES (Invitrogen)-buffered DMEM (Invitrogen) supplemented with 10% FCS (Sigma-Aldrich), 0.2 mM ascorbic acid 2-phosphate (Invitrogen), 0.1 mM non-essential amino acids (Sigma-Aldrich), 0.4 mM proline (Sigma-Aldrich), 100 units/ml penicillin (Invitrogen), and 100 µg/ml streptomycin (Invitrogen) at 37°C to allow for scaffold hydration and attachment of serum proteins.

Cell Seeding and Culture

Chondrocytes were isolated from articular cartilage of the femoral condyles of 6-month-old bovine calves as described previously [302]. Isolated chondrocytes were seeded on the cylindrical (4 x 4 mm) scaffolds at a density of 3 million cells per scaffold. Seeding and tissue culture were performed in spinner flasks stirred at 60 rpm, and contained at 37°C in a humidified 5% CO₂ incubator up to 42 days. Culture medium was replaced every 2-3 days.

In vivo Implantation

Chondrocytes cultured for 14 days on cylindrical PEGT/PBT scaffolds as described above were implanted in subcutaneous pockets of 6-week-old nude mice (HdCpb:NMRI-nu, Harlan, The Netherlands). Animals were sacrificed after either 7, 14, 21 or 28 days after implantation.

Measurement of Oxygen Gradients

Glass oxygen microelectrodes [412] connected to a picoammeter, were mounted in a micromanipulator. The micro-electrode (tip $\varnothing = 5 \mu\text{m}$) in combination with a micromanipulator, allows the determination of oxygen profiles with a spatial resolution of about 10 µm [307, 372, 406]. Before each measurement, the electrode was calibrated using a two-point calibration with air saturated culture medium and saturated (anoxic) Na₂SO₃ solution. Samples were confined in order to prevent diffusion from the sides or the bottom and then placed in a flow cell, which was perfused with air saturated (21% oxygen) culture medium at 37°C. After 1 hour of equilibration, the electrode was introduced into the sample

to a depth of 2500 μm at different locations (i.e. in the centre, 1.0 mm from the centre and 1.5 mm from the centre) while mounting the construct surface and microelectrode tip microscopically. Oxygen concentration was recorded until a stable reading was obtained. Subsequently, the electrode was retracted stepwise (100 μm) from the sample and the readout was registered electronically. This procedure was repeated three times for each location and data obtained for the different locations were averaged.

Cell Distribution Measurements

Construct samples ($n=3$) for biochemical quantification of DNA were taken after 3, 14 and 35 days of culture and after 14 days *in vitro* and an additional 14 days *in vivo*. Constructs were placed in a solution containing proteinase K (1 mg/ml), pepstatin A (10 $\mu\text{g/ml}$) and iodoacetamide (185 $\mu\text{g/ml}$) (Sigma-Aldrich) overnight at 56°C to digest the extra-cellular matrix (ECM) formed during culture. Quantification of total DNA was as described previously [304].

Spatial distributions within constructs were determined from histological sections. Samples were stained with Vectashield mounting medium containing DAPI (Vector laboratories) and colour images ($n = 7-11$ per sample) were acquired at successive tissue depths. Images were obtained using a digital camera (Progressive 3CCD, Sony) mounted on a fluorescence microscope (E600, Nikon). DAPI staining was visualized using a XF-57 filter (Omega Optical). The number of blue pixels per area was determined and assumed to be proportional to the number of cells in that area. By combining the obtained data with the results of the DNA assay, cell distributions were calculated. Cell distributions were obtained by averaging 8 measurements.

Statistics

Statistical significance was assessed by analysis of variance (ANOVA) followed by Student-Newman-Kuels posthoc test using Sigma Stat software (Jandal Corp.) with $p < 0.05$ as the criteria for statistical significance.

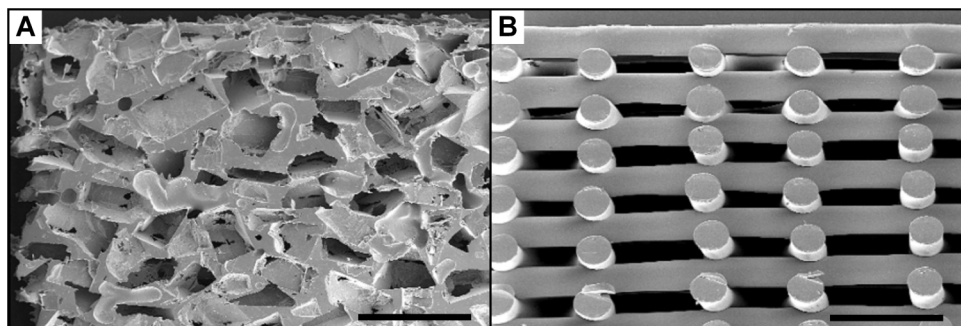


Figure 1 - Scanning electron micrograph of (A) a compression-moulded and particle-leached sponge (CM), and (B) a 3D-deposited fibre (3DF) scaffold. Scale bar represents 1 mm.

Results and Discussion:

In the present study we evaluated the effect of scaffold architecture on oxygen gradients in tissue engineered cartilaginous construct. Two different polymer scaffolds of the same bulk composition were used, a tortuous compression-moulded / particle-leached sponge (CM) and an organised 3D-deposited fibre (3DF). Constructs for the evaluation of oxygen gradients were cultured *in vitro* and *in vivo*. The effects of these two scaffold architectures regarding cartilaginous tissue formation has been described in detail elsewhere [307].

Scaffolds implanted without cultured chondrocytes had, besides the presence of tissue with a fibroblast-like morphology (results not shown), a macroscopically red appearance and contained numerous blood vessels at the time-point of explantation, regardless of scaffold architecture (Fig 2A, 2B). In contrast, implants containing cultured chondrocytes, did not show any signs of vascularization within the construct, whereas some superficial vascularization was observed on the outside of the implants at all time points assessed (arrow Fig 2C, 2D).

The absence of blood vessels in tissue-engineered cartilaginous constructs, likely to be related to the secretion of anti-angiogenic factors by the cells [343], has been reported previously by other investigators [125].

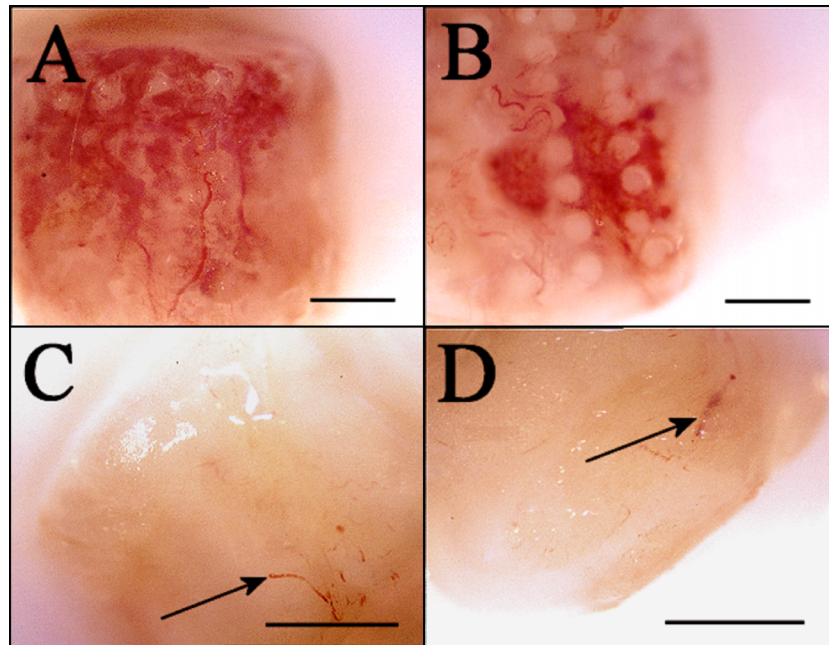


Figure 2 - Photomicrograph of CM (A, C) and 3D (B, D) constructs after 28 days *in vivo* containing no cells at time point of implantation (cross section) (A, B) and seeded with 3 million cells and pre-cultured cultured for 14 days *in vitro* (C, D). Arrow indicates superficial blood vessels. Scale bar represents 1 mm. ► p212.

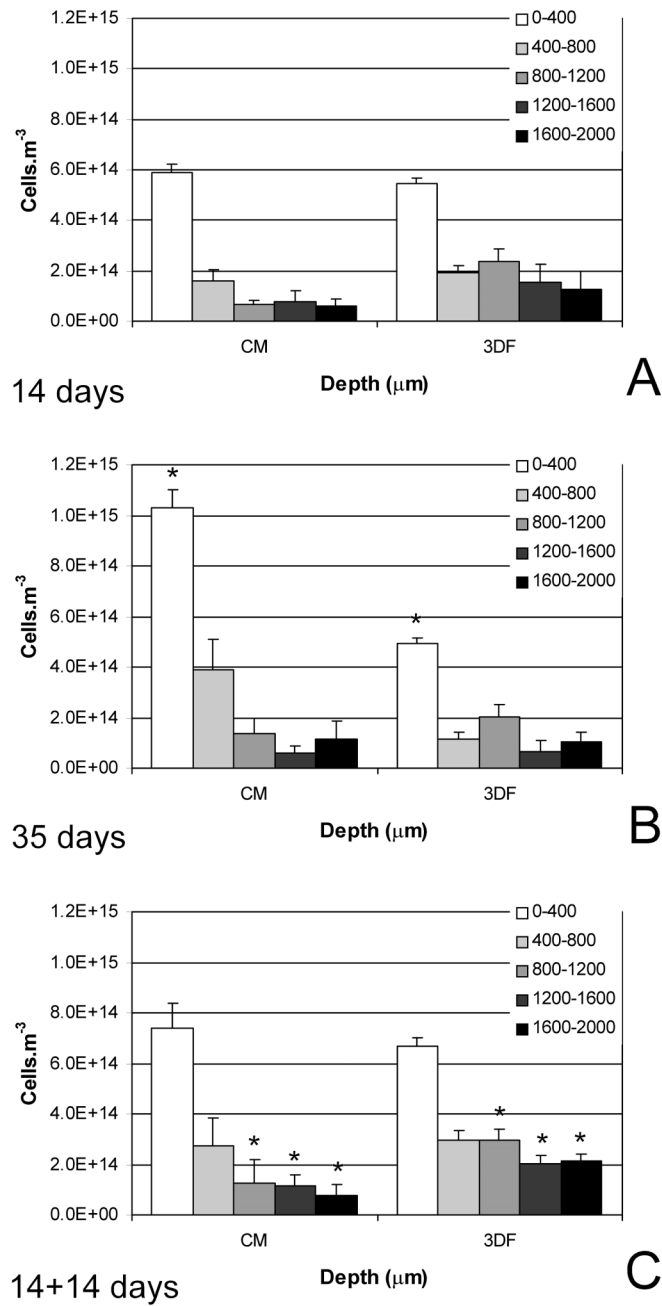


Figure 3 - Cell distribution within CM and 3DF scaffolds after 14 days (A) and 35 days in vitro (B) and 14 days in vitro and an additional 14 days in vivo (14+14 days) (C). 0 = outside, 2000 = centre, * = significantly different from other scaffold.

Cell Distribution Measurements

Within CM constructs, cell density within the peripheral boundaries significantly increased during *in vitro* culture (Fig 3A, 3B), whereas in the inner regions (1200-2000 μm), only small numbers of cells were present (Fig 3). Similarly, peripheral cell densities of 3DF constructs were higher than those observed centrally, however, the difference between the different depth regions was not as distinct as observed in CM constructs (Fig 3). Moreover, cell density within the first 400 μm was about twice as high in CM constructs in comparison to 3DF constructs after 35 days of *in vitro* culture (Fig 3B). In addition, overall cell densities observed *in vivo* in the inner regions (800-2000 μm) of 3DF constructs were significantly higher in comparison to CM constructs (Fig 3C).

We previously demonstrated [307] that more surface area for cell attachment is available in the CM scaffolds and, consequently, more cell-aggregates were formed in the 3DF scaffolds. Within these aggregates re-differentiation can be enhanced by the so-called community effect [160]. Due to the possible excretion of signalling agents by these activated cells, proliferation within the peripheral boundaries of 3DF constructs could be inhibited, resulting in a less pronounced fibrous capsule surrounding the construct, as was demonstrated by image analysis after 35 days (Fig 3B). Especially at later time points, no noticeable changes in cell density were observed in the centre *in vitro* and minimal amounts of matrix were deposited. On the other hand, cells in 3DF samples are more homogeneously distributed and more cartilage-like tissue was deposited *in vivo* [307]. Due to the significantly higher number of cells observed in the inner regions of 3DF scaffolds, oxygen requirements could increase.

Microelectrode Oxygen Measurements

Oxygen profiles could be measured reproducibly with the microelectrodes. Measurements, up to 2000 μm of depth, confirmed that oxygen concentrations decrease with depth within cartilaginous tissue-engineered constructs. The shape of the oxygen profiles considerably changed over the first 14 days of culture as is shown in Figure 4. From 3 to 14 days onward the oxygen gradient became steeper for both constructs. This effect may have been caused by the increase in cell density in combination with the development of the fibrous capsule, which typically forms around a cartilaginous construct [131, 365]. Alternatively, continual matrix formation within the pores, may block any potential convection through the scaffold and, thus, potentially decreasing the permeability of nutrients within the construct [128].

To facilitate comparison of samples taken at multiple time points, the area under the oxygen gradient curve was calculated between 0 and 2000 μm for CM as well as 3DF constructs at all time points (Fig 5). Data was normalized to the curves obtained from empty control scaffolds (*i.e.* no gradient). Within both constructs, gradients intensified during the first 14 days of culture (see also Fig 4) and were more pronounced within CM constructs (Fig 5). Oxygen gradients within constructs implanted subcutaneous in nude mice after 14 days of *in vitro* culture, became markedly less steep within 7 days of implantation. However, at subsequent time points (14, 21 and 28 days of implantation), no further changes in oxygen gradient profile of *in vivo*-constructs were observed. *In vitro*, gradients levelled off gradually with culture time, after they had intensified during the first 14 days. Moreover, after 42 days of *in vitro*-culture, gradient profiles were comparable to those observed for the *in vivo*-samples. No distinct

difference in oxygen gradient development with time was observed between the two scaffold architectures (CM and 3DF).

A decrease in surface area under the oxygen gradient curve (Fig 5), can be explained by an increase in cell density and/or specific oxygen consumption and by a decrease of the overall diffusion coefficient. Cell density *in vitro*, increases in the outer layers of the CM construct whereas, in 3DF constructs the concentration stays relatively constant (Fig 3). In addition, the oxygen diffusion coefficient *in vitro*, could change slightly by the deposited tissue. Consequently, the most likely cause of the increase in surface area under the oxygen gradient curve is a decrease of the specific oxygen consumption rate. Like wise, *in vivo* cell concentrations appear relatively constant and the oxygen diffusion coefficient remains constant or decreases slightly, again leading to a decrease in specific oxygen consumption rates of the transplanted cells.

Given the low oxygen availability in the *in vivo*-environment, in addition to the presence of growth factors supplied by the host, cells may have been stimulated to adapt to the low oxygen conditions. It has previously been demonstrated that chondrocytes can adapt to low oxygen conditions [409], and hypoxia inducible factor 1 (HIF-1) is one of the major regulators of the hypoxic response, controlling the expression of genes associated with metabolic function [283, 430, 435]. Accordingly, re-differentiating chondrocytes [78, 365] have, like chondrocytes in native cartilage [415], a lower specific oxygen consumption in comparison to chondrocytes maintained as single cells [168, 356].

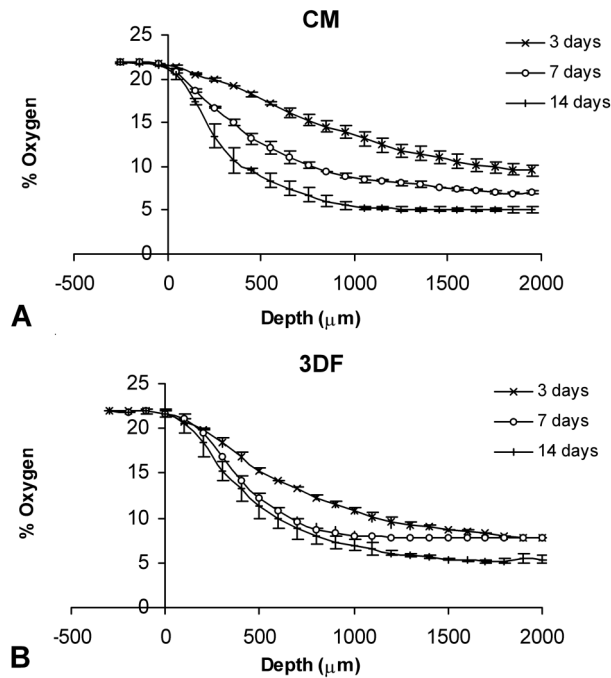


Figure 4 - Oxygen concentrations with depth in CM (A) and 3DF (B) constructs cultured for 3, 7 and 14 days.

Oxygen measurements were performed *ex-vivo*. Therefore, differences observed for *in-vivo* samples may be attributed to confounding effects of experimental setup, e.g. cells could respond to the transfer to the *ex-vivo* environment by changing their metabolism.

Vascularization of the implants can be excluded as a cause for the weakening of the gradients and the gradual increase in minimal oxygen concentration measured after subcutaneous implantation. While explants of polymer scaffolds without cultured chondrocytes were highly vascularized, explants with cultured chondrocytes contained no blood vessels except for some superficial vascularization within the fibrous capsule around the implants.

Overall, it was noted that oxygen levels in cartilaginous constructs reached a non-zero plateau at a depth of approximately 1000 μm , indicating that oxygen is not the first nutrient to become limiting. Similarly, Horner and Urban [190] demonstrated that, in studies on the supply of nutrients to cells from the nucleus pulposus of the intervertebral disc, glucose rather than oxygen was the critical nutrient. In this case, glucose could also be the limiting factor, since these cells obtain the majority of their energy mainly by glycolysis [437]. Alternatively, the observed effect could also be caused by limited diffusion of lactate out of the constructs. Given that chondrocyte metabolism is mainly anaerobic, lactate might have accumulated and caused the pH within the constructs to decrease [455], possibly creating a harmful environment for the chondrocyte.

Figure 6 shows the minimal oxygen tension measured in the centre of the constructs (depth = 2000 μm) over the entire culture period. Minimal oxygen concentrations followed a similar trend as was observed in Figure 5. Minimal oxygen concentration decreased gradually during the first 14 days to about 5%, whereas at later time-points the concentration gradually increased to approximately 13% and 15.5% for *in vitro*- and *in vivo*-samples, respectively. Overall, the minimal oxygen concentrations observed at 21 till 42 days *in vivo* are higher in comparison to the concentrations measured in samples maintained *in vitro*. However, it should be stressed that oxygen measurements of these samples were performed *ex-vivo*.

Thus, the measured values do not reflect the oxygen concentrations experienced by the cells prior to harvesting. Before the analysis, the samples were equilibrated under aerobic conditions, which may explain the rather mild gradients and high oxygen concentrations observed within these constructs.

Kellner *et al.* [232] recently determined oxygen gradients in PGA-cartilage constructs *in vitro* during a 3-week culture at 21% oxygen using a fluorescent sensor. In line with our observations, they found that gradients were intensified at day 21 in comparison to day 1. However, oxygen concentrations observed by Kellner *et al.* in the centre of the constructs were low (<1%) and did not change significantly with time, whereas we found higher values that did change with culture time. The use of a static culture system and slightly larger constructs (5 mm diameter) are likely causes for the observed differences.

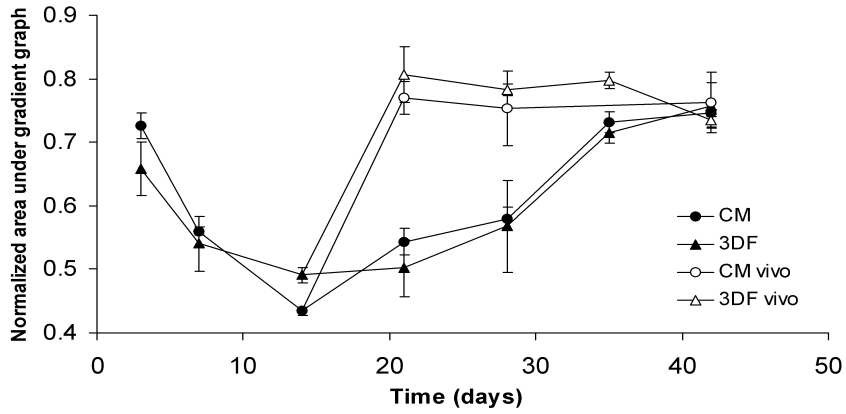


Figure 5 - Average surface area under the oxygen gradient curves of CM and 3DF constructs *in vitro* and *in vivo*. Normalized to surface area under the curve when no gradient is present. Data represent average \pm SD of three or four independent measurements.

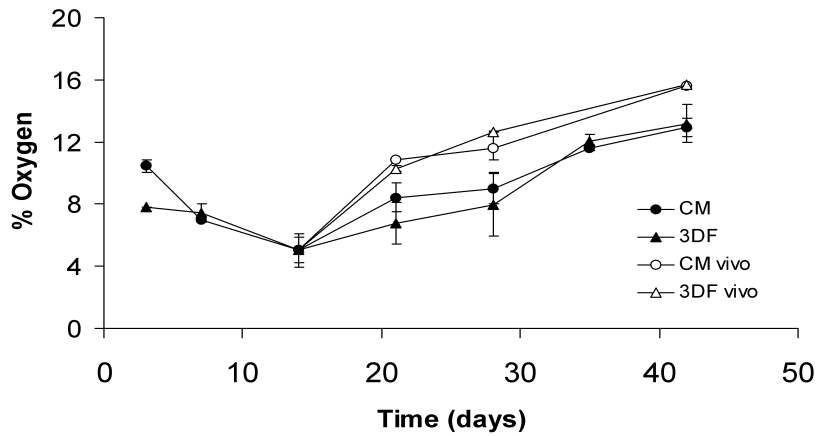


Figure 6 - Minimum of oxygen partial pressure within the construct that was reached within 2000 μ m of depth. Data represent the average \pm SD of three or four independent measurements. All samples were equilibrated at 21% oxygen prior analysis.

Conclusions:

Our results demonstrate that oxygen gradients are present in polymer-cartilage constructs, *in vitro* as well as *in vivo*. In addition, we showed that these gradients intensify during the first 14 days of culture under the conditions applied. Subsequently, regardless of scaffold architecture employed, gradients within *in vivo* constructs rapidly decreased with time, whilst *in vitro*, a gradual decrease in gradient intensity was observed. However, the organised pores of the 3DF scaffold, with its less tortuous and more open structure than the CM scaffold, did not result in less pronounced oxygen gradient within the constructs. Nevertheless, cell distribution on 3DF scaffolds was more homogeneous and cartilage-like tissue deposition *in vivo* is enhanced compared to CM scaffolds. Most likely, the more homogeneous cell distribution in 3DF constructs is compensated by a lowered specific oxygen consumption of the cells caused by the presence of surrounding cartilaginous extra-cellular matrix.

In conclusion, we did not observe an effect of scaffold architecture on oxygen gradients within the present study. However, cell distribution and matrix deposition were enhanced in 3DF scaffolds, stressing the importance of a rationally designed scaffold for cartilage tissue-engineering applications, that offers possibilities for regulation of nutrient supply.

Acknowledgments:

The authors gratefully acknowledge Bert van Groen and Paul le Comte (Department of Chemical Engineering, University of Amsterdam, The Netherlands) for their excellent assistance with the oxygen microelectrode measurements.

Chapter 6

Polymer Scaffolds Fabricated with Organised Pore-Size Gradient Structures as a Model for Studying the Zonal Organisation Within Tissue Engineered Cartilage Constructs

Woodfield T.B.F.^{‡1,2}, van Blitterswijk C.A.¹, de Wijn J.², Sims T.J.³, Hollander A.P.³, Riesle, J.^{1,2}

¹ Institute for Biomedical Technology, University of Twente, Enschede, The Netherlands

² IsoTis S.A., Bilthoven, The Netherlands

³ Department of Rheumatology, University of Bristol, Bristol, United Kingdom

Abstract:

The zonal organization of cells and extracellular matrix constituents within articular cartilage are important for its biomechanical function in diarthroidal joints. Tissue engineering strategies adopting porous three-dimensional (3D) scaffolds offer significant promise for the repair of articular cartilage defects, yet few approaches have accounted for the zonal structural organization as in native articular cartilage. In this study, the ability of anisotropic pore architectures to influence the zonal organization of chondrocytes and ECM components was investigated.

Using a novel 3D fibre deposition (3DF) technique, we designed and produced 100% interconnecting scaffolds containing either homogenously-spaced pores (1 mm fibre spacing, $\approx \text{Ø}650 \mu\text{m}$ pore size) or pore-size gradients (0.5 – 2.0 mm fibre spacing, $\approx \text{Ø}250\text{--}1650 \mu\text{m}$ range), but with similar overall vol% porosity ($\approx 80\%$) and volume fraction available for cell attachment and ECM formation.

In vitro cell seeding showed that pore-size gradients promoted a similar anisotropic cell distribution as the superficial (S), middle (M) and lower (L) zones in immature bovine articular cartilage, irrespective of dynamic or static seeding methods. There was a direct correlation between zonal scaffold volume fraction and both DNA and GAG content. Prolonged tissue culture *in vitro* showed similar inhomogeneous distributions in zonal GAG and collagen type II accumulation but not GAG/DNA, and levels were an order of magnitude less than in native cartilage.

In this model system, we illustrated how scaffold design and novel processing techniques can be used to develop anisotropic pore architectures for instructing zonal cell and tissue distribution in tissue engineered cartilage constructs.

[‡] Woodfield TBF, van Blitterswijk CA, de Wijn J, Sims TJ, Hollander AP, Riesle, J. Polymer Scaffolds Fabricated with Organised Pore-size Gradient Structures as a Model for Studying the Zonal Organisation Within Tissue Engineered Cartilage Constructs. *Tissue Eng* **2004** (submitted).

Introduction:

It is well established that the regenerative capacity in damaged or diseased articular cartilage is limited [60, 62, 203, 436, 517]. Numerous strategies have been employed to deliver or recruit reparative cells to the defect, with or without a three-dimensional (3D) scaffold, for the expressed purpose of production and organization of extracellular matrix (ECM) components [49, 61, 62, 203, 205, 517]. It has been noted, however, that virtually none of these cell- or scaffold-based cartilage repair strategies employed to date account for the high degree of topographical organization of cells and ECM constituents within native hyaline cartilage [203, 517].

Chondrocytes are responsible for the synthesis and maintenance of articular cartilage, and yet occupy only a small portion (typically less than 2%) of the total volume of adult tissue [207] compared with the remaining interstitial water ($\approx 80\%$) and ECM components ($\approx 20\%$), such as type II collagen, non-collagenous proteins and a high concentration of cartilage proteoglycans [61, 314]. Mature chondrocytes are well differentiated in their lineage and the ECM in which they assemble has a highly organised internal structure [61, 207]. Distinct variations in cell density and morphology, collagen fibril diameter and orientation, water concentration, and glycosaminoglycan (GAG) concentration exist with depth from the surface [61, 62, 207, 314, 410, 472] and can be divided into four zones: the superficial, middle, and deep zones, and the zone of calcified cartilage, as described in Figure 1. Furthermore, chondrocytes from superficial, middle and deep zones have been shown to exhibit different metabolic activities [516], and in 3D culture experiments maintain their ability to synthesize ECM components specific to their zonal origin [234, 501].

The complex zonal organization and interaction between solid ECM and fluid components within articular cartilage are directly related to its biomechanical function [85, 157, 268, 281, 288, 344, 346, 429, 475, 503]. It provides the tissue with near frictionless articulation and remarkable load bearing abilities due to its viscoelastic behaviour, as well as zone- and frequency-dependant stiffness under mechanical compression. The inexorable functional demands necessary in load bearing cartilage may require the repair tissue to closely resemble that of native tissue in terms of composition and organization for long term success [157, 288, 346, 517]. Since chondrocytes are responsible for synthesis of cartilage ECM, the hypothesis is that by imitating the zonal organization within native tissue, the local cell environment will also stimulate synthesis of an organised cartilage construct.

As a step in this direction, recent studies have investigated the possibility of incorporating biological recognition or "instructive" features into biomaterial implants [197, 198, 517]. With respect to cartilage tissue engineering, polymer scaffolds with cell-excluding barriers or vertically oriented pores or channels have been developed [209, 274, 445], as well as seeding methods using cells suspended in photopolymerizing hydrogels [234, 438], agarose [359] or alginate [16]. Moreover, instead of using a heterogeneous mixture of cells isolated from full-thickness cartilage, these studies in gels typically involved separate expansion and/or culture of zonal cell populations, isolated from the superficial, middle and deep zone cartilage, and have assisted in tailoring an anisotropic cell distribution or tissue exhibiting specific superficial zone proteins [238, 474]. To our knowledge, experiments using porous 3D scaffolds designed to investigate the zonal organization of tissue-engineered cartilage (e.g. using pore

gradients) have not been reported. These studies, which attempt to embed biological recognition or cell instructive features within scaffolds, offer considerable challenges based on the ability to both fabricate and characterize complex, anisotropic scaffold architectures in order to relate concomitant tissue responses to these architectures.

We previously described a novel 3D fibre deposition technique which allows accurate design of polymer scaffolds with controlled porosity, pore size and mechanical properties for cartilage tissue-engineering applications [519]. By further adapting this 3D scaffold technology, the initial aim of this study was to design model 3D fibre-deposited scaffolds containing: (a) homogeneously-sized pores or pore-size gradients, (b) similar scaffold volume fraction (*i.e.* surface to volume ratio), (c) similar overall porosity for cell attachment and ECM synthesis, and (d) a 100% interconnecting pore volume to promote cell infiltration and maximize nutrient/waste exchange throughout. Since seeding techniques can also influence the distribution of cells within porous polymeric scaffolds [495], we adopted two techniques that allowed either a random cell distribution or the direct placement of cells, *i.e.* dynamic seeding in stirred suspension (spinner flask) and static cell injection respectively. For the static seeding method, scaffolds containing homogeneously-sized pores or pore-size gradient were constructed with a dense basal film to prevent cell loss through the highly interconnected pore volume.

Finally, the main aim of the study was to quantitatively evaluate zonal chondrocyte distribution and organization of cartilage ECM components, as measured by DNA, glycosaminoglycan (GAG) and collagen type II content, in response to these model scaffold geometries and seeding regimes following *in vitro* culture. Furthermore, results comparing zonal cell and ECM formation on scaffolds *in vitro* with native bovine articular cartilage are reported herein.

Materials & Methods:

3D-Deposited Scaffolds:

Porous poly(ethylene glycol)-terephthalate - poly(butylene terephthalate) (PEGT/PBT) co-polymer scaffolds (PEG molecular weight = 300, PEGT wt% = 55, PBT wt% = 45) were produced using a novel 3D fibre-deposition technique described previously [519]. Briefly, scaffolds were constructed by successively layering a 0°-90° pattern of molten co-polymer from a Ø250 µm nozzle onto a computer controlled x-y-z table. By programming different fibre deposition paths into the computer software, it was possible to generate a range of scaffold architectures by accurately controlling the fibre spacing from one layer to another [519].

In this study, scaffolds were produced with either a homogeneous 1 mm fibre spacing (*1mm*) or a gradient in fibre spacing (*Grad*) throughout the height of the construct. More specifically, *Grad* scaffolds were constructed by initially depositing four 0°-90° layers with a fibre spacing of 2.0 mm, followed by another four layers at 1.0 mm, and finally only one layer at 0.5 mm at the upper surface (Fig 2). Therefore, the 2.0 mm spaced region represented the deep zone, or lower 45% of the scaffold (labelled *L*); the 1.0 mm spaced region represented

the middle, or middle 45% of the scaffold (labelled M); and the 0.5 mm spaced region represented the upper, or superficial 10% of the scaffold (labelled S).

In addition, scaffolds with a homogenous 1 mm fibre spacing (*1mmF*) or a pore gradient (*GradF*) were also produced by directly depositing fibres on a dense PEGT/PBT film approximately 50 μm in thickness in order to provide a barrier to cell and nutrient infiltration, similar to that present within the bone-cartilage interface in articulating joints (Fig 2). Films were solution-cast from the same PEGT/PBT co-polymer composition as the 3D scaffolds using a technique described previously [375].

For cell culture experiments, $\varnothing 7$ mm by 4 mm cylindrical samples were cored from bulk 3D-deposited *Grad*, *1mm*, *GradF* and *1mmF* blocks. Prior to cell seeding, scaffolds were sterilized by gamma irradiation (minimum dose 25 kGy) in a JS6500 Tote Box Irradiator at Isotron B.V. (Ede, The Netherlands).

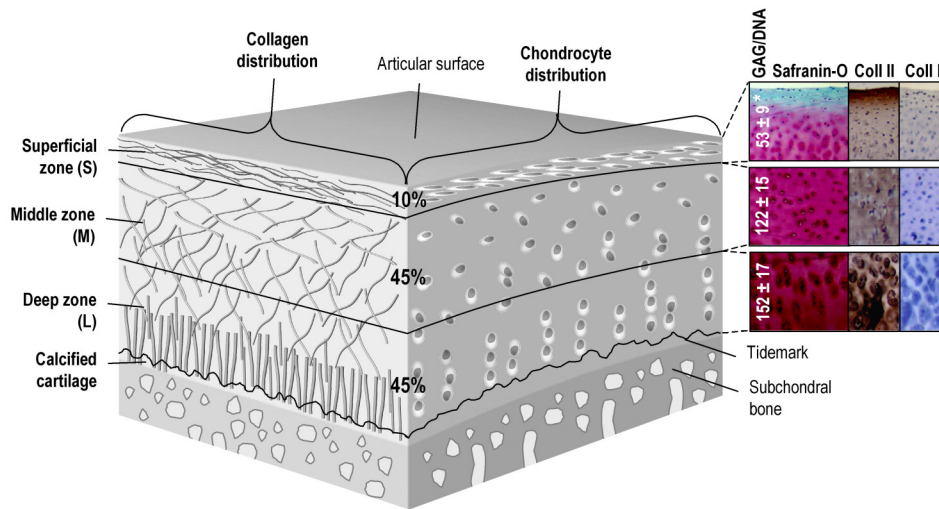


Figure 1 – Anisotropic distribution and orientation of collagen fibres (left face), chondrocytes (right face) and glycosaminoglycan (GAG) within the superficial (S, 10%), middle (M, 45%) and deep or lower (L, 45%) zones of articular cartilage. GAG/DNA content, and safranin-O staining for GAG and immunohistochemistry for collagen type II and type I are illustrated at right. The superficial (S) zone contains flattened chondrocytes and thin, densely packed collagen fibrils ($\varnothing 20$ nm) oriented tangentially to the articular surface. The middle (M) zone contains larger, randomly oriented collagen fibres and chondrocytes have a more rounded appearance. The lower (L), or deep zone, consists of large, spherical chondrocytes aligned in a columnar fashion, and thicker collagen fibres ($\varnothing 120$ nm) oriented perpendicular to the joint surface. A zone of calcified cartilage follows, whose thickness and intermediate stiffness modulate the transfer of forces through articular cartilage to subchondral bone (* indicates significant difference in GAG/DNA content; illustration adapted from Woodfield et al., [517] with permission from publisher). ► p213.

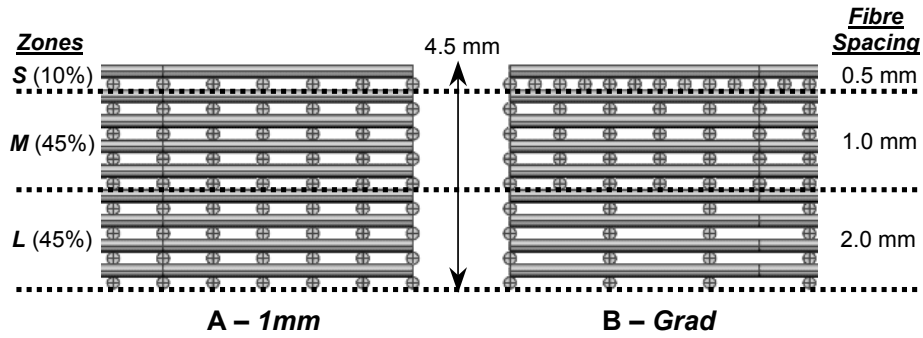


Figure 2 – Schematic of 3D-deposited scaffolds containing a homogeneous 1 mm fibre spacing (A), and a pore-size gradient (B). Regions corresponding to the upper (S), middle (M) and deep zones (L) are indicated on the left, while on the right, the associated fibre spacing used in the gradient scaffolds (0.5, 1.0 and 2.0 mm) are indicated.

Scaffold Characterisation:

Due to the regular pore geometry, determining the interconnecting pore size of the resulting scaffolds was possible using scanning electron microscopy (SEM). Theoretical volume percent (vol%) porosity was calculated for each scaffold using deposition geometries based on a unit cube, whereby the fibre diameter and spacing between layers were equal (*i.e.* no overlap due to the fusion between fibres from one layer to another was assumed), as described previously [519].

The scaffold volume fraction within each of the S, M and L zones was also calculated from deposition geometry data. Assuming a unit cube, the fibre surface area (mm^2) equalled $\pi d.l.n$, where d , l and n represent the fibre diameter (250 μm), fibre length, and the total number of fibres in a given zone respectively. Values were normalized to the associated volume (mm^3) of each of the S, M and L zones, by calculating the cross sectional area (l^2) and height (h) of each zone, yielding the zone volume fraction (mm^{-1}) as follows:

$$\text{Zone Volume Fraction} = \frac{\pi d.l.n}{l^2.h} = \frac{\pi d.n}{l.h} \quad \text{Eq. (1)}$$

Tissue Culture:

Chondrocytes were isolated via collagenase digestion (0.15% type II collagenase, Worthington Biochemical) from articular cartilage harvested from the parapatellar groove of freshly slaughtered, 6-month old bovine knee joints. For *Grad* and *1mm* scaffolds, primary cells were dynamically seeded on $\varnothing 7$ mm by 4 mm thick scaffolds in spinner flasks (Bellco Glassware, 100 mL working volume, 50 rpm) at a density of 8×10^6 cells per scaffold (56 scaffolds in total). For *GradF* and *1mmF* scaffolds, primary cells were statically seeded by placing a highly concentrated cell suspension directly on top of the constructs (8×10^6 cells in 40 μL cell suspension per scaffold) using a micropipette. To prevent cell loss through the highly interconnected pores of the 3D scaffolds, *GradF* and *1mmF* constructs were placed within sterile tubing prior to seeding. Therefore, with the radial borders of the scaffold surrounded by tubing, and a dense film present at the base of the scaffold, only the upper surface remained open. Cells were allowed to settle for 3 hours within the scaffolds before being transferred to

12-well plates containing 3 mL of medium. For all samples, the culture medium contained HEPES (Invitrogen)-buffered DMEM (Invitrogen) supplemented with 10% fetal bovine serum (FBS, Sigma-Aldrich), 0.2 mM ascorbic acid 2-phosphate (Invitrogen), 0.1 mM non-essential amino acids (Sigma-Aldrich), 0.4 mM proline (Sigma-Aldrich), 100 units/ml penicillin (Invitrogen), and 100 µg/ml streptomycin (Invitrogen).

Seeding was evaluated after 3 days of spinner flask (*Grad* and *1mm*) or static culture (*GradF* and *1mmF*) conditions. After removing the tubing on statically seeded scaffolds, all remaining samples were dynamically cultured in spinner flasks until day 21, with medium refreshment every 3-4 days. *Grad*, *GradF* and *1mmF* scaffolds were oriented vertically in spinner flasks so that 0.5 mm spaced fibres were on top, and the 2 mm spaced or dense films were at the bottom.

Biochemical Analysis:

Constructs for biochemical analysis (n=3 per condition at each time point) were sectioned in the three *S*, *M* and *L* zones indicated in Figure 2 using a custom designed device allowing perpendicular sections of desired thickness to be made using a micrometer. The diameter and thickness of each of the sections were measured using digital callipers (Matsushita, Japan) so that quantitative data from each zone could be normalized by volume as described below. Sections were then placed in a solution containing proteinase-K (1 mg/ml), pepstatin A (10 µg/ml) and iodoacetamide (185 µg/ml) (Sigma-Aldrich) overnight at 56°C to digest the cells and extra-cellular matrix (ECM) formed during culture. These samples were then evaluated for DNA, GAG, and collagen type II content as follows:

DNA content: Quantification of total DNA was performed with a Cyquant dye kit (Molecular Probes) as per manufacturer's instructions using a fluorescent plate reader (Perkin Elmer).

GAG content: GAG was quantitatively determined by reaction with dimethyl-methylene blue dye (Sigma-Aldrich) [122]. Intensity of colour change was immediately measured using a microplate reader (EL 312e, Bio-TEK Instruments) at an absorbance 520 nm. Values were compared to those from a standard of chondroitin sulphate B (Sigma-Aldrich).

Collagen type II content: Using an enzyme-linked immunosorbent assay on aliquots from proteinase-K digests, collagen type II content was determined as described previously [183, 227].

To allow comparison with native articular cartilage organization, the above biochemical assays were performed on corresponding zones (*i.e.* *S*, *M*, and *L*) of bovine articular cartilage cylinders (Ø4 mm by 4 mm thick), harvested from the same tissue used for cell isolation. Furthermore, in order to compare the results between the different *S*, *M* and *L* zones, quantitative biochemical data were normalized by available pore volume (mm³) within each zone. This was calculated by taking the total volume of the sample ($\pi/4 \cdot D_c^2 \cdot t$) based on direct diameter (D_c) and thickness (t) measurements of the construct taken during sectioning, and subtracting the fibre volume. Since the scaffold diameter (D), height (h), and vol% porosity (P), for each zone (excluding tissue) were known from deposition geometries, fibre volume of each zone could be determined according to the following equation:

$$\text{Fiber Volume} = \text{Scaffold Volume} \cdot \frac{(100 - \% \text{Porosity})}{100} = \frac{\pi}{4} D^2 h \cdot \frac{(100 - P)}{100} \quad \text{Eq. (2)}$$

Histological Analysis:

Histology: Samples were fixed overnight in 0.14M cacodylate buffer (pH = 7.2 - 7.4) containing 0.25% glutaraldehyde (Merck). Samples were then dehydrated in sequential ethanol series, plastic embedded in glycol-methacrylate (Merck) and cut using a microtome to yield 5 μ m thick sections. Sections were stained with haematoxylin (Sigma-Aldrich) and fast green (Merck) to visualize cells/cell nuclei and safranin-O (Sigma-Aldrich) to visualize extracellular glycosaminoglycan (GAG).

Immunohistochemistry: Constructs were embedded in optimal cutting temperature compound (OCT, Tissue-Tek) and snap frozen at -60°C. Cryo-sections, 5 μ m in thickness, were made (Cryotome, Thermo Shandon) and fixed in acetone for 8 minutes. Collagen type I and II were immuno-localized using an Animal Research Kit (Dako) in combination with collagen type I (1:1000, Ab-1, Calbiochem, EMD Biosciences, CA) and II antibodies (1:200, II-II6B3, Developmental Studies Hybridoma Bank) as described previously [305]. Staining was visualized using DAB-solution (Dako) for 5 minutes in addition to counter staining with haematoxylin (Sigma-Aldrich).

All histological sections were mounted and examined under a light microscope (Nikon Eclipse E600) with representative images captured using a digital camera (Sony Corporation, Japan) and Matrix Vision software (Matrix Vision GmbH, Germany).

Scanning Electron Microscopy (SEM): Samples were fixed and dehydrated as described above, and critical point dried from liquid carbon dioxide using a Balzers CPD 030 Critical Point Dryer. Dried tissue-cultured samples or as-produced scaffolds were then sputter-coated (Cressington) with a thin gold layer and studied using a Philips XL30 Environmental Scanning Electron Microscope (ESEM).

Statistics:

To compare biochemical composition between the various zones within each scaffold (n=3), one-way analysis of variance (ANOVA) was performed using SigmaStat statistical software (SPSS Inc.). If tests for normality and variance passed, then one-way ANOVA was performed, whereas if variance tests failed, then one-way ANOVA-on-ranks was performed with Student-Newman-Keuls post hoc tests for significance ($p < 0.05$) used in both cases.

Results:

Scaffold Characterisation:

As shown in Figure 3, the desired overall volume percent porosity (80.1% and 78.0%) and volume fraction (3.25 mm^{-1} and 3.69 mm^{-1}) available for cell attachment and ECM formation were similar for both *Grad* and *1mm* scaffolds respectively. As expected the *S* zone, with a 0.5 mm fibre spacing in *Grad* and *GradF* scaffolds, had the lowest porosity and highest volume fraction (59.2% and 6.67 mm^{-1} respectively), while the *L* zone, with a 2.0 mm fibre spacing, had the highest porosity and lowest volume fraction (87.4% and 2.05 mm^{-1} respectively). The middle *M* zone, with a 1.0 mm fibre spacing, had a porosity and volume fraction of 78.0% and 3.59 mm^{-1} respectively. These porosity and volume fraction values of the latter were also characteristic of each of the *S*, *M* and *L* zones in *1mm* and *1mmF* scaffolds, as they contained the same homogeneous 1.0 mm fibre spacing throughout.

Previous studies on 3D-deposited scaffolds have shown that, for the geometries chosen in this experiment, the pore size present within scaffolds based on a $250 \mu\text{m}$ fibre diameter and a 0.5 mm, 1.0 mm or 2.0 mm fibre spacing were approximately $250 \mu\text{m}$, $650 \mu\text{m}$ and $1650 \mu\text{m}$ respectively [519]. Therefore, considerably different and distinct pore sizes were available in *Grad* scaffolds for observing cellular responses.

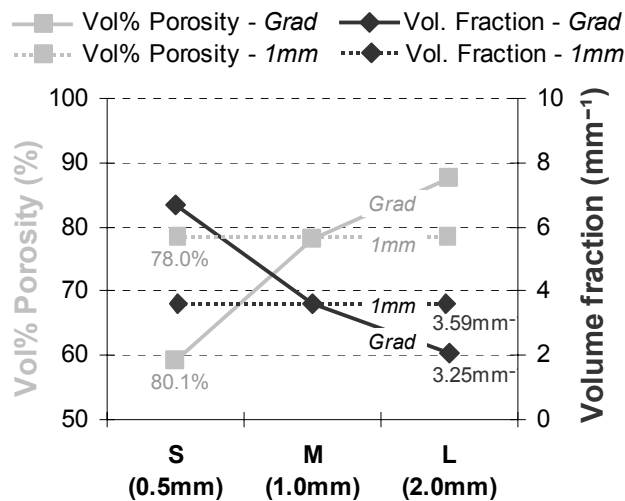


Figure 3 – Zonal scaffold volume percent (vol%) porosity (■) and volume fraction (◆) characteristics for *S*, *M* and *L* zones within *Grad* and *1mm* scaffolds. Overall vol% porosity and volume fraction for all zones within *Grad* and *1mm* scaffolds are indicated under each of the respective curves (zonal fibre spacing for *Grad* scaffolds indicated in brackets).

Biochemical Analysis:

DNA: DNA results showed a significantly higher concentration of cells per unit volume in *Grad* and *GradF S* zones than in corresponding *M* and *L* zones respectively at both day 3 and day 21 (Fig 4A). This anisotropic cell distribution, particularly at day 3, was similar to that measured in bovine articular cartilage explants where we observed a significantly higher concentration of cells per unit volume within the *S* zone compared with *M* and *L* zones (Fig 4B). In comparison, *1mm* and *1mmF* scaffolds, without a pore volume gradient, showed a more homogeneous distribution of cells per unit volume across the three *S*, *M* and *L* zones. In these scaffolds, a significant difference in cell number was observed only between *1mmF S* and *M* zones and was likely the result of the static seeding technique which resulted in the cells settling either within the upper fibres or deep near the dense film (Fig 6C).

When comparing the DNA per unit volume to the volume fraction for *Grad* and *GradF* scaffolds (Fig 5A, 5C), we saw a direct correct correlation between cellularity and scaffold volume fraction at day 3 in gradient scaffolds ($R^2 = 0.997$ and 0.908 respectively), but to a lesser extent after 21 days culture ($R^2 = 0.715$ and 0.706 respectively).

GAG: GAG results showed a similar anisotropic distribution as the DNA data. Again, *Grad* and *GradF S* zones contained a significantly higher GAG content than *M* and *L* zones respectively at both day 3 and day 21 (Fig 4C). These significant trends were not seen in *1mm* and *1mmF* scaffolds. GAG per unit volume in native bovine articular cartilage explants was highest in the *L* zone, however, this was not significantly higher than in *S* and *M* zones (Fig 4D). Furthermore, the amount of GAG measured in native cartilage was approximately 5 to 10 times higher than in the corresponding zones within cultured scaffolds.

As shown in Figure 5B and 5D, there was also a direct correlation between GAG content and volume fraction for *Grad* scaffolds at day 3 ($R^2 = 0.970$), but to a lesser extent for *GradF* scaffolds ($R^2 = 0.855$). Conversely, at day 21, GAG content more directly correlated with volume fraction in *GradF* scaffolds ($R^2 = 0.904$) compared with *Grad* scaffolds ($R^2 = 0.762$).

GAG/DNA: When GAG content was normalized to DNA for each zone in native cartilage explants, significantly higher GAG/DNA was present in the *L* zone compared with *M* and *S* zones respectively (Fig 1). There was no significant difference in GAG/DNA within respective zones of cultured scaffolds with and without pore volume gradients (not shown). However, GAG/DNA content in *Grad* and *1mm* scaffolds increased between day 3 and day 21, whereas, for *GradF* and *1mmF* scaffolds, GAG/DNA remained unchanged with culture time (not shown).

Collagen Type II: An anisotropic distribution in collagen type II content per unit volume was also observed in *Grad* and *GradF* scaffolds at day 3 and day 21, although some significant differences were seen in *1mm* and *1mmF* scaffolds at day 3 (Fig 4E). In general, *S* zones of *Grad* and *GradF* contained significantly higher collagen type II compared with *M* and *L* zones. The exception was between *Grad S* and *L* zones, which exhibited the highest levels of collagen type II, but were not significantly different to one another. Notably, however, a 10-fold increase in collagen II content was observed between day 3 and day 21 from zone *L*, whereas only a 2-fold increase was observed in the *S* zone (Fig 4E). Therefore, based on the rate of collagen synthesis, longer culture periods might result in a distribution of collagen type II more similar to native articular cartilage explants illustrated in Figure 4F. In this case, we observed significantly greater amounts of collagen type II per unit volume in *L* and *M* zones

than the S zone (Fig 4F). Similar to GAG data, collagen type II content per unit volume within native cartilage was approximately 10 times higher than values measured in cultured samples, and compared with *Grad* and *1mm* scaffolds, increases in collagen content between day 3 and day 21 for *GradF* and *1mmF* scaffolds remained limited.

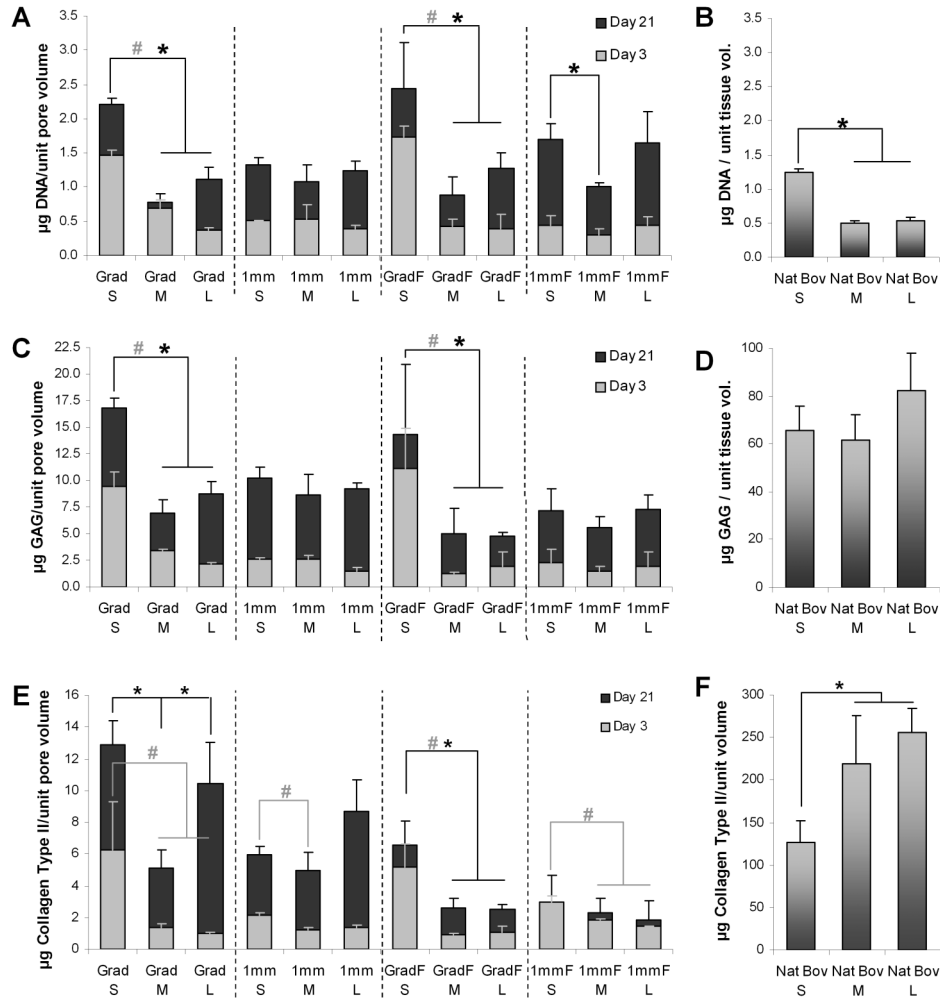


Figure 4 – Distribution of (A, B) DNA, (C, D) GAG, and (E, F) collagen type II content within *Grad*, *1mm*, *GradF* and *1mmF* scaffolds at day 3 and day 21 compared with native bovine articular cartilage explants (B, D, F). Significant difference denoted by: # = day 3, * = day 21.

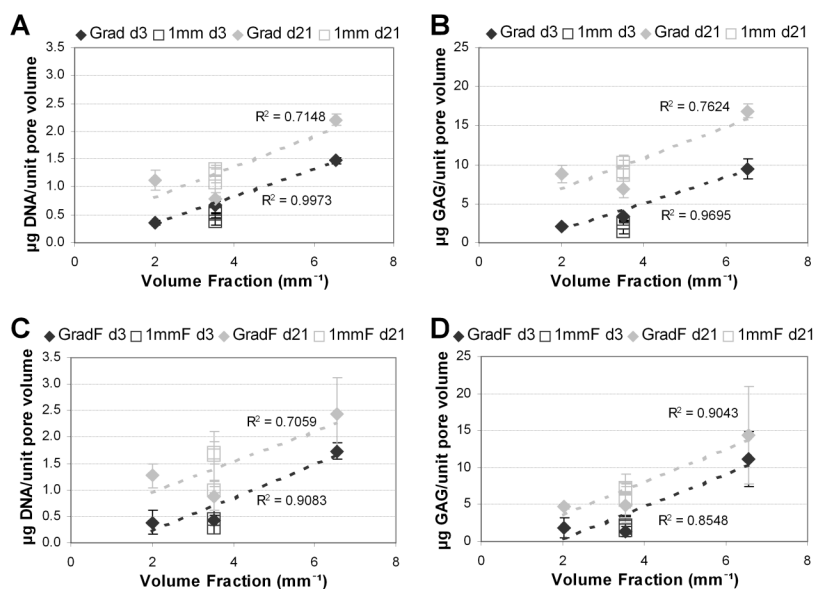


Figure 5 – Correlation between DNA (A, C) and GAG (B, D) content with scaffold volume fraction in Grad / 1mm scaffolds (A, B) and GradF / 1mmF scaffolds (C, D) at day 3 and day 21.

Histological Analysis:

SEM and GAG: SEM and safranin-O stained sections showed that, after 3 days dynamic seeding in spinner flasks, chondrocytes were homogeneously distributed throughout 1mm and Grad scaffolds, essentially covering all available fibre surface area (Fig 6A, 6B). Due to the higher density of fibres in the upper S zone of Grad scaffolds, there appeared to be a greater concentration of cells in this zone compared with M and L zones respectively (Fig 6B), as previously confirmed in DNA assays (Fig 4A).

In contrast to the more random seeding of cells in spinner flasks, static seeding of a highly concentrated cell suspension on GradF (not shown) and 1mmF (Fig 6C) scaffolds resulted a less homogeneous cell distribution. This was likely due to the homogenous 1 mm fibre spacing which allowed cells to more easily pass through the interconnecting pore volume with static seeding. Importantly, the dense basal film prevented these cells from exiting the scaffold, thereby maintaining suitable seeding efficiency. Positive safranin-O staining for GAG was evident in the tissue surrounding fibres in all scaffolds after 3 days (e.g. Grad shown in Fig 6D). The intensity of GAG staining within scaffolds tended to be greatest in regions of highest cell concentration, and therefore, S zones in Grad and GradF scaffolds exhibited more regions of positive GAG staining (e.g. Grad shown in Fig 6D), thus confirming our biochemical GAG findings (Fig 4C). In all cases, attached cells had aggregated around the PEGT/PBT fibres in multiple cell layers and had a rounded morphology (e.g. Grad shown in Fig 6D).

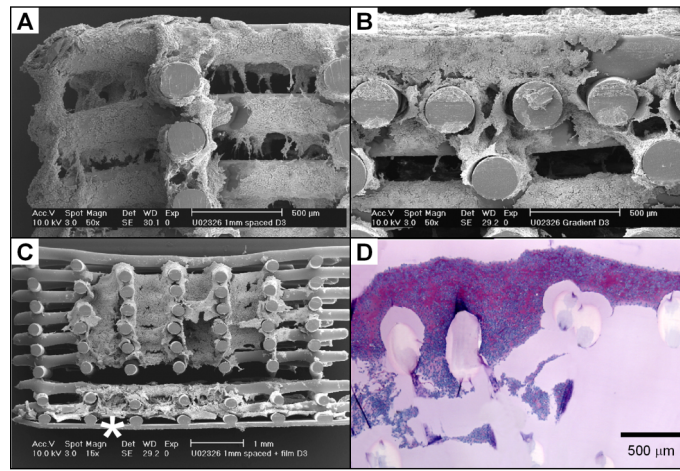


Figure 6 – SEM (A-C) and safranin-O stained sections (D) showing cell attachment and GAG staining on 1mm (A), Grad (B, D), 1mmF (C) scaffolds after 3 days seeding. Available fibre surfaces of spinner flask seeded 1mm and Grad scaffolds were near completely covered with a layer of chondrocytes (A, B). Statically seeded scaffolds (1mmF shown in C) contained more localized regions of high cell density (* indicates dense film). ▶ p214.

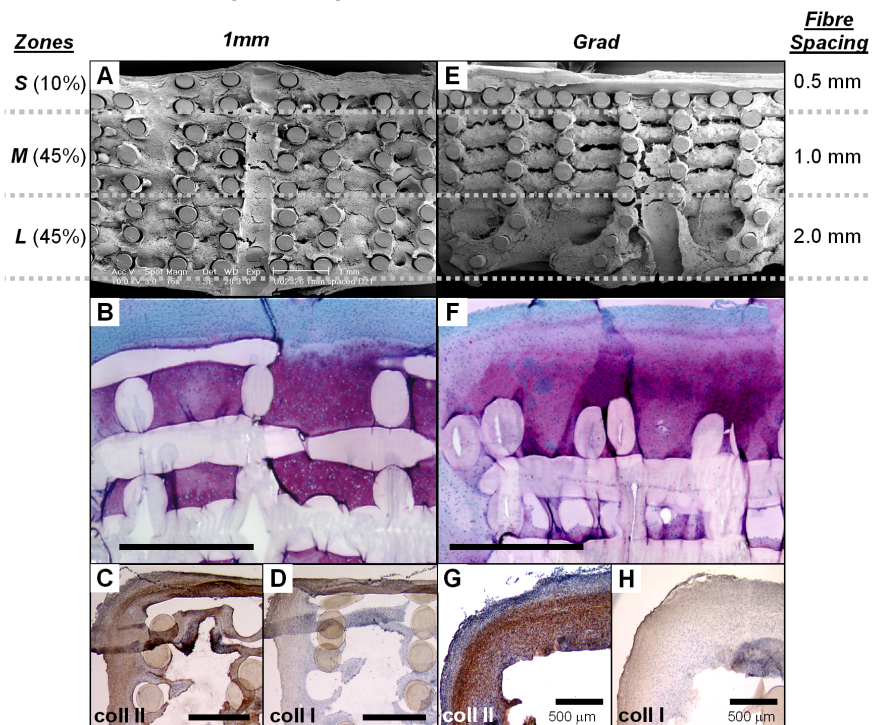


Figure 7 – SEM (A, E), safranin-O (B, F) and collagen type II (C, G) and type I (D, H) immunohistology sections showing extra cellular matrix (ECM) formation within 1mm (A-D) and Grad scaffolds (E-H) after 21 days dynamic culture. Regions corresponding to S, M and L zones are indicated on the left, with associated fibre spacing indicated on the right (scale bar = 1 mm unless otherwise stated). ▶ p214.

After 21 days culture, SEM and safranin-O stained sections showed tissue formation throughout interconnected pores of all scaffolds with ECM bridging the gaps between fibres and resulting in consistent GAG staining (e.g. *1mm* and *Grad* shown Fig 7B, 7F). The exception was ECM formation within *L* zones in *Grad* and *GradF* scaffolds, where there was incomplete bridging between fibres and areas of void space still remaining unfilled (e.g. *Grad* shown Fig 7E). Qualitatively, the amount of cells and GAG staining present within the various *S*, *M* and *L* zones was consistent with biochemical DNA and GAG data, particularly with the higher content of DNA and GAG within the upper *S* zone of *Grad* and *GradF* scaffolds. In contrast, the homogeneous pore distribution in *1mm* and *1mmF* scaffolds tended to result in a more homogeneous cell and GAG distribution (e.g. *1mm* shown Fig 7A, 7B). In all scaffolds, a thin fibrous capsule, approximately 100 μm thick, was present at the periphery of all scaffolds cultured for 21 days (e.g. *1mm* and *Grad* shown Fig 7B, 7F), and was likely related to the dynamic fluid flow imparted on the cells at the periphery of the scaffold during spinner flask culture [494]. ECM within this thin layer did not stain positively for GAG and contained flattened, more fibroblast-like cells similar to the superficial zone of native bovine cartilage (Fig 1).

Immunohistochemistry: Collagen type I and II immunostaining was performed on scaffolds cultured for 21 days only, as we expected limited collagen synthesis to have occurred at the 3 day time point. Within *Grad*, *1mm*, *GradF* and *1mmF* scaffolds, collagen type II was clearly expressed in each zone (e.g. *1mm* and *Grad* shown in Fig 7E, 7F). Collagen type I was expressed only at the very periphery of the scaffolds in correlation with the fibrous capsule (e.g. *1mm* and *Grad* shown in Fig 7D, 7H). Interestingly, due to the film in *GradF* and *1mmF* scaffolds, no fibrous capsule formed in *L* zones resulting in only collagen type II expression and not type I (not shown). With respect to collagen orientation in scaffolds, we were unable to clearly comment on a recapitulation of the radial collagen orientation native cartilage after 21 days.

Discussion & Conclusions:

The aim of this study was not to completely recapitulate the zonal cell and ECM distribution of articular cartilage, but to describe a preliminary model to investigate if scaffolds designed with a pore volume gradient could be instructive for cell and/or ECM distribution. Using a novel computer-controlled 3D fibre deposition technique [519], we successfully produced scaffolds with a 100% interconnecting porous architectures with either a homogeneous (*Imm*) or a gradient (*Grad*) in pore size (Fig 2). This accurate control over scaffold design allowed direct comparisons to be made relating cell and tissue responses to scaffold pore architectures. For comparison with tissue-engineered constructs, we also described a technique to determine the zonal distribution of DNA, GAG and collagen type II within *S*, *M* and *L* zones in 4 mm thick native bovine articular cartilage explants. This technique was verified by quantitative biochemical data and qualitative histology and immunohistochemistry techniques, and were consistent with previous studies demonstrating the organizational structure of native articular cartilage [207, 234]. Cell attachment to PEGT/PBT fibres was achieved using two seeding techniques. Dynamic spinner flask seeding was used as method to randomly introduce cells to various scaffolds, while static cell seeding was used to offer a level of control over cell placement within various scaffolds. Statically seeded scaffolds (*GradF* and *ImmF*) contained a dense film to confine cells within the porous architectures. By using a static seeding method, we hoped to further control the placement of cells based on the expectation that most of the cell suspension would remain in the upper *S* zone of *GradF* and *ImmF* scaffolds, with some cells gravitating towards the basal dense film due to the large interconnecting pores.

Previous studies have investigated the effect of pore size on chondrocyte behaviour [35, 276, 355], and it has been suggested that in scaffolds containing small pore sizes (<20 μm), cell-cell interactions are enhanced, resulting in improved chondrocyte proliferation, whereas total collagen content is little effected by pore size and geometry [35, 355]. Investigators have not typically evaluated scaffolds with the large variation in pore size used in this study (*i.e.* typically 20-300 μm compared with 250-1650 μm), or investigated how collagen type II is distributed throughout porous scaffolds. Other reports suggest that pellet- or mass-cultures, which allow close cell-cell interactions enhance chondrocyte (re)differentiation (*i.e.* GAG/DNA content) and ECM matrix production [432, 453]. We hypothesized that differences in biochemical content may exist between zones where cell-cell interactions varied greatly *i.e.* *S* zones (0.5 mm fibre spacing) compared with *L* zones (2.0 mm spacing). Based purely on available zonal pore volume and the fact that chondrocytes in native cartilage occupy a very small percentage of the overall tissue volume (< 2%), we had hypothesized that there were physical volumetric limits to the amount of GAG and collagen type II synthesis per cell in *S* zones as opposed to *L* zones, if cells were provided with suitable nutrients and a 3D environment. For example, chondrocytes on *S* zones with high cell-cell interaction would be stimulated to proliferate and rapidly synthesize ECM until the available pore volume was filled, whereupon further ECM formation might reach an equilibrium. Whereas chondrocytes in *L* zones, with low cell density, fewer cell-cell interactions and fewer volumetric limitations could proliferate and, on a per cell basis, synthesize greater GAG and collagen type II, more akin the levels synthesized by cells in the deep zone of native articular cartilage.

By incorporating pore size gradients based on *S*, *M* and *L* zones, we were able to demonstrate an anisotropic cell and ECM distribution, whereby, direct correlations between cell number (DNA content) and GAG content with volume fraction were observed in *Grad* and *GradF* scaffolds after 3 days seeding, which was maintained in spinner flask culture up to 21 days. Moreover, this zonal distribution in DNA content within *Grad* and *GradF* scaffolds was shown to be almost identical to that measured in native bovine articular cartilage. The slightly lower GAG content observed in *GradF* and *1mmF* scaffolds could be related to the dense film blocking fluid flow and/or nutrition to the cells, or that the injection seeding technique may have caused greater damage to cells than dynamic seeding (although cell viability was not determined in this case). Pore volume gradients, within the ranges used in this experiment, were not sufficient to elicit noticeable differences in GAG/DNA, particularly in relation to the zonal variations seen in native cartilage.

Similar to DNA and GAG results, anisotropic distributions of collagen type II content per unit volume were observed in *Grad* and *GradF* scaffolds (Fig 4). Interestingly, after 21 days culture the collagen type II content in the *Grad L* zone was not significantly different to the *S* zone, with a 10-fold increase in accumulation from day 3 (Fig 4E). Since DNA content in the *L* zone was significantly lower than the *S* zone at day 21 (Fig 4A), this suggests that in the *L* zone, containing a low volume fraction and high porosity, a greater amount of collagen type II was being synthesized per cell than other zones. This observation was not present, however, in the *L* zone of *GradF* scaffolds, where significantly higher collagen type II content existed in *S* zone compared with both *M* and *L* zones. It is intuitive to expect zones of high cell density per unit volume to synthesize greater amounts of collagen (*i.e.* the *S* zone), however, there must be another mechanism operating in the *L* zone of *Grad* scaffolds related to the low cell number, low volume fraction, and large pore size. SEM and safranin-O sections demonstrated that few of the large pores within *Grad* scaffolds were completely filled with ECM after 21 days (Fig 7E). Therefore, with fewer cell-cell interactions and incomplete bridging of 1650 μm sized pores compared with *S* and *M* zones, it was likely that more cells were exposed to dynamic fluid flow conditions resulting in stimulation of higher collagen type II synthesis per cell [142]. This is further evidenced in *GradF* scaffolds where, even though few of the large pores were filled with ECM after 21 days, fluid flow was likely inhibited in the *L* zone by the dense film, resulting in reduced collagen type II synthesis compared to the *L* zone of *Grad* scaffolds. These results also raise the possibility that pore geometry affects the synthesis of GAG and collagen II differently, even by cells within the same scaffold. Perhaps longer culture periods would allow ECM to completely fill these *L* zones, resulting in significant variations in zonal collagen type II content more in line with that present in native articular cartilage (Fig 6B). While we did observe zonal variations in collagen type II synthesis per cell based on available pore volume in this study, we could not confirm this hypothesis, and further studies are required to understand possible mechanisms and/or adopt alternative methods for controlling zonal cell behaviour.

Other recent studies have attempted to address the need for developing scaffolds or culture techniques which (re)create repair tissue which resembles the zonal organization within articular cartilage. In general, these studies have adopted the use of polymer, alginate or agarose gels to spatially distribute chondrocytes isolated from superficial, middle and deep zone cartilage [234, 238, 359, 438]. While these studies have promising advantages in that the desired cells and cell concentrations can be easily incorporated in a 3D environment, and

that specific zonal markers, such as superficial zone protein, or differential accumulation of GAG and total collagen can be achieved, they do offer some limitations. Firstly, it is difficult to isolate chondrocytes from separate zones in articular cartilage, particularly for human tissue where the zonal differences are less distinct and biopsies are limited in size. Secondly, these gels typically have limited mechanical properties compared with native cartilage and the gels also contain distinct boundaries between zones which could delaminate due to shear stresses.

We describe in this study an alternative method for studying zonal organization within tissue-engineered cartilage constructs. By having complete control over scaffold design using 3D fibre deposition, we were able to influence the number and distribution of cells and, to a certain extent, their ability to produce zonal ECM components by varying the volume fraction and pore volume distribution within a single scaffold. The computer controlled nature of the 3D fibre deposition process also allows accurate and reproducible bonding of PEGT/PBT fibres from layer to another, irrespective of architecture, thereby eliminating concerns of delamination between zones and allowing complex gradient scaffolds to be produced with similar thickness to articular cartilage (2-6 mm). Furthermore, we have previously demonstrated how fibre spacing and deposition patterns can be tailored to produce scaffolds with similar compressive static and dynamic mechanical properties to articular cartilage [519]. While gel techniques offer limited mechanical properties, particularly from one zone to another, some studies are emerging, however, where different concentrations of agarose gels have been combined to produce zonal constructs with varying stiffness [359], however these are far from those necessary to match articular cartilage.

For clinical applications, the ability to incorporate a dense basal layer into the construct, which prevents infiltration of blood- and/or marrow-derived progenitor cells into the wound site, a repair consequence which typically results in an inferior fibrocartilage *in vivo* as opposed to the desired hyaline cartilage, may be an important feature in future scaffold designs [206]. We demonstrated that the dense film in *GradF* and *ImmF* scaffolds assisted cell retention with static seeding techniques and could be incorporated into future *in vivo* studies where a both zonal pore gradients and solid barriers to host cell infiltration can be evaluated. It is worth noting that the natural barrier, the layer of calcified cartilage which anchors cartilage to subchondral bone was not addressed in this zonal study. This limitation should be addressed in future as the calcified cartilage layer forms a critical link with the remaining zonal organization for successful biomechanical function of the articulating joints [55, 228].

One other limitation of the technique presented in this study is that a heterogeneous chondrocyte population (*i.e.* cells from superficial, middle and deep zones) was introduced into the scaffold offering little control over the placement of cells in specific zones, as achieved using previously mentioned gel encapsulation techniques. Previous studies within our group have demonstrated that different compositions of PEGT/PBT co-polymers can influence the attachment and phenotypic expression of human articular chondrocytes on both 2D films [299] and on 3D deposited fibre scaffolds [333]. The extreme flexibility of the 3D fibre deposition technique would allow us in the future to not only control the gradient in pore volume and volume fraction, but also incorporate gradients in PEGT/PBT composition within scaffolds to regulate chondrocyte phenotype, irrespective of heterogeneity or zonal origin of the cell. For instance, a high density of fibres from a PEGT/PBT composition which promotes cell attachment, proliferation and a more de-differentiated phenotype (*i.e.* a lower

GAG/DNA and collagen II content indicative of more superficial chondrocytes) could be applied at the superficial zone. This would also provide sufficient mechanical properties to withstand tensile forces at the articulating surface. Whereas, at the deep zone, a lower density of fibres with a PEGT/PBT composition which promotes a more differentiated phenotype (*i.e.* higher GAG/DNA and collagen II content) could result in a zonal organization and biomechanical properties more similar to native articular cartilage. The flexibility in PEGT/PBT co-polymer composition may also allow us in future to influence zonal scaffold biodegradation rate [111], another feature which has recently been shown to influence deposition of ECM components *in vitro* in hydrogels [59]. In future studies, we intend to address whether such scaffolds will result in even greater instructive characteristics to those presented in this study.

In conclusion, this study provides insight into ways in which instructive characteristics could be incorporated into 3D scaffold designs for tissue engineering articular cartilage which resembles the native zonal cell, structural and mechanical organization. We demonstrated an experimental model for developing porous, 100% interconnected scaffolds with similar pore volume, but containing either homogenous pores or pore-size gradients. *In vitro* cell seeding showed that pore-size gradients promoted an inhomogeneous cell distribution mimicking that of immature bovine cartilage, irrespective of dynamic or static seeding methods. Prolonged *in vitro* tissue culture showed similar inhomogeneous distributions in zonal GAG and collagen type II. Gradients in cell-cell interactions based on controlled changes in pore size within *Grad* and *GradF* scaffolds did not influence the zonal distribution of GAG/DNA. Further research employing the techniques used in this study are required in order to recreate the same distributions of GAG and collagen II *in vitro* and *in vivo* as native cartilage.

Acknowledgements:

The authors acknowledge funding from the European Commission ("Scafcart" project G5RD-CT-1999-00050).

III.

Instructive Scaffolds: Composition, Pore Architecture and Chondrocyte Re-differentiation

Chapter 7

Gas Plasma Treatment and PEGT/PBT Substrate Composition Affect Human Chondrocyte Adhesion and Re-differentiation Capacity

Chapter 8

The Effect of Scaffold Composition and Architecture on Human Nasal Chondrocyte Re-differentiation and Cartilaginous Matrix Deposition Capacity

"Since we cannot know all that there is to be known about anything,
we ought to know a little about everything."
[Blaise Pascal, 1623-1662]

50 μ m

Exp

WD

Spot Magn

Acc.V

Chapter 7

Gas Plasma Treatment and Substrate Composition Affect Expanded Human Chondrocyte Adhesion and Re-differentiation Capacity

Woodfield T.B.F.^{‡1,2}, van Blitterswijk C.A.¹, Miot S.³, Martin I.³, Riesle J.^{1,2}

¹ Institute for Biomedical Technology, University of Twente, Enschede, The Netherlands

² IsoTis S.A., Bilthoven, The Netherlands

³ Departments of Surgery and of Research, University of Basel, Switzerland

Abstract:

We investigated whether controlled changes in substrate surface chemistry via gas plasma surface modification and substrate composition can regulate the adhesion and post-expansion re-differentiation of human chondrocytes in serum containing (S+) and serum free (SF) media. Expanded human chondrocytes were plated on gas plasma treated (GP+) or untreated (GP-) poly(ethylene glycol)-terephthalate – poly(butylene terephthalate) (PEGT/PBT) block co-polymers films with two compositions (low or high PEG content). Total cellularity (DNA content) and immunofluorescent staining of vitronectin (VN) and fibronectin (FN) integrin receptors were evaluated, while post-expansion chondrogenic phenotype was assessed by collagen type I and type II mRNA expression.

We observed a direct relationship between cellularity, cell morphology and re-differentiation potential. Independent of PEGT/PBT composition, GP treatment enhanced cell spreading and total cellularity, but only in S+ media suggesting that protein adsorption mechanisms were involved. There was a significant influence of PEGT/PBT composition on cellularity in both S+ or SF media. Substrates supporting high cellularity and a spread cell morphology (i.e. GP+ and low PEG content PEGT/PBT compositions), showed greater FN integrin receptor staining intensity, concomitant with reduced collagen type II/I mRNA gene expression. The cause of these observations was likely preferential FN adsorption, due to the low PEG content and preferential PEG etching during GP treatment, resulting in a FN-rich surface. Substrates supporting low cellularity and a spherical cell morphology (GP- and high PEG content PEGT/PBT compositions) were likely FN-deficient, thereby promoting chondrocyte re-differentiation as assessed by collagen type II/I gene expression.

This study highlights the need to carefully assess cell-substrate interactions and the use of S+ or SF culture conditions to improve cellular adhesion whilst maintaining suitable re-differentiation capacity.

[‡] Woodfield TBF, van Blitterswijk CA, Miot S, Martin I, Riesle J. Gas Plasma Treatment and Substrate Composition Regulate Expanded Human Chondrocyte Adhesion and Re-differentiation Capacity. *Exp Cell Res* **2004** (submitted).

Introduction:

The ability of polymeric substrates to influence the attachment, proliferation and gene expression in anchorage dependent cells has long been established [186, 290, 291, 315]. More recently, with the development of tissue engineering strategies, aimed at combining reparative cells and porous scaffolds for repairing or regenerating damaged tissues (e.g. articular cartilage defects), the role of cell-biomaterial interactions in regulating specific cellular functions has received considerable attention [28, 214, 215, 408, 517]. The ability of chondrocytes to alter their gene expression profile following attachment makes them an interesting cell type for studying phenotype modulation by controlled variations in substrate composition and/or surface modification.

Scaffold-based therapies for repairing articular cartilage defects require attachment and retention of large numbers of chondrogenic cells within a three-dimensional (3D) environment to regenerate damaged extra-cellular matrix (ECM) [517]. In order to obtain suitable numbers of cells to seed within a porous scaffolds of clinically relevant size (0.5 – 12.5 cm²) [182], extensive *in vitro* cell expansion is required. It is well established that during expansion in monolayer, chondrocytes lose their phenotype, or de-differentiate [186, 489], resulting most noticeably in a change in collagen synthesis from type II to type I, as well as a change in cell morphology from a spherical to a flattened, fibroblast-like appearance [24, 467, 505]. Chondrocyte-biomaterial interactions are influenced by sequential events starting from integrin-mediated interactions with serum-derived proteins adsorbed on the biomaterial surface, subsequent adhesion and morphological changes, finally regulating the differentiation stage, and thus the quality and quantity of ECM deposition. Therefore, in developing successful cell based technologies, the optimization of biomaterial substrates and/or associated surface modification techniques which regulate, or are "instructive" for, attachment and re-differentiation of de-differentiated (i.e. expanded) human chondrocytes is of significant clinical importance and offers a considerable challenge.

We previously established a model system to study chondrocyte-material interactions using poly (ethylene glycol)-terephthalate - poly (butylene terephthalate) (PEGT/PBT) block co-polymer substrates [299]. The advantage of this co-polymer system is that during synthesis, the molecular weight (MW) of poly (ethylene glycol) (PEG) and the weight percent (wt%) ratio of hydrophilic PEGT and hydrophobic PBT blocks can be tailored, making it possible to modulate substrate properties such as wettability [371], protein adsorption [299], swelling, biodegradation rate [111], and mechanical properties [519]. Two dimensional (2D) studies performed on PEGT/PBT films with low PEG MW have shown that preferential surface adsorption of fibronectin (FN) compared to vitronectin (VN) was positively correlated with cell attachment, and negatively correlated with chondrocyte re-differentiation [299]. In contrast, hydrophilic PEGT/PBT substrates presenting a high PEG MW exhibited a low FN to VN adsorption ratio and resulted in an increased ability to maintain phenotype of primary bovine [375] and human chondrocytes [299]. Using hydrophilic PEGT/PBT substrates may result in better maintenance of chondrocyte phenotype, however, getting chondrocytes (in particular expanded human chondrocytes) to attach to hydrophilic PEGT/PBT substrates in sufficient number is problematic [518], thereby requiring the assistance of surface modification techniques.

Surface modification via glow discharge gas plasma (GP) is used commercially to treat tissue-culture polystyrene (TCPS) surfaces, and has been shown to enhance cell attachment, growth and differentiation [233, 458]. These features are reportedly caused by etching and incorporation of hydroxyl and carboxyl groups in the most superficial layers (i.e. at a nano-scale level) during GP treatment through a cascade of chemical reactions [83, 371]. GP surface modification has been shown to enhance bone progenitor-cell attachment and function on 2D polymer films and 3D polymer scaffolds [88, 96], potentially making it a simple and highly desirable technique for modification of polymeric scaffolds for tissue engineering. In preliminary studies using primary bovine chondrocytes, we observed increased attachment and chondrogenesis on GP treated 3D PEGT/PBT scaffolds compared with untreated scaffolds [518]. However, little is known about the effect of GP on expanded human chondrocyte attachment and phenotypic expression. Studies have shown that argon GP treatment of PEGT/PBT block co-polymers resulted in the preferential removal of PEG blocks, as well as significantly increasing substrate hydrophilicity due to the introduction of polar functional groups at the surface [371]. Given that more hydrophilic PEGT/PBT surfaces tend to enhance maintenance of chondrocyte phenotype [299, 375], GP treatment of varying compositions of PEGT/PBT substrates may also regulate phenotypic expression of cells exposed to these surfaces.

It still remains unclear which exact surface properties are altered following GP treatment and whether surface hydrophilicity, protein adsorption, or the bulk properties of the substrate are responsible for eliciting different adhesion and phenotypic responses in expanded human chondrocytes. We hypothesized that physico-chemical modification of the upper-most surface of PEGT/PBT substrates via GP treatment may influence cell attachment via mechanisms independent of adsorption of serum-derived proteins. As a mechanistic approach to understand the effects of protein adsorption, we evaluated attachment mechanisms and chondrocyte phenotype in serum-containing (S+) and serum free (SF) media, both shown to stimulate re-differentiation of expanded human chondrocytes [226].

Therefore, the purpose of this study was to evaluate cell attachment and re-differentiation capacity of expanded human chondrocytes by culturing:

- (i) on varying compositions of PEGT/PBT films,
- (ii) with (GP+) or without (GP-) gas plasma treatment,
- (iii) in serum-containing (S+) or serum-free (SF) media.

Cell attachment and proliferation were investigated by means of DNA quantification and cellular expression of FN and VN integrin receptors was analyzed by immunofluorescence. Post expansion re-differentiation capacity was assessed by quantification of collagen type I and II gene expression using real time RT-PCR.

Materials & Methods:

Material:

PEGT/PBT co-polymers were obtained from IsoTis S.A. (Bilthoven, The Netherlands) with a composition denoted as $a / b / c$, where a represents the PEG MW (g/mol), and b and c represent the wt% of the PEGT and PBT respectively. Cell-substrate interactions were evaluated on PEGT/PBT co-polymer films produced from 1000/70/30 and 300/55/45 compositions differing in hydrophilicity (Table I). PEGT/PBT co-polymer resin was dissolved in chloroform (Sigma Aldrich) and films, approximately 50 μm in thickness, were solution-cast using a technique described previously [375]. Due to the swelling behaviour of hydrophilic 1000/70/30 films (approximately 20%), $\varnothing 8.5$ mm discs were punched out whereas for hydrophobic 300/55/45 films with limited swelling behaviour (approximately 2%) $\varnothing 10$ mm discs were punched out.

Gas Plasma (GP) Treatment:

Films for GP treatment were placed in a cylindrical, radio-frequency glow-discharge glass bell chamber (Harrik Scientific Corp, NY). A vacuum was applied to the chamber (0.01 mbar) and subsequently flushed 4 times with argon (Ar, purity $\geq 99.999\%$, Hoekloos B.V., The Netherlands). The films were then treated under an Ar plasma (0.1-0.2 mbar) for 30 minutes. GP treated and untreated films were then vacuum sealed in foil purged with nitrogen and sterilized by gamma irradiation (minimum dose 25 kGy) at Isotron B.V. (Ede, The Netherlands). Samples were stored in foil at -20°C prior to use.

The ability of GP treatment to increase the hydrophilicity of PEGT/PBT films has been characterized previously [371]. Compared to untreated films, a 30 minute Ar gas plasma treatment resulted in a decrease in contact angle (as determined using a captive bubble technique) on water-equilibrated 1000/70/30 and 300/55/45 films (Table 1). Previously reported contact angles for TCPS have been included for comparison [218].

Table 1 – Contact angles of gas plasma (argon) treated and untreated 1000/70/30 and 300/55/45 films in comparison with TCPS.

Sample	Untreated film	Gas plasma treated film (30 min Ar)
1000/70/30 [371]	$39^{\circ} \pm 1^{\circ}$	$34^{\circ} \pm 2^{\circ}$
300/55/45 [371]	$48^{\circ} \pm 3^{\circ}$	$24^{\circ} \pm 3^{\circ}$
TCPS [218]		$62^{\circ} \pm 2^{\circ}$

Tissue Culture:

Human nasal chondrocytes were isolated via collagenase digestion (collagenase type-II, Worthington), plated on tissue-culture polystyrene (TCPS, NUNC) at a density of 3,500 cells/cm² and culture-expanded until passage two. In order to obtain a suitable number of cells, an expansion medium containing DMEM (Invitrogen) supplemented with 10% fetal bovine serum (FBS, Sigma Aldrich), 0.29 mg/ml L-glutamine (Sigma Aldrich), 1 mM sodium pyruvate (Invitrogen), 0.1 mM non-essential amino acids (NEAA, Sigma Aldrich), 100 units/ml penicillin (Invitrogen), 100 µg/ml streptomycin (Invitrogen), 10 mM HEPES buffer (Invitrogen), 1 ng/ml TGFβ₁ (R&D Systems), 5 ng/ml bFGF-2 (R&D Systems), 10 ng/ml PDGF-bb (R&D Systems) was used. This specific combination of growth factors has previously been shown to enhance human chondrocytes proliferation and re-differentiation capacity [19]. Expanded human nasal chondrocytes were selected for this study since they were a clinically relevant cell source, and have been shown to de- and re-differentiate in a similar manner to articular chondrocytes [469], but also proliferate faster and exhibit a greater chondrogenic capacity after expansion [226].

GP+ and GP- 1000/70/30 and 300/55/45 films were placed in sterile 12-well plates (NUNC) and allowed to equilibrate for 3 hours at 37°C in appropriate serum containing (S+) or serum free (SF) media (described below). Expanded chondrocytes were trypsinized (0.15% trypsin-EDTA, Invitrogen), seeded at a density of 10,000 cells/cm² on GP treated (GP+) or untreated (GP-) PEGT/PBT films and cultured in S+ or SF media, both shown to stimulate re-differentiation of human nasal chondrocytes [226]. Specifically, the S+ medium contained DMEM-Glutamax (Invitrogen) supplemented with 10% FBS, 0.1 mM NEAA, 100 units/ml penicillin, 100 µg/ml streptomycin, 10 mM HEPES buffer, 0.1 mM ascorbic acid 2-phosphate (Invitrogen), and 10 µg/ml insulin (Sigma Aldrich), whereas the SF medium contained DMEM-Glutamax supplemented with ITS+1 (1x, Sigma Aldrich), 0.1 mM NEAA, 100 units/ml penicillin, 100 µg/ml streptomycin, 10 mM HEPES buffer, 0.1 mM ascorbic acid 2-phosphate, 1.25 mg/ml human serum albumin (HSA, Sigma Aldrich), 10⁻⁷M dexamethasone (Sigma Aldrich), 10 ng/ml TGFβ₁ (R&D Systems). Pellet cultures (0.5x10⁶ cells/pellet) and TCPS (10,000 cells/cm²) served as positive and negative controls for cell re-differentiation respectively, with the abovementioned S+ and SF media used in both cases.

Evaluation:

DNA content: To determine the number of cells adhering to the various polymer substrata, films were harvested at days 3 and 10 ($n=3$) and frozen at -80°C. Films were placed in a solution containing proteinase-K (1 mg/ml), pepstatin-A (10 µg/ml) and iodoacetamide (185 µg/ml) (Sigma-Aldrich) overnight at 56°C to digest the cells and extra-cellular matrix (ECM). Quantification of total DNA was performed with a Cyquant dye kit (Molecular Probes) as per manufacturer's instructions using a fluorescent plate reader (Perkin Elmer).

Histology: Pellets were harvested at day 10 ($n=3$) and fixed overnight in 0.14M cacodylate buffer (pH = 7.2-7.4) containing 0.25% glutaraldehyde (Merck). Samples were then dehydrated in sequential ethanol series, plastic embedded in glycol-methacrylate (Merck) and cut using a microtome to yield 5 µm thick sections. Sections were stained with

haematoxylin (Sigma-Aldrich) and fast green (Merck) to visualize cells/cell nuclei and safranin-O (Sigma-Aldrich) to visualize extracellular glycosaminoglycans (GAG).

Scanning Electron Microscopy (SEM): To examine cell morphology, samples harvested at day 3 and day 10 ($n=2$) were fixed and dehydrated as described above, and critical point dried from liquid carbon dioxide using a Balzers CPD 030 Critical Point Dryer. Films were then sputter-coated (Cressington) with a thin gold layer and studied using a Philips XL30 Environmental Scanning Electron Microscope.

Integrin receptor detection: Fibronectin (FN) and vitronectin (VN) integrin receptors were detected by immunofluorescence. At days 3 and 10, films ($n=3$) were fixed for 15 minutes with 10% formalin (Sigma), rinsed with phosphate buffered saline (PBS, Invitrogen), and cells permeabilized with 0.2% Triton X-100 for 20 minutes. Films were rinsed in PBS and blocked for 15 minutes with 0.1 M glycine, and for a further 15 minutes using serum-free protein block (Dako). Films were again rinsed in PBS and incubated separately with monoclonal antibodies directed against the $\alpha 5 \beta 1$ fibronectin receptor (clone P1D6, dilution 1:500, Covance); or against the $\alpha v \beta 3$ vitronectin receptor (anti-CD61, dilution 1:100, Pharmingen). Films were rinsed in PBS and further incubated for 30 minutes with a goat anti-mouse secondary antibody conjugated with Alexa 488 (dilution 1:100, Molecular Probes). The films were rinsed 3 times in PBS and mounted with Vectashield (Vector Labs, CA) containing DAPI to visualize cell nuclei. Slides were examined under a fluorescence microscope (Nikon Eclipse E600) using a F-T filter (FITC/Texas Red, Nikon) for integrin receptors detection (labelled green) and a quad-band filter (XF 113-2, Omega Optical) for DAPI stained cell nuclei (labelled blue). Representative images using both filters were captured at the same exposure using a digital camera (Sony Corporation, Japan) and merged using Paintshop Pro (Jasc Software) yielding a single image locating cell nuclei combined with either FN or VN integrin receptor staining.

RT-PCR: Samples harvested at day 10 were analyzed by quantitative real time RT-PCR for collagen type I and II messenger RNA (mRNA) expression ($n=3$). Films were carefully rinsed in PBS and frozen in Trizol reagent (Life Technologies) at -80°C . RNA were extracted from films using 250 μl Trizol (Life Technologies) according to the manufacturer's instructions. cDNA were generated from total RNA using reverse-transcriptase Stratascript (Stratagene). Real-time RT-PCR reactions were performed and monitored using a ABI prism 7700 Sequence Detection System and the Sequence Detector V program (Perkin Elmer Applied Biosystems). The PCR master mix was based on AmpliTaq Gold DNA polymerase (Perkin Elmer Applied Biosystems). In the same reaction, cDNA samples were analyzed both for collagen type I or collagen type II and for a housekeeping gene (18S ribosomal RNA), using previously described sequences of primers and probes [19]. Each cDNA sample was assessed at least in duplicate, with collagen type I and type II mRNA expression levels normalized to the corresponding 18S rRNA levels. Since collagen type II is a typical marker of differentiated chondrocytes in hyaline cartilage, as opposed to collagen type I, expressed in de-differentiated chondrocytes, we used the ratio of mRNA levels of collagen type II to I (CII/CI) as a chondrocyte differentiation index.

Protein adsorption: To give an indication of protein adsorption capacity of GP+ and GP- films of varying composition, cell-free films ($n=3$) were incubated overnight in 50 mg/ml FITC-conjugated bovine serum albumin (BSA, Molecular Probes). Films were rinsed 3 times in PBS and protein adsorption (labelled green) visualized under a fluorescence microscope (Nikon Eclipse E600) using a F-T filter (FITC/Texas Red, Nikon) with representative images captured at the same exposure using a digital camera (Sony Corporation, Japan). Semi-quantitative BSA

adsorption results were obtained by calculating the percentage of green BSA-expressing pixels to the total number of pixels using Image J (NIH) image analysis software.

Statistics:

Data were represented as a mean \pm standard deviation ($n=3$). To test levels of significance in DNA content and collagen II/I mRNA ratio, one-way analysis of variance (ANOVA) was performed using SigmaStat statistical software (SPSS Inc.). If tests for normality and variance passed, then one-way ANOVA was performed, whereas if variance tests failed, then one-way ANOVA-on-ranks was performed with Student-Newman-Keuls post hoc tests for significance ($P<0.05$) used in both cases.

Results:

Cell Adhesion:

DNA analysis showed that after 10 days culture in S+ media, the number of cells adhering to GP+ 1000/70/30 and 300/55/45 films was significantly greater compared with GP- films. There was no significant difference in DNA content between TCPS, GP+ 1000/70/30 and GP+ 300/55/45 substrates after 3 days (data not shown). However, after 10 days, TCPS had significantly higher DNA content than all other substrates, while GP+ 1000/70/30 and GP+ 300/55/45 films maintained a similar DNA content (Fig 1A). Among all conditions tested, the lowest number of cells was found on GP- 1000/70/30 films, which exhibited a significantly lower DNA content than GP- 300/55/45 films. These results demonstrate that PEGT/PBT composition clearly has an effect on DNA content/film, and when GP treatment was applied, significantly greater DNA content was observed, and appeared to be independent of PEGT/PBT composition.

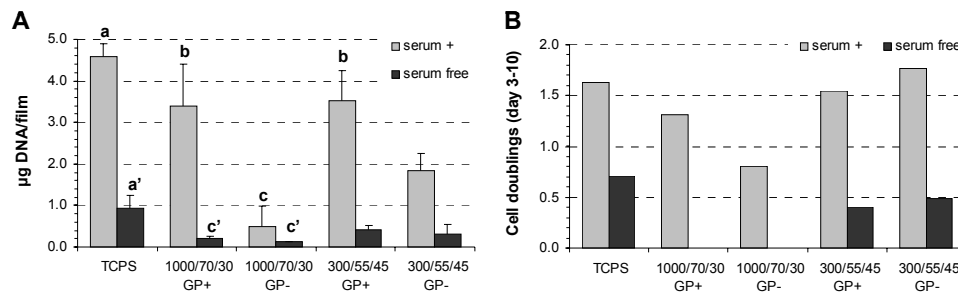


Figure 1 – (A) DNA content per film at day 10 in serum containing (S+) or serum free (SF) media on gas plasma treated (GP+) and untreated (GP-) substrates compared with TCPS. (B) The number of cell doublings on each of the substrata between day 3 and day 10. Significant differences in S+ (a, b, c) and SF media (a', b', c') denoted by: a, a' = > all substrates; b, b' = > GP- films; c, c' = < 300/55/45 films.

Due to the absence of potent cell attachment proteins in SF media, cell numbers were significantly reduced on TCPS, GP- and GP+ substrates compared with S+ media (Fig 1A). GP treatment of PEGT/PBT films did not enhance DNA content/film over TCPS in the absence of serum, as TCPS had significantly greater DNA content than GP+ and GP- films. When comparing cell number between films in SF media, no significant difference in DNA content was observed between GP+ and GP- 300/55/45 films, or between GP+ and GP- 1000/70/30. However, DNA content was significantly greater on 300/55/45 films than 1000/70/30 films, suggesting that composition and not GP treatment of PEGT/PBT films was responsible for increased cell number in the absence of serum.

When the DNA data were expressed in terms of cell proliferation (Fig 1B), the number of cell doublings between day 3 and day 10 in S+ media was greatest on GP- 300/55/45 (1.8) films, followed by GP+ 300/55/45 (1.5), GP+ 1000/70/30 (1.3) and GP- 1000/70/30 (0.8), compared with 1.6 cell doublings on TCPS. Cell proliferation remained limited in SF media, with greatest cell doublings observed on GP- 300/55/45 (0.5) and GP+ 300/55/45 (0.4), compared with 0.7 cell doublings on TCPS (Fig 1B). No cell proliferation was observed on treated and untreated 1000/70/30 substrates between day 3 and day using SF media, and was likely due to limited cell adhesion (Fig 1A). Therefore, out of all the substrates, TCPS and GP- 300/55/45 films provided greater cell proliferation capacity in both S+ and SF media, whereas GP- 1000/70/30 provided the least cell proliferative capacity. Comparing treated and untreated substrates, GP seemed to only influence cell proliferation in S+ medium on 1000/70/30 films.

Scanning Electron Microscopy (SEM):

Cell morphology was assessed for each of the substrates and media conditions at day 3 and 10. Since cell morphology was generally similar in S+ or SF media at each of the time points, only samples from day 10 are illustrated in Fig 2. With respect to number of adherent cells in S+ medium, SEM analysis confirmed our DNA results, with surfaces of GP+ 1000/70/30 (Fig 2A) and GP+ 300/55/45 films (Fig 2C) and TCPS (Fig 2E) confluent with chondrocytes, exhibiting a spread morphology and numerous pseudopodia. Fewer cells were present on GP- 300/55/45 films, again exhibiting a spread morphology, although, as shown in Figure 2D, some cells still retained their spherical appearance. Few cells were present on GP- 1000/70/30 films and tended to exhibit a spherical appearance, as illustrated by the single cell at high magnification (x2000) in Figure 2B. These chondrocytes resisted adhesion and spreading, instead forming aggregates of 10-20 cells resembling a micron-scale pellet above the substrate. These observations are more clearly illustrated and discussed later in Figure 4 following immunofluorescent staining.

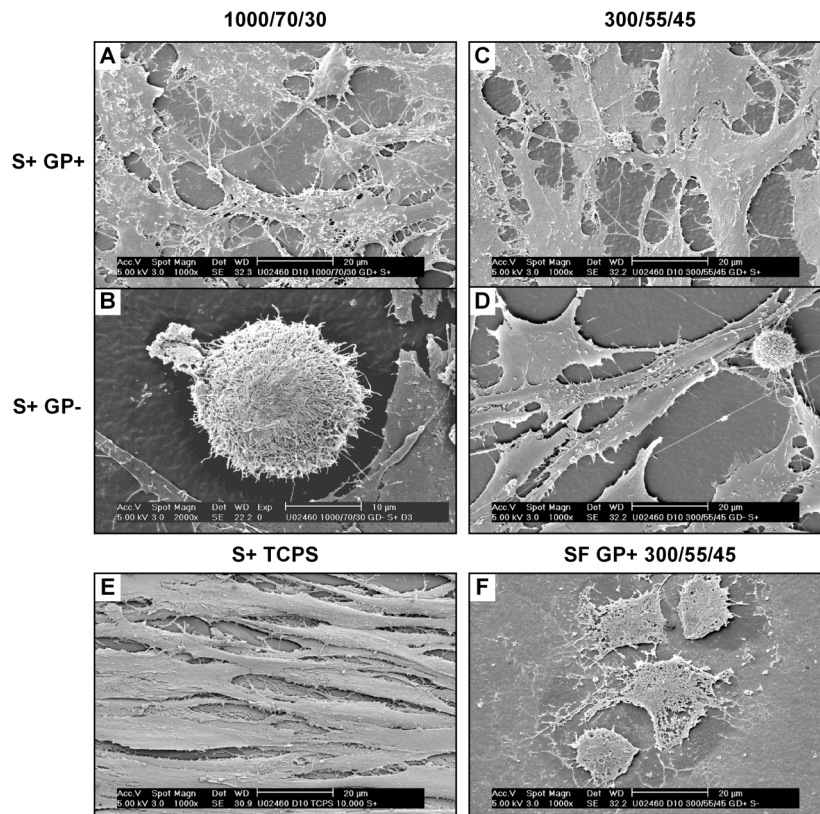


Figure 2 – (A-D) SEM pictures of expanded human chondrocytes after 10 days culture in S+ medium on 1000/70/30 (A x1000, B x2000) and 300/55/45 substrates (C, D x1000) either with (A, C) or without (B, D) GP treatment. (E) TCPS control in S+ media. (F) Example of cell morphology in SF media on GP+ 300/55/45.

Histology and RT-PCR:

Pellets cultured in S+ and SF media showed cell re-differentiation after 10 days, as indicated by spherical cells embedded in lacunae and intense safranin-O staining (inset Fig 3) of sulphated extra-cellular glycosaminoglycan (GAG) resembling that of articular cartilage. Furthermore, the re-differentiation index, taken as a ratio of collagen type II to I mRNA, was significantly higher in S+ and SF pellets compared with cells cultured on TCPS for 10 days (Fig 3). Pellet cultures represented a positive control for cell re-differentiation as previously described for human nasal chondrocytes expanded and re-differentiated in similar conditions described in this study [226].

Although fewest cells adhered to GP- 1000/70/30 films in S+ medium compared with all other conditions (Fig 1A), these substrates promoted chondrocyte re-differentiation in 2D most similar to that shown in pellet cultures, resulting in collagen II/I mRNA ratios 2- and 3-orders of

magnitude greater than GP- 300/55/45 and both GP+ compositions respectively (Fig 3). However, when treated with gas plasma, both 1000/70/30 and 300/55/45 films exhibited only marginally higher collagen II/I mRNA ratios than TCPS in S+ media, suggesting that GP treated PEGT/PBT films tend to promote a more de-differentiated, fibroblast-like phenotype and lower CII/CI mRNA ratio (Fig 3). While all substrates showed a higher re-differentiation index than TCPS in SF media, no significant differences in CII/CI mRNA ratios between groups were observed (except between TCPS and pellet cultures) and these ratios were all noticeably lower than in S+ medium. Interestingly, more cells were present on TCPS substrates in SF media at day 10 compared with PEGT/PBT films (Fig 1) and yet the films exhibited greater re-differentiation capacity. In SF medium, the chondrogenic index was not significantly enhanced on GP- 1000/70/30 as compared to other substrates, suggesting that the interaction between cells and serum proteins adsorbed to the substrate play a large role in chondrocyte re-differentiation. While we demonstrated that expanded (*i.e.* de-differentiated) human nasal chondrocytes are capable of responding to changes in substrate composition and chemistry and re-express a chondrogenic phenotype, our results confirm the general paradigm that substrates which promote adhesion and proliferation of chondrocytes (*i.e.* GP treated and 300/55/45 films), limit cell re-differentiation capacity.

Integrin Receptor Detection:

To study the effect of substrate composition and GP treatment on chondrocyte adhesion mechanisms, immunofluorescent staining for $\alpha V\beta 3$ and $\alpha 5\beta 1$ integrin receptors for vitronectin and fibronectin respectively was performed. As discussed previously, spherical cell aggregates containing 10-20 cells formed on top of GP- 1000/70/30 films (Fig 4B₁, 4B₃), whereas individual cells adhered to GP+ 1000/70/30 and 300/55/45 films (Fig 4A₁₋₄) exhibited a spread morphology. In S+ medium, greater cell numbers were observed on GP+ films (Fig 4A₁₋₄) than GP- films (Fig 4B₁₋₄), whereas in SF medium, greater cell numbers were observed on 300/55/45 films (Fig 4C_{2-D₂}, 4C_{4-D₄}) than 1000/70/30 films (Fig 4C_{1-D₁}, 4C_{3-D₃}), verifying DNA and SEM results. In both S+ and SF media, the intensity of staining for FN and VN receptors was greater in GP treated films (Fig 4A₁₋₄, 4C₁₋₄) than in untreated films (Fig 4B₂, 4B₄, 4D₁₋₄), with the exception of spherical aggregates which formed on top of GP- 1000/70/30 films, where integrins were actively expressed more as a result of cell-cell interactions, rather than cell-substrate interactions (Fig 4B₁, 4B₃). Furthermore, expression of integrin receptors for both VN and FN, appeared to be greater on GP+ 300/55/45 films (Fig 4A₂, 4C₂, 4A₄, 4C₄) than GP+ 1000/70/30 films (Fig 4A₁, 4C₁, 4A₃, 4C₃) irrespective of culture in S+ or SF media, although in general, integrin expression on all films was more pronounced in S+ medium (Fig 4A₁₋₄) than SF medium (Fig 4C₁₋₄). Interestingly, FN integrin receptor expression on all substrates (Fig 4A_{3-D₄}) appeared to be greater in comparison to VN expression in corresponding substrates (Fig 4A_{1-D₂}), the exception being GP+ 300/55/45 (Fig 4A₂, 4A₄) and GP- 1000/70/30 films (Fig 4B₁, 4B₃) in S+ medium where high expression of both VN and FN were observed.

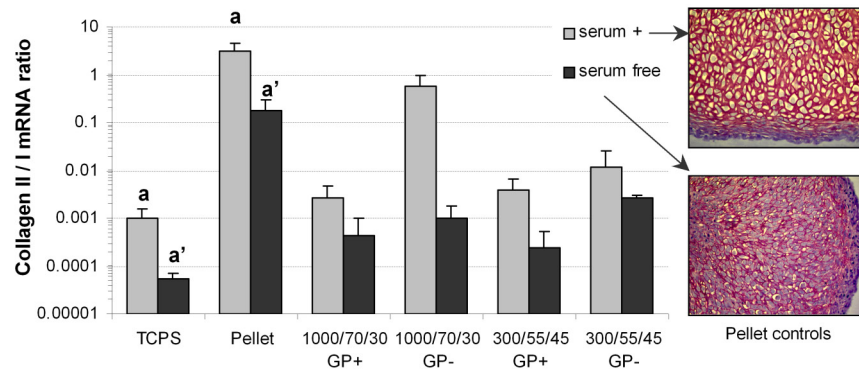


Figure 3 - Re-differentiation potential (collagen II/I mRNA ratio) of expanded (P2) human nasal chondrocytes on gas plasma treated (GP+) and untreated (GP-) substrates after 10 days culture in serum containing (S+) or serum free (SF) media. Negative control for re-differentiation = TCPS; positive control for re-differentiation = pellet. Inset pictures show positive safranin-O staining in pellet cultures in both S+ and SF media ($\times 100$). Significant difference between substrates denoted by: S+ media = a ; SF media = a'. ► p215.

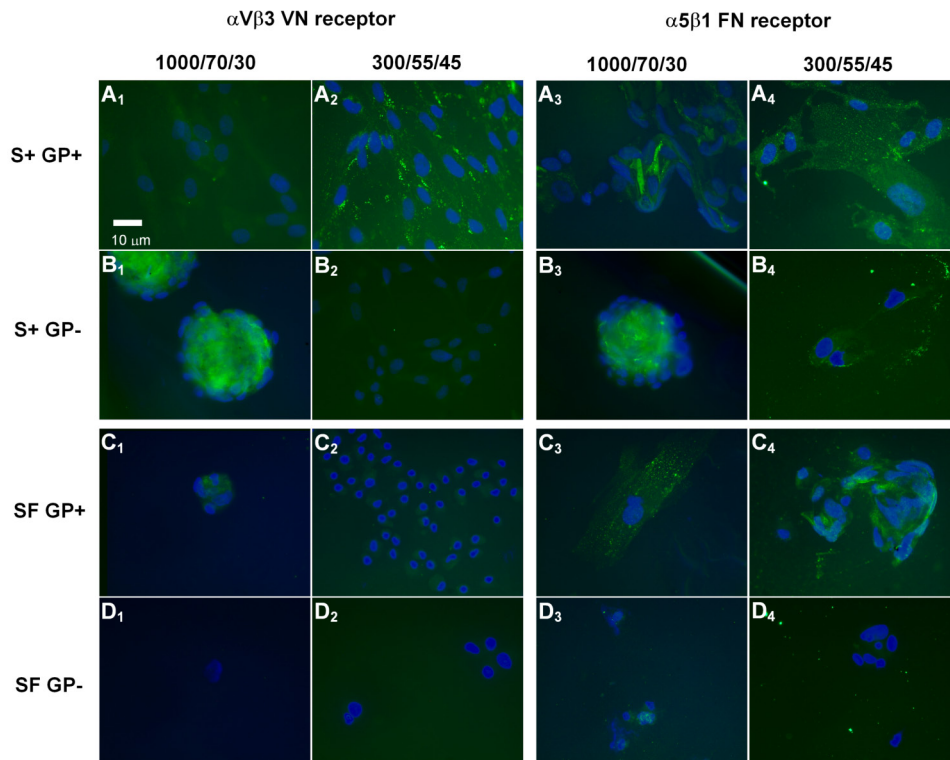


Figure 4 – Immunofluorescence images showing $\alpha V\beta 3$ vitronectin (VN, A₁-D₂) and $\alpha 5\beta 1$ fibronectin (FN, A₃-D₄) integrin intensity in expanded human nasal chondrocytes at day 10. Cells were plated on GP+ (A₁-₄, C₁-₄) and GP- films (B₁-₄, D₁-₄) with 1000/70/30 (A₁-D₁, A₃-D₃) and 300/55/45 compositions (A₂-D₂, A₄-D₄), and cultured in S+ (A₁-B₄) or SF media (C₁-D₄). Cell nuclei stained blue with DAPI. ► p215.

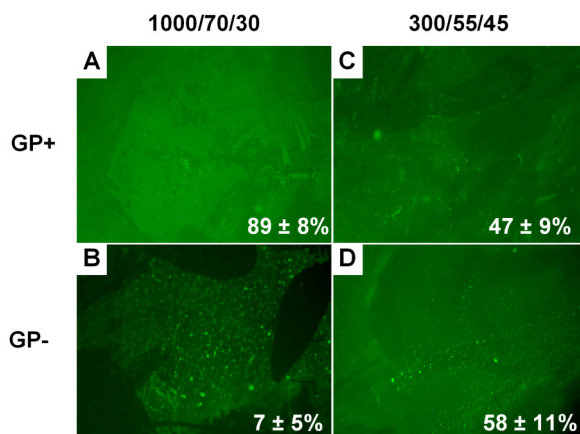


Figure 5 – Fluorescence images (x100) showing adsorption of FITC bovine serum albumin (BSA) on GP+ (A, C) and GP- (B, D) films with 1000/70/30 (A, B) and 300/55/45 compositions (C, D). Image analysis was used to estimate the percentage intensity of FITC-BSA and are included in each image. ► p216.

Protein Adsorption:

To give an indication of the effect of substrate composition and GP treatment on protein adsorption capacity of PEGT/PBT films, immunofluorescent detection of adsorbed FITC-conjugated bovine serum albumin (BSA) was performed, and semi-quantitative results were obtained using image analysis. As illustrated in Figure 5, GP treatment of 1000/70/30 films (Fig 5A) resulted in considerably greater BSA adsorption ($89\% \pm 8\%$) than on untreated films where protein adsorption was limited ($6.8\% \pm 5\%$, Fig 5B). There was no obvious effect of GP treatment on BSA adsorption between GP+ and GP- 300/55/45 films ($47\% \pm 9\%$ and $58\% \pm 11\%$ respectively).

Discussion & Conclusions:

The goal of this study was to evaluate whether controlled changes in substrate surface chemistry via gas plasma surface modification and substrate composition can regulate the adhesion and post-expansion re-differentiation of human chondrocytes in serum containing (S+) and serum free (SF) media. These two main issues, relating to chondrocyte adhesion mechanisms and downstream re-differentiation capacity, are discussed accordingly below.

Cell Adhesion: In this study, we demonstrated that PEGT/PBT composition clearly had an effect on the adhesion of expanded human nasal chondrocytes, with greater DNA content measured on 300/55/45 films as compared to 1000/70/30 films irrespective of whether S+ or SF media were used (Fig 1A). Independent of PEGT/PBT composition, GP treatment of 2D films promoted significantly higher DNA content as compared to untreated films, but only when serum was present in the culture medium. This suggests that GP surface treatment modified the adsorption of serum-derived attachment proteins, such as FN and VN. Mahmood *et al.* [299] recently demonstrated a positive correlation between FN adsorption and attachment of primary human articular chondrocytes on PEGT/PBT substrates of varying composition. In

this case, preferential adsorption of FN over VN and greater cell attachment was observed on 300/55/45 substrates, as compared to 1000/70/30 substrates. Increased adsorption of FN on 300/55/45 co-polymers might result from reduced steric interference by pendant PEG chains, or preferential binding to PBT regions at the surface. While expanded rather than primary human nasal chondrocytes were used in this study, preferential FN adsorption was the likely reason why GP- 300/55/45 films also promoted greater cell adhesion as compared to GP- 1000/70/30 films. Although we did not directly measure FN and VN adsorption in this study (only protein adsorption via BSA), we hypothesize that GP treatment overrules the mechanism by which proteins normally compete on various PEGT/PBT substrates, allowing preferential adsorption of FN directly, and thereby allowing enhanced cell adhesion in both GP+ 300/55/45 and 1000/70/30 films (Fig 1A). Although these direct mechanisms are unclear, the typical role of PEG might be affected by GP treatment. PEG incorporation at biomaterial surfaces is commonly employed to limit protein adsorption as a result of PEG hydrophilicity and high surface mobility [9, 351]. In our case, PEG incorporation was achieved by synthesizing long (MW 1000) or short (MW 300) PEG chains within the 70:30 or 55:45 wt% ratio of PEGT and PBT respectively, making up the PEGT/PBT block co-polymers. In an Ar gas plasma, sputtering and ultraviolet etching play a predominant role in modifying polymer surfaces [473]. Furthermore, it has been shown that in an Ar gas plasma, the etching rate of the amorphous PEG phase is approximately 4 times higher than for the more crystalline PBT phase [371], thereby selectively removing mobile, hydrophilic PEG from PEGT/PBT block co-polymer surfaces. This would suggest that wettability decreases with GP treatment, yet that was not the case (Table 1). The increase in wettability of PEGT/PBT co-polymers following Ar GP treatment is more likely attributed to surface oxidation, due to the introduction of polar functional groups by reactions of surface free radicals with oxygen in air (post-oxidation) [371]. The fact that lower PEG MW compositions (i.e. 300/55/45) have been shown to preferentially adsorb FN, resulting in improved chondrocyte attachment, and that Ar GP treatment likely exposes additional PBT regions (via preferential etching of PEG) for any given composition of PEGT/PBT substrate (i.e. 300/55/45 or 1000/70/30), suggests that preferential FN adsorption is greatly enhanced following GP treatment, allowing significantly greater cell adhesion to similar levels as TCPS (which itself is commercially GP treated). Clearly, cell adhesion is severely impaired in the absence of serum proteins, and GP surface modification provides no additional effect (via surface charge for instance) to improve matters. If preferential PEG etching occurs then additional PBT regions are not influencing physico-chemical mechanisms by which chondrocytes adhere in the absence of serum. While the mechanism is unclear, PEGT/PBT composition alone (i.e. 300/55/45 compared with 1000/70/30) does have an influence in assisting cell adhesion in SF conditions (Fig 2). However, since TCPS allowed greatest cell adhesion in SF media, it seems that substrate chemical composition, and not surface wettability, has a significant role to play.

Gene Expression: Fewest cells adhered to GP- 1000/70/30 films in S+ medium compared with all other conditions (Fig 1A). However, with respect to cell re-differentiation, these substrates promoted chondrocyte re-differentiation in 2D most similar to those shown in pellet cultures, resulting in collagen II/I mRNA ratios 2- and 3-orders of magnitude greater than GP- 300/55/45 and both GP+ compositions respectively (Fig 3). Our data confirmed those of Mahmood *et al.* [299] showing reduced chondrocyte re-differentiation on FN-rich 300/55/45 films, and supports previous studies where FN has been shown to enhance chondrocyte de-

differentiation in monolayer culture [384, 507]. Following our hypothesis that GP treated PEGT/PBT substrates preferentially adsorb FN, it is understandable that GP+ 1000/70/30 and 300/55/45 films resulted in least chondrocyte re-differentiation as measured by collagen II/I mRNA levels (Fig 3). We also observed that scaffold wettability likely had little effect on chondrocyte re-differentiation. For example, we cannot assume hydrophilic substrates support re-differentiation since, according to contact angle data (Table 1), the most hydrophilic substrates (GP+ 300/55/45 and 1000/70/30) actually showed least re-differentiation, whereas the most hydrophobic substrate (GP- 300/55/45) also had limited re-differentiation potential.

Integrin Receptor Detection: Previous studies have shown that $\alpha 5\beta 1$ is a primary chondrocyte fibronectin receptor. Knudson *et al.* [241] showed that antibodies directed against $\alpha 5$ or $\beta 1$ integrin subunits inhibited more than 80% of cell adhesion to FN, or more than 90% of chondrocyte adhesion to FN and types II and VI collagen respectively. We generally observed that the intensity of staining for FN receptor was higher than for VN receptor. Specifically, we observed greater $\alpha 5\beta 1$ FN integrin receptor expression in general on GP+ treated films in S+ and SF media than $\alpha V\beta 3$ VN receptor expression, and may be the reason why chondrocytes adhered to GP+ films displayed limited re-differentiation capacity. Previous studies have demonstrated $\alpha V\beta 3$ VN- and $\alpha 5\beta 1$ FN-receptor expression of primary human articular chondrocytes in serum containing medium on 300/55/45 but not 1000/70/30 films [299]. We observed similar results in this study for expanded human nasal chondrocytes, however, in our case VN and FN integrin expression in GP- 1000/70/30 was observed between cell-cell interaction within aggregates, rather than cell-substrate interactions. In SEM and immunofluorescence images, there were clear relationships between cell morphology and re-differentiation. Substrates showing enhanced cell adhesion and spreading resulted in low collagen II/I mRNA ratios more similar to TCPS (negative control), whereas substrates promoting a more spherical cell morphology (i.e. GP- 1000/70/30) resulted in greater collagen II/I mRNA ratios, more similar to pellet cultures (positive control).

Conclusion: We demonstrated that PEGT/PBT composition had an effect on adhesion of expanded human nasal chondrocytes irrespective of whether S+ or SF media was used (Fig 1). We also demonstrated a simple GP surface modification process which significantly improved chondrocyte adhesion on PEGT/PBT substrates, but only in S+ media. Based on protein (BSA) adsorption and previous FN and VN adsorption studies on PEGT/PBT substrates, we suggest that GP treatment enhances FN adsorption, thereby improving adhesion but limiting the re-differentiation capacity of expanded human chondrocytes. We further demonstrated that PEGT/PBT composition affects re-differentiation potential of de-differentiated human chondrocytes, evidenced by greater collagen II/I mRNA in 1000/70/30 compositions which promoted a more spherical cell morphology. This study highlights the need to carefully assess cell-substrate interactions and the use of S+ or SF culture conditions to optimize the engineering of cartilage constructs, particularly with respect to surface modification to improve cellular adhesion whilst maintaining suitable re-differentiation capacity.

Chapter 8

The Effect of Scaffold Composition and Architecture on Human Nasal Chondrocyte Re-differentiation and Cartilaginous Matrix Deposition Capacity

Woodfield T.B.F.^{2,3‡}, Miot S.^{1‡}, Daniels A.U.⁴, Suetterlin R.⁵, Peterschmitt I.⁶, Heberer M.¹, van Blitterswijk C.A.², Riesle J.³, Martin I.¹

¹ Departments of Surgery and of Research, University Hospital Basel, Switzerland.

² Institute for Biomedical Technology, University of Twente, Enschede, The Netherlands

³ IsoTis S.A., Bilthoven, The Netherlands

⁴ Laboratory for Orthopaedic Biomechanics, Felix Platter Hospital, Basel, Switzerland

⁵ M.E. Muller Institute at the Biozentrum, University of Basel, Switzerland

⁶ UFR Pluridisciplinaire Enseignement Professionnalise Supérieur, Université Haute Alsace, Colmar, France.

Abstract:

We investigated whether the post-expansion re-differentiation and cartilage tissue formation capacity of adult human chondrocytes can be regulated by controlled modifications of scaffold composition and architecture. As a model system, we used poly(ethylene glycol terephthalate)-poly(butylene terephthalate) block copolymer scaffolds from 2 compositions (low or high PEG content, resulting in different wettability) and 2 architectures (generated by compression moulding or 3D fibre deposition) with similar porosity and mechanical properties, but different interconnecting pore architectures. Scaffolds were seeded with expanded human chondrocytes and the resulting constructs assessed immunohistochemically, biochemically and at the mRNA expression level following up to 4 weeks culture.

For a given 3D architecture, the more hydrophilic scaffold enhanced cell re-differentiation and cartilaginous tissue formation after 4 weeks culture, as assessed by higher mRNA expression of collagen type II, increased deposition of glycosaminoglycan (GAG) and predominance of type II over type I collagen immunostaining. The fibre deposited scaffolds, with a more accessible pore volume and larger interconnecting pores, supported increased GAG deposition, but only if the more hydrophilic composition was used.

By applying controlled and selective modifications of chemico-physical scaffold parameters, we demonstrate that both scaffold composition and architecture are instructive for expanded human chondrocytes in the generation of 3D cartilaginous tissues. The observed effects of composition and architecture were likely mediated respectively by differential serum protein adsorption and efficiency of nutrient/waste exchange.

[‡] Equally contributing authors. Miot S, Woodfield TBF, Daniels AU, Suetterlin R, Peterschmitt I, Heberer M, van Blitterswijk CA, Riesle J, Martin I. The Effect of Scaffold Composition and Architecture on Human Nasal Chondrocyte Re-differentiation and Cartilaginous Matrix Deposition Capacity. *Biomater* **2004** (accepted).

Introduction:

One of the challenges in tissue engineering is the design and fabrication of biodegradable scaffolds which are 'instructive' for specific cellular functions, and may thus regulate in a predictable and controlled fashion cell adhesion, proliferation, expression of a specific phenotype and extracellular matrix deposition. It has long been known that cell behaviour on synthetic polymers is related to both the physical and chemical properties of the substratum [291]. Scaffold physical structure may control cell function by regulating the diffusion of nutrients, waste products and cell-cell interactions [535], whereas scaffold surface chemistry indirectly affects cell adhesion, morphology and subsequent cellular activity by controlling adsorption of ions, proteins and other molecules from the culture medium [291, 443]. It is then this molecularly populated surface that the cells sense and respond to biochemically by means of specific receptors (e.g., integrins) [278].

Cartilage cells are an ideal model for the study of cell-substrate interactions, due to the tight relationships which have been established between chondrocyte morphology and function [285]. When chondrocytes are released from their extracellular matrix and cultured under conditions promoting a spread morphology, such as on 2D tissue culture plastic, they progressively lose their original phenotype (*i.e.*, expression of collagen type II and aggrecan) and display fibroblastic, pre-chondrogenic features (*i.e.*, expression of collagen type I and versican), a process typically described as dedifferentiation [24, 36]. Chondrocyte dedifferentiation can be reversed by culturing cells in substrates supporting a spherical morphology, such as polymer gels [24, 42] or porous polymer scaffolds [153, 318]. The influence of specific surface properties of various biomaterials on chondrocyte behaviour has been so far mostly investigated using 2D films [161, 215, 249, 263, 375]. However, the growing appreciation that cell behaviour in 2D cultures does not necessarily translate into 3D systems [1, 103] prompts for extended studies in 3D scaffolds where the introduction of an additional parameter, the 3D architecture, could modulate the effects of changes in the substrate composition.

As a model scaffold system, we selected a segmented block co-polymer consisting of soft, hydrophilic poly(ethylene glycol)-terephthalate (PEGT) segments and hard, hydrophobic poly(butylene terephthalate) (PBT) segments, denoted as *a/b/c*, whereby, *a* represents the PEG molecular weight (MW, g/mol), and *b* and *c* represent the weight percentage of PEGT and PBT blocks respectively. By varying the PEGT MW and the weight percentage ratio between PEGT and PBT, it is possible to modulate the wettability, protein adsorption, swelling and mechanical properties of the substrate [299, 519]. Furthermore, by changing the fabrication technique (*i.e.*, compression moulding or 3D fibre deposition) for a given PEGT/PBT composition, it is possible to fabricate 3D scaffolds with the same bulk composition and overall porosity but different interconnecting pore architectures [307].

Previously, Papadaki et al [375] reported that primary bovine chondrocytes seeded on 2D PEGT/PBT films best retained their chondrocytic phenotype when a 1000/70/30 composition was used. More recently, Mahmood et al [299] confirmed that 2D PEGT/PBT films produced from 1000/70/30 compositions better maintained the phenotype of primary adult human articular chondrocytes as compared to 300/55/45 compositions. The latter composition,

however, allowed re-differentiation of expanded human chondrocytes in 3D scaffolds produced by compression moulding [302].

In the present study, we produced 3D scaffolds in the two above described PEGT/PBT compositions either by compression moulding or 3D fibre deposition. We then used the generated scaffolds to investigate whether the post-expansion re-differentiation and cartilage tissue formation capacity of adult human chondrocytes can be regulated by controlled changes in PEGT/PBT composition and architecture.

Material and Methods:

Scaffold Fabrication

PEGT/PBT co-polymers were obtained from IsoTis S.A. (Bilthoven, The Netherlands). 3D scaffolds made from 300/55/45 and 1000/70/30 compositions (Fig. 1A) were produced using either a compression moulding and particle leaching technique (CM) [117] or a 3D fibre deposition technique (3DF) [307, 519]. Briefly, CM scaffolds were prepared by mixing PEGT/PBT granules with sodium chloride grains (75% by volume), sieved to obtain particles ranging in size from 400 – 600 μm . After compression moulding under heat and pressure, the polymerized PEGT/PBT block was then immersed in demineralised water for 48 h to remove the sodium chloride, and dried under reduced pressure in a vacuum oven. Porous 3DF scaffolds were constructed by successively layering a 0°-90° pattern of molten PEGT/PBT fibres from a $\text{\O}250$ μm nozzle onto a computer controlled x-y-z table. Fibres within each layer were spaced 1.0 mm apart, but were offset (staggered) by 0.5 mm between layers to optimize the “visible” surface available for cell seeding (Fig. 1B). Square blocks of 30 x 30 x 4 mm were produced with a consistent pore size and 100% interconnecting pore volume (Fig. 1B). Cylindrical scaffolds, $\text{\O}5$ x 4 mm, were cored from the bulk porous CM and 3DF blocks prior to cell seeding. Previous thermal analysis studies have demonstrated that CM and 3DF processing techniques do not result in changes of PEG MW or PEGT/PBT composition [519], and therefore, any differences seen in this study between architectures of CM and 3DF scaffolds could not be related to differences in scaffold composition.

Scaffold Characterisation

Scaffold architecture was analyzed using micro-computed tomography (μCT) using a desktop MicroCT machine (μCT -40, Scanco Medical, Bassersdorf, Switzerland) as described previously [307]. Briefly, two hundred 2D slices (2048x2048 pixels, 12 μm resolution) were scanned of every sample covering a height of 2.4 mm. The resulting grey-scale images were segmented and a threshold applied to extract the polymer phase and then inverted to extract the pore phase. This allowed 3D reconstruction of the scaffold volume (SV) and pore volume (PV) from stacked 2D images (Fig. 1B), which in turn could be analyzed to give information on scaffold volume percent (vol%) porosity, surface area to volume ratio, pore size and accessible pore volume using previously described techniques [251, 307, 348, 419, 535]. In addition to μCT , scaffold porosity was also determined using mass/volume techniques [307].

To characterize the mechanical properties of scaffolds with varying composition and architecture, unconfined static and dynamic compression tests were carried out on hydrated scaffolds to determine the equilibrium modulus (20% strain) and dynamic stiffness (0.1 Hz) for comparison with native articular cartilage tissue, as explained previously [307, 519].

Chondrocyte Isolation and Expansion

The source of hyaline cartilage was the human nasal septum, collected in the University Hospital of Basel after informed consent. Nasal chondrocytes were selected for this study since they de- and re-differentiate similarly to articular chondrocytes [469] but proliferate faster and exhibit a higher chondrogenic capacity after expansion [226]. Independent experiments were performed with cells from 2 patients (31 and 28 years old). Chondrocytes were isolated upon 22-hour incubation at 37°C in 0.15% type II collagenase and re-suspended in Dulbecco's Modified Eagle's Medium (DMEM) containing 10% fetal bovine serum, 4.5 mg/ml D-glucose, 0.1 mM non essential amino acids, 1 mM sodium pyruvate, 100 mM HEPES buffer, 100 U/ml penicillin, 100 µg/ml streptomycin and 0.29 mg/ml glutamine (complete medium). Chondrocytes were plated in plastic dishes at a density of 10⁴ cells/cm² in complete medium further supplemented with 1 ng/ml transforming growth factor-β1 (TGF-β1), 5 ng/ml fibroblast growth factor-2 (FGF-2) and 10 ng/ml platelet-derived growth factor-bb (PDGF-bb) (all from R&D Systems, Minneapolis, MN). This specific combination of growth factors has previously been shown to enhance human nasal chondrocyte proliferation and post-expansion differentiation ability [469]. When cells were sub-confluent, they were detached by treatment with 0.3% type II collagenase, followed by 0.05% trypsin/0.53 mM EDTA, and re-plated at 5x10³ cells/cm². When cells again approached confluence, second passage cells were detached and seeded on scaffolds as described below.

Chondrocyte Seeding and Culture on 3D Scaffolds

Cylindrical scaffolds (Ø5 mm by 4 mm thick) were pre-wet with 70% ethanol, extensively rinsed in complete medium and blotted dry. Cells (5 x 10⁶ /scaffold, re-suspended in 54 µl of complete medium) were statically seeded on the scaffolds placed in dishes coated with a thin film of 1% agarose. Constructs were statically cultured for 2 and 4 weeks in complete medium supplemented with 10 µg/ml insulin and 0.1 mM ascorbic acid, with culture medium completely replaced twice a week. Duplicate specimens were generated and assessed for each experimental group (e.g. type of scaffold and time point). After harvesting, each construct was divided into three parts which were independently processed for histological and immunohistochemical, biochemical or gene expression analysis.

Histological and Immunohistochemical Analysis

Tissue constructs were fixed in 4% formalin for 24 hours at 4°C, dehydrated, embedded in paraffin and cross-sectioned (7 µm thick). For histological analysis, sections were stained with Safranin-O for sulphated glycosaminoglycans (GAG). Immunohistochemical analysis was performed as described by Baschong *et al.* [20]. Sections were treated with 0.25% ammonia (NH₃) in 70% ethanol for 1 h during de-paraffinisation in order to eliminate autofluorescence. Sections were then sequentially treated with 10 mg/ml sodium borohydride (NaBH₄) for 40 min at 4°C and 1 mg/ml testicular hyaluronidase for 30 min at 37°C. Non-specific sites were

blocked by incubation with swine serum diluted 1:10 in PBS for 10 min at room temperature (RT). Sections were double labelled by incubation with a polyclonal antibody against collagen type I (T40111R, Biodesign International, Saco, ME) followed by a goat anti-rabbit secondary antibody conjugated with Alexa 488 (Molecular Probes) and with a monoclonal antibody against collagen type II (II-II6B3, Developmental Studies Hybridoma Bank, Iowa City, IA) followed by a donkey anti-mouse secondary antibody labelled with Cy3 (Jackson Immuno Research, Lab). Other sections were labelled with a monoclonal antibody against smooth muscle α -actin (SMA, clone 1A4, Sigma) followed by a donkey anti-mouse secondary antibody labelled with Cy3. All incubations with the antibodies were performed for 60 min at RT. All sections were mounted with Mowial-1188 (Hoechst, Frankfurt, Germany), dried overnight and stored in the dark until microscopic imaging using a confocal laser scanning microscope (TCS 4-D CLSM, Leica AG, Heidelberg). The image stacks were generated as 0.5 μ m optical sections in parallel in the 488 nm (green) and 568 nm (red) channels. As a control for tissue quality, a series of differential interference contrast (DIC) images was acquired in a subsequent scan of the same field.

Biochemical Analysis

Tissue constructs were digested in 1 ml of proteinase-K solution (1 mg/ml proteinase-K in 50 mM Tris with 1 mM EDTA, 1 mM iodoacetamide and 10 μ g/ml pepstatin-A) for 15 hours at 56°C. GAG contents were measured spectrophotometrically after reaction with dimethylmethylene blue dye [122] with chondroitin sulphate as a standard. The GAG content was normalized to the amount of DNA which was measured using a Cyquant cell proliferation assay kit (Molecular Probes), with calf thymus DNA as a standard.

Gene Expression Analysis

RNA was extracted from tissue constructs using 250 μ l Trizol (Life Technologies, Basel, CH) according to the manufacturer's instructions. cDNA was generated from total RNA using reverse-transcriptase Stratascript (Stratagene) in the presence of dNTP and DTT. Real-time PCR reactions were performed and monitored using a ABI prism 7700 Sequence Detection System and the Sequence Detector V program (Perkin Elmer Applied Biosystems). The PCR master mix was based on AmpliTaq Gold DNA polymerase (Perkin Elmer Applied Biosystems). In the same reaction, cDNA samples were analyzed both for collagen type II and for the housekeeping gene (18S ribosomal RNA), using previously described sequences of primers and probes [19]. Each cDNA sample was assessed at least in duplicate and collagen type II mRNA expression levels normalized to the corresponding 18S rRNA levels.

Statistical Analysis

Data are presented as mean \pm standard deviation. The normality of the populations to be analyzed was tested by Shapiro-Wilk tests. Means were compared by Student's t-tests in case of normal population or by Mann Whitney tests in case of failure of normality. Statistical analyses were performed using the Sigma Stat software (SPSS Inc. version 7.5), with $p < 0.05$ as the criteria for statistical significance.

Results:

Scaffold Characterisation

Two processing techniques (CM and 3DF) were used to fabricate porous scaffolds from two different PEGT/PBT co-polymer compositions, resulting in reproducible and comparable volume percent porosities, as determined by mass-volume (m/V) and 3D μ CT techniques (Table 1). The scaffold surface area per volume ratio was approximately 3 times greater in CM scaffolds than in 3DF scaffolds.

Figure 2 shows the accessible pore volume distribution and pore size distribution for both 300/55/45 and 1000/70/30 compositions of CM and 3DF scaffolds represented as a percentage of total pore volume (PV). The accessible pore volumes in both CM and 3DF scaffolds were approximately 100% interconnected. However, 3DF scaffolds had a considerably greater accessibility cut-off value of $\sim 360 \mu\text{m}$ (taken as the pore size guaranteeing at least 90% of the pore volume was accessible) compared with $\sim 100 \mu\text{m}$ in CM scaffolds (Fig. 2A). Indeed, for the pore range investigated in this study (excluding the pore size extremes of $6 \mu\text{m}$ and $1000 \mu\text{m}$ pores), a greater percentage of the pore volume was accessible in 3DF scaffolds as compared with CM scaffolds, and typically corresponded to between 300-400 μm greater accessible pore size for a given percentage pore volume. Furthermore, as shown in Figure 2B, 300/55/45 and 1000/70/30 3DF scaffolds had considerably greater average pore sizes (388 μm and 380 μm respectively) than CM scaffolds (182 μm and 160 μm respectively). The leftward shift in the average pore size distribution observed in CM and 3DF scaffolds of different composition (Fig. 2B) was likely due to the documented swelling characteristics of the more hydrophilic 1000/70/30 compositions [519]. To give an indirect measure of scaffold tortuosity or complexity, 3D μ CT analysis also allowed determination of a connectivity density (CD) index, defined as the maximal number of pore walls that may be cut without completely separating the scaffold structure [366]. For CM scaffolds, the CD ranged between 246.2 – 407.7 as opposed to a range of 5.1 – 7.3 in 3DF scaffolds. Given that 3DF scaffolds show a very low CD and a pore volume that is 90% accessible at pore sizes greater than 360 μm demonstrates a simple, less tortuous pore architecture, whereas CM scaffolds exhibited a high CD and a pore volume that is 90% accessible at pore sizes greater than 100 μm , indicative of a more complex, tortuous pore architecture.

Table 1 - Structural characterisation of scaffold architecture.

Sample	Measured Vol% Porosity		Scaffold Vol. Fraction $\mu\text{CT} (\text{mm}^{-1})$	Avg. Pore Size $\mu\text{CT} (\mu\text{m})$	Pore Size Range $\mu\text{CT} (\mu\text{m})$	Pore Size at $\geq 90\%$ Accessible Pore Vol. $\mu\text{CT} (\mu\text{m})$
	m/V (%)	$\mu\text{CT} (\%)$				
CM 300/55/45	75.6 ± 1.9	81.8	10.0	182	6 – 450	98
CM 1000/70/30	76.0 ± 2.1	77.8	12.2	160	6 – 444	95
3DF 300/55/45	70.2 ± 1.2	74.4	3.8	380	132 – 450	380
3DF 1000/70/30	71.5 ± 1.8	71.2	4.0	388	156 – 600	360

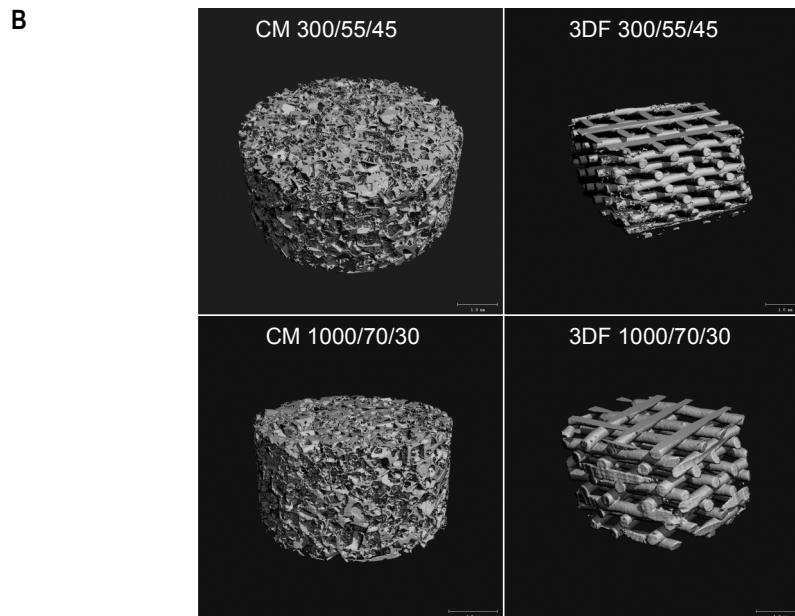
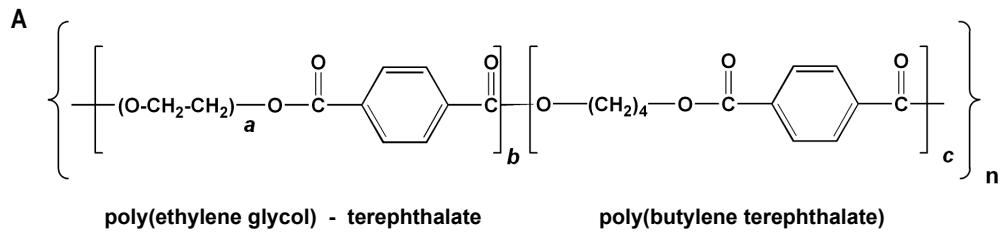


Figure 1 - (A) Chemical structure of poly(ethylene glycol) terephthalate - poly(butylene terephthalate) (PEGT/PBT) block copolymers. The molecular weight of PEG (*a*) and the weight ratio between PEGT and PBT (*b/c*) defines the specific composition obtained (*a/b/c*). (B) 3D reconstruction by micro-computed tomography scans of different PEGT/PBT scaffold architectures generated by compression moulding (CM) or 3D fibre deposition technique (3DF) and compositions (300/55/45 and 1000/70/30).

Similar equilibrium modulus and dynamic stiffness properties were obtained for both CM and 3DF scaffolds. 300/55/45 scaffolds yielded higher equilibrium modulus and dynamic stiffness values than 1000/70/30 scaffolds of the same geometry (Fig. 3). This was likely due to the lower PEG MW and greater weight percentage ratio of "stiff" PBT blocks to "soft" PEGT blocks present in the 300/55/45 scaffolds, and limited water uptake. Furthermore, 300/55/45 scaffolds yielded equilibrium modulus values approximately 200-300% higher than native immature bovine and human articular cartilage, whereas dynamic stiffness values were approximately 50% of native tissues.

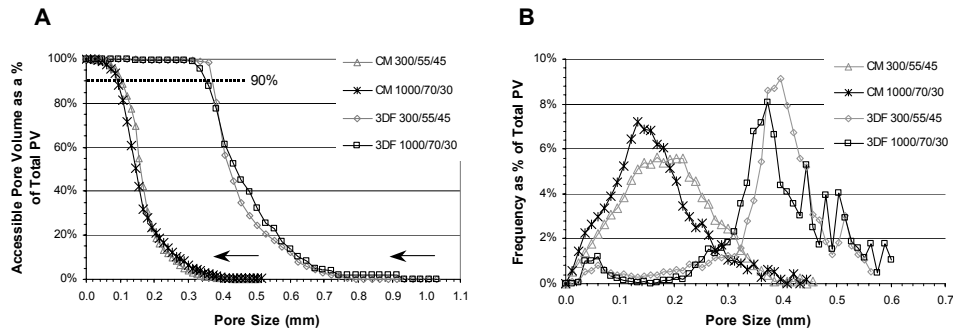


Figure 2 - Accessible pore volume distribution (A) and pore size distribution (B) for both 300/55/45 and 1000/70/30 compositions of CM and 3DF scaffolds represented as a percentage of total pore volume (PV). The dotted line in (A) represents the 90% cut-off value, used to determine the pore size at which 90% of the pore volume was no longer accessible. Arrows in (A) indicate direction of pore accessibility measurement, from scaffold periphery towards scaffold interior.

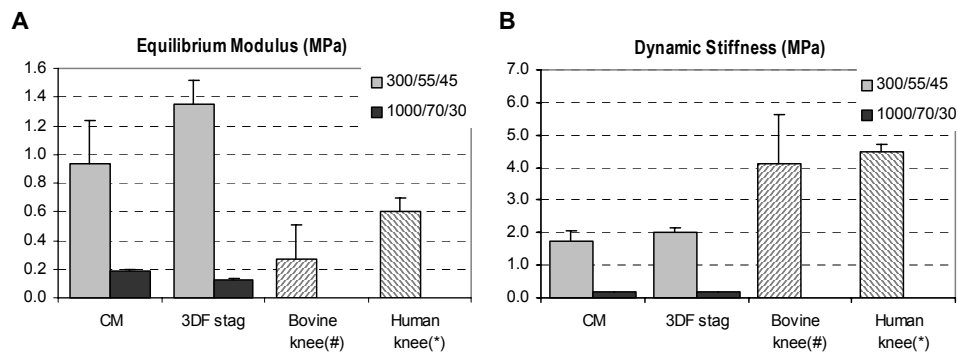


Figure 3 - Equilibrium modulus (20% strain) (A) and dynamic stiffness (0.1 Hz) (B) of hydrated CM and 3DF scaffolds compared with natural articular cartilage; # taken from [519], * taken from [475].

Histological and Immunohistochemical Analysis

After expansion in monolayer for 2 passages, nasal chondrocytes were seeded and cultured in CM and 3DF PEGT/PBT scaffolds based on the composition 300/55/45 or 1000/70/30. After 4 weeks of cultivation in constructs based on 300/55/45 scaffolds, most cells appeared elongated, indicating a dedifferentiated phenotype, and Safranin-O staining intensity was relatively faint (Fig. 4A, C). In constructs based on 1000/70/30 scaffolds, cells exhibited a rounded morphology, characteristic of a more differentiated phenotype, and the extracellular matrix was intensely stained for sulphated GAG (Fig. 4B, D). A similar trend was observed after 2 weeks of culture, although GAG staining intensity was generally weaker than at 4 weeks (data not shown). For each composition of PEGT/PBT, the Safranin-O staining was relatively more intense in the constructs based on 3DF scaffolds (Fig. 4C, D) than in those based on CM scaffolds (Fig. 4A, B). After 4 weeks of culture, in all experimental groups,

staining for Safranin-O was preferential at the periphery of the constructs, while the centre was generally only faintly stained. This pattern of GAG distribution is consistent with previous observations reported for tissue engineered cartilage constructs of similar dimensions cultured under static conditions [365].

After 4 weeks of culture, immunohistochemical staining for collagen type I was positive in constructs from all experimental groups (Fig. 5A, C, E, G), whereas staining for collagen type II was not detected in constructs based on CM 300/55/45 scaffolds (Fig. 5B). Collagen type II staining was predominant to that for collagen type I in constructs based on 1000/70/30 scaffolds, both in the CM (Fig. 5F) and 3DF (Fig. 5H) architectures, whilst it was of similar intensity to collagen type I staining in constructs based on 3DF 300/55/45 scaffolds (Fig. 5D). Constructs were also immunohistochemically stained for smooth muscle α -actin (SMA), a contractile actin isoform expressed by fibroblastic cells [33] and dedifferentiated chondrocytes [236, 318]. After 2 and 4 weeks of culture, cells were faintly stained in the constructs based on 300/55/45 scaffolds, independently of their architecture, whilst no SMA staining was detected in constructs based on 1000/70/30 scaffolds (data not shown).

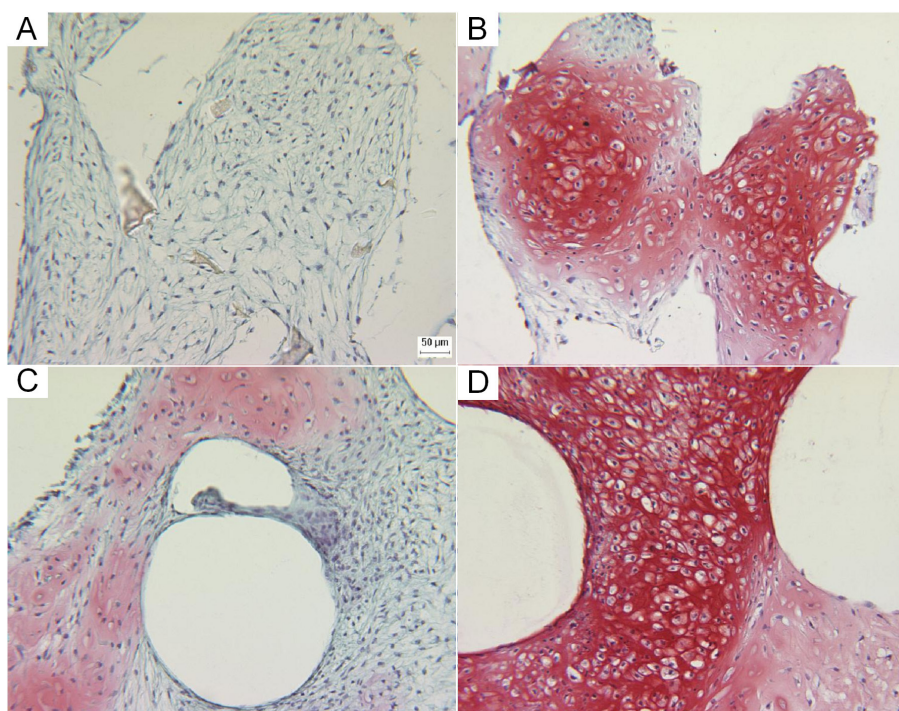


Figure 4 - Representative cross-sectional fields of constructs generated by 4 weeks culture of human nasal chondrocytes on CM 300/55/45 (A), CM 1000/70/30 (B), 3DF 300/55/45 (C), or 3DF 1000/70/30 (D) scaffolds. Histological sections were stained by Safranin-O. Scale bar = 50 μ m. ► p217.

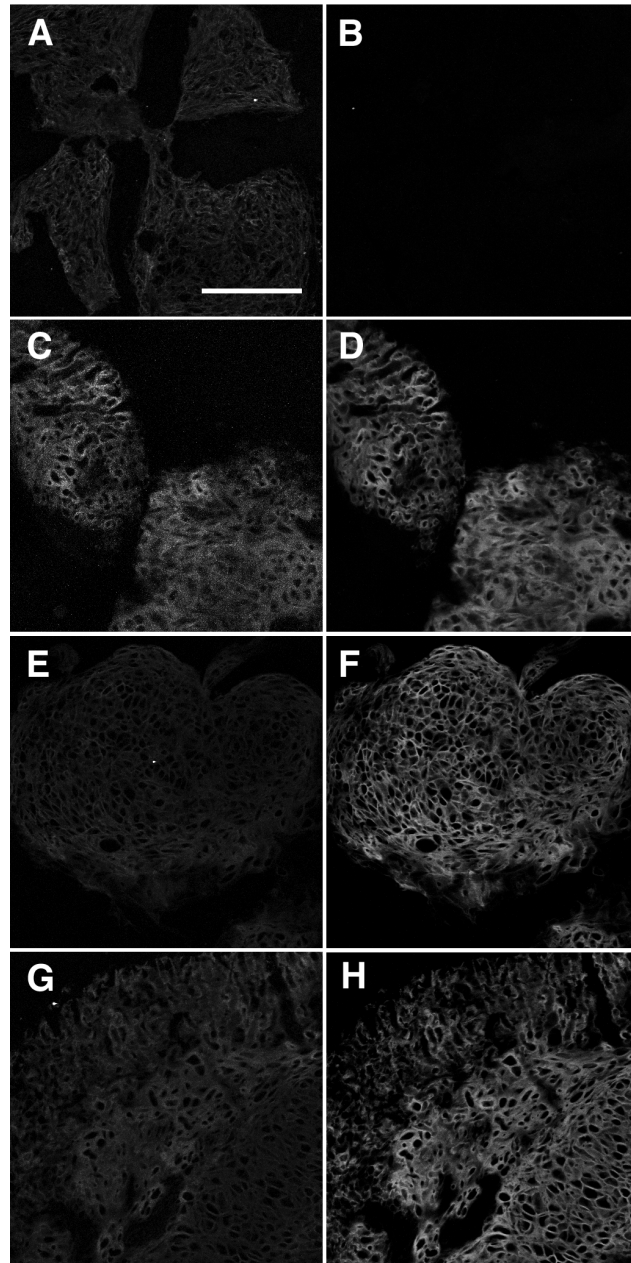


Figure 5 - Collagen type I (left column) and type II (right column) immunostaining of chondrocytes cultured for 4 weeks in the scaffolds CM 300/55/45 (A, B), 3DF 300/55/45 (C, D), CM 1000/70/30 (E, F), or 3DF 1000/70/30 (G, H). Scale bar = 200 μ m.

Biochemical Analysis

The amounts of DNA were not significantly different in the constructs based on the four types of scaffolds and cultured for 2 or 4 weeks (data not shown). The amounts of accumulated GAG normalized to the DNA content (GAG/DNA) significantly increased from 2 to 4 weeks of culture in all experimental groups (Fig. 6), indicating a temporal development of cartilaginous tissue, in agreement with the histological observations.

After 4 weeks of culture, constructs based on 1000/70/30 scaffolds contained significantly higher GAG/DNA ratios than those based on 300/55/45 scaffolds, both for CM ($p=0.021$) and 3DF ($p=0.021$) architectures. Constructs based on 3DF scaffolds contained significantly higher GAG/DNA ratios than those based on CM scaffolds, but only if the 1000/70/30 composition was used ($p=0.021$) (Fig. 6).

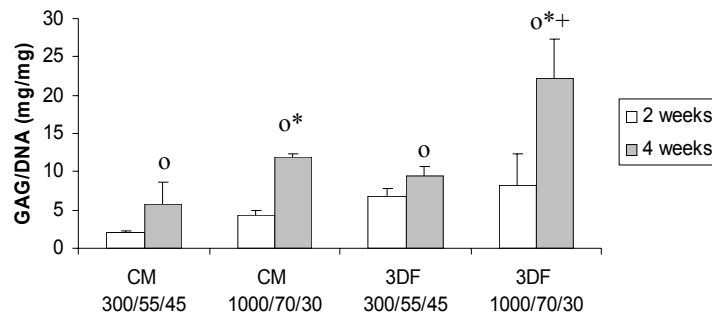


Figure 6 - Glycosaminoglycan (GAG) content normalized to the DNA amount of constructs generated by chondrocytes cultured for 2 (white bars) or 4 weeks (grey bars) in the scaffolds CM 300/55/45, CM 1000/70/30, 3DF 300/55/45 and 3DF 1000/70/30. Statistically significant differences ($p<0.05$) are indicated as follows. *: different from composition 300/55/45 for the same architecture; +: different from architecture CM for the same composition; o: different from 2 weeks of culture for the same architecture and composition.

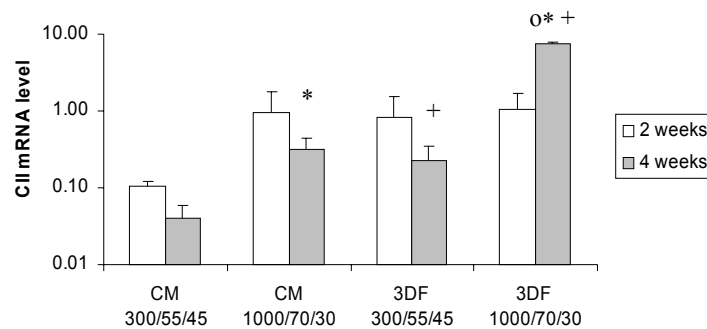


Figure 7 - Collagen type II mRNA expression level normalized to 18S rRNA (arbitrary units) by chondrocytes cultured for 2 (white bars) or 4 weeks (grey bars) in the scaffolds CM 300/55/45, CM 1000/70/30, 3DF 300/55/45 and 3DF 1000/70/30. Statistically significant differences ($p<0.05$) are indicated as follows. *: different from composition 300/55/45 for the same architecture; +: different from architecture CM for the same composition; o: different from 2 weeks of culture for the same architecture and composition.

Collagen Type II Gene Expression

From 2 to 4 weeks of culture, the collagen type II mRNA expression levels increased significantly in the constructs based on 3DF 1000/70/30 scaffolds ($p=0.021$), and decreased significantly in those based on CM 300/55/45 scaffolds ($p=0.019$). No statistically significant temporal change was detected in the other experimental groups (Fig. 7).

After 4 weeks of culture, chondrocytes in 1000/70/30 scaffolds expressed significantly higher collagen type II mRNA levels than in 300/55/45 scaffolds, both for CM ($p=0.020$) and 3DF ($p=0.020$) architectures. Chondrocytes cultured in 3DF scaffolds expressed significantly higher collagen type II mRNA levels than in CM scaffolds, both for 1000/70/30 ($p=0.020$) and 300/55/45 ($p=0.019$) compositions.

Collagen type II mRNA expression levels as a function of scaffold composition and architecture were in agreement with collagen type II protein deposition, assessed immunohistochemically. In particular, after 4 weeks of culture, constructs based on CM 300/55/45 scaffolds, where collagen type II protein was not detected (Fig. 5B), displayed the lowest collagen type II mRNA expression levels (Fig. 7).

Discussion:

Summary

In the present study, we demonstrated that a PEGT/PBT composition previously reported to support maintenance of the chondrocytic phenotype in 2D films (*i.e.*, 1000/70/30) [299] is also capable of promoting chondrocyte re-differentiation and cartilaginous matrix accumulation in 3D porous scaffolds. This result was obtained for both of the 3D architectures studied, although a highly interconnecting and accessible pore architecture (*i.e.*, 3DF scaffolds) further improved chondrogenesis in 1000/70/30 scaffolds.

Cell/Biomaterial Interactions

The behaviour of chondrocytes cultured on a specific substrate is determined by sequential events starting from integrin-mediated interactions with the proteins adsorbed on the biomaterial [189], subsequent adhesion and morphological changes, finally regulating the differentiation stage and thus the quality and quantity of ECM deposition. As compared to the 300/55/45 substrate, the higher wettability of the 1000/70/30 material (contact angle of $39^\circ \pm 1^\circ$ versus $48^\circ \pm 3^\circ$ [111, 519]), combined with a larger size and density of the hydrophilic PEG chains [146, 152], is expected to generate a greater volume of moving water molecules at the scaffold surface, which is known to reduce unspecific adsorption of serum proteins, including fibronectin [262, 299]. Increased fibronectin adsorption is generally associated with cell spreading [299, 533], and is consistent with our result that chondrocytes displayed a more round shape and expressed reduced amounts of smooth muscle α -actin in the hydrophilic 1000/70/30 scaffolds. Based on known structure-function relationships in chondrocyte biology [533], these morphological and cytoskeletal features would then explain the greater extent of cell re-differentiation, assessed by the higher mRNA expression of collagen type II, and the

generation of superior cartilaginous tissues, assessed by the increased deposition of GAG and the predominance of type II over type I collagen. The observation that a more hydrophilic substrate supports differentiated cellular functions is consistent with previous studies performed using fetal bovine and human chondrocytes [276, 299], rat marrow stromal cells [146], rat hepatocytes [107] and human hepatoblastoma cells [243]. One of the most innovative aspects of our work is the indication that the composition of a porous 3D scaffold is instructive for the development of engineered cartilage in the same direction predicted by studies of chondrocyte differentiation performed in 2D membranes [299].

Scaffold Architecture

As compared to cells cultured in 1000/70/30 CM scaffolds, those cultured in 1000/70/30 3DF scaffolds displayed an increased extent of re-differentiation and generated tissues which were closer to natural cartilage, histologically and biochemically. Since the two scaffolds share an identical composition and are characterised by similar percent porosity and mechanical properties, the result was likely due to the higher accessibility cut-off value, average pore size and lower connectivity density of the 3DF scaffolds. This conclusion, which is relying on the unique opportunity of applying controlled modifications of selective physical parameters in the scaffolds investigated, underlines the importance of designing 3D architectures with highly accessible and interconnecting pore volumes, thereby facilitating the diffusion rate of nutrients and gases as well as waste removal [306]. The change in the scaffold architecture from CM to 3DF did not result in increased GAG fractions if a 300/55/45 composition was used. This observation is consistent with a previous study in which GAG accumulation by primary bovine chondrocytes cultured for 2 weeks in scaffolds based on 300/55/45 composition was similar in both 3DF and CM architectures, although when implanted subcutaneously in nude mice, 3DF constructs showed significantly higher GAG deposition than CM constructs [307]. Taken together, these findings suggest that, in a static *in vitro* environment, scaffold architectures with a highly accessible and interconnecting pore volume can better modulate the generation of engineered cartilage if certain pre-requisites necessary to promote chondrogenesis (e.g., a supportive substrate composition) are met.

Conclusions:

This study advances in the identification of criteria for design or selection of scaffolds with properties which are instructive for the re-differentiation of human expanded chondrocytes and supportive for the generation of 3D cartilaginous tissues. Specifically, we demonstrated the importance of a hydrophilic composition containing large and densely distributed PEG chains (e.g., 1000/70/30), combined with an highly interconnecting and accessible pore architecture (e.g., 3DF). Issues that have not been addressed in this study are related to the mechanical properties and degradation rate of the scaffolds. Indeed, in contrast to 300/55/45 scaffolds, those based on the 1000/70/30 composition poorly matched the equilibrium modulus and dynamic stiffness of native cartilage and are expected to further decrease their mechanical properties in a short period of time due to a relatively fast degradation rate [111]. In this regard, it has to be underlined that the choice of the scaffold composition could be related to the cartilage repair strategy selected (e.g., graft of a cell-

free scaffold, of a freshly cell-seeded construct or of a more developed engineered tissue). For example, if constructs are pre-cultured for a sufficient period of time, the presence of deposited ECM could compensate for intrinsically lower mechanical properties of the scaffold, which are on the other hand essential for a direct implantation approach. While a highly interconnecting and accessible pore architecture which also provides suitable mechanical properties may always be recommended (e.g., 3DF), for a strategy relying on grafting of immature cartilage constructs, one could envision a composite composition where a backbone with appropriate mechanical properties (e.g., 300/55/45) is coated with another substrate capable of promoting chondrocyte re-differentiation and cartilaginous matrix deposition (e.g., 1000/70/30). Further work is required to verify these principles in appropriate animal models.

Acknowledgments:

This work was supported by the Swiss Federal Office for Education and Science (B.B.W.) under the Fifth European Framework Growth Program (FP5 project SCAFCART, grant Nr. 99.0291). We are grateful to the Ear-Nose-Throat Department, University Hospital of Basel (head of clinic: Prof. Dr. R. Probst) for providing cartilage biopsies.



IV.

Instructive Anatomically-Shaped Scaffolds: Tissue-Engineered Implants for Joint Reconstruction.

Chapter 9

Towards Anatomically-Shaped Tissue-Engineered Implants for Reconstruction of Small Articulating Joints - A Preliminary *in vitro* and *in vivo* Study in Rabbits.

"The most exciting phrase to hear in science, the one that heralds new discoveries, is not 'Eureka!' but 'That's funny'..."

[Isaac Asimov, 1920-1992]

Chapter 9

Towards Anatomically-Shaped Tissue-Engineered Implants for Reconstruction of Small Articulating Joints - A Preliminary *in vitro* and *in vivo* Study in Rabbits

Woodfield T.B.F.^{‡1,2}, Wedler V.³, von Rechenberg B.⁴, Schneller M.³, Riesle J.², van Blitterswijk C.A.¹

¹ Institute for Biomedical Technology, University of Twente, Enschede, The Netherlands

² IsoTis S.A., Bilthoven, The Netherlands

³ Division for Plastic-, Hand- and Reconstructive Surgery, University Hospital Zurich, Switzerland

⁴ Musculoskeletal Research Unit, Dept. of Equine Sciences, University of Zurich, Switzerland

Abstract:

The ability to engineer functional, anatomically-shaped implants for treating focal or surface wide damage to articular cartilage represents a significant clinical demand. We describe preliminary studies investigating the feasibility of a tissue-engineering concept, from imaging of the joint to an anatomically-shaped implant for small joint reconstruction using an autologous rabbit knee model. Combinatorial approaches including computed tomography (CT); three-dimensional (3D) computer aided design (CAD); scaffold rapid prototyping (RP) via computer numerical controlled (CNC) milling and 3D fibre deposition (3DF); and bioreactor culture were used to engineer customized femoral and tibial cartilagenous implants with varying internal pore architecture, but identical external anatomic shape.

Prior to implantation, the effect of scaffold architecture, produced using compression moulding/particulate leaching (CM) or 3D fibre deposition (3DF), on chondrocyte differentiation and mechanical properties were evaluated following *in vitro* culture and subcutaneous implantation *in vivo* in nude mice. 3DF architectures promoted a homogeneous distribution of viable cells, glycosaminoglycan (GAG) and collagen type II as well as significantly greater GAG content and differentiation capacity (*i.e.* GAG/DNA), compared to CM architectures. Mechanical evaluation showed that 3DF scaffold/neo-tissue constructs exhibited significantly higher equilibrium modulus and dynamic stiffness (0.1 Hz) compared to CM scaffolds, which increased with culture time, and were similar to native cartilage. Following joint osteotomy and autologous implantation in rabbits, the goal was to evaluate implant fixation and joint function after short-term follow-up. After 6 weeks (*n*=2), femoral and tibial implants had integrated with the host bone and rabbits had regained limited function and knee flexion/extension. Histology indicated the presence of articulating surfaces between femoral and tibial implants, however for both CM and 3DF architectures, repair tissue was fibrous-like in appearance and did not resemble the cartilage-like tissue present prior to implantation.

New strategies adopting anatomically-shaped, tissue-engineering implants with designed internal pore architecture and mechanical properties may offer significant advantages for the repair or total joint resurfacing of damaged articular cartilage.

[‡] Woodfield TBF, Wedler V, von Rechenberg B, Schneller M, Riesle J, van Blitterswijk CA. Towards Anatomically-Shaped Tissue-Engineered Implants for Reconstruction of Small Articulating Joints - A Preliminary *in vitro* and *in vitro* Study in Rabbits. *Arth Rheum* **2004** (submitted).

Introduction:

Articular cartilage lesions resulting from trauma or degenerative diseases are commonly encountered clinical problems [60, 62, 313]. It is well established that damaged adult articular cartilage has limited regenerative capacity [436] resulting in joint pain, loss of mobility and associated secondary affects such as osteoarthritis [62]. Current treatment protocols employed clinically include osteochondral drilling, debridement, periosteal or perichondrial grafting, osteochondral autografts (mosaicplasty) or allografts, and autologous chondrocyte implantation [52, 65, 205, 220, 313, 369]. However, short of total joint replacement, few of these approaches are capable of consistently restoring long term function to damaged articular cartilage [54, 65, 203, 205, 313]. Tissue engineering approaches, adopting three dimensional (3D) scaffold conduits for delivery or recruitment of reparative cells in an organised manner to bridge voids within cartilage defects, offer considerable promise as alternative repair strategies [149, 452].

Over the past few years, our group has focused on developing model scaffold systems for studying functional articular cartilage repair using biodegradable, multi-block co-polymers based on poly(ethylene glycol)-terephthalate – poly(butylene terephthalate) (PEGT/PBT) [307, 375, 517, 519]. Central to this work has been the development model porous PEGT/PBT scaffolds with controlled porous architectures using conventional compression moulding/particulate leaching (CM) techniques [301, 307], and novel rapid prototyping (RP) techniques, such as 3D fibre deposition (3DF) [517, 519]. Rapid prototyping (RP) techniques allow construction of highly reproducible structures with complex geometries from computer aided design (CAD) models and advanced computer numerical controlled (CNC) manufacturing processes [209]. Application of this technology in combination with modern clinical imaging techniques, such as computed tomography (CT) and magnetic resonance imaging (MRI), has resulted in recent advances in producing customized metallic implants typically for total joint replacement, and more recently in scaffold development [185, 460, 461, 488]. Transferring RP and imaging technologies to encompass porous, biodegradable, biomaterials for cartilage tissue engineering poses a significant challenge.

The motivation for this study was the feasibility of developing anatomically-shaped, tissue-engineered cartilage implants for resurfacing and/or reconstruction of damaged finger joints in an *in vitro* and *in vivo* model. While previous attempts have been made to tissue-engineer various cartilagenous, bone and tendon components in the form of a finger joint, function was never evaluated in a load bearing environment *in vivo* [217]. In developing a functional implant, design issues, such as the restoration of articulating surfaces and contours; implant fixation to bone; and implant mechanical properties, needed to be addressed, in addition to tissue-engineering considerations, such as obtaining a suitable reparative cell source; cell expansion; cell re-differentiation and extra-cellular matrix formation. It was clear that in attempting to address these issues, the scope of this study was considerably greater, encompassing feasibility of a design process for developing functional, anatomically-shaped implants which could be widely applicable in the field of tissue engineering for repairing focal defects, or joint resurfacing/reconstruction.

To assess scaffold design criteria and feasibility in the current study, we chose an autologous rabbit knee model for evaluating joint reconstruction following osteotomy of femoral and

tibial articulating surfaces. Based on 3D imaging of the rabbit knee, two RP technologies were then chosen to develop anatomically-shaped femoral and tibial PEGT/PBT scaffolds with two distinctly different porous CM and 3DF architectures. *In vitro* and *in vivo* performance of tissue-engineered implants were evaluated in a stepwise approach in two separate experiments, as described below.

The general tissue engineering paradigm states that successful repair or replacement of articular cartilage will require grown tissue possessing the functional properties of the native tissue as well as graft-to-host tissue integration [204, 517]. A viable approach being to elaborate constructs *in vitro* which achieve biochemical compositions and mechanical properties that match those of native tissue, prior to implantation [200]. Therefore, in a preliminary study (experiment 1), our initial goal was to evaluate cartilage tissue formation and mechanical properties of CM and 3DF PEGT/PBT constructs following *in vitro* culture and subcutaneous implantation in nude mice. Cylindrical CM and 3DF PEGT/PBT scaffolds with the same overall porosity but different interconnecting pore architectures were produced. Static and dynamic mechanical properties of tissue-engineered CM and 3DF constructs were determined. Cartilage tissue formation was evaluated by means of safranin-O staining, scanning electron microscopy (SEM), cell viability, and collagen type I and type II immunolocalisation, as well as quantification of glycosaminoglycan (GAG) and DNA.

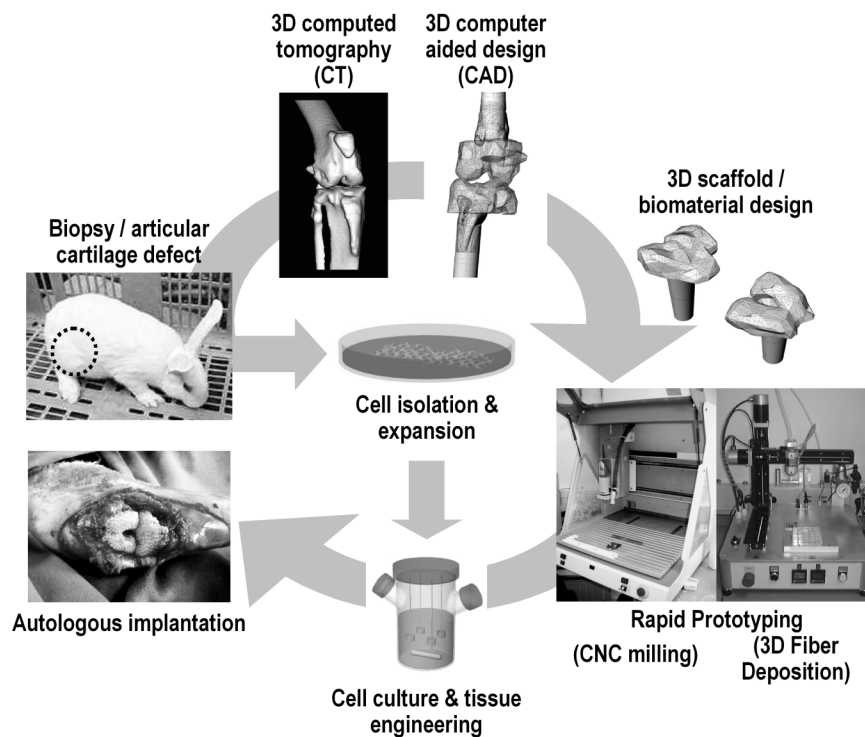


Figure 1 – Process for developing anatomically-shaped tissue-engineered constructs for total joint resurfacing of damaged articular cartilage.

The goal of the *in vivo* study (experiment 2) was determine feasibility of designing anatomically-shaped tissue-engineered implants for resurfacing of small articulating joints with a short term follow-up in rabbit knee model (Fig 1). Using medical imaging and two novel RP techniques, we aimed to develop porous PEGT/PBT with anatomically-shaped external contours but different CM and 3DF internal pore architectures described and evaluated in experiment 1 above. Cartilage tissue formation was evaluated in tissue-engineered femoral and tibial constructs prior to implantation as described above (experiment 1), and at 6 weeks follow up *in vivo* to ultimately determine implant function, fixation but also histological appearance of repair tissue. Due to the limited size of cartilage biopsy and the clinical relevance of obtaining chondrogenic re-differentiation and ECM formation in 3D scaffolds, expanded rabbit chondrocytes were used in this study and an autologous tissue culture and implantation approach adopted.

Materials and Methods:

Materials:

Bio-degradable poly(ethylene glycol) terephthalate – poly(butylene terephthalate) (PEGT/PBT) block co-polymers were obtained from IsoTis S.A. (Bilthoven, The Netherlands). Various *in vitro* and *in vivo* studies have demonstrated both the biocompatibility and biodegradable nature of PEGT/PBT co-polymers [28, 111, 402, 480] and are currently applied for a range of biomedical applications [29, 95, 375, 403, 517]. PEGT/PBT co-polymer composition used in this study was defined by a PEG molecular weight (MW) of 300 g/mol, and a PEGT: PBT weight percent (wt%) ratio of 55:45. This composition (denoted as 300/55/45) was selected as a model biomaterial system based on a number of previous studies demonstrating applicability to an extensive range of processing techniques for producing dense and porous 3D architectures [34, 95, 111, 307] including selected RP techniques [519], suitable thermal and mechanical stability [519], as well as the ability to promote chondrocyte attachment and cartilagenous matrix deposition [301, 307, 519].

Design and Rapid Prototyping (RP) of Anatomic Scaffolds:

Computer Aided Design (CAD) model: 3D computed tomography (CT) scans (Siemens, Germany), of the distal femur and proximal tibia of 6-month old New Zealand white rabbits were taken (0.5 mm slice thickness) and rendered to form an anatomic surface model of hard tissue in the knee joint (Fig 2A). CT surface models were imported (in STL format) into CAD software (Rhinoceros, Seattle, USA) and geometries converted to solid 3D CAD models (DXF format). The solid CAD models were re-designed to isolate femoral and tibial surfaces and integrate anatomic positioning of stem for medullary fixation. A 15 mm long stem was designed to allow a press fixation into the medullary cavity (Fig 2B, 2C). Preliminary osteotomy studies in cadaver rabbits indicated the average diameter of the medullary canal to be 7 mm. To ease implantation and press fixation, the stem was tapered from Ø7 mm to Ø5 mm a along its 15 mm length. Two RP techniques, computer numerical controlled (CNC) milling and 3D fibre deposition (3DF), were then used to produce anatomically-shaped scaffolds with different pore architectures, as described below. For each technique, RP specific CAD

models (in STL and DXF format) for femoral and tibial scaffolds, including support structures, were developed (Fig 3A, 3B), allowing RP specific tool paths (G-code) to be generated.

Computer Controlled (CNC) milling: This process required the pre-fabrication of 25 mm thick blocks of porous compression moulded (CM) and salt leached PEGT/PBT foam, produced by compressing a mixture of PEGT/PBT resin and salt crystals (75% by volume and 400-600 μm in size) under heat and pressure, as described previously [116]. Tool paths were generated from CAD models using DeskProto CNC software (Delft Spine Systems, The Netherlands) and the desired 3D scaffolds “cut” from the CM foam using a CNC milling machine (CPM 4030, illustrated in Fig 1) and a 2 mm ball ended cutter in a 2-sided process (Fig 3A).

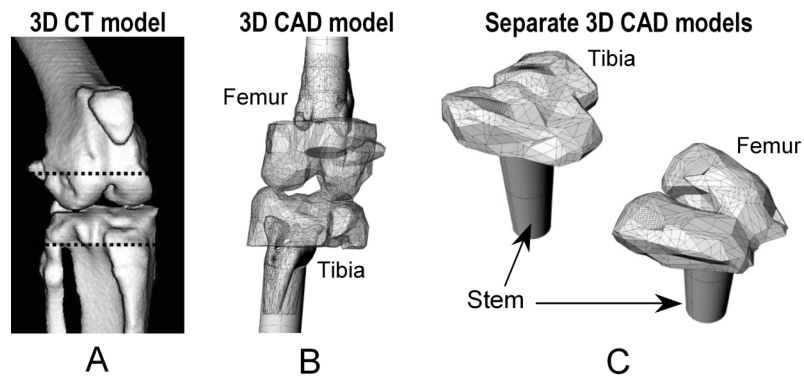


Figure 2 – (A) 3D CT surface model of rabbit knee, (B) solid 3D CAD model re-designed to isolate articulating surfaces and integrate anatomic positioning of stem for medullary fixation, (C) solid 3D femoral and tibial models for generating final RP model. Dotted lines in (A) illustrate approximate surgical cutting planes for osteotomy.

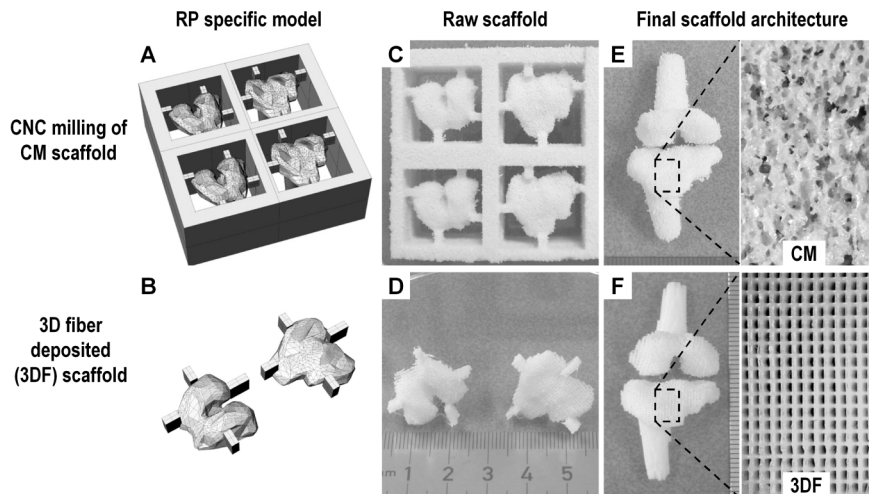


Figure 3 – Rapid prototyping of porous anatomically-shaped scaffolds using CNC milling of a block of compression moulded PEGT/PBT foam (A, C, E), and 3D fibre deposition of molten PEGT/PBT (B, D, E). Separate RP specific models (A, B) were generated from which a raw scaffold could be manufactured (C, D). After removal of support structures, identical, anatomically-shaped CM (E) and 3DF (F) scaffolds were produced but with distinctly different internal pore architectures.

3D Fibre Deposition (3DF): We previously described a novel technique for producing 3D fibre deposited scaffolds by successive layering of molten PEGT/PBT fibres in a computer controlled process [519]. Using similar principles on a 3D BioPlotter™ machine (EnvisionTec, Marl, Germany, illustrated in Fig 1) [253, 256], more complex anatomically-shaped PEGT/PBT scaffolds were constructed for this study. Briefly, a custom designed, stainless-steel syringe containing PEGT/PBT resin under heat (200°C) and pressure (nitrogen gas, 5 bar), was connected to the x-y-z axes of the BioPlotter device. RP specific models (Fig 3B) and fibre deposition criteria, such as x-y-z axis speed (210 mm/min), fibre spacing (0.6 mm), fibre orientation (0°–90°), layer thickness (0.15 mm) based on a nozzle diameter of 250 µm, were used to generate deposition paths from BioPlotter software. Molten fibres, which rapidly solidified, were deposited layer at a time, “building” the desired anatomic femoral and tibial scaffolds in a 2-part process while having complete control over the internal pore structure (Fig 3B). To illustrate this point, after “building” the porous femoral and tibial geometries (part 1), the tapered stem (part 2) was rigidly attached to femoral and tibial regions by initially depositing a dense layer of fibres before resuming the usual 0.6 mm fibre spacing on subsequent layers. The high contact density of fibres in the dense layer ensured rigid fixation and also served as a barrier to prevent chondrocytes leaving, or host cells infiltrating, the femoral and tibial pore spaces during seeding and *in vivo* implantation.

Cylindrical scaffolds (Ø7 x 4 mm) for use in the preliminary scaffold evaluation study were cored from simple rectangular blocks of CM and 3DF material, produced using the identical processing techniques described above.

To promote adhesion and a homogeneous cell distribution throughout the scaffolds [518], porous CM and 3DF femoral and tibial implants were gas plasma treated under an argon plasma (0.1-0.2 mbar) for 30 minutes. However, to prevent cell adhesion to the stem component, and thereby localize tissue formation only within the articulating regions of femoral and tibial implants, PVC tubing was placed over the entire length of the stem of each scaffold. Scaffolds including tubing were then autoclave sterilized (121°C for 30 min) prior to use in tissue culture experiments

Biopsy and Joint Preparation:

Ethical approval for use of a total of four, 6-month old New Zealand white rabbits was obtained for implantation studies in accordance with animal studies guidelines of the University Hospital, Zurich. Rabbits were operated under general anaesthesia with a respirator. During the first surgery, a lateral incision (~4 cm) was made in the left knee and the joint capsule exposed longitudinally. Care was taken to preserve the patella and medial quadriceps tendon and patella ligament by pushing structures medially. Both posterior and anterior cruciate ligaments were disconnected and the medial and lateral meniscus removed. Osteotomy of the femoral and tibial articulating surfaces (~2 mm in height) was performed and the medullary canal bored open and freed of marrow tissue. Cutting planes were determined prior to surgery based on 3D CT models used to develop the 3D anatomic scaffolds (Fig 2A). Femoral and tibial biopsies for each rabbit were labelled and immediately processed for autologous cell isolation and tissue culture (described below). A temporary silicon prosthesis (Swanson) was placed within the femoral and tibial medullary cavities to stabilize the knee for a 5-week period while tissue culture was taking place. The medial

quadriceps tendon and patella ligament were repositioned, the joint capsule, subcutaneous layer and skin closed with resorbable Polyglactin (Vicryl 3/0) sutures, and a spray plaster was applied.

Tissue Culture:

Rabbit chondrocytes were isolated from femoral and tibial biopsies via collagenase digestion (collagenase type-II, Worthington). Cells were culture-expanded (3,500 cells/cm²) for approximately 2-weeks until passage 2 in HEPES-buffered DMEM (Invitrogen) supplemented with 20 mM ascorbic acid, 0.4 mM proline (Sigma Aldrich), 0.1 mM non-essential amino acids (NEAA, Sigma Aldrich), 100 units/ml penicillin (Invitrogen), 100 µg/ml streptomycin (Invitrogen), and 10% fetal bovine serum (FBS, Sigma Aldrich). Pairs of femoral and tibial scaffolds were placed on sterile needles and seeded (20x10⁶ cells/scaffold) in spinner flasks (50 mL working volume, 60 rpm) for 3 days, and then remained in dynamic spinner flask culture *in vitro* for 21 days (40 rpm), with medium replacement every 3 days.

For the preliminary study, cylindrical CM and 3DF scaffolds (Ø7 x 4 mm) were seeded at a density of 8x10⁶ cells per scaffold and also cultured *in vitro* for 21 days as described above. Constructs were subsequently implanted in subcutaneous pockets of 6-week old nude mice (HdCpb:NMRI-nu, Harlan, The Netherlands). Animals were sacrificed 28 days after implantation and constructs processed histologically and biochemically, as described below.

Autologous Implantation in vivo:

After a 5-week cell expansion and tissue culture period, tissue engineered femoral and tibial constructs were implanted using an autologous approach (see Fig 1). This second operation, was performed in an identical manner to the first osteotomy procedure described above. The left knee joint was exposed as explained previously and the Swanson prosthesis and any visible scar tissue was carefully removed. A fresh bone bed was prepared by additional osteotomy (~1 mm thick) of bone from the remaining distal femur and proximal tibia surfaces. Tissue-engineered femoral and tibial implants ($n=2$) were press fit into the medullary cavities with additional resorbable suture fixation (Vicryl 3/0) between the border of the construct and the adjacent periosteum. After verifying secure positioning and articulation between the implants, the joint was closed as described above. Rabbits were monitored for a 6-week period for signs of infection or inflammation. Plaster casts were initially to be used to stabilize the joint within the first 2 weeks post-surgery, however, the rabbits naturally maintained a full extension of the knee during this period and casts were not used. Rabbits had freedom to move and their progress in terms of mobility and joint function was monitored daily. The animals were allowed to naturally initiate joint motion and partial load bearing on operated joints as soon as functionally comfortable (typically 2-4 weeks). After 6 weeks, rabbits were sacrificed, and operated (left) and control (right) joints harvested for observation and histological analysis as described below.

Evaluation - Preliminary Study:

Scaffold characterisation: Methods for characterizing porosity, average pore size, pore geometry, and accessible pore volume of CM and 3DF scaffolds have been described previously [307, 519] using techniques such as micro computed tomography (μ CT) and SEM, as well as calculations from mass/volume measurements and fibre deposition geometries.

Cell viability: A live/dead assay (Molecular Probes) was used to assess cell viability as described previously [519]. Briefly, constructs were harvested and 1 mm thick sections incubated in a PBS solution containing 6 μ mol/L ethidium bromide homodimer and 2 μ mol/L calcein AM for 30 minutes at 37°C and immediately examined in an inverted fluorescent microscope (Nikon Eclipse E400) using a FITC Texas Red filter.

Biochemical analysis: CM and 3DF constructs ($n=4$ per time point) were placed in a solution containing proteinase-K (1 mg/ml), pepstatin-A (10 μ g/ml) and iodoacetamide (185 μ g/ml) (Sigma-Aldrich) overnight at 56°C to digest the cells and extra-cellular matrix (ECM). GAG was quantitatively determined by reaction with dimethyl-methylene blue dye (Sigma-Aldrich) [122]. Intensity of colour change was immediately measured using a microplate reader (EL 312e, Bio-TEK Instruments) at an absorbance 520 nm. Values were compared to those from a standard of chondroitin sulphate B (Sigma-Aldrich). GAG content was normalized to total DNA, which was measured using a Cyquant dye kit (Molecular Probes) as per manufacturer's instructions using a fluorescent plate reader (Perkin Elmer).

Histological analysis: CM and 3DF constructs were fixed overnight in 0.14M cacodylate buffer (pH = 7.2-7.4) containing 0.25% glutaraldehyde (Merck). Samples were then dehydrated in sequential ethanol series, plastic embedded in glycol-methacrylate (Merck) and cut using a microtome to yield 5 μ m thick sections. Sections were stained with haematoxylin (Sigma-Aldrich) and fast green (Merck) to visualize cells/cell nuclei, and safranin-O (Sigma-Aldrich) to visualize sulphated extracellular glycosaminoglycan (GAG).

Scanning Electron Microscopy (SEM): To examine scaffold architecture and cell morphology, scaffolds were fixed and dehydrated as described above, and critical point dried from liquid carbon dioxide using a Balzers CPD 030 Critical Point Dryer. Samples were then sputter-coated (Cressington) with a thin gold layer and studied using a Philips XL30 Environmental Scanning Electron Microscope (ESEM).

Immunohistochemistry: Collagen type I and type II were immuno-localized using an Animal Research Kit (Dako) in combination with collagen type I (1:1000, Ab-1, Calbiochem, EMD Biosciences) and II antibodies (1:200, II-116B3, Developmental Studies Hybridoma Bank) as described previously [305]. Staining was visualized using DAB-solution (Dako) for 5 minutes in addition to counter staining with haematoxylin (Sigma-Aldrich).

Mechanical Properties: Static and dynamic unconfined compression tests were performed on hydrated, cylindrical CM and 3DP scaffolds, as well as on tissue engineered constructs after 21 days *in vitro* culture and 28 days subcutaneous implantation ($n=4$ per time point). Constructs were allowed to equilibrate for 3 hours in phosphate buffered saline (PBS) prior to testing. Equilibrium modulus (20% strain) and dynamic stiffness (15-20% strain deformation at 0.1 Hz) were determined as described previously [519], and compared with native articular cartilage properties from literature [475, 519].

Evaluation - Autologous Rabbit Knee Model:

Day 21 prior to implantation: Anatomic femoral and tibial implants cultured *in vitro* for 21 days were analyzed qualitatively for cell viability as well as distribution and composition of ECM components prior to implantation. Cell viability, histological analysis, SEM and immunohistochemistry were performed as described above.

6-week follow up in vivo: General observations of operated knees were made prior to joint harvesting and histological analysis. The operated joints were checked for range of movement. In addition, a small region of the joint capsule was exposed and observations relating to articulation between femoral and tibial implants, implant fixation, synovial fluid appearance made. The entire joint containing intact femoral and tibial implants were harvested and evaluated histologically as described below.

Histological analysis: Histology was performed on non-decalcified bone and cartilage samples from both operated and control knee joints as described previously [490]. Briefly, entire joints were fixed in 4% buffered paraformaldehyde for 2–3 weeks, dehydrated in increasing grades of ethanol, defatted and cleared with xylene and embedded in acrylic resin (HistoDur®, Leica, Switzerland, 500 ml methyl methacrylate base, 30 ml phthalic acid dibutylester plasticizer, and 5×1g activator). From the polymerized blocks, 200 µm sections were cut using a sawing microtome (Leica SP 1600). These sections were then mounted on acrylic Plexiglas slides (Wachendorf, Perspex GS Acrylicglas Opal 1013), and polished. Sections were etched for 5 minutes and surface stained with basic fuchsin (5 min) and methylene blue (5 min) to visualize bone and soft tissues respectively. Alternatively, thionine (10 min) was used to visualize soft tissue as well as extracellular GAG.

Statistics:

All data was represented as a mean ± standard deviation. To test levels on significance in GAG/DNA content and mechanical properties, one-way analysis of variance (ANOVA) was performed using SigmaStat statistical software (SPSS Inc.) with Student-Newman-Keuls post hoc testing ($P < 0.05$).

Results:

Preliminary Study:

Scaffold characterisation: Previous characterisation studies in our group on CM and 3DF 300/55/45 PEGT/PBT scaffolds [307, 519] demonstrated that designed 3DF scaffolds contained a simple, highly accessible pore volume due to large interconnecting pores, whereas as a result of the more random particle-leaching production process, CM scaffolds contained a more tortuous, less accessible pore volume due to smaller interconnecting pores [307]. Based on fibre deposition geometries ($\text{\O}175\ \mu\text{m}$ fibre diameter and 0.6 mm fibre spacing) and mass volume techniques, 3DF scaffolds used in this study were approximately 76% porous, compared with 80% in CM scaffolds. This indicated that similar pore volumes were available in both scaffold architectures to compare cell infiltration, tissue formation and nutrient/waste exchange. However, 3DF scaffolds had a considerably larger average pore size ($415\ \mu\text{m}$) than CM scaffolds ($182\ \mu\text{m}$) [307]. The surface area to volume ratio in 3DF and CM scaffolds was $5.5\ \text{mm}^{-1}$ and $10.0\ \text{mm}^{-1}$ respectively.

Histological analysis & cell viability: Dynamic seeding of expanded (passage 2) rabbit chondrocytes resulted in a homogeneous distribution of cells throughout cylindrical CM and 3DF scaffolds (not shown). After 21 days spinner flask culture, SEM images demonstrated considerable ECM formation (Fig 4A, 4B), and after 28 days subcutaneous implantation, cartilage-like tissue formation was observed in both CM and 3DF scaffolds as indicated by positive safranin-O staining for GAG (Fig C, F) and collagen type II staining (not shown). However, tissue formation and fluorescent staining for live (green) cells was limited to peripheral regions of CM scaffolds (Fig 4C, 4E), whereas in 3DF scaffolds, positive safranin-O staining, collagen type II expression and viable cells were more predominantly observed throughout the highly accessible and interconnected pore volume (Fig 4D, 4F).

Biochemical analysis: To determine the effects of scaffold architecture on cartilage tissue formation, quantitative assays for GAG and DNA were performed. Significantly higher GAG per wet weight was measured in 3DF compared with CM scaffolds irrespective of *in vitro* culture or subcutaneous implantation *in vivo*. However, *in vivo* samples contained significantly higher GAG per wet weight than *in vitro* samples of the same architecture. When normalized to cell number, greater GAG/DNA was measured in 3DF compared with CM scaffolds at both 21 days *in vitro* and 28 days *in vivo*. This suggests that for expanded rabbit chondrocytes, porous 3DF architectures provide conditions which stimulate chondrogenic ECM formation.

Mechanical properties: Irrespective of culture duration, mechanical data showed that 3DF scaffolds had significantly greater equilibrium modulus and dynamic stiffness (at 0.1 Hz) compared with CM scaffolds of the same porosity ($\approx 80\%$). This was likely due to the organised network of PEGT/PBT fibres in 3DF scaffolds compared with more random architecture in CM scaffolds [307]. *In vitro* cultured 3DF scaffolds had a similar dynamic stiffness prior to implantation as natural bovine [519] and human articular cartilage at 0.1 Hz [475], whereas CM scaffolds were approximately 50% as stiff. Steadily increasing GAG content and ECM formation during *in vitro* and *in vivo* culture (Fig 5A, 5B) resulted in synergistic increase in

mechanical properties in both CM and 3DF with time over non cell-seeded scaffolds (Fig 5C, 5D), however, 3DF scaffolds cultured *in vivo* were significantly stiffer under dynamic compression than *in vitro* cultured 3DF scaffolds. Due to the limited size of biopsies, mechanical properties of rabbit articular cartilage were not determined in this study, although previous studies have demonstrated similar properties exist between distal femoral cartilage in rabbit, human and bovine species [13, 353].

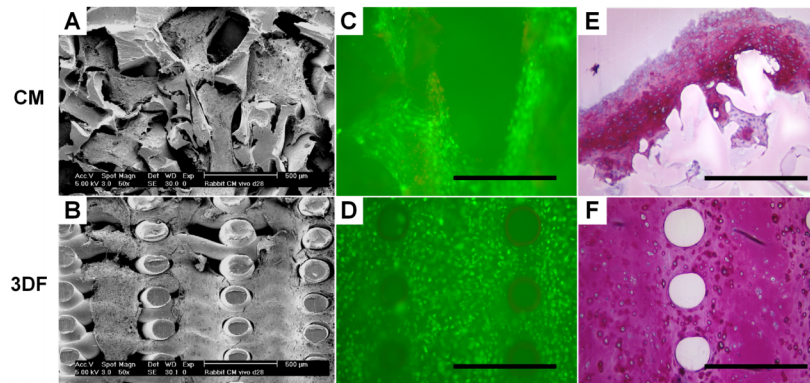


Figure 4 – Results from preliminary study in cylindrical CM (A, C, E) and 3DF (B, D, F) scaffolds illustrating tissue formation in SEM images (A, B) after 21 days *in vitro* culture and cell viability (C, D) and safranin-O staining (E, F) after 28 days subcutaneous implantation (scale bar = 500 μ m). ► p218.

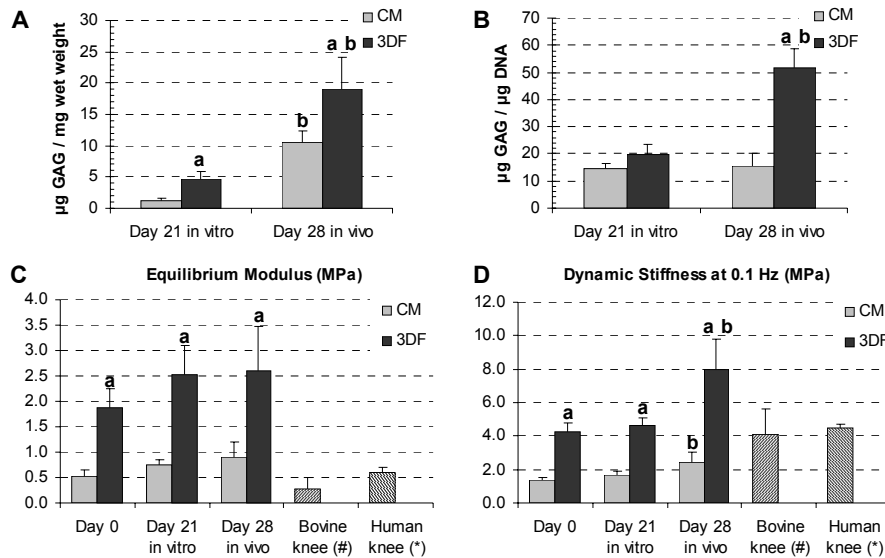


Figure 5 – (A) GAG per wet weight and (B) GAG per DNA data for CM and 3DF scaffolds after 21 days *in vitro* culture and 28 days subcutaneous implantation. (C) Static (equilibrium modulus) and (D) cyclic (dynamic stiffness) compressive mechanical properties of CM and 3DF scaffolds compared with native bovine and human articular cartilage. Significant differences denoted by: a = between CM, b = between other time points for the same architecture; # from Woodfield et al. [519]; * from Treppo et al. [475].

Autologous Rabbit Knee Model – day 21 prior to implantation

Due to the large size of the implants (Fig 6), and limited number of expanded rabbit chondrocytes (20×10^6 cells/scaffold) available for seeding in both implantation and control experiments, obtaining a homogeneous distribution of cells and ECM formation was challenging. Nonetheless, after 21 days spinner flask culture, tissue formation was observed on the surfaces of CM and 3DF femoral and tibial implants with a translucent, glossy gross appearance (Fig 6A, 6B). Furthermore, after *in vitro* culture, femoral and tibial implants scaffolds had maintained their original anatomic shape.

SEM: SEM analysis of sectioned implants demonstrated that even in these large implants, the interconnecting pore volume in 3DF scaffolds was near completely filled with ECM prior to implantation (Fig 6D). While cells and ECM were observed within central regions of CM scaffolds, most ECM formation occurred at the periphery of the scaffold (Fig 6C).

Histological analysis & cell viability: Safranin-O staining showed cartilage-like tissue formation and GAG staining in both CM (Fig 6E) and 3DF scaffolds (Fig 6F). Consistent with tissue distribution results from SEM images, GAG staining (Fig 6E) and collagen type II (Fig 6G) immunostaining were limited to superficial regions of CM scaffolds, but were observed more homogeneously throughout the interconnected pore volume of 3DF scaffolds (Fig 6F, 6H). Diffusional limitations related to implant size did not appear to limit cell viability in 3DF scaffolds, with live (green) cells observed throughout the thickness of the implant (Fig 6F inset). In CM implants, live cells were observed within a 1-2 mm peripheral border whereas central regions were almost acellular rather than containing large numbers of dead (red) cells (Fig 6E inset).

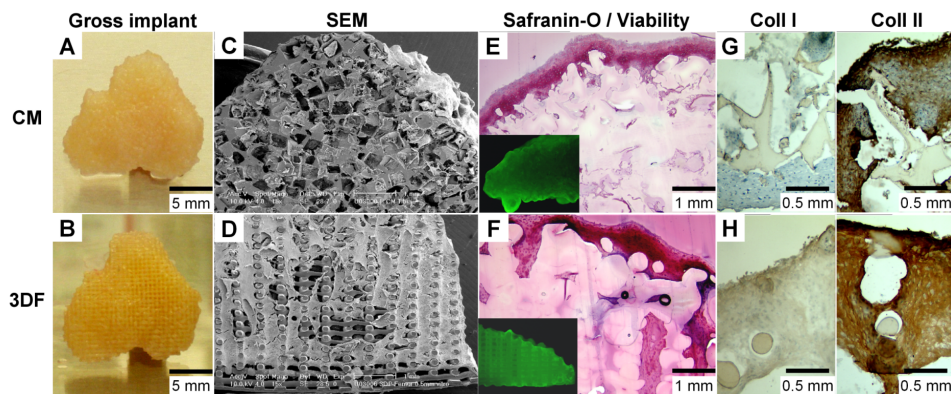


Figure 6 – Gross appearance of tissue-engineered tibial implants (A, B), and cross-sectional SEM (C, D), cell viability (inset) and safranin-O (E, F) and collagen type I/II immunostaining images (G, H) after 21 days *in vitro* culture. (A, C, E, G) CNC milled CM scaffold, (B, D, F, H) 3DF scaffold. ► p218.

Autologous Rabbit Knee Model – 6-week follow up in vivo

Surgeries for joint osteotomy and implantation of tissue-engineered femoral and fibial implantation occurred without incident. In one rabbit, dislocation of the temporary Swanson prosthesis occurred and was re-operated without additional complication. After 6 weeks, rabbits had regained limited function in operated joints. Knee stability and articulation were sufficient to allow partial load bearing with hopping and voluntary grooming movements using the operated (left) leg observed. There were no signs of excessive joint infection or inflammation other than expected scar tissue formation following osteotomy and temporary Swanson prosthesis placement. The joint capsule had healed at 6 weeks and synovium appeared clear.

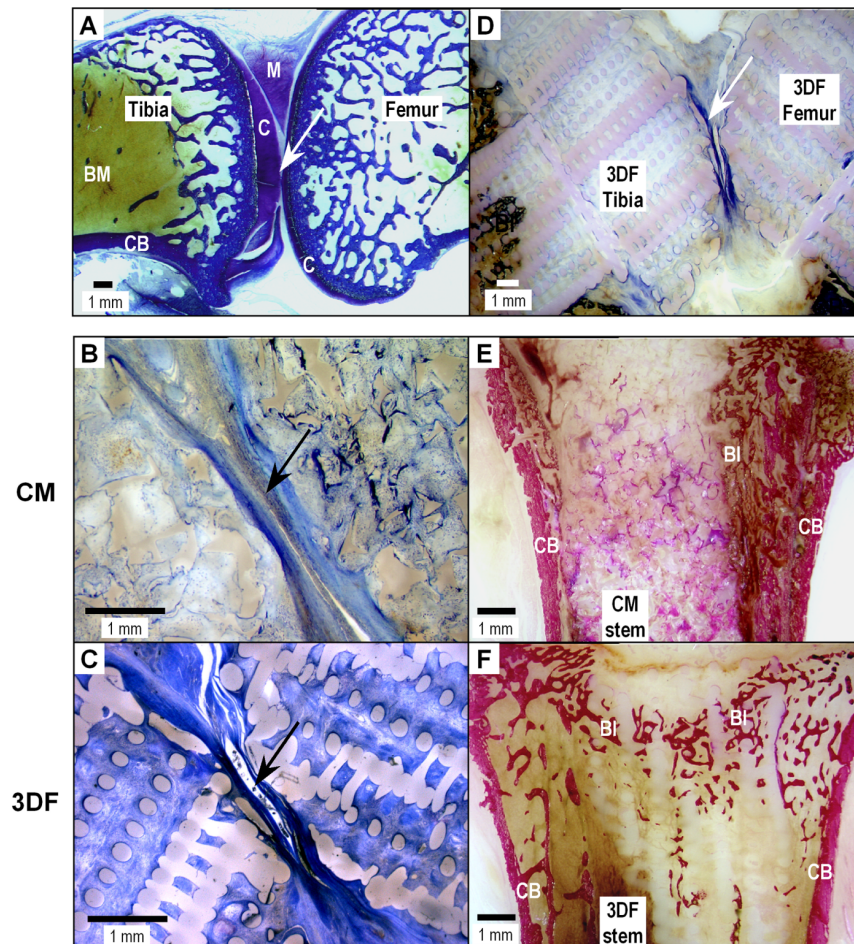


Figure 7 – Histological sections of control (A) and operated joints (B-F) at 6 week follow-up using anatomically-shaped CM (B, E) and 3DF implants (C, F). Example of 3DF femoral and tibial implants shown in D. Samples were stained with thionine (A-D) and basic fucshin/methylene blue (E, F). Arrow indicates articulating surface; C = articular cartilage; M = meniscus; CB = cortical bone; BM = bone marrow; BI = bone in-growth. ▶ p219.

Histology: Histological evaluation of control and operated joints showed that a significant proportion of the articulating cartilage surfaces and underlying cancellous bone were removed during osteotomy. Nonetheless, the precise anatomic design of the articulating surfaces and stem assisted press-fit implantation and the re-establishment of articulating surfaces between the femur and tibia. Although the 4 rabbits evaluated in this feasibility study had resumed limited function in operated knees, the engineered cartilage-like tissue that was evident within *in vitro* cultured CM and 3DF femoral and tibial implants prior to implantation (Fig 6) was not maintained after 6 weeks implantation *in vivo*. Instead, the tissue filling pores throughout the articulating regions in 3DF implants contained a mixture of rounded and flattened cells and little- to no- staining for GAG (Fig 7B, 7C), indicative of a predominantly fibrous-like tissue repair. Limited amounts of tissue were present filling pores in the articulating regions of CM implants, but it was similar in appearance to that seen in 3DF implants. However, at the articulating surface of both CM and 3DF implants, a dense layer of fibrous tissue, aligned tangentially to the implant surface, was observed (Fig 7B, 7C arrows) allowing the implants to facilitate joint articulation. 3DF implants appeared to have maintained their original shape and had not deformed or fragmented after 6-weeks implantation (Fig 7C, 7D, 7F), and was likely due to their desirable mechanical stiffness. While bulk shape was maintained in general for CM implants, certain regions appeared to be less resistant to deformation (not shown). This may have been related to a lower dynamic stiffness compared to 3DF implants, although differences in tissue formation, animal variability and joint use may also have had an effect.

In terms of fixation, new cancellous bone in-growth was observed distally in the stem of 3DF implants after 6 weeks, bridging the entire joint space and rigidly fixing the tapered stem of the implant to the cortical bone wall. Bone formation was observed in the stem of CM implants, but more proximally and to a lesser extent than 3DF implants.

Discussion and Conclusions:

In this study, we investigated the process feasibility of designing anatomically-shaped tissue-engineered implants for resurfacing of small articulating joints (*i.e.* with a short term follow-up in rabbit knee model). This process introduced a number of combinatorial methods for the development of 3D anatomic models from CT scans of the rabbit knee and computer aided design (CAD); rapid prototyping (RP) of porous PEGT/PBT implants with anatomically-shaped external contours but different internal pore architectures; *in vitro* seeding and tissue culture of expanded rabbit chondrocytes on implants; static and dynamic mechanical evaluation and biochemical composition prior to implantation; and finally re-implantation in an autologous approach in the rabbit knee following tibial and femoral osteotomy.

Previous studies have attempted to tissue-engineer finger joints *in vitro* using poly-glycolic and poly-L-lactic acid co-polymer non-woven mesh scaffolds and selective placement of periosteum, chondrocytes, and tenocytes [217]. While individual cartilage, bone and tenocapsule components, with a similar structure human phalanges, were observed following subcutaneous implantation in mice, the scaffold components were only sutured together and no functional evaluation *in vitro* or *in vivo* was performed. In other studies, tissue-engineered cartilage suitable for craniofacial reconstruction has been described via injection

moulding of alginate seeded with auricular sheep chondrocytes [81, 82]. Here the moulds were standard facial implant moulds and so construct shape was not further customizable. In general, moulding techniques are inflexible in that new and expensive moulds need to be produced any time the anatomic geometry needs to be altered, and provides limited control over the design and mechanical properties of implants. Other approaches for repairing osteochondral defects have developed porous, biphasic scaffolds with optimized properties for promoting tissue formation and integration in for cartilage and bone compartments [244, 425, 426, 441]. In a recent study Mauck *et al.* [199] described a paradigm for tissue engineering anatomically-shaped biphasic osteochondral implants. Their process involved medical imaging and RP techniques to design moulds for casting cell-seeded agarose constructs with anatomic contours. They further describe interesting techniques to integrate the contoured agarose with explanted trabecular bone as well as provide *in vitro* mechanical conditioning criteria. Disadvantages of these techniques are the inflexibility of moulding techniques as mentioned previously, and the inability to reproducibly create tissue-engineered chondrocyte-agarose constructs with similar static and dynamic mechanical properties to native articular cartilage (*i.e.* compressive, or Young's modulus, was 12.5% of native bovine cartilage).

While *in vitro* studies are emerging, no studies, to our knowledge, have assessed the feasibility of developing anatomically-shaped tissue-engineered implants for resurfacing or reconstruction of damaged cartilage in small articulating joints *in vivo*. We chose an autologous rabbit knee model in this study based on the similar dimensions to human finger joint, and extensive use for focal and osteochondral defect repair [204]. Although the knee presents a more complex joint to the finger in terms of stability, it was important to evaluate feasibility if implants for this study in a load bearing capacity.

The novel aspect of this study is that with the CT imaging and RP techniques described herein (*i.e.* CNC milling of CM scaffolds and 3D fibre deposition), not only were we able to design and engineer the anatomic external shape of PEGT/PBT scaffolds, but also engineer the internal pore architecture concurrently. RP techniques based on 3D fibre deposition, which directly allow control of complex shape as well pore architecture, offer greater flexibility and control [211, 427, 428] particularly in the design of porous scaffolds to meet specific anatomic and functional mechanical requirements [519]. Based on *in vitro* data from the preliminary study (experiment 1), we observed that large interconnecting pores and highly accessible pore volume in 3DF scaffold enhanced cartilage tissue formation, with a homogeneous distribution, compared with CM scaffolds. This was consistent with previous studies evaluating cartilage tissue formation *in vitro* and *in vivo* on CM and 3DF scaffolds using bovine [306, 307] and expanded human nasal chondrocytes [333]. This data suggests that, for the design of large, anatomically-shaped implants of clinically relevant size, interconnecting 3DF scaffold architectures provide a porous 3D environment which promotes chondrocyte attachment and ECM synthesis with minimal nutrient limitations, and was likely the reason we observed homogenous distributions of viable cells throughout femoral and fibial 3DF implants compared with CM implants.

3DF constructs also exhibited significantly higher equilibrium modulus and dynamic stiffness properties to CM scaffolds, which increased with *in vitro* and *in vivo* culture time. Based on previous studies [519], we designed 3D fibre deposition patterns to produce interconnecting porous architectures with similar dynamic stiffness (at 0.1 Hz) to native articular cartilage,

thereby providing suitable mechanical stability to allow early implantation and load bearing of an immature tissue-engineered cartilage construct. In adopting this early implantation strategy, extended *in vitro* culture periods and mechanical pre-conditioning of the tissue-engineered implant to achieve sufficient mechanical properties were avoided. Previous studies have also shown that implantation of immature (2 week-old) tissue-engineered cartilage constructs promoted better integration to host tissue than more mature (8 week-old) constructs [364].

Following implantation of *in vitro* cultured femoral and tibial implants in the rabbit osteotomy model (experiment 2) and a short follow-up after 6 weeks, we observed that limited joint function and weight bearing had been regained. Regrettably, histological analysis of operated joints indicated that the repair tissue present within femoral and tibial CM and 3DF implants did not resemble the level of cartilage-like tissue present prior to implantation, and was predominantly fibrous-like. Collagen type I and II immunohistochemistry was not evaluated for *in vivo* samples. Nevertheless, implant geometry had been maintained and a functional articulating layer, albeit fibrous-like, was observed. Moreover, the tapered stem and press-fit design of the implants, particularly in 3DF constructs, provided a suitable environment for rapid cancellous bone growth, providing excellent implant fixation after 6 weeks. Although a suitable outcome in terms of implant fixation and function in the short-term was obtained, there are several possible explanations for not observing a hyaline-like repair tissue. Firstly, we did not investigate cell viability or cell retention in the tissue-engineered constructs after implantation. Although an autologous approach was adopted, it is possible that cells did not survive the implantation procedure, and that due to excessive infiltration of blood- or marrow-derived host cells and the associated wound healing response, maintenance of the tissue-engineered cartilage present at implantation was compromised. In osteochondral cartilage repair experiments in rabbits, Ostrander *et al.* [373] demonstrated that tissue engineered implants are rapidly infiltrated with host cells after implantation, thereby affecting repair responses. Furthermore, the rabbit osteotomy model required 2 surgeries, thereby subjecting the tissue-engineered implants to a severely degenerated joint environment at the second surgery. It is unlikely that re-establishment of the synovial capsule occurred soon after either operation, and subsequent nutrients supplied by the synovial fluid necessary for maintaining chondrocyte function were limited.

This study raised a number of additional issues. Firstly, it is important to note that the anatomically-shaped implants developed in this study were based on 3D CT data, thereby imaging only dense bone tissue. Therefore, none of the cartilagenous or soft tissue anatomy was incorporated into the model scaffolds. Nevertheless, we were able to demonstrate feasibility of the process, and in future, MRI scans (which are capable of imaging soft tissue) may provide even greater anatomic detail. Such soft tissue imaging may be particularly applicable for developing customized implants for plastic and reconstructive surgeries.

Secondly, the aim of this study was not directed to total joint reconstruction, and in our model system we only addressed a single tissue type in this study, *i.e.* tissue-engineered cartilage, and not bone, ligament or tendon. With the current interest in development of biphasic osteochondral implants however, combinations of RP techniques to encompass bone specific scaffolds as recently described by Wilson *et al.* [514] will be possible for generating synthetic anatomically-shaped osteochondral implants.

While only a few rabbits were analyzed in this feasibility study, these results provide promising evidence to proceed in a larger, long term study in rabbits using 3DF scaffold architectures. Using advanced RP techniques, this study demonstrated the ability to tissue-engineer, anatomically-shaped cartilage constructs *in vitro*. Porous, interconnected 3DF scaffold architectures promoted chondrocyte attachment and re-differentiation capacity whilst exhibiting mechanical properties similar to native articular cartilage explants. The flexibility of the RP technologies such as 3D fibre deposition of PEGT/PBT copolymers described in this study offer a considerable promise as a technique for developing model scaffold architectures

Acknowledgements:

The authors gratefully acknowledge the assistance of M. Krupa, University Hospital Zurich, for performing rabbit CT scans and 3D surface model rendering, as well as financial assistance from SUVA (Swiss National Accident Insurance Fund).

Discussion and Conclusions

Chapter 10

- I. Designed scaffolds: rapid prototyping for cartilage tissue engineering.
- II. Instructive scaffolds: pore architecture and chondrocyte differentiation.
- III. Instructive scaffolds: composition, pore architecture and chondrocyte re-differentiation
- IV. Instructive anatomically-shaped scaffolds: tissue-engineered implants for joint reconstruction.

Implications for Cartilage Tissue Engineering:
Future Directions

"There must be a beginning of any great adventure, but the continuing
unto the end until it is thoroughly finished yields the true glory."

[Francis Drake, 1577]

Chapter 10

Discussion and Conclusions

In **Chapter 1** and **Chapter 2**, we reviewed and discussed critical design considerations and current limitations related to the development, material selection and processing of scaffolds for articular cartilage tissue engineering. While addressing all these design criteria was beyond the scope of this thesis, we did, however, emphasize that one of the challenges in tissue engineering is the design and fabrication of biodegradable scaffolds which are "instructive" for specific cellular functions. In adopting a less conventional approach to scaffold-based tissue engineering, we started with the question:

In what ways can we design porous scaffolds to influence or instruct cell function in 3D?

To address this question, we designed and evaluated a number of *in vitro* and *in vivo* experimental model systems based on controlled changes in 3D PEGT/PBT scaffold architecture and substrate composition. As proposed in **Chapter 1**, these model systems were evaluated in four separate phases in this thesis.

In this chapter, the achievements of each phase are reviewed based on the findings that have been discussed in detail in Chapters 3-9, and their implications for cartilage tissue engineering and future directions are discussed accordingly.

I. Designed scaffolds: rapid prototyping for cartilage tissue engineering.

In **Chapter 3** we described the development of a novel 3D fibre deposition (3DF) technique which allowed us to reproducibly "*design-in*" desired scaffold characteristics, such as porosity, pore size and pore interconnectivity. Computer-controlled deposition of molten PEGT/PBT fibres resulted in: scaffolds with staggered fibre spacing; anisotropic scaffolds with pore size gradients; and scaffolds with complete dense layers. Mechanical data indicated that it was possible to design 3DF scaffold architectures which match the static and dynamic properties of articular cartilage. Preliminary *in vitro* and *in vivo* culture experiments showed that 3DF scaffolds were capable of supporting chondrocyte differentiation, as well as providing a suitable 3D architecture for attachment and homogeneous distribution of viable, human articular chondrocytes.

This rapid prototyping (RP) technique offered considerable advantages over traditional scaffold processing techniques (Chapter 1) resulting in the design of porous scaffolds capable of meeting 9 out of the 10 the critical design criteria (bioactivity/gene delivery was not investigated) described in Table 2 from Chapter 2. The flexibility of the 3DF method and *designed* model scaffolds described in Chapter 3 provided an elegant method to further investigate the effects of scaffold architecture on cartilage tissue formation *in vitro* and *in vivo*.

II. Instructive scaffolds: pore architecture and chondrocyte differentiation.

In **Chapter 4** and **Chapter 5**, two processing techniques, compression-moulding/particulate-leaching (CM) and 3D fibre deposition (3DF), were used to develop model porous scaffolds with similar vol% porosity but varying pore accessibility. In **Chapter 6** 3DF scaffolds were designed and produced containing either homogeneously-spaced pores or pore-size gradients, but with similar overall vol% porosity and volume fraction available for cell attachment and ECM formation. Using these model scaffold architectures, we addressed the following question:

What influences do controlled changes in 3D PEGT/PBT scaffold architecture have on chondrocyte differentiation capacity and zonal organisation within tissue-engineered constructs?

Following subcutaneous implantation *in vivo*, we demonstrated that 3DF scaffold architectures, containing a highly accessible pore volume and large interconnecting pores (average $\text{Ø}525 \mu\text{m}$), promoted a more homogeneous distribution of chondrocytes and ECM components, and significantly enhanced GAG synthesis and chondrocyte differentiation capacity (*i.e.* GAG/DNA) compared to CM scaffold architectures, which contained a tortuous and less accessible pore volume, and small interconnecting pores (average $\text{Ø}182 \mu\text{m}$). This effect, however, was not observed with prolonged dynamic culture *in vitro*, and may have been related to the dense fibrous cell layer present at the periphery of *in vitro* cultured constructs thereby reducing nutrient diffusion and sensitivity of the *in vitro* model. Although 3DF scaffolds presented a less tortuous and more accessible pore volume than CM scaffolds, we did not observe an effect of scaffold architecture on oxygen gradients *in vitro* or *in vivo* (Chapter 5). Gradients were less severe in constructs cultured *in vivo*, and due to the more homogeneous cell and ECM distribution in 3DF constructs, it cannot be excluded that a lower specific oxygen consumption of the cells, in addition to enhanced diffusion of other nutrients such as glucose [179] were instructive for cell differentiation as well as cell viability, particularly in central regions of the scaffold. The conditions which favoured cartilage ECM formation *in vivo* were likely enhanced by the availability of host-derived growth factors following subcutaneous implantation [309, 467].

In Chapter 6, the ability of anisotropic 3DF pore architectures to instruct the zonal organisation of chondrocytes and ECM components was investigated. *In vitro* cell seeding showed that pore-size gradients promoted a similar anisotropic cell distribution to superficial (S), middle (M) and lower (L) zones in immature bovine articular cartilage, irrespective of dynamic or static seeding methods. There was a direct correlation between zonal scaffold volume fraction with DNA and GAG content. Prolonged tissue culture *in vitro* showed similar inhomogeneous distributions in zonal GAG and collagen type II synthesis but not GAG/DNA, and levels were an order of magnitude less than in native cartilage. The high rate of collagen type II accumulation observed only in L zones (2 mm fibre spacing) of *Grad* scaffolds suggested that large interconnecting pore size, with greater access to dynamic medium flow conditions, may stimulate collagen type II synthesis independently of GAG.

III. Instructive scaffolds: composition, pore architecture and chondrocyte re-differentiation

The ability to design 3D biomaterial substrates which stimulate post-expansion re-differentiation of human chondrocytes represents a clinically significant research objective. In **Chapter 7**, PEGT/PBT substrate composition and gas plasma (GP) surface modification were evaluated in serum containing (S+) or serum free (SF) media. In **Chapter 8**, the combination of CM and 3DF scaffold architectures described in Chapters 4-5 and PEGT/PBT compositions described in Chapter 7 were evaluated. In this section, we attempted to address the following question:

What influences do controlled changes in PEGT/PBT surface composition and 3D scaffold architecture have on human chondrocyte re-differentiation and cartilage tissue formation capacity?

In Chapter 7, we observed a direct relationship between cellularity, cell morphology and re-differentiation potential on PEGT/PBT substrates. There was a significant influence of PEGT/PBT composition on cellularity in both S+ or SF media. In PEGT/PBT compositions supporting high cellularity and a spread cell morphology (300/55/45), the post-expansion re-differentiation of human chondrocytes (as evidenced by collagen II/I mRNA expression) was reduced, whereas in PEGT/PBT compositions with low cellularity and a spherical cell morphology (1000/70/30), collagen II/I mRNA expression was increased. Independent of PEGT/PBT composition, GP treatment enhanced cell spreading and total cellularity in S+ media, but had no effect in SF media suggesting protein adsorption mechanisms were involved. Enhanced $\alpha 5\beta 1$ (FN) integrin receptor intensity was also observed, concomitant with reduced collagen type II/I mRNA expression compared to untreated films. The fact that lower PEG MW compositions (e.g. 300/55/45) show preferential adsorption of fibronectin (FN) compared to vitronectin (VN) [299] and that GP treatment preferentially etches PEG rather than PBT copolymer blocks [371], suggests that these PEGT/PBT substrates were FN-rich, thereby supporting cell adhesion and spreading but detrimentally affecting the re-differentiation capacity of expanded human chondrocytes, whereas FN-deficient substrates enhance re-differentiation capacity.

In Chapter 8, we demonstrated that high MW PEGT/PBT compositions (e.g. 1000/70/30) supporting maintenance of the chondrogenic phenotype on 2D films (Chapter 7) [299] were capable of promoting chondrocyte re-differentiation and cartilaginous matrix accumulation in porous CM and 3DF scaffolds *in vitro*. 3DF scaffolds architectures, with a more accessible pore volume and larger interconnecting pores, supported increased GAG/DNA deposition compared to CM scaffolds, but only if a 1000/70/30 composition was used. Interestingly, enhanced collagen type II mRNA was observed in 3DF compared with CM scaffolds irrespective of composition, suggesting that at the mRNA level, architecture alone is capable of instructing collagen type II synthesis pathways in human chondrocytes, and operate independently to GAG synthesis pathways.

The synergistic instructive effects of both PEGT/PBT composition and 3DF scaffold architecture were likely mediated by preferential serum protein adsorption to high PEG MW 1000/70/30 materials, promoting a FN-deficient substrate, a more rounded cell morphology (Chapter 7) [299], as well as the efficient exchange of nutrients/wastes respectively (Chapters 3-4). This

synergistic effect was further highlighted, given that, in Chapter 3, the significant influence of 3DF scaffold architecture on chondrocyte differentiation was only observed following subcutaneous implantation *in vivo*. Although human chondrocyte re-differentiation potential was not evaluated *in vivo* in this thesis, our data from Chapters 4 and 5 suggests that more distinct differences in cartilage formation between CM and 3DF architectures may be possible.

IV. Instructive anatomically-shaped scaffolds: tissue-engineered implants for joint reconstruction.

In **Chapter 9** we amalgamated RP technologies and model systems developed in Chapters 2-8 to describe the feasibility an entire tissue-engineering concept, from imaging of the defect to a functional, anatomically-shaped tissue-engineered implant for small joint reconstruction using an autologous rabbit knee model. In order to obtain suitable static and dynamic mechanical properties (Chapters 3-4) to support *in vivo* loading, only 300/55/45 PEGT/PBT compositions were investigated.

In a preliminary experiment studying the re-differentiation potential of expanded *rabbit* chondrocytes on cylindrical CM and 3DF scaffolds, we observed identical results to those described for differentiation of bovine chondrocytes in Chapters 4-5. Notably, 3DF constructs also exhibited significantly higher equilibrium modulus and dynamic stiffness (0.1 Hz) properties to CM scaffolds, which increased with *in vitro* and *in vivo* culture time, thereby providing suitable mechanical stability to allow early implantation and load bearing of an immature tissue-engineered cartilage construct. To our knowledge, tissue-engineered constructs possessing *dynamic* mechanical properties that match those of native articular cartilage prior to implantation have yet to be described. Our data suggested that, for the design of large, anatomically-shaped implants of clinically relevant size, interconnecting 3DF scaffold architectures provide a porous 3D environment which promotes chondrocyte attachment and ECM synthesis (*i.e.* GAG and collagen type II) with minimal nutrient limitations. This was likely the reason we observed homogenous distributions of viable cells throughout femoral and tibial 3DF implants compared with CM implants *in vitro* prior to autologous implantation in rabbits.

The main goal of *in vivo* implantation was to evaluate implant fixation and joint function. After a short-term 6 week follow-up in 4 rabbits, the stem of femoral and tibial implants had integrated with the host bone (particularly in 3DF implants) and rabbits had regained limited function and knee flexion/extension. Following explanation, histology indicated the presence of articulating surfaces between femoral and tibial implants, with 3DF implants better maintaining their original geometry after loading compared with CM implants. Unfortunately, the repair tissue was fibrous-like in appearance and did not resemble the cartilage-like tissue present prior to implantation. Due to the debilitated joint environment following osteotomy and/or the influx of blood- or marrow-derived cells associated with the wound healing response, maintenance of the tissue-engineered cartilage present at implantation was likely compromised.

Based on the feasibility data presented in Chapter 9, longer follow-up experiments (3 months and 6 months) using 3DF femoral and tibial implants are currently being undertaken in 12

rabbits. This data will provide additional information as to the long term fate of the implants with respect to the type of repair tissue, implant fixation and implant integrity following extended load bearing conditions *in vivo*.

Implications for Cartilage Tissue Engineering:

Scaffolds are central to tissue engineering strategies because they provide a 3D framework for cells to attach and produce necessary ECM to repair or regenerate damaged tissues which cannot be simply emulated by cells cultured in 2D. As the scaffold provides the basic foundation for tissue engineering approaches, its various properties need to be carefully designed and optimised [517]. While model systems were predominantly investigated in this thesis, a number of issues were addressed which have direct implications towards cartilage tissue engineering, and are discussed briefly below:

Scaffold architecture:

Based on the research presented in this thesis, the most optimal scaffold architectures for instructing a homogeneous ECM distribution and chondrocyte (re)differentiation in tissue-engineered constructs were 3DF scaffolds, containing a highly accessible pore volume in combination with large, interconnecting pores (see summary Table B.1 in Appendix B). These results stress the importance of a rationally designed scaffold architecture for cartilage tissue-engineering applications that allow for the regulation of nutrient supply (e.g. oxygen and glucose), particularly for large clinically sized implants where nutrient limitations become more critical [411].

3DF processing techniques offer considerable flexibility in the design of porous architectures for tissue engineering. For our model scaffolds, the specific fibre spacing and fibre diameter adopted were related to obtaining comparable vol% porosity to CM scaffolds while still providing optimal dynamic stiffness and large interconnecting pores. Alternating to a staggered fibre spacing likely provided a more suitable architecture for seeding (Chapter 8) compared with a homogeneous fibre spacing, although mechanical properties were decreased by approximately 50% (Chapter 3, 8). Although we did not systematically evaluate tissue formation on a range of 3DF pore architectures, we demonstrated in Chapter 6 that pore-size gradients (Ø250–1650 µm in range) within scaffolds influenced the amount and distribution of GAG and collagen type II, but did not effect cell differentiation (GAG/DNA) *in vitro*. Based on data from Chapters 4 and 5, subcutaneous implantation of scaffolds *in vivo* may yield more distinct differences in the instructive abilities of scaffold architectures containing gradients in volume fraction and pore size. While the development of anisotropic tissue-engineered constructs which promote the zonal organisation of native cartilage are important, we demonstrated in Chapter 8 that additional factors instructing (re)differentiation such as synergistic effects of scaffold composition are necessary (discussed later).

Scaffold characterisation using novel µCT techniques presented in this thesis were essential to gaining a complete understanding of pore architecture and accessibility. The sensitivity and wide applicability of these techniques offer considerable advantages for the characterisation of scaffolds for tissue engineering.

Scaffold composition:

Based on the research presented in this thesis, the most optimal scaffold composition for instructing chondrocyte (re)differentiation on 2D films and 3D scaffolds were high PEG MW 1000/70/30 co-polymer compositions. Our data suggests that, for tissue engineering approaches which expose 3D scaffolds to serum containing media, and thereby preferential protein adsorption, a FN-rich substrate-protein milieu promotes chondrocyte adhesion and a de-differentiated phenotype, whereas a FN-deficient substrate-protein milieu promotes a spherical morphology and maintenance of differentiated chondrocyte phenotype. This confirms data which suggests that increased FN adsorption enhances cell spreading and de-differentiation [299, 533]. While we observed synergistic effects of both composition and 3D scaffold architecture on human chondrocytes re-differentiation capacity, our data suggests that comparatively, scaffold composition and the subsequent influence of protein adsorption, has a more significant influence on (re)differentiation than architecture alone.

Scaffold materials other than PEGT/PBT were not investigated in this thesis. We were primarily interested in studying the effects of controlled changes in scaffold composition and pore architecture, and PEGT/PBT co-polymers provided an ideal model substrate. Other promising scaffolds (described in Chapter 2) such as HYAFF-11 (hyaluronic acid derivative) have been described for their instructive chondrogenic ability in human articular chondrocytes [153, 451]. The ability for these, and other, promising biomaterials to be processed using 3DF or other RP techniques remains uncertain. However, the development and *in vitro* and *in vivo* evaluation of standardised 3DF scaffold architectures from a range of natural or synthetic biomaterials in parallel, would offer significant advantages in comparing the success of scaffold-based tissue engineering approaches to articular cartilage repair.

Mechanical properties:

Given the frequency dependant, viscoelastic response of articular cartilage under dynamic compression [113, 173, 194, 376], we postulated that the dynamic, rather than static, properties of articular cartilage provides a more appropriate benchmark with which to emulate into scaffolds designed for articular cartilage repair. While other investigators have reported the development of scaffolds with similar (static) compressive modulus to articular cartilage [360, 445], the development of scaffolds with similar dynamic stiffness properties to articular cartilage have not been reported previously. The mechanical data presented in this thesis (Chapter 3, 4, 8 and 9) indicated that it was possible to design 3DF PEGT/PBT scaffolds which match the static and dynamic properties of articular cartilage (see summary in Table B.2 in Appendix B). After cell seeding and *in vitro* culture or subcutaneous implantation *in vivo*, we also demonstrated that the combination of scaffold and engineered tissue not only maintains but further increased equilibrium modulus and dynamic stiffness properties with culture duration (Chapter 9).

It has been shown that *in vitro* culture time (*i.e.* the developmental stage of the tissue-engineered construct) can have a significant effect on the integration between repair and native tissue [114, 364]. Obradovic *et al.* [364] demonstrated enhanced integration between immature constructs (1-week culture) compared with mature constructs (8-week culture). The mechanical properties of immature constructs were insufficient compared with mature constructs however. Scaffold designs, such as 3DF architectures demonstrated in this thesis, that support rapid re-differentiation and ECM synthesis to enhance integration – but on the

other hand have sufficient mechanical stability to protect this newly formed tissue from *in vivo* joint loading – could offer significant promise. Furthermore, in adopting an early implantation strategy, extended *in vitro* culture periods and mechanical pre-conditioning of the tissue-engineered implant to achieve sufficient mechanical properties were avoided. By implanting anatomically-shaped CM and 3DF scaffolds in rabbits (Chapter 9) we were able to forgo integration issues between tissue-engineered and host cartilage given that total joint resurfacing was evaluated. While 3DF implants had improved mechanical properties than CM implants, both constructs were capable of supporting short-term *in vivo* loading. We emphasize that mechanical properties are very important, however, longer *in vivo* follow up studies and a greater contrast in scaffold mechanical properties to those studied in this thesis may be necessary if definite conclusions are to be drawn regarding the influence of mechanical properties on the success of articular cartilage repair.

Future Directions:

The flexibility of RP and CAD/CAM techniques, such as 3DF, in combination with the processibility and instructive cell response of PEGT/PBT biomaterial provides enormous potential in a number of avenues in tissue engineering. With the introduction of bi-phasic scaffold designs (Chapter 2), one can envisage that recent developments in rapid prototyping of ceramic biomaterials for bone tissue-engineering [514] could be combined with 3DF techniques to create bi- or multi-phasic osteochondral implants. Scaffold composition and pore architectures could be designed and produced which instruct specific chondrogenic and osteogenic responses *in vitro* or *in vivo* enhancing repair and tissue integration.

With respect to 3DF techniques described in this thesis (particularly in Chapter 9), in addition to varying scaffold fibre spacing, nozzles and/or syringes could be interchanged during processing in the future in order to deposit fibres with different diameter and PEGT/PBT composition. As a result, interconnecting pore size, volume fraction, fibre orientation, surface chemistry, degradation behaviour and mechanical properties could be controlled from one layer to another. In all these cases, the ability to produce anatomically-shaped or customized implants may provide a significant clinical impact [427, 428]. For example, all of the abovementioned scaffold architectures and compositions could be produced with simple or complex anatomical geometries based directly on 3D CAD models and/or CT/MRI scans of actual defects.

We emphasized that a highly interconnecting and accessible pore architecture (e.g. 3DF) which also provides suitable mechanical properties is recommended. In repair strategies relying on implantation of immature cartilage constructs, future composite scaffolds containing a bulk substrate with appropriate mechanical properties (e.g. 300/55/45), coated with another substrate capable of promoting chondrocyte (re)differentiation and cartilaginous matrix deposition (e.g. 1000/70/30) would be advantageous. Preliminary efforts to achieve this have already been performed using a novel emulsion coating technique [449] as described in Fig B.1 (Appendix B). Furthermore, based on the demonstrated ability to incorporate proteins into the emulsion coating technique [449], this may offer additional advantages in the controlled release of instructive bioactive factors, such as TGF- β 1.

Mechanical cues are crucial for normal skeletal development, growth and maturation [212]. Mechanical conditioning or stimulation of cartilage constructs *in vitro* has been shown to be instructive for chondrocyte (re)differentiation [76, 77, 159, 399]. As an alternative to currently adopted short-term loading in gels (e.g. agarose, alginate), mechanically stable 3DF scaffolds with designed pore architectures should be evaluated in future to determine the effects of long-term mechanical stimulation and predict what effects physiological load bearing will have on cell-seeded constructs *in vivo*. Preliminary studies by Mandl *et al.* (unpublished data, Orthopaedic Research Laboratory, Erasmus University Medical Centre, Rotterdam) using an *in vitro* cyclic compression bioreactor demonstrated that 3DF scaffold stiffness and elastic response remained unchanged following cyclic loading (450,000 cycles @ 0.3 Hz, 15% strain) for 21 days in synovial fluid.

To evaluate the success of scaffold-based tissue engineering approaches in cartilage repair, the long-term functional stability of repair tissue *in vivo* is critical for patients to regain joint function and alleviate pain. Lamentably, the length of time needed to clinically evaluate novel scaffold technologies and treatment options limits rapid innovation and development of repair strategies. Better *in vitro* models and more rapid *in situ* evaluation techniques, such as high resolution MRI [394] or imaging of luciferase markers in transgenic mice [97, 150, 178], that are capable of providing biochemical data (e.g. GAG) as well as structural and morphological images in real-time are necessary. Furthermore, future studies need to address the retention and fate of implanted cells using scaffold-based tissue engineering techniques [373].

In creating articular cartilage, Nature has developed a truly remarkable material both structurally and functionally. While we demonstrated advanced processing techniques and biomaterials with instructive compositions and architectures for stimulating tissue engineering of articular cartilage, it is clear we still have work to do in order to match the ultimate "tissue-engineer", Nature herself.

Appendix

Appendix A

Enhanced Cell Attachment and Onset of Chondrogenesis on Gas Plasma Treated 2D and 3D PEGT/PBT Scaffolds

Appendix B

Tables B.1, B.2 and Figures B.1, B.2

200 μm

Exp

WD

Det

Magn

Spot

Acc.V



Appendix A:

Enhanced Cell Attachment and Onset of Chondrogenesis on Gas Plasma Treated 2D and 3D PEGT/PBT Scaffolds

Woodfield T.B.F.,^{1,2} Mahmood T.A.,^{1,2} Riesle J.,² van Blitterswijk C.A.^{1,2}

¹ Institute for Biomedical Technology, University of Twente, Enschede, The Netherlands

² IsoTis S.A., Bilthoven, The Netherlands

Trans. Orthop. Res. Soc., Dallas, USA, **2002**; **27**: 473.

Introduction:

At present we are evaluating a family of poly (ethylene glycol)-terephthalate - poly (butylene terephthalate) (PEGT/PBT) block copolymer materials as carriers for cell-based therapies for cartilage defect repair. PEGT/PBT block co-polymers consist of hydrophilic PEGT soft segments and hydrophobic PBT hard segments denoted using the following notation **a/b/c** (a = PEG molecular weight, b = wt% PEGT, c = wt% PBT). To promote early onset of chondrogenesis *in vitro*, and hence, earlier implantation and load bearing in the patient, it is important to provide cells with a porous, 3D and interconnected substrate with suitable surface chemistry allowing cell attachment, proliferation, and differentiation throughout the scaffold.

Gas plasma (GP) treatment is commonly used commercially to treat tissue-culture polystyrene surfaces, enhancing cell attachment and proliferation, reportedly caused by etching and incorporation of hydroxyl groups in the most superficial layers through a cascade of chemical reactions [83]. Previous GP experiments on dense and porous PEGT/PBT substrates using SVK14 epithelial cells and dermal fibroblasts respectively, resulted in improved cell attachment and growth [27], however, little is known about the behaviour of chondrocytes towards GP treated surfaces. The purpose of this study was to investigate the effects of chondrocyte attachment and chondrogenesis on PEGT/PBT substrates either with or without GP surface modification. 2D and 3D substrates composed of 1000PEGT70PBT30 were selected as previous studies suggested such compositions would provide a sensitive surface model.

Materials and Methods:

Material: 2D dense films with an average thickness of 67 μm were solvent cast from PA 1000/70/30 resin. 3D porous 1000/70/30 scaffolds were produced using two different processing techniques. Compression moulding and salt leaching produced scaffolds with approximately 75% porosity and pore sizes ranging between 500-600 μm . Scaffolds were also produced using a novel 3D fibre deposition technique. Briefly, scaffolds were constructed by successively layering a 0°-90° pattern of molten PEGT/PBT from a $\text{\O}250$ μm nozzle onto a

computer controlled table translating in the x-y plane. After a number of layer iterations, the resulting 4 mm thick construct had 100% interconnected pores ranging between 700 μ m and 200 μ m in the horizontal and vertical planes respectively, and was approximately 70% porous. All constructs were glow discharge treated under a CO₂ (4.5 purity) plasma (50W). To allow full penetration of the plasma, top and bottom surfaces of the constructs were treated for 15 minutes each.

Tissue Culture: Primary bovine chondrocytes were isolated via collagenase digestion from tissue harvested from freshly slaughtered mature and immature animals. For 2D experiments, mature cells were seeded at a density of 10,000 cells/cm² per polymer disc (\varnothing = 1.55 cm), which were cored from the dense films. Porous 3D scaffolds, \varnothing 7 mm x 4 mm thick, were dynamically seeded in spinner flasks for 3 days at a density of 7.5x10⁶ immature cells/scaffold. Scaffolds were then dynamically cultured in spinner flasks for 12 days. HEPES buffered DMEM supplemented with 20 mM ascorbic acid, 0.4 mM proline, 0.1 mM NEAA, pen/strep and 10% FBS was used for both 2D and 3D culture.

Evaluation: 2D cultures were assessed after 1.5 and 7 days and cell morphology examined under light microscopy. Cellularity per cell seeded was determined by DNA quantitation using a Cyquant assay ($n=3$). 3D cultures were assessed after 3 and 12 days. Following fixation and dehydration, samples were plastic embedded and stained with Safranin-O (haematoxylin/fast-green counter-stain) to assess tissue morphology as well as chondrogenesis via glycosaminoglycan (GAG) expression. Non-embedded samples were also sectioned, critically point dried and gold sputter-coated for scanning electron microscopy (SEM) analysis.

Results:

DNA data indicated that significantly greater numbers of cells ($p<0.03$) initially attached to GP treated than untreated PA 1000/70/30 films after 1.5 days (Fig 1). Light microscopy after 1.5 days showed both rounded as well as spread cells were evident on GP treated surfaces, whilst at day 7, cells were spread and had reached confluency. In contrast, cells attached to the untreated films maintained a rounded morphology at both 1.5 and 7 days. Cell proliferation data at day 7 showed that GP treated films continued to demonstrate significantly greater cell numbers ($p<0.01$) compared to untreated films.

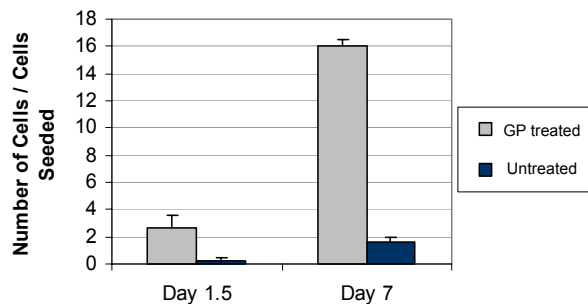


Figure A.1 – Cell attachment and proliferation on glow discharge (GP) treated and untreated 1000/70/30 PEGT/PBT dense films.

SEM analysis after 3 days dynamic seeding on 3D scaffolds also showed increased cell attachment and tissue formation on GP treated scaffolds compared with controls. This was particularly true for GP treated 3D-deposited scaffolds (Fig 2A, 2B) where a tissue layer completely surrounded fibres within the scaffold and stained positively for GAG (Fig 2D). In contrast, early chondrogenesis was limited to only a few areas in untreated scaffolds stained with safranin-O (Fig 2C). Whilst considerable subsequent tissue formation resulted following 12 days dynamic culture on untreated 1000/70/30 (inset Fig 2C), it was less than treated scaffolds, where almost all pores were lined or filled with cartilage-like tissue staining positively for GAG (inset Fig 2D).

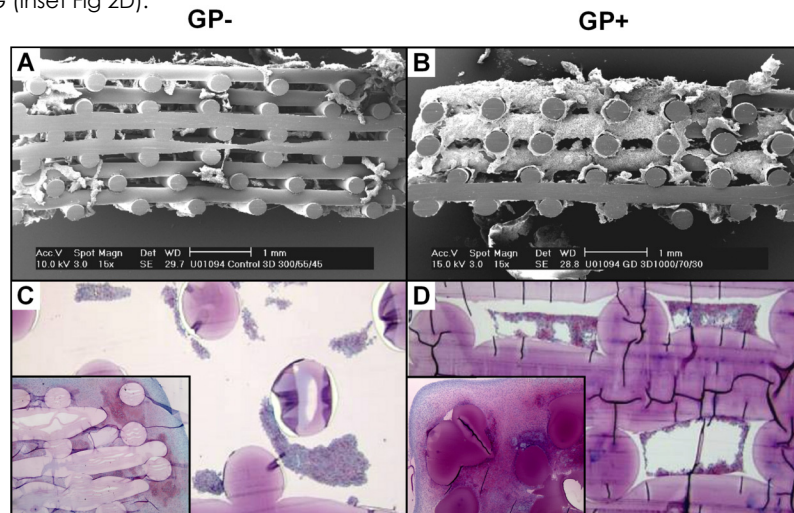


Figure A.2 – Day 3 (A) SEM x-section of untreated 3D 1000/70/30 (B) GP treated 3D 1000/70/30; (C) Saf-O untreated 3D 1000/70/30; (D) Saf-O GP treated 3D 1000/70/30 showing positive GAG formation. Inset (C, D) shows Saf-O staining at day 12. ► p220.

Conclusions:

We have demonstrated a simple surface modification process which significantly improved chondrocyte attachment and proliferation in 2D/3D model scaffolds. Whilst it still remains unclear as to which exact surface properties are positively altered following GP treatment, enhanced cell attachment resulted in more rapid synthesis of cartilage-like tissue following dynamic seeding and culture on 3D scaffolds compared with untreated 3D scaffolds. We believe providing structured scaffolds which promote rapid cell attachment and proliferation with concomitant cartilage tissue formation may allow early implantation and *in-vivo* loading stimuli in the future.

Acknowledgements:

The authors would like to acknowledge L. Groenewoud (GP treatment), as well as funding from the European Commission (FP5 project "Scafcart" G5RD-CT-1999-00050).

Appendix B:

Table B.1 – Summary of scaffold characterisation data.

Sample	Measured Vol% Porosity		Scaffold Vol. Fraction	Avg. Pore Size	Pore Size Range	Pore Size at $\geq 90\%$ Accessible Pore Vol.
	m/V (%)	μ CT (%)	μ CT (mm^{-1})	μ CT (μm)	μ CT (μm)	μ CT (μm)
CM 300/55/45	75.6 \pm 1.9	81.8	10.0	182	6 – 450	98
CM 1000/70/30	76.0 \pm 2.1	77.8	12.2	160	6 – 444	95
3DF 1mm 300/55/45	70.2 \pm 1.8	77.6	3.3	525	132 – 852	680
3DF 1mm 1000/70/30	70.2 \pm 1.2	72.8	4.0	450	108 – 828	500
3DF 1mm stag 300/55/45	70.2 \pm 1.2	74.4	3.8	380	132 – 450	380
3DF 1mm stag 1000/70/30	71.5 \pm 1.8	71.2	4.0	388	156 – 600	360

Table B.2 – Summary of scaffold mechanical properties data.

Sample	Equilibrium Modulus (MPa)	Dynamic Stiffness @ 0.1 Hz (MPa)
CM 300/55/45	0.93 \pm 0.31	1.72 \pm 0.33
CM 1000/70/30	0.18 \pm 0.01	0.17 \pm 0.02
3DF 1mm 300/55/45	2.50 \pm 0.82	4.33 \pm 0.52
3DF 1mm stag 300/55/45	1.35 \pm 0.17	2.01 \pm 0.14
3DF 2mm 300/55/45	0.05 \pm 0.02	0.21 \pm 0.10
3DF 0.5mm 1000/70/30	0.98 \pm 0.39	2.10 \pm 0.44
3DF 1mm 1000/70/30	0.24 \pm 0.02	0.44 \pm 0.01
3DF 1mm stag 1000/70/30	0.13 \pm 0.01	0.16 \pm 0.01
Bovine femoral AC	0.27 \pm 0.24	4.10 \pm 1.57
Human femoral AC [475]	0.60	4.50

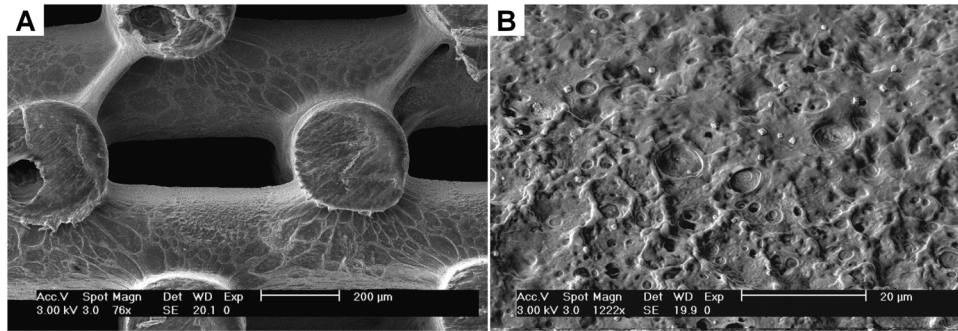


Figure B.1 – (A) Emulsion coating of 3DF 300/55/45 scaffold (staggered fibre spacing) with a thin layer of 1000/70/30. While the bulk 300/55/45 scaffold provides necessary mechanical properties, the micro-porous 1000/70/30 coating (B) provides a rough and instructive substrate for promoting chondrocyte re-differentiation and cartilaginous ECM deposition.

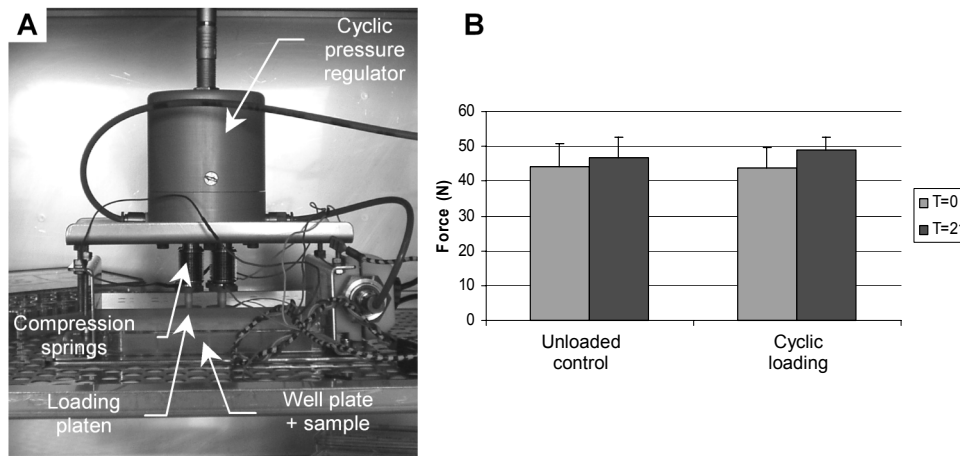


Figure B.2 – (A) Cyclic compression bioreactor. Cyclic pressure regulation controls vertical motion of compression springs which impart deformation to cell-seeded constructs placed in well-plates. (B) The equilibrium force at 15% strain (i.e. stiffness) in 3DF scaffolds remained unchanged following cyclic loading (450,000 cycles @ 0.3 Hz, 15% strain) for 21 days in synovial fluid (unpublished data, Orthopaedic Research Laboratory, Erasmus University Medical Centre, Rotterdam).

Summary

Recent advances in the fields of biological science and materials engineering have resulted in the evolution of the field of "tissue engineering" - aimed at combining cell therapy and biodegradable biomaterials for the repair or regeneration of damaged tissues (*i.e.* articular cartilage). Few of the currently employed clinical techniques for repairing damaged articular cartilage are capable of restoring long-term function, and while tissue engineering strategies have shown promising results, their relative success over traditional techniques remains uncertain (Chapter 1-2). One of the challenges in cartilage tissue engineering is the design and fabrication of 3D scaffolds which are capable of instructing, or guiding, specific cellular functions in order to obtain functional repair tissue. Important scaffold design criteria include not only the ability to provide suitable mechanical properties and interconnecting 3D pore volume for cell adhesion and proliferation, but also an architecture and surface chemistry which are "instructive" for chondrocyte (re)differentiation and subsequent ECM formation to initiate repair.

In Chapter 3, the development of a novel 3D fibre deposition (3DF) technique was introduced which allowed us to reproducibly "design in" desired scaffold characteristics such as porosity, pore size and pore interconnectivity. This rapid prototyping technique allowed computer controlled deposition of sequential layers of molten PEGT/PBT co-polymer fibres ($\varnothing 175\text{-}250\ \mu\text{m}$) resulting in scaffolds with established biocompatibility, surface chemistry promoting cell adhesion and differentiation, a highly interconnecting pore volume, dynamic mechanical properties matching native articular cartilage, controllable internal 3D pore architectures incorporating pore-size gradients or anisotropic features, as well as controllable external scaffold shape based on computer aided design (CAD) models (Chapter 9).

With respect to structure-function relationships between scaffold pore architecture and cartilage tissue formation, we demonstrated that controlled changes in 3D PEGT/PBT scaffold architecture effects chondrocyte differentiation capacity *in vivo* (Chapters 4-5). 3DF scaffold architectures containing a highly accessible pore volume and large, 100% interconnecting pores (average $\varnothing 525\ \mu\text{m}$) instructed cells to synthesise significantly greater GAG and GAG/DNA content compared to compression moulded and particle leached (CM) scaffold architectures with the same porosity (80%). These latter scaffolds contained a less accessible pore volume and smaller interconnecting pores (average $\varnothing 182\ \mu\text{m}$). These effects were likely the result of enhanced nutrient/waste exchange throughout 3DF scaffolds, although they could not be directly correlated to differences in oxygen gradient between scaffold architectures (Chapter 5). However, both the amount and homogeneous distribution of cells and ECM (*i.e.* GAG and collagen type II) were enhanced throughout 3DF scaffolds. Anisotropic 3DF scaffolds with designed pore-size gradients were capable of instructing an inhomogeneous (zonal) distribution of cells, GAG and collagen type II within tissue-engineered constructs *in vitro* (Chapter 6), but did not influence the zonal distribution of GAG/DNA.

The ability of PEGT/PBT scaffold composition and architecture to instruct post-expansion re-differentiation of human chondrocytes was investigated in Chapters 7 and 8. We demonstrated in Chapter 7 that low PEG molecular weight (MW) PEGT/PBT compositions (*e.g.*

300/55/45) supported cell adhesion and reduced post-expansion re-differentiation (evidenced by collagen type II/I mRNA expression) of human nasal chondrocytes on 2D films. In contrast, on high PEG MW PEGT/PBT compositions (e.g. 1000/70/30), cell adhesion was limited but collagen II/I mRNA expression was increased, and was likely related to fibronectin (FN) adsorption from serum containing (S+) culture media. Independent of PEGT/PBT composition, surface modification of 300/55/45 or 1000/70/30 films via gas plasma treatment enhanced cell adhesion and cellularity, resulting in increased $\alpha 5\beta 1$ (FN) integrin receptor expression intensity and reduced re-differentiation capacity. These effects were related to preferential etching of PEG over PBT blocks, thereby influencing surface protein adsorption (e.g. FN-rich), as similar effects were not observed when serum free (SF) culture media was used.

When extrapolated to 3D scaffolds in Chapter 8, synergistic instructive effects of both PEGT/PBT composition and architecture were observed in high MW (*i.e.* 1000/70/30) 3DF compared to CM scaffolds, indicated by increased GAG/DNA deposition and enhanced collagen II mRNA expression *in vitro*. Comparatively, scaffold composition and the subsequent influence of protein adsorption (*i.e.* FN-deficient surfaces) appeared to be more instructive for chondrocyte re-differentiation than architecture alone. However, 3DF scaffold architectures (with a simple, highly accessible pore volume and large interconnecting pores $\varnothing 380 \mu\text{m}$) were capable of instructing enhanced collagen II mRNA expression compared with CM scaffolds, irrespective of composition, and suggests collagen and GAG synthesis pathways operate independently.

In Chapter 9, we described a preliminary *in vivo* study in rabbits in an attempt to amalgamate novel RP technologies, scaffold design criteria and culture techniques developed in Chapters 2-8 to produce anatomically-shaped tissue-engineering cartilage implants for joint reconstruction. Using computed tomography (CT) scans to generate a 3D CAD models of the rabbit knee, RP techniques including computer numerical controlled (CNC) milling of CM blocks and 3DF allowed anatomically-shaped tibial and femoral scaffolds to be produced. Prior to implantation, 3DF scaffolds contained significantly greater GAG and GAG/DNA content, exhibiting significantly higher and comparable dynamic mechanical properties (at 0.1Hz) to native articular cartilage, compared to CM scaffolds. Following knee osteotomy surgery and *in vivo* implantation, 3DF and CM implants were evaluated after a short-term 6 week follow-up. Histology indicated bone in-growth and implant fixation, as well as an articulating layer between femoral and tibial implants as a result of limited load bearing and knee function in rabbits over the 6 week period. However, for both 3DF and CM architectures, the cartilage-like tissue present prior to implantation was not maintained and the repair tissue was predominantly fibrous-like in appearance. Although we successfully developed a concept for anatomically-designed tissue-engineered cartilage implants, longer-term load bearing studies are necessary to further evaluate the type of tissue repair, implant fixation and implant integrity and are currently ongoing.

A complete summary and discussion of the results presented in this thesis were described in Chapter 10. Furthermore, the implications of this research in cartilage repair strategies and future directions were discussed.

Samenvatting

Recente ontwikkelingen in het biotechnologische en (bio)materialen onderzoek hebben geresulteerd in de ontwikkeling van "tissue engineering" als een nieuwe wetenschappelijke discipline. In tissue engineering, worden cel therapie and biologische degradeerbare biomaterialen gecombineerd voor de klinische behandeling van weefsel defecten (b.v in articulair kraakbeen). Van de klinische technieken die tegenwoordig worden toegepast in de behandeling van articulaire kraakbeen defecten, zijn er weinigen in staat tot functioneel herstel op de lange termijn. Ondanks dat de ontwikkelingen in tissue engineering veel belovend zijn, zal in de toekomst blijken of ze een additioneel effect hebben dat conventionele technieken ontstijgt (Hoofdstuk 1-2). Een van de uitdaging in kraakbeen tissue engineering is het ontwikkelen en maken van 3D drager materialen die cellen kunnen instrueren en sturen in de herstelreactie naar functioneel kraakbeen. Criteria die belangrijk zijn voor het ontwerpen van een geschikt dragermateriaal zijn onder anderen het verschaffen van geschikte mechanische eigenschappen en het voorzien in interconnectiviteit en porositeit die cel adhesie and proliferatie stimuleren. Maar ook chemische en morfologische eigenschappen van het dragermateriaal oppervlak kunnen instructief zijn voor de (re)differentiatie van kraakbeencellen en vorming van extracellulaire matrix die noodzakelijk is voor een herstelreactie.

In Hoofdstuk 3 wordt de ontwikkeling geïntroduceerd van een nieuwe 3D-print techniek voor vezels (3DF). Deze techniek die we "rapid prototyping" noemen, maakt het mogelijk om de gewenste dragermateriaal karakteristieken zoals porositeit, poriegrootte and interconnectiviteit reproduceerbaar in een construct te bouwen. Met rapid prototyping worden opeenvolgende lagen PEGT/PBT co-polymeer vezels ($\varnothing 175\text{-}250\ \mu\text{m}$) geprint op een computer gestuurde manier. Dit resulteert in biocompatibele dragermaterialen voorzien van chemische oppervlakte eigenschappen die cel adhesie en differentiatie stimuleren, hoge interconnectiviteit tussen de poriën, dynamisch mechanische eigenschappen vergelijkbaar met natuurlijk kraakbeen, controleerbare interne 3D porie architectuur waardoor gradiënten in poriegrootte kunnen worden aangebracht en een door CAD (computer aided design) gemoduleerde en controleerbare vorm van het construct (Hoofdstuk 9).

Met betrekking tot de relatie tussen architectuur van een construct en kraakbeen vorming, hebben we aangetoond dat aangebrachte veranderingen in architectuur van 3D PEGT/PBT dragermaterialen, kraakbeencel differentiatie in vivo beïnvloeden (Hoofdstuk 4-5). De architectuur van 3DF dragermaterialen voorzien cellen van een uitermate hoog toegankelijk porievolume en grote poriën die 100% interconnectief zijn ($\varnothing 525\ \mu\text{m}$). Als we de differentiatie van kraakbeen cellen in deze constructen vergelijken met differentiatie in constructen met dezelfde porositeit (80%) die gemaakt zijn met een thermoplastische perstechniek (CM), zien we dat in 3DF constructen significant meer GAG en GAG/DNA wordt gemaakt. CM constructen blijken een klein toegankelijk porie volume te hebben en de interconnectiviteit tussen poriën was kleiner (gemiddeld $\varnothing 182\ \mu\text{m}$). Ook al hebben we geen direct correlatie tussen constructarchitectuur en zuurstofgradiënten kunnen aantonen, het effect van 3DF constructen op differentiatie is mogelijk het resultaat van een verhoogde mate van nutriënt/afvalproduct uitwisseling door het hele construct (Hoofdstuk 5). Zowel de hoeveelheid als de homogeniteit van celdistributie en kraakbeenmatrix (b.v GAG and collagentype II) is verhoogd in 3DF constructen. Met anisotropische 3DF constructen die een gradiënt in poriegrootte hebben, zijn we in staat cellen in vitro te voorzien van instructieve signalen waardoor ze zich inhomogeen en zone afhankelijk distribueren en GAG en collageentype II synthetiseren. Echter we hebben geen zone-afhankelijk verschil in GAG/DNA in deze constructen aangetoond.

In Hoofdstuk 7 en 8 hebben we de mogelijkheid bestudeerd om redifferentiatie van gekweekte chondrocyten te beïnvloeden door veranderingen in PEGT/PBT dragermateriaal compositie and architectuur aan te brengen. In hoofdstuk 7 hebben we beschreven dat PEGT/PBT2D- films met een laag PEG molecuair gewicht (MW) (b.v 300/55/45) cel adhesie stimuleren en tegelijkertijd redifferentiatie van humane gekweekte chondrocyten uit neus kraakbeen onderdrukken (aangetoond door collageentype II/I mRNA expressie). Aan de andere kant is cel adhesie op PEGT/PBT composities met een hoog PEG MW gelimiteerd en tegelijkertijd is collageen II/I mRNA expressie verhoogd. Dit is hoogstwaarschijnlijk gerelateerd aan fibronectine (FN) adsorptie uit serum dataanwezig is in het kweekmedium. Onafhankelijk van de PEGT/PBT compositie verhogen modificaties van het oppervlak van 300/55/45 of 1000/70/30 films door gas plasma behandeling, de cel adhesie. Dit resulteert in verhoogde expressie van $\alpha 5\beta 1$ (FN) integrin receptor en gereduceerde redifferentiatie. Dit effect is gerelateerd aan het preferentieel etsen van PEG boven PBT blokken door de gasplasma behandeling waardoor eiwit adsorptie aan het oppervlak (b.v FN-rijk) beïnvloed wordt. Dit concluderen we omdat we in medium zonder serum (SF) niet dezelfde effecten konden aantonen.

In hoofdstuk 8 extrapoleren we het bovenstaande naar 3D vezelconstructen. Hier wordt namelijk het synergetisch instructieve effect van zowel de PEGT/PBT compositie als de architectuur van 3DF constructen (b.v 1000/70/30) met een hoog MW t.o.v CM constructen aangetoond door meer GAG/DNA depositie en verhoogde collageen II mRNA expressie in vitro. Als we dit vergelijken met de invloed van de dragermateriaalcompositie op eiwit adsorptie (b.v FN-loze oppervlakken) en de daarop volgende invloed op redifferentiatie van kraakbeencellen alleen, lijkt compositie meer instructieve invloed te hebben dan architectuur alleen. In vergelijking met CM constructen voorziet de architectuur van 3DF constructen de cel echter wel met instructieve signalen die resulteren in verhoogde collageen II mRNA expressie. Omdat dit onafhankelijk is van compositie suggereren deze resultaten dat collageen en GAG synthese routes autonoom van elkaar lopen.

In Hoofdstuk 9 beschrijven we een in vivo studie in konijnen waarin een eerste poging wordt gedaan om rapid prototyping technologie, dragermateriaal vormgeving en kweek technieken ontwikkeling omschreven in Hoofdstuk 2-8, te combineren om een anatomische gevormd tissue-engineered kraakbeenimplantaat te maken voor gewrichtreconstructie. Met CT (computed tomography)scan hebben we 3D CAD modellen gemaakt van een konijnenknie. Vervolgens is het mogelijk gebleken om met RP technieken zoals o.a. CNC (computer numerical controlled) freesen van CM blokken en 3DF een anatomisch gevormde reconstructies van de tibia en femur uit dragermateriaal te produceren. Vóór implantatie hebben de 3DF constructen t.o.v CM constructen significant meer GAG en GAG/DNA, vertonen ze significant hogere dynamisch mechanische eigenschappen die in vergelijking meer lijken op die van articulaire kraakbeen (bij 0.1 Hz). Na osteotomie van de knie en in vivo implantatie van de 3DF en CM constructen, zijn de implantaten weer geëxplanteerd en geevalueerd na 6 weken. Histologische data laten botingroei en fixatie van het implantaat aan het bot zien. Bovendien zien we, als gevolg van de gelimiteerde belasting en flexie van de knie, een articulaire laag tussen de femurale en de fibiale implantaten. Echter, in zowel 3DF als CM constructen is extracellulaire matrix die aanwezig was op het moment van implantatie niet gehandhaafd en bestond het herstel weefsel voornamelijk uit weefsel met een fibreusachtige morfologie. Hoewel we een succesvol concept hebben ontwikkeld voor het maken van anatomisch gevormde tissue-engineerd kraakbeenimplantaten, is verdere evaluatie van het herstel weefsel, implantaat fixatie en implantaat integriteit op de lange termijn noodzakelijk.

Een complete samenvatting en de discussie van de resultaten die in dit proefschrift worden omschreven is in hoofdstuk 10 gegeven. Bovendien worden hier de implicaties van deze studie op het ontwikkelen van strategieën voor het behandelen van kraakbeen defecten besproken.

References

- [1] Abbott A. Cell culture: biology's new dimension. *Nature* **2003**; 424(6951): 870-872.
- [2] Abell A, Willis K, Lange D. Mercury Intrusion Porosimetry and Image Analysis of Cement-Based Materials. *J Colloid Interface Sci* **1999**; 211(1): 39-44.
- [3] Aeschlimann D, Lyons P, Masterlark T, Hayashi K, Graf B, Vanderby R. Repair of cartilage defects with autogenous osteochondral transplants (mosaicplasty) in a sheep model. *Trans Orthop Res Soc* **2001**; 26: 183.
- [4] Agrawal CM, Ray RB. Biodegradable polymeric scaffolds for musculoskeletal tissue engineering. *J Biomed Mater Res* **2001**; 55(2): 141-150.
- [5] Ahsan T, Sah R. Biomechanics of integrative cartilage repair. *Osteo Cart* **1999**; 7(1): 29-40.
- [6] Aichroth P, Ellis H. Transplantation of joint surfaces by cartilage grafts. *Br J Surg* **1970**; 57(11): 855.
- [7] Aigner J, Tegeler J, Hutzler P, Campoccia D, Pavesio A, Hammer C, Kastenbauer E, Naumann A. Cartilage tissue engineering with novel nonwoven structured biomaterial based on hyaluronic acid benzyl ester. *J Biomed Mater Res* **1998**; 42(2): 172-181.
- [8] Allemann F, Mizuno S, Eid K, Yates K, Zaleske D, Glowacki J. Effects of hyaluronan on engineered articular cartilage extracellular matrix gene expression in 3-dimensional collagen scaffolds. *J Biomed Mater Res* **2001**; 55(1): 13-19.
- [9] Altankov G, Thom V, Groth T, Jankova K, Jonsson G, Ulbricht M. Modulating the biocompatibility of polymer surfaces with poly(ethylene glycol): effect of fibronectin. *J Biomed Mater Res* **2000**; 52(1): 219-230.
- [10] Anderson AF, Mandelbaum BR, Erggelet C, Micheli LJ, Fu F, Moseley JB, Browne JE. A controlled study of autologous chondrocyte implantation versus marrow stimulation techniques for full-thickness articular cartilage lesions of the femur. *Trans AAOs* **2002**; 29: 607.
- [11] Angermann P, Riegels-Nielsen P, Pedersen H. Osteochondritis dissecans of the femoral condyle treated with periosteal transplantation. Poor outcome in 14 patients followed for 6-9 years. *Acta Orthop Scand* **1998**; 69(6): 595-597.
- [12] Armstrong CG, Lai WM, Mow VC. An analysis of the unconfined compression of articular cartilage. *J Biomech Eng* **1984**; 106: 165-173.
- [13] Athanasiou KA, Rosenwasser MP, Buckwalter JA, Malinin TI, Mow VC. Interspecies comparisons of in situ intrinsic mechanical properties of distal femoral cartilage. *J Orthop Res* **1991**; 9(3): 330-340.
- [14] Aubin P, Cheah H, Davis A, Gross A. Long-term followup of fresh femoral osteochondral allografts for posttraumatic knee defects. *Clin Orthop* **2001**; 391(Suppl): S318-S327.
- [15] Aulthouse A, Beck M, Griffey E. Expression of the human chondrocyte phenotype in vitro. *In Vitro Cell Dev Biol Anim* **1989**; 25: 659-668.
- [16] Aydelotte M, Thonar E, Mollenhauer J, Flechtenmacher J. Culture of chondrocytes in alginate gel: variations in conditions of gelation influence the structure of the alginate gel, and the arrangement and morphology of proliferating chondrocytes. *In Vitro Cell Dev Biol Anim* **1998**; 34(2): 123-130.
- [17] Bahuaud J, Maitrot R, Bouvet R, Kerdiles N, Tovagliari F, Synave J, Buisson P, Thierry J, Versier A, Romanet J, Chauvin F, Gillet J, Allizard J, de Belenet H. Implantation of autologous chondrocytes for cartilagenous lesions in young patients. A study of 24 cases. *Chirurgie* **1998**; 123(6): 568-571.
- [18] Bakker D, van Blitterswijk C, Hesselting S, Koerten H, Kuijpers W, Grote J. Biocompatibility of a polyether urethane, polypropylene oxide, and a polyether polyester copolymer. A qualitative and quantitative study of three alloplastic tympanic membrane materials in the rat middle ear. *J Biomed Mater Res* **1990**; 24(4): 489-515.
- [19] Barbero A, Ploegert S, Heberer M, Martin I. Plasticity of clonal populations of dedifferentiated adult human articular chondrocytes. *Arthritis Rheum* **2003**; 48(5): 1315-1325.
- [20] Baschong W, Suetterlin R, Laeng RH. Control of autofluorescence of archival formaldehyde-fixed, paraffin-embedded tissue in confocal laser scanning microscopy (CLSM). *J Histochem Cytochem* **2001**; 49(12): 1565-1572.
- [21] Beaver R, Mahomed M, Backstein D, Davis A, Zukor D, Gross A. Fresh osteochondral allografts for post-traumatic defects in the knee. A survivorship analysis. *J Bone Joint Surg Br* **1992**; 74(1): 105-110.
- [22] Behravesh E, Shung A, Jo S, Mikos A. Synthesis and Characterization of Triblock Copolymers of Methoxy Poly(ethylene glycol) and Poly(propylene fumarate). *Biomacromolecules* **2002**; 3(1): 153-158.

- [23] Bentley G, Biant L, Carrington R, Akmal M, Goldberg A, Williams A, Skinner J, Pringle J. A prospective, randomised comparison of autologous chondrocyte implantation versus mosaicplasty for osteochondral defects in the knee. *J Bone Joint Surg Br* **2003**; 85(2): 223-230.
- [24] Benya P, Shaffer J. Dedifferentiated chondrocytes re-express the differentiated collagen phenotype when cultured in agarose gels. *Cell* **1982**; 30: 215-224.
- [25] Berend ME, Thong AE, Faris GW, Newbern G, Pierson JL, Ritter MA. Total joint arthroplasty in the extremely elderly: hip and knee arthroplasty after entering the 89th year of life. *J Arthroplasty* **2003**; 18(7): 817-821.
- [26] Bert J, Maschka K. The arthroscopic treatment of unicompartmental gonarthrosis: a five-year follow-up study of abrasion arthroplasty plus arthroscopic debridement and arthroscopic debridement alone. *Arthroscopy* **1989**; 5(1): 25-32.
- [27] Beumer GJ. *Synthetic Biodegradable Polymers in the Regeneration of Skin*. PhD Thesis, University of Leiden, The Netherlands, **1993**; 158
- [28] Beumer GJ, van Blitterswijk CA, Bakker D, Ponec M. Cell-seeding and in vitro biocompatibility evaluation of polymeric matrices of PEO/PBT copolymers and PLLA. *Biomaf* **1993**; 14(8): 598-604.
- [29] Beumer GJ, van Blitterswijk CA, Ponec M. Biocompatibility of a biodegradable matrix used as a skin substitute: an in vivo evaluation. *J Biomed Mater Res* **1994**; 28(5): 545-552.
- [30] Bezemer JM, Grijpma DW, Dijkstra PJ, van Blitterswijk CA, Feijen J. A controlled release system for proteins based on poly(ether ester) block-copolymers: polymer network characterization. *J Controlled Release* **1999**; 62(3): 393-405.
- [31] Bezemer JM, Grijpma DW, Dijkstra PJ, van Blitterswijk CA, Feijen J. Control of protein delivery from amphiphilic poly(ether ester) multiblock copolymers by varying their water content using emulsification techniques. *J Controlled Release* **2000**; 66(2-3): 307-320.
- [32] Bezemer JM, Oude Weme P, Grijpma DW, Dijkstra PJ, van Blitterswijk CA, Feijen J. Amphiphilic poly(ether ester amide) multiblock copolymers as biodegradable matrices for the controlled release of proteins. *J Biomed Mater Res* **2000**; 52(1): 8-17.
- [33] Bezemer JM, Radersma R, Grijpma DW, Dijkstra PJ, Feijen J, van Blitterswijk CA. Zero-order release of lysozyme from poly(ethylene glycol)/poly(butylene terephthalate) matrices. *J Controlled Release* **2000**; 64(1-3): 179-192.
- [34] Bezemer JM, Radersma R, Grijpma DW, Dijkstra PJ, van Blitterswijk CA, Feijen J. Microspheres for protein delivery prepared from amphiphilic multiblock copolymers. 1. Influence of preparation techniques on particle characteristics and protein delivery. *J Controlled Release* **2000**; 67(2-3): 233-248.
- [35] Bhardwaj T, Pilliar R, Grynypas M, Kandel R. Effect of material geometry on cartilagenous tissue formation in vitro. *J Biomed Mater Res* **2001**; 57(2): 190-199.
- [36] Binette F, McQuaid D, Haudenschild D, Yaeger P, McPherson J, Tubo R. Expression of a stable articular cartilage phenotype without evidence of hypertrophy by adult human articular chondrocytes in vitro. *J Orthop Res* **1998**; 16(2): 207-216.
- [37] Black J. "Biological Performance of Materials: Fundamentals and Biocompatibility." 2nd ed., New York: Marcel Dekker Inc., **1992**.
- [38] Blunk T, Sieminski A, Gooch K, Courter D, Hollander A, Nahir A, Langer R, Vunjak-Novakovic G, Freed L. Differential effects of growth factors on tissue-engineered cartilage. *Tissue Eng* **2002**; 8(1): 73-84.
- [39] Bobic V. Arthroscopic osteochondral autograft transplantation in anterior cruciate ligament reconstruction: a preliminary clinical study. *Knee Surg Sports Traumatol Arthrosc* **1996**; 3(4): 262-264.
- [40] Bobic V, Noble J. Articular cartilage, to repair or not to repair. *J Bone Joint Surg Br* **2000**; 82(2): 165-166.
- [41] Bonassar LJ, Grodzinsky AJ, Frank EH, Davila SG, Bhaktav NR, Trippel SB. The effect of dynamic compression on the response of articular cartilage to insulin-like growth factor-I. *J Orthop Res* **2001**; 19(1): 11-17.
- [42] Bonaventure J, Kadhom N, Cohen-Sodal L, Ng K, Bourguignon J, Lasselin C, Freisinger P. Reexpression of cartilage-specific genes by dedifferentiated human articular chondrocytes cultured in alginate beads. *Exp Cell Res* **1994**; 212(1): 97-104.
- [43] Borden M, Attawia M, Khan Y, Laurencin CT. Tissue engineered microsphere-based matrices for bone repair: design and evaluation. *Biomaf* **2002**; 23(2): 551-559.
- [44] Borden M, Attawia M, Laurencin CT. The sintered microsphere matrix for bone tissue engineering: in vitro osteoconductivity studies. *J Biomed Mater Res* **2002**; 61(3): 421-429.
- [45] Bouhadir KH, Mooney DJ. Promoting angiogenesis in engineered tissues. *J Drug Target* **2001**; 9(6): 397-406.

- [46] Bouwmeester P, Kuijjer R, Homminga G, Bulstra S, Geesink R. A retrospective analysis of two independent prospective cartilage repair studies: autogenous perichondrial grafting versus subchondral drilling 10 years post-surgery. *J Orthop Res* **2002**; 20(2): 267-273.
- [47] Bouwmeester S, Beckers J, Kuijjer R, van der Linden A, Bulstra S. Long-term results of rib perichondrial grafts for repair of cartilage defects in the human knee. *Int Orthop* **1997**; 21(5): 313-317.
- [48] Boyan BD, Hummert TW, Dean DD, Schwartz Z. Role of material surfaces in regulating bone and cartilage cell response. *Biomater* **1996**; 17(2): 137-146.
- [49] Boyan BD, Lohmann CH, Romero J, Schwartz Z. Bone and cartilage tissue engineering. *Clin Plast Surg* **1999**; 26(4): 629-645, ix.
- [50] Breinan HA, Minas T, Hsu HP, Nehrer S, Shortkroff S, Spector M. Autologous chondrocyte implantation in a canine model: change in composition of reparative tissue with time. *J Orthop Res* **2001**; 19(3): 482-492.
- [51] Brittberg M. Autologous chondrocyte transplantation. *Clin Orthop* **1999**; 367(Suppl): S147-155.
- [52] Brittberg M, Lindahl A, Nilsson A, Ohlsson C, Isaksson O, Peterson L. Treatment of deep cartilage defects in the knee with autologous chondrocyte transplantation. *N Engl J Med* **1994**; 331(14): 889-895.
- [53] Brittberg M, Sjogren-Jansson E, Lindahl A, Peterson L. Influence of fibrin sealant (Tisseel) on osteochondral defect repair in the rabbit knee. *Biomater* **1997**; 18(3): 235-242.
- [54] Brittberg M, Tallheden T, Sjogren-Jansson B, Lindahl A, Peterson L. Autologous chondrocytes used for articular cartilage repair: an update. *Clin Orthop* **2001**; 391(Suppl): S337-348.
- [55] Broom ND, Oloyede A, Flachsmann R, Hows M. Dynamic fracture characteristics of the osteochondral junction undergoing shear deformation. *Med Eng Phys* **1996**; 18(5): 396-404.
- [56] Brown TD. Techniques for mechanical stimulation of cells in vitro: a review. *J Biomech* **2000**; 33(1): 3-14.
- [57] Brun P, Abatangelo G, Radice M, Zacchi V, Guidolin D, Daga Gordini D, Cortivo R. Chondrocyte aggregation and reorganization into three-dimensional scaffolds. *J Biomed Mater Res* **1999**; 46(3): 337-346.
- [58] Bryant S, Anseth K. The effects of scaffold thickness on tissue engineered cartilage in photocrosslinked poly(ethylene oxide) hydrogels. *Biomater* **2001**; 22(6): 619-626.
- [59] Bryant S, Anseth K. Controlling the spatial distribution of ECM components in degradable PEG hydrogels for tissue engineering cartilage. *J Biomed Mater Res* **2003**; 64(1): 70-79.
- [60] Buckwalter J. Articular cartilage injuries. *Clin Orthop* **2002**; 402: 21-37.
- [61] Buckwalter J, Mankin H. Instructional Course Lectures, The American Academy of Orthopaedic Surgeons - Articular Cartilage. Part I: Tissue Design and Chondrocyte-Matrix Interactions. *J Bone Joint Surg Am* **1997**; 79(4): 600-611.
- [62] Buckwalter J, Mankin H. Instructional Course Lectures, The American Academy of Orthopaedic Surgeons - Articular Cartilage. Part II: Degeneration and Osteoarthritis, Repair, Regeneration, and Transplantation. *J Bone Joint Surg Am* **1997**; 79(4): 612-632.
- [63] Buckwalter J, Mankin H. Articular cartilage repair and transplantation. *Arthritis Rheum* **1998**; 41(8): 1331-1342.
- [64] Buckwalter JA. Articular cartilage: injuries and potential for healing. *J Orthop Sports Phys Ther* **1998**; 28(4): 192-202.
- [65] Buckwalter JA. Evaluating methods of restoring cartilaginous articular surfaces. *Clin Orthop* **1999**; 367(Suppl): S224-238.
- [66] Buckwalter JA, Mankin HJ. Articular cartilage: degeneration and osteoarthritis, repair, regeneration, and transplantation. *AAOS Instr Course Lect* **1998**; 47: 487-504.
- [67] Buckwalter JA, Mankin HJ. Articular cartilage: tissue design and chondrocyte-matrix interactions. *AAOS Instr Course Lect* **1998**; 47: 477-486.
- [68] Bujia J, Wilmes E, Kastenbauer E, Gurtler L. Influence of chemical allograft preservation procedures on the human immunodeficiency virus. *Laryngoscope* **1996**; 106(5 Pt 1): 645-647.
- [69] Burgarski B, Jovanovic D, Vunjak-Novakovic G. Bioreactor systems based on microencapsulated animal cell cultures. In "Fundamentals of animal cell immobilization and microencapsulation." Goosen M, Ed.; CRC Press: Boca Raton, **1993**; 267-296.
- [70] Buschmann MD, Gluzband YA, Grodzinsky AJ, Hunziker EB. Mechanical compression modulates matrix biosynthesis in chondrocyte/agarose culture. *J Cell Sci* **1995**; 108 (Pt 4): 1497-1508.
- [71] Buschmann MD, Kim YJ, Wong M, Frank E, Hunziker EB, Grodzinsky AJ. Stimulation of aggrecan synthesis in cartilage explants by cyclic loading is localized to regions of high interstitial fluid flow. *Arch Biochem Biophys* **1999**; 366(1): 1-7.

- [72] Butler D, Goldstein S, Guilak F. Functional tissue engineering: the role of biomechanics. *J Biomech Eng* **2000**; 122(6): 570-575.
- [73] Cao Y, Rodriguez A, Vacanti M, Ibarra C, Arevalo C, Vacanti C. Comparative study of the use of poly(glycolic acid), calcium alginate and pluronics in the engineering of autologous porcine cartilage. *J Biomater Sci Polym Ed* **1998**; 9(5): 475-487.
- [74] Caplan A. Mesenchymal stem cells. *J Orthop Res* **1991**; 9(5): 641-650.
- [75] Carraher CE. "Polymer Chemistry." 5th ed., New York: Marcel Dekker Inc., **2000**.
- [76] Carver SE, Heath CA. Increasing extracellular matrix production in regenerating cartilage with intermittent physiological pressure. *Biotechnol Bioeng* **1999**; 62(2): 166-174.
- [77] Carver SE, Heath CA. Influence of intermittent pressure, fluid flow, and mixing on the regenerative properties of articular chondrocytes. *Biotechnol Bioeng* **1999**; 65(3): 274-281.
- [78] Carver SE, Heath CA. Semi-continuous perfusion system for delivering intermittent physiological pressure to regenerating cartilage. *Tissue Eng* **1999**; 5(1): 1-11.
- [79] Caterson EJ, Nesti LJ, Li WJ, Danielson KG, Albert TJ, Vaccaro AR, Tuan RS. Three-dimensional cartilage formation by bone marrow-derived cells seeded in polylactide/alginate amalgam. *J Biomed Mater Res* **2001**; 57(3): 394-403.
- [80] Chang R, Falconer J, Stulberg S, Arnold W, Manheim L, Dyer A. A randomized controlled trial of arthroscopic surgery versus closed-needle joint lavage for patients with osteoarthritis of the knee. *Arthritis Rheum* **1993**; 36: 289-296.
- [81] Chang S, Rowley J, Tobias G, Genes N, Roy A, Mooney D, Vacanti C, Bonassar L. Injection molding of chondrocyte/alginate constructs in the shape of facial implants. *J Biomed Mater Res* **2001**; 55(4): 503-511.
- [82] Chang SC, Tobias G, Roy AK, Vacanti CA, Bonassar LJ. Tissue engineering of autologous cartilage for craniofacial reconstruction by injection molding. *Plast Reconstr Surg* **2003**; 112(3): 793-799.
- [83] Chawla AS. Plasma polymerization and plasma modification or surfaces for biomaterial applications. In "Polymeric Biomaterials." Piskin and Hoffman, (Ed); Nyhoff: Dordrecht, The Netherlands, **1986**; 221.
- [84] Cheah CM, Leong KF, Chua CK, Low KH, Quek HS. Characterization of microfeatures in selective laser sintered drug delivery devices. *Proc Inst Mech Eng [H]* **2002**; 216(6): 369-383.
- [85] Chen A, Bae W, Schinagl R, Sah R. Depth- and strain-dependent mechanical and electromechanical properties of full-thickness bovine articular cartilage in confined compression. *J Biomech* **2001**; 34(1): 1-12.
- [86] Chen JH, Laiw RF, Jiang SF, Lee YD. Microporous segmented polyetherurethane vascular graft: I. Dependency of graft morphology and mechanical properties on compositions and fabrication conditions. *J Biomed Mater Res* **1999**; 48(3): 235-245.
- [87] Chenite A, Chaput C, Wang D, Combes C, Buschmann MD, Hoemann CD, Leroux JC, Atkinson BL, Binette F, Selmani A. Novel injectable neutral solutions of chitosan form biodegradable gels in situ. *Biomater* **2000**; 21(21): 2155-2161.
- [88] Chim H, Ong JL, Schantz JT, Huttmacher DW, Agrawal CM. Efficacy of glow discharge gas plasma treatment as a surface modification process for three-dimensional poly (D,L-lactide) scaffolds. *J Biomed Mater Res* **2003**; 65A(3): 327-335.
- [89] Chow KS, Khor E. Novel fabrication of open-pore chitin matrixes. *Biomacromolecules* **2000**; 1(1): 61-67.
- [90] Chu CR, Coutts RD, Yoshioka M, Harwood FL, Monosov AZ, Amiel D. Articular cartilage repair using allogeneic perichondrocyte-seeded biodegradable porous polylactic acid (PLA): a tissue-engineering study. *J Biomed Mater Res* **1995**; 29(9): 1147-1154.
- [91] Chu CR, Monosov AZ, Amiel D. In situ assessment of cell viability within biodegradable polylactic acid polymer matrices. *Biomater* **1995**; 16(18): 1381-1384.
- [92] Cicutinni FM, Wluka AE, Wang Y, Davis SR, Hankin J, Ebeling P. Compartment differences in knee cartilage volume in healthy adults. *J Rheumatol* **2002**; 29(3): 554-556.
- [93] Cima LG, Vacanti JP, Vacanti C, Ingber D, Mooney D, Langer R. Tissue engineering by cell transplantation using degradable polymer substrates. *J Biomech Eng* **1991**; 113(2): 143-151.
- [94] Claase MB. *Cell-seeded scaffolds based on poly(ethylene oxide) and poly(butylene terephthalate) block copolymers for bone tissue engineering*. PhD Thesis - University of Twente, The Netherlands, **2004**;
- [95] Claase MB, Grijpma DW, Mendes SC, de Bruijn JD, Feijen J. Porous PEOT/PBT scaffolds for bone tissue engineering: Preparation, characterization, and in vitro bone marrow cell culturing. *J Biomed Mater Res* **2003**; 64A(2): 291-300.

- [96] Claase MB, Olde Riekerink MB, de Bruijn JD, Grijpma DW, Engbers GH, Feijen J. Enhanced bone marrow stromal cell adhesion and growth on segmented poly(ether ester)s based on poly(ethylene oxide) and poly(butylene terephthalate). *Biomacromolecules* **2003**; 4(1): 57-63.
- [97] Clemens TL, Tang H, Maeda S, Kesterson RA, Demayo F, Pike JW, Gundberg CM. Analysis of osteocalcin expression in transgenic mice reveals a species difference in vitamin D regulation of mouse and human osteocalcin genes. *J Bone Miner Res* **1997**; 12(10): 1570-1576.
- [98] Clements K, Bee Z, Crossingham G, Adams M, Sharif M. How severe must repetitive loading be to kill chondrocytes in articular cartilage? *Osteo Cart* **2001**; 9(5): 499-507.
- [99] Colton C. Implantable biohybrid artificial organs. *Cell Transplant* **1995**; 4(4): 415-436.
- [100] Cooke M, Fisher J, Dean D, Rimnac C, Mikos A. Use of stereolithography to manufacture critical-sized 3D biodegradable scaffolds for bone ingrowth. *J Biomed Mater Res* **2003**; 64B(2): 65-69.
- [101] Couvreur P, Puisieux F. Nano- and microparticles for the delivery of polypeptides and proteins. *Adv Drug Deliv Rev* **1993**; 10: 141-162.
- [102] Crofts G, Sah H, Park T. Adsorption determines in-vitro protein release rate from biodegradable microspheres: quantitative analysis of surface area during degradation. *J Controlled Release* **1997**; 47: 101-111.
- [103] Cukierman E, Pankov R, Stevens DR, Yamada KM. Taking cell-matrix adhesions to the third dimension. *Science* **2001**; 294(5547): 1708-1712.
- [104] Czitrom A, Keating S, Gross A. The viability of articular cartilage in fresh osteochondral allografts after clinical transplantation. *J Bone Joint Surg Am* **1990**; 72(4): 574-581.
- [105] Czitrom A, Langer F, McKnee N, Gross A. Bone and cartilage allotransplantation. A review of 14 years of research and clinical studies. *Clin Orthop* **1986**; 208: 141-145.
- [106] Dahlberg L, Kreicbergs A. Demineralized allogeneic bone matrix for cartilage repair. *J Orthop Res* **1991**; 9(1): 11-19.
- [107] de Bartolo L, Morelli S, Bader A, Dioli E. Evaluation of cell behaviour related to physico-chemical properties of polymeric membranes to be used in bioartificial organs. *Biomater* **2002**; 23(12): 2485-2497.
- [108] Dee K, Anderson T, Bizios R. Design and function of novel osteoblast-adhesive peptides for chemical modification of biomaterials. *J Biomed Mater Res* **1998**; 40: 371-377.
- [109] Demarteau O, Jakob M, Schafer D, Heberer M, Martin I. Development and validation of a bioreactor for physical stimulation of engineered cartilage. *Biorheology* **2003**; 40(1-3): 331-336.
- [110] Démarteau O, Schäfer D, Jacob M, Heberer M, Martin I. Dynamic compression increases expression of cartilage-specific genes by adult human chondrocytes seeded into hyaluronic acid-based scaffolds. *Trans Orthop Res Soc* **2002**; 27: 254.
- [111] Deschamps AA, Claase MB, Slijster WJ, de Bruijn JD, Grijpma DW, Feijen J. Design of segmented poly(ether ester) materials and structures for the tissue engineering of bone. *J Controlled Release* **2002**; 78(1-3): 175-186.
- [112] Deschamps AA, van Apeldoorn AA, Hayen H, de Bruijn JD, Karst U, Grijpma DW, Feijen J. In vivo and in vitro degradation of poly(ether ester) block copolymers based on poly(ethylene glycol) and poly(butylene terephthalate). *Biomater* **2004**; 25(2): 247-258.
- [113] Di SM, Suh J. Biphasic poroviscoelastic characteristics of proteoglycan-depleted articular cartilage: simulation of degeneration. *Ann Biomed Eng* **2002**; 30(6): 792-800.
- [114] DiMicco M, Waters S, Akeson W, Sah R. Integrative cartilage repair: dependence on developmental stage and collagen metabolism. *Osteo Cart* **2002**; 10(3): 218-225.
- [115] DiSilvestro MR, Zhu Q, Wong M, Jurvelin JS, Suh JK. Biphasic poroviscoelastic simulation of the unconfined compression of articular cartilage: I-Simultaneous prediction of reaction force and lateral displacement. *J Biomech Eng* **2001**; 123(2): 191-197.
- [116] Du C, Klasens P, Haan RE, Bezemer J, Cui FZ, de Groot K, Layrolle P. Biomimetic calcium phosphate coatings on Polyactive 1000/70/30. *J Biomed Mater Res* **2002**; 59(3): 535-546.
- [117] Du C, Meijer GJ, van de Valk C, Haan RE, Bezemer JM, Hesselting SC, Cui FZ, de Groot K, Layrolle P. Bone growth in biomimetic apatite coated porous Polyactive 1000PEG70PBT30 implants. *Biomater* **2002**; 23(23): 4649-4656.
- [118] Duke PJ, Daane EL, Montufar-Solis D. Studies of chondrogenesis in rotating systems. *J Cell Biochem* **1993**; 51(3): 274-282.
- [119] Dunham B, Koch R. Basic fibroblast growth factor and insulinlike growth factor I support the growth of human septal chondrocytes in a serum-free environment. *Arch Otolaryngol Head Neck Surg* **1998**; 124(12): 1325-1330.

- [120] Elder SH, Goldstein SA, Kimura JH, Soslowsky LJ, Spengler DM. Chondrocyte differentiation is modulated by frequency and duration of cyclic compressive loading. *Ann Biomed Eng* **2001**; 29(6): 476-482.
- [121] Elisseeff J, Anseth K, Sims D, McIntosh W, Randolph M, Yaremchuk M, Langer R. Transdermal photopolymerization of poly(ethylene oxide)-based injectable hydrogels for tissue-engineered cartilage. *Plast Reconstr Surg* **1999**; 104(4): 1014-1022.
- [122] Farndale R, Buttle D, Barrett A. Improved quantitation and discrimination of sulphated glycosaminoglycans by use of dimethylmethylene blue. *Biochim Biophys Acta* **1986**; 883(2): 173-177.
- [123] Felson DT. Osteoarthritis new insights. Part I: The disease and its risk factors. *Ann Intern Med* **2000**; 133: 635-646.
- [124] Freed L, Grande D, Lingbin Z, Emmanuel J, Marquis J, Langer R. Joint resurfacing using allograft chondrocytes and synthetic biodegradable polymer scaffolds. *J Biomed Mater Res* **1994**; 28(8): 891-899.
- [125] Freed L, Marquis J, Nohria A, Emmanuel J, Mikos A, Langer R. Neocartilage formation in vitro and in vivo using cells cultured on synthetic biodegradable polymers. *J Biomed Mater Res* **1993**; 27(1): 11-23.
- [126] Freed L, Vunjak-Novakovic G, Langer R. Cultivation of cell-polymer cartilage implants in bioreactors. *J Cell Biochem* **1993**; 51(3): 257-264.
- [127] Freed LE, Hollander AP, Martin I, Barry JR, Langer R, Vunjak-Novakovic G. Chondrogenesis in a cell-polymer-bioreactor system. *Exp Cell Res* **1998**; 240(1): 58-65.
- [128] Freed LE, Marquis JC, Vunjak-Novakovic G, Emmanuel J, Langer R. Composition of Cell-Polymer Cartilage Implants. *Biotech Bioeng* **1994**; 43(7): 605-614.
- [129] Freed LE, Martin I, Vunjak-Novakovic G. Frontiers in tissue engineering: In vitro modulation of chondrogenesis. *Clin Orthop* **1999**; 367(Suppl): S46-58.
- [130] Freed LE, Vunjak-Novakovic G. Cultivation of Cell-Polymer Tissue Constructs in Simulated Microgravity. *Biotechnol Bioeng* **1995**; 46(4): 306-313.
- [131] Freed LE, Vunjak-Novakovic G, Biron RJ, Eagles DB, Lesnoy DC, Barlow SK, Langer R. Biodegradable polymer scaffolds for tissue engineering. *Biotechnology (N Y)* **1994**; 12(7): 689-693.
- [132] Frenkel S, Toolan B, Menche D, Pitman M, Pachence J. Chondrocyte transplantation using a collagen bilayer matrix for cartilage repair. *J Bone Joint Surg Br* **1997**; 79(5): 831-836.
- [133] Frondoza C, Sohrabi A, Hungerford D. Human chondrocytes proliferate and produce matrix components in microcarrier suspension culture. *Biomater* **1996**; 17(9): 879-888.
- [134] Gao J, Dennis J, Solchaga L, Awadallah A, Goldberg V, Caplan A. Tissue-engineered fabrication of an osteochondral composite graft using rat bone marrow-derived mesenchymal stem cells. *Tissue Eng* **2001**; 7(4): 363-371.
- [135] Garrett J. Osteochondral allografts. *Instr Course Lect* **1993**; 42: 355-358.
- [136] Genes N, Bonassar L. The effect of substrate stiffness on chondrocytes adhesion to RGD-alginate. *Trans Orthop Res Soc* **2002**; 27: 265.
- [137] Gilbert JE. Current treatment options for the restoration of articular cartilage. *Am J Knee Surg* **1998**; 11(1): 42-46.
- [138] Gilligly SD, Voight M, Blackburn T. Treatment of articular cartilage defects of the knee with autologous chondrocyte implantation. *J Orthop Sports Phys Ther* **1998**; 28(4): 241-251.
- [139] Glowacki J. In vitro engineering of cartilage. *J Rehabil Res Dev* **2000**; 37(2): 171-177.
- [140] Godbey W, Mikos A. Recent progress in gene delivery using non-viral transfer complexes. *J Controlled Release* **2001**; 72(1-3): 115-125.
- [141] Goldstein A, Zhu G, Morris G, Meszlenyi R, Mikos A. Effect of osteoblastic culture conditions on the structure of poly(DL-lactic-co-glycolic acid) foam scaffolds. *Tissue Eng* **1999**; 5(5): 421-434.
- [142] Gooch K, Kwon J, Blunk T, Langer R, Freed L, Vunjak-Novakovic G. Effects of mixing intensity on tissue-engineered cartilage. *Biotechnol Bioeng* **2001**; 72(4): 402-407.
- [143] Gooch KJ, Blunk T, Courter DL, Sieminski AL, Bursac PM, Vunjak-Novakovic G, Freed LE. IGF-I and mechanical environment interact to modulate engineered cartilage development. *Biochem Biophys Res Commun* **2001**; 286(5): 909-915.
- [144] Goodwin K, Lydon F, Tighe B, Wong M. Compressive properties of semi-IPN hydrogels are comparable to cartilage tissue. *Trans Orthop Res Soc* **2002**; 27: 1072.
- [145] Goomer R, Deftos L, Terkeltaub R, Maris T, Lee M, Harwood F, Amiel D. High-efficiency non-viral transfection of primary chondrocytes and perichondrial cells for ex-vivo gene therapy to repair articular cartilage defects. *Osteo Cart* **2001**; 9(3): 248-256.

- [146] Gopferich A, Peter S, Lucke A, Lu L, Mikos A. Modulation of marrow stromal cell function using poly(D,L-lactic acid)-block-poly(ethylene glycol)-monomethyl ether surfaces. *J Biomed Mater Res* **1999**; 46(3): 390-398.
- [147] Grande D, Halberstadt C, Naughton G, Schwartz R, Manji R. Evaluation of matrix scaffolds for tissue engineering of articular cartilage grafts. *J Biomed Mater Res* **1997**; 34(2): 211-220.
- [148] Grande D, Pitman M, Peterson L, Menche D, Klein M. The repair of experimentally produced defects in rabbit articular cartilage by autologous chondrocyte transplantation. *J Orthop Res* **1989**; 7(2): 208-218.
- [149] Grande DA, Breitbart AS, Mason J, Paulino C, Laser J, Schwartz RE. Cartilage tissue engineering: current limitations and solutions. *Clin Orthop* **1999**; 367(Suppl): S176-185.
- [150] Grant T, Cho J, Ariail K, Weksler N, Smith R, Horton W. Col2-GFP reporter marks chondrocyte lineage and chondrogenesis during mouse skeletal development. *Dev Dyn* **2000**; 218(2): 394-400.
- [151] Green W. Articular cartilage repair. Behavior of rabbit chondrocytes during tissue culture and subsequent allografting. *Clin Orthop* **1977**; 124: 237-250.
- [152] Gref R, Minamitake Y, Peracchia MT, Trubetskov V, Torchilin V, Langer R. Biodegradable long-circulating polymeric nanospheres. *Science* **1994**; 263(5153): 1600-1603.
- [153] Grigolo B, Lisignoli G, Piacentini A, Fiorini M, Gobbi P, Mazzotti G, Duca M, Pavesio A, Facchini A. Evidence for redifferentiation of human chondrocytes grown on a hyaluronan-based biomaterial (HYAff 11): molecular, immunohistochemical and ultrastructural analysis. *Biomater* **2002**; 23(4): 1187-1195.
- [154] Grigolo B, Roseti L, Fiorini M, Fini M, Giavaresi G, Aldini N, Giardino R, Facchini A. Transplantation of chondrocytes seeded on a hyaluronan derivative (HYAff-11) into cartilage defects in rabbits. *Biomater* **2001**; 22(17): 2417-2424.
- [155] Grimshaw M, Mason R. Bovine articular chondrocyte function in vitro depends upon oxygen tension. *Osteo Cart* **2000**; 8(5): 386-392.
- [156] Grote JJ, Bakker D, Hesseling SC, van Blitterswijk CA. New alloplastic tympanic membrane material. *Am J Otol* **1991**; 12(5): 329-335.
- [157] Guilak F, Butler DL, Goldstein SA. Functional tissue engineering: the role of biomechanics in articular cartilage repair. *Clin Orthop* **2001**; 391(Suppl): S295-305.
- [158] Guilak F, Jones W, Ting-Beall H, Lee G. The deformation behavior and mechanical properties of chondrocytes in articular cartilage. *Osteo Cart* **1999**; 7(1): 59-70.
- [159] Guilak F, Meyer BC, Ratcliffe A, Mow VC. The effects of matrix compression on proteoglycan metabolism in articular cartilage explants. *Osteo Cart* **1994**; 2(2): 91-101.
- [160] Gurdon J. A community effect in animal development. *Nature* **1988**; 336: 772-774.
- [161] Hambleton J, Schwartz Z, Khare A, Windeler SW, Luna M, Brooks BP, Dean DD, Boyan BD. Culture surfaces coated with various implant materials affect chondrocyte growth and metabolism. *J Orthop Res* **1994**; 12(4): 542-552.
- [162] Hangody L, Feczko P, Bartha L, Bodo G, Kish G. Mosaicplasty for the Treatment of Articular Defects of the Knee and Ankle. *Clin Orthop* **2001**; 391(Suppl): S328-S336.
- [163] Hangody L, Kish G, Karpati Z, Szerb I, Eberhardt R. Treatment of osteochondritis dissecans of the talus: use of the mosaicplasty technique—a preliminary report. *Foot Ankle Int* **1997**; 18(10): 628-634.
- [164] Hangody L, Kish G, Karpati Z, Szerb I, Udvarhelyi I. Arthroscopic autogenous osteochondral mosaicplasty for the treatment of femoral condylar articular defects. A preliminary report. *Knee Surg Sports Traumatol Arthrosc* **1997**; 5(4): 262-267.
- [165] Hansen U, Schunke M, Domm C, Ioannidis N, Hassenpflug J, Gehrke T, Kurz B. Combination of reduced oxygen tension and intermittent hydrostatic pressure: a useful tool in articular cartilage tissue engineering. *J Biomech* **2001**; 34(7): 941-949.
- [166] Harris LD, Kim BS, Mooney DJ. Open pore biodegradable matrices formed with gas foaming. *J Biomed Mater Res* **1998**; 42(3): 396-402.
- [167] Harwin S. Arthroscopic debridement for osteoarthritis of the knee: predictors of patient satisfaction. *Arthroscopy* **1999**; 15(2): 142-146.
- [168] Haselgrove J, Shapiro I, Silverton S. Computer modeling of the oxygen supply and demand of cells of the avian growth cartilage. *Am J Physiol* **1993**; 265: C97-506.
- [169] Hasler EM, Herzog W, Wu JZ, Muller W, Wyss U. Articular cartilage biomechanics: theoretical models, material properties, and biosynthetic response. *Crit Rev Biomed Eng* **1999**; 27(6): 415-488.
- [170] Haugland RP. "Handbook of Fluorescent Probes and Research Chemicals." 7th ed., Eugene, OR: Molecular Probes, **1999**.

- [171] Hauselmann HJ, Masuda K, Hunziker EB, Neidhart M, Mok SS, Michel BA, Thonar EJ. Adult human chondrocytes cultured in alginate form a matrix similar to native human articular cartilage. *Am J Physiol* **1996**; 271(3 Pt 1): C742-752.
- [172] Hayes DW, Jr., Brower RL, John KJ. Articular cartilage. Anatomy, injury, and repair. *Clin Podiatr Med Surg* **2001**; 18(1): 35-53.
- [173] Hayes WC, Mockros LF. Viscoelastic properties of human articular cartilage. *J Appl Physiol* **1971**; 31(4): 562-568.
- [174] He S, Yaszemski M, Yasko A, Engel P, Mikos A. Injectable biodegradable polymer composites based on poly(propylene fumarate) crosslinked with poly(ethylene glycol)-dimethacrylate. *Biomater* **2000**; 21(23): 2389-2394.
- [175] Healy KE, Reznick A, Stile RA. Designing Biomaterials to Direct Biological Responses. *Ann NY Acad Sci* **1999**; 875(1): 24-35.
- [176] Heath CA, Magari SR. Mini-review: Mechanical factors affecting cartilage regeneration in vitro. *Biotechnol Bioeng* **1996**; 50(4): 430-437.
- [177] Hem DL, Hubbell JA. Incorporation of adhesion peptides into nonadhesive hydrogels useful for tissue resurfacing. *J Biomed Mater Res* **1998**; 39(2): 266-276.
- [178] Herschman HR. Molecular imaging: looking at problems, seeing solutions. *Science* **2003**; 302(5645): 605-608.
- [179] Heywood HK, Bongers M, Bader DL, Lee DA. Glucose depletion induces an upregulation of oxygen utilisation by chondrocytes. *Trans Orthop Res Soc* **2004**; 29: 261.
- [180] Hildebrand T, Rügsegger P. A new method for the model independent assessment of thickness in three dimensional images. *J Microsc* **1997**; 185: 67-75.
- [181] Hiraki Y, Inoue H, Shigeno C, Sanma Y, Bentz H, Rosen D, Asada A, Suzuki F. Bone morphogenetic proteins (BMP-2 and BMP-3) promote growth and expression of the differentiated phenotype of rabbit chondrocytes and osteoblastic MC3T3-E1 cells in vitro. *J Bone Miner Res* **1991**; 6(12): 1373-1385.
- [182] Hjelle K, Solheim E, Strand T, Muri R, Brittberg M. Articular cartilage defects in 1,000 knee arthroscopies. *Arthroscopy* **2002**; 18(7): 730-734.
- [183] Hollander AP, Heathfield TF, Webber C, Iwata Y, Bourne R, Rorabeck C, Poole AR. Increased damage to type II collagen in osteoarthritic articular cartilage detected by a new immunoassay. *J Clin Invest* **1994**; 93(4): 1722-1732.
- [184] Hollister S, Maddox R, Taboas J. Optimal design and fabrication of scaffolds to mimic tissue properties and satisfy biological constraints. *Biomater* **2002**; 23(20): 4095-4103.
- [185] Hollister SJ, Levy RA, Chu TM, Halloran JW, Feinberg SE. An image-based approach for designing and manufacturing craniofacial scaffolds. *Int J Oral Maxillofac Surg* **2000**; 29(1): 67-71.
- [186] Holtzer H, Abbott J, Lash J, Holtzer A. The loss of phenotypic traits by differentiated cell in vitro. I. Dedifferentiation of cartilage cells. *Proc Natl Acad Sci USA* **1960**; 46: 1533-1542.
- [187] Holy CE, Dang SM, Davies JE, Shoichet MS. In vitro degradation of a novel poly(lactide-co-glycolide) 75/25 foam. *Biomater* **1999**; 20(13): 1177-1185.
- [188] Homminga G, Buma P, Koot H, van der Kraan P, van den Berg W. Chondrocyte behavior in fibrin glue in vitro. *Acta Orthop Scand* **1993**; 64(4): 441-445.
- [189] Horbett TA. Principles underlying the role of adsorbed plasma proteins in blood interactions with foreign materials. *Cardiovasc Pathol* **1993**; 2: 137S-148S.
- [190] Homer HA, Urban JP. 2001 Volvo Award Winner in Basic Science Studies: Effect of nutrient supply on the viability of cells from the nucleus pulposus of the intervertebral disc. *Spine* **2001**; 26(23): 2543-2549.
- [191] Hou Q, Grijpma DW, Feijen J. Porous polymeric structures for tissue engineering prepared by a coagulation, compression moulding and salt leaching technique. *Biomater* **2003**; 24(11): 1937-1947.
- [192] Hou Q, Grijpma DW, Feijen J. Preparation of interconnected highly porous polymeric structures by a replication and freeze-drying process. *J Biomed Mater Res* **2003**; 67B(2): 732-740.
- [193] Hu Y, Grainger DW, Winn SR, Hollinger JO. Fabrication of poly(alpha-hydroxy acid) foam scaffolds using multiple solvent systems. *J Biomed Mater Res* **2002**; 59(3): 563-572.
- [194] Huang CY, Mow VC, Ateshian GA. The role of flow-independent viscoelasticity in the biphasic tensile and compressive responses of articular cartilage. *J Biomech Eng* **2001**; 123(5): 410-417.
- [195] Huang Q, Goh J, Huttmacher D, Lee E. In Vivo Mesenchymal Cell Recruitment by a Scaffold Loaded with Transforming Growth Factor beta1 and the Potential for in Situ Chondrogenesis. *Tissue Eng* **2002**; 8(3): 469-482.

- [196] Hubbard M. Articular debridement versus washout for degeneration of the medial femoral condyle. A five-year study. *J Bone Joint Surg Br* **1996**; 78(2): 217-219.
- [197] Hubbell JA. Biomaterials in tissue engineering. *Biotechnology (N Y)* **1995**; 13(6): 565-576.
- [198] Hubbell JA. Bioactive biomaterials. *Curr Opin Biotechnol* **1999**; 10(2): 123-129.
- [199] Hung CT, Lima EG, Mauck RL, Taki E, LeRoux MA, Lu HH, Stark RG, Guo XE, Ateshian GA. Anatomically shaped osteochondral constructs for articular cartilage repair. *J Biomech* **2003**; 36(12): 1853-1864.
- [200] Hung CT, Mauck RL, Wang CC, Lima EG, Ateshian GA. A paradigm for functional tissue engineering of articular cartilage via applied physiologic deformational loading. *Ann Biomed Eng* **2004**; 32(1): 35-49.
- [201] Hungerford DS, Krackow KA. Total joint arthroplasty of the knee. *Clin Orthop* **1985**; (192): 23-33.
- [202] Hunter W. On the structure and diseases of articulating cartilage. *Phil. Trans. R. Soc. London* **1743**; 42: 514-521.
- [203] Hunziker EB. Articular cartilage repair: are the intrinsic biological constraints undermining this process insuperable? *Osteo Cart* **1999**; 7(1): 15-28.
- [204] Hunziker EB. Biologic repair of articular cartilage. Defect models in experimental animals and matrix requirements. *Clin Orthop* **1999**; 367(Suppl): S135-146.
- [205] Hunziker EB. Articular cartilage repair: basic science and clinical progress. A review of the current status and prospects. *Osteo Cart* **2002**; 10(6): 432-463.
- [206] Hunziker EB, Driesang IM, Saager C. Structural barrier principle for growth factor-based articular cartilage repair. *Clin Orthop* **2001**; 391(Suppl): S182-189.
- [207] Hunziker EB, Quinn TM, Hauselmann HJ. Quantitative Structural Organization of Normal Adult Human Articular Cartilage. *Osteo Cart* **2002**; 10(7): 564-572.
- [208] Hunziker EB, Rosenberg LC. Repair of partial-thickness defects in articular cartilage: cell recruitment from the synovial membrane. *J Bone Joint Surg Am* **1996**; 78(5): 721-733.
- [209] Hutmacher DW. Scaffolds in tissue engineering bone and cartilage. *Biomater* **2000**; 21(24): 2529-2543.
- [210] Hutmacher DW. Scaffold design and fabrication technologies for engineering tissues--state of the art and future perspectives. *J Biomater Sci Polym Ed* **2001**; 12(1): 107-124.
- [211] Hutmacher DW, Schantz T, Zein I, Ng KW, Teoh SH, Tan KC. Mechanical properties and cell cultural response of polycaprolactone scaffolds designed and fabricated via fused deposition modeling. *J Biomed Mater Res* **2001**; 55(2): 203-216.
- [212] Iannotti JP, Goldstein S, Kuhn J, Lipiello L, Kaplan FS, Zaleske DJ. The formation and growth of skeletal tissues. In "Orthopaedic Basic Science: Biology and Biomechanics of the Musculoskeletal System." Buckwalter JA, Einhorn TA and Simon SR, (Ed), 2nd ed.; American Academy of Orthopaedic Surgeons: Rosemount, IL, **2000**; 77-110.
- [213] Insall J, Joseph D, Msika C. High fibial osteotomy for varus gonarthrosis. A long-term follow-up study. *J Bone Joint Surg Am* **1984**; 66(7): 1040-1048.
- [214] Ishaug-Riley S, Yaszemski M, Bizios R, Mikos A. Osteoblast function on synthetic biodegradable polymers. *J Biomed Mater Res* **1994**; 28(12): 1445-1453.
- [215] Ishaug-Riley SL, Okun LE, Prado G, Applegate MA, Ratcliffe A. Human articular chondrocyte adhesion and proliferation on synthetic biodegradable polymer films. *Biomater* **1999**; 20(23-24): 2245-2256.
- [216] Ishida O, Tanaka Y, Morimoto I, Takigawa M, Eto S. Chondrocytes are regulated by cellular adhesion through CD44 and hyaluronic acid pathway. *J Biomed Mater Res* **1997**; 12: 1657-1663.
- [217] Isogai N, Landis W, Kim TH, Gerstenfeld LC, Upton J, Vacanti JP. Formation of phalanges and small joints by tissue-engineering. *J Bone Joint Surg Am* **1999**; 81(3): 306-316.
- [218] Ito Y, Kajihara M, Imanishi Y. Materials for enhancing cell adhesion by immobilization of cell-adhesive peptide. *J Biomed Mater Res* **1991**; 25(11): 1325-1337.
- [219] Jackson D, Scheer M, Simon T. Cartilage substitutes: Overview of basic science and treatment options. *J Am Acad Orthop Surg* **2001**; 9(1): 37-52.
- [220] Jackson DW, Lalor PA, Aberman HM, Simon TM. Spontaneous Repair of Full-Thickness Defects of Articular Cartilage in a Goat Model: A Preliminary Study. *J Bone Joint Surg Am* **2001**; 83-A(1): 53-64.
- [221] Jakob M, Demarteau O, Schafer D, Hintermann B, Dick W, Heberer M, Martin I. Specific growth factors during the expansion and redifferentiation of adult human articular chondrocytes enhance chondrogenesis and cartilaginous tissue formation in vitro. *J Cell Biochem* **2001**; 81(2): 368-377.
- [222] Jo S, Shin H, Mikos A. Modification of Oligo(poly(ethylene glycol) fumarate) Macromer with a GRGD Peptide for the Preparation of Functionalized Polymer Networks. *Biomacromolecules* **2001**; 2(1): 255-261.

- [223] Johnson LL. Arthroscopic abrasion arthroplasty: a review. *Clin Orthop* **2001**; 391(Suppl): S306-317.
- [224] Johnstone B, Yoo J. Mesenchymal cell transfer for articular cartilage repair. *Expert Opin Biol Ther* **2001**; 1(6): 915-921.
- [225] Jurvelin J, Buschmann M, Hunziker E. Optical and mechanical determination of Poisson's ratio of adult bovine humeral articular cartilage. *J Biomech* **1997**; 30(3): 235-241.
- [226] Kafienah W, Jakob M, Demarteau O, Frazer A, Barker M, Martin I, Hollander A. Three-dimensional tissue engineering of hyaline cartilage: comparison of adult nasal and articular chondrocytes. *Tissue Eng* **2002**; 8(5): 817-826.
- [227] Kafienah W, Sims TJ. Biochemical methods for the analysis of tissue-engineered cartilage. In "Biopolymer Methods in Tissue Engineering." Hatton PV and Hollander AP, (Ed); Humana Press: Totowa, NJ, **2003**; 217-229.
- [228] Kandel R, Boyle J, Gibson G, Cruz T, Speagle M. In vitro formation of mineralized cartilagenous tissue by articular chondrocytes. *In Vitro Cell Dev Biol Anim* **1997**; 33(3): 174-181.
- [229] Kang R, Marui T, Ghivizzani SC, Nifa IM, Georgescu HI, Suh JK, Robbins PD, Evans CH. Ex vivo gene transfer to chondrocytes in full-thickness articular cartilage defects: a feasibility study. *Osteo Cart* **1997**; 5(2): 139-143.
- [230] Kawabe N, Yoshinai M. The repair of full-thickness articular cartilage defects. Immune responses to reparative tissue formed by allogeneic growth plate chondrocyte implants. *Clin Orthop* **1991**; 268: 279-293.
- [231] Kawamura S, Wakitani S, Kimura T, Maeda A, Caplan A, Shino K, Ochi T. Articular cartilage repair. Rabbit experiments with a collagen gel-biomatrix and chondrocytes cultured in it. *Acta Orthop Scand* **1998**; 69(1): 56-62.
- [232] Kellner K, Liebsch G, Klimant I, Wolfbeis O, Blunk T, Schulz M, Gopferich A. Determination of oxygen gradients in engineered tissue using a fluorescent sensor. *Biotechnol Bioeng* **2002**; 80(1): 73-83.
- [233] Khang G, Jeon J, Lee J, Cho S, Lee H. Cell and platelet adhesions on plasma glow discharge-treated poly(lactide-co-glycolide). *Biomed Mater Eng* **1997**; 7(6): 357-368.
- [234] Kim TK, Sharma B, Williams CG, Ruffner MA, Malik A, McFarland EG, Elisseeff JH. Experimental model for cartilage tissue engineering to regenerate the zonal organization of articular cartilage. *Osteo Cart* **2003**; 11(9): 653-664.
- [235] Kim YJ, Sah RL, Grodzinsky AJ, Plaas AH, Sandy JD. Mechanical regulation of cartilage biosynthetic behavior: physical stimuli. *Arch Biochem Biophys* **1994**; 311(1): 1-12.
- [236] Kinner B, Spector M. Smooth muscle actin expression by human articular chondrocytes and their contraction of a collagen-glycosaminoglycan matrix in vitro. *J Orthop Res* **2001**; 19(2): 233-241.
- [237] Kladny B, Martus P, Schiwy-Bochat K, Weseloh G, Swoboda B. Measurement of cartilage thickness in the human knee joint by magnetic resonance imaging using a three-dimensional gradient echo sequence. *Int Orthop* **1999**; 23: 264-267.
- [238] Klein TJ, Schumacher BL, Li KW, Voegtline M, Masuda K, Thonar EJ, Sah RL. Tissue engineered articular cartilage with functional stratification: targeted delivery of chondrocytes expressing superficial zone protein. *Trans Orthop Res Soc* **2002**; 27: 212.
- [239] Klein TJ, Schumacher BL, Masuda K, Thonar EJ, Sah RL. Fabrication of a stratified cartilage construct with localized superficial zone protein expression. *Trans Biomed Eng Soc* **2001**; 29S1: 12.17.14.
- [240] Knight M, Ross J, Sherwin A, Lee D, Bader D, Poole C. Chondrocyte deformation within mechanically and enzymatically extracted chondrons compressed in agarose. *Biochim Biophys Acta* **2001**; 1526(2): 141-146.
- [241] Knudson W, Loeser R. CD44 and integrin matrix receptors participate in cartilage homeostasis. *Cell Mol Life Sci* **2002**; 59(1): 36-44.
- [242] Korhonen R, Laasanen M, Toyras J, Rieppo J, Hirvonen J, Helminen H, Jurvelin J. Comparison of the equilibrium response of articular cartilage in unconfined compression, confined compression and indentation. *J Biomech* **2002**; 35(7): 903-909.
- [243] Krasteva N, Harms U, Albrecht W, Seifert B, Hopp M, Altankov G, Groth T. Membranes for biohybrid liver support systems--investigations on hepatocyte attachment, morphology and growth. *Biomater* **2002**; 23(12): 2467-2478.
- [244] Kreklau B, Siffinger M, Mensing MB, Voigt C, Berger G, Burmester GR, Rahmzadeh R, Gross U. Tissue engineering of biphasic joint cartilage transplants. *Biomater* **1999**; 20(18): 1743-1749.
- [245] Kruger T, Wohlrab D, Birke A, Hein W. Results of arthroscopic joint debridement in different stages of chondromalacia of the knee joint. *Arch Orthop Trauma Surg* **2000**; 120(5-6): 338-342.
- [246] Kuboki Y, Jin Q, Takita H. Geometry of carriers controlling phenotypic expression in BMP-induced osteogenesis and chondrogenesis. *J Bone Joint Surg Am* **2001**; 83-A Suppl 1(Pt 2): S105-115.

- [247] Kuettnner KE. Biochemistry of articular cartilage in health and disease. *Clin Biochem* **1992**; 25(3): 155-163.
- [248] Kujawa M, Caplan A. Hyaluronic acid bonded to cell-culture surfaces stimulates chondrogenesis in stage 24 limb mesenchyme cell cultures. *Dev Biol* **1986**; 114(2): 504-518.
- [249] Lahiji A, Sohrabi A, Hungerford D, Frondoza C. Chitosan supports the expression of extracellular matrix proteins in human osteoblasts and chondrocytes. *J Biomed Mater Res* **2000**; 51(4): 586-595.
- [250] Lai WM, Mow VC. Drag-induced compression of articular cartilage during a permeation experiment. *Biorheology* **1980**; 17(1-2): 111-123.
- [251] Laib A, Barou O, Vico L, Lafage-Proust M, Alexandre C, Rugsegger P. 3D micro-computed tomography of trabecular and cortical bone architecture with application to a rat model of immobilisation osteoporosis. *Med Biol Eng Comput* **2000**; 38(3): 326-332.
- [252] Laib A, Kumer J, Majumdar S, Lane N. The temporal changes of trabecular architecture in ovariectomized rats assessed by MicroCT. *Osteoporos Int* **2001**; 12(11): 936-941.
- [253] Landers R, Hubner U, Schmelzeisen R, Mulhaupt R. Rapid prototyping of scaffolds derived from thermoreversible hydrogels and tailored for applications in tissue engineering. *Biomater* **2002**; 23(23): 4437-4447.
- [254] Landers R, Mulhaupt R. Desktop manufacturing of complex objects, prototypes and biomedical scaffolds by means of computer-assisted design combined with computer-guided 3D plotting of polymers and reactive oligomers. *Macromolec Mater Eng* **2000**; 282: 17-21.
- [255] Landers R, Mulhaupt R. Rapid prototyping of hydrogel scaffolds for use in tissue engineering. *Tissue Eng: Proc Eur Tissue Eng Soc* **2001**; 7(5): 629.
- [256] Landers R, Pfister A, Hubner U, John H, Schmelzeisen R, Mulhaupt R. Fabrication of soft tissue engineering scaffolds by means of rapid prototyping techniques. *J Mater Sci* **2002**; 37(15): 3107-3116.
- [257] Langer R, Vacanti JP. Tissue engineering. *Science* **1993**; 260(5110): 920-926.
- [258] Lanza R, Langer R, Vacanti J. "Principles of Tissue Engineering." 2 ed., London: Academic Press, **2000**.
- [259] Le Baron RG, Athanasiou KA. Extracellular matrix cell adhesion peptides: functional applications in orthopedic materials. *Tissue Eng* **2000**; 6(2): 85-103.
- [260] Lee DA, Noguchi T, Freaun SP, Lees P, Bader DL. The influence of mechanical loading on isolated chondrocytes seeded in agarose constructs. *Biorheology* **2000**; 37(1-2): 149-161.
- [261] Lee G, Poole C, Kelley S, Chang J, Caterson B. Isolated chondrons: a viable alternative for studies of chondrocyte metabolism in vitro. *Osteo Cart* **1997**; 5(4): 261-274.
- [262] Lee JH, Kopecek J, Andrade JD. Protein-resistant surfaces prepared by PEO-containing block copolymer surfactants. *J Biomed Mater Res* **1989**; 23(3): 351-368.
- [263] Lee S, Khang G, Lee Y, Lee H. Interaction of human chondrocytes and NIH/3T3 fibroblasts on chloric acid-treated biodegradable polymer surfaces. *J Biomater Sci Polym Ed* **2002**; 13(2): 197-212.
- [264] Lee SJ. Cytokine delivery and tissue engineering. *Yonsei Med J* **2000**; 41(6): 704-719.
- [265] Leidner J, Wong EW, MacGregor DC, Wilson GJ. A novel process for the manufacturing of porous grafts: process description and product evaluation. *J Biomed Mater Res* **1983**; 17(2): 229-247.
- [266] Leong KF, Cheah CM, Chua CK. Solid freeform fabrication of three-dimensional scaffolds for engineering replacement tissues and organs. *Biomater* **2003**; 24(13): 2363-2378.
- [267] Li L, Buschmann M, Shirazi-Adl A. A fibril reinforced nonhomogeneous poroelastic model for articular cartilage: inhomogeneous response in unconfined compression. *J Biomech* **2000**; 33(12): 1533-1541.
- [268] Li L, Shirazi-Adl A, Buschmann M. Alterations in mechanical behaviour of articular cartilage due to changes in depth varying material properties—a nonhomogeneous poroelastic model study. *Comput Methods Biomech Biomed Engin* **2002**; 5(1): 45-52.
- [269] Li LP, Soulhat J, Buschmann MD, Shirazi-Adl A. Nonlinear analysis of cartilage in unconfined ramp compression using a fibril reinforced poroelastic model. *Clin Biomech (Bristol, Avon)* **1999**; 14(9): 673-682.
- [270] Li P, Bakker D, van Blitterswijk CA. The bone-bonding polymer Polyactive 80/20 induces hydroxycarbonate apatite formation in vitro. *J Biomed Mater Res* **1997**; 34(1): 79-86.
- [271] Li S, de Wijn J, Li J, Layrolle P, de Groot K. Macroporous biphasic calcium phosphate scaffold with high permeability/porosity ratio. *Tissue Eng* **2003**; 9(3): 535-548.

- [272] Liao CJ, Chen CF, Chen JH, Chiang SF, Lin YJ, Chang KY. Fabrication of porous biodegradable polymer scaffolds using a solvent merging/particulate leaching method. *J Biomed Mater Res* **2002**; 59(4): 676-681.
- [273] Lightfoot E. "Transport phenomena and living systems." New York: John Wiley, **1974**.
- [274] Lin ASP, Barrows TH, Cartmella SH, Guldberg RE. Microarchitectural and mechanical characterization of oriented porous polymer scaffolds. *Biomater* **2003**; 24.
- [275] Liu SQ, Kodama M. Porous polyurethane vascular prostheses with variable compliances. *J Biomed Mater Res* **1992**; 26(11): 1489-1502.
- [276] LiVecchi A, Tombes R, Laberge M. In vitro chondrocyte collagen deposition within porous HDPE: substrate microstructure and wettability effects. *J Biomed Mater Res* **1994**; 28(8): 839-850.
- [277] Lo H, Kadiyala S, Guggino S, Leong K. Poly(L-lactic acid) foams with cell seeding and controlled-release capacity. *J Biomed Mater Res* **1996**; 30(4): 475-484.
- [278] Loeser RF. Integrin-mediated attachment of articular chondrocytes to extracellular matrix proteins. *Arthritis Rheum* **1993**; 36(8): 1103-1110.
- [279] Loeser RF. Chondrocyte integrin expression and function. *Biorheology* **2000**; 37(1-2): 109-116.
- [280] Loeser RF. Integrins and cell signaling in chondrocytes. *Biorheology* **2002**; 39(1-2): 119-124.
- [281] Lohmander L. Tissue engineering of cartilage: do we need it, can we do it, is it good and can we prove it? *Novartis Found Symp* **2003**; 249: 2-10; discussion 10-16, 170-174, 239-141.
- [282] Lohnert J. Regeneration of hyalin cartilage in the knee joint by treatment with autologous chondrocyte transplants. Initial clinical results. *Langenbecks Arch Chir Suppl Kongressbd* **1998**; 115: 1205-1207.
- [283] Lopez-Barneo J, Pardal R, Ortega-Saenz P. Cellular mechanism of oxygen sensing. *Annu Rev Physiol* **2001**; 63: 259-287.
- [284] Lorensen W, Cline H. Marching cubes: a high resolution 3D surface construct algorithm. *Comput Graph* **1987**; 21: 163-169.
- [285] Loty S, Forest N, Boulekbache H, Sautier JM. Cytochalasin D induces changes in cell shape and promotes in vitro chondrogenesis: a morphological study. *Biol Cell* **1995**; 83(2-3): 149-161.
- [286] Lu L, Mikos A. The importance of new processing techniques in tissue engineering. *MRS Bull* **1996**; 21(11): 28-32.
- [287] Lu L, Valenzuela R, Yaszemski M. Articular cartilage tissue engineering. *e-biomed* **2000**; 2: 99-114.
- [288] Lu L, Zhu X, Valenzuela RG, Currier BL, Yaszemski MJ. Biodegradable polymer scaffolds for cartilage tissue engineering. *Clin Orthop* **2001**; 391(Suppl): S251-270.
- [289] Lu W, Park T. Protein release from poly(lactic-co-glycolic acid) microspheres: protein stability problems. *PDA J Pharm Sci Technol* **1995**; 49(1): 13-19.
- [290] Lydon MJ, Clay CS. Substratum topography and cell traction on sulphuric acid treated bacteriological-grade plastic. *Cell Biol Int Rep* **1985**; 9(10): 911-921.
- [291] Lydon MJ, Minett TW, Tighe BJ. Cellular interactions with synthetic polymer surfaces in culture. *Biomater* **1985**; 6(6): 396-402.
- [292] Lysaght M, Nguy N, Sullivan K. An economic survey of the emerging tissue engineering industry. *Tissue Eng* **1998**; 4: 231-238.
- [293] Lysaght MJ, Reyes J. The growth of tissue engineering. *Tissue Eng* **2001**; 7(5): 485-493.
- [294] Ma PX, Langer R. Morphology and mechanical function of long-term in vitro engineered cartilage. *J Biomed Mater Res* **1999**; 44(2): 217-221.
- [295] Ma PX, Schloo B, Mooney D, Langer R. Development of biomechanical properties and morphogenesis of in vitro tissue engineered cartilage. *J Biomed Mater Res* **1995**; 29(12): 1587-1595.
- [296] Ma PX, Zhang R. Microtubular architecture of biodegradable polymer scaffolds. *J Biomed Mater Res* **2001**; 56(4): 469-477.
- [297] Mader K, Bittner B, Li Y, Wohlauf W, Kissel T. Monitoring microviscosity and microacidity of the albumin microenvironment inside degrading microparticles from poly(lactide-co-glycolide) (PLG) or ABA-triblock polymers containing hydrophobic poly(lactide-co-glycolide) A blocks and hydrophilic poly(ethylene oxide) B blocks. *Pharm Res* **1998**; 15(5): 787-793.
- [298] Mahmood T. *Chondrocyte-biomaterial interactions: a mechanistic approach to cartilage tissue engineering*. PhD Thesis - University of Twente, Enschede, The Netherlands, **2004**; 171
- [299] Mahmood TA, Miot S, Frank O, van Blitterswijk CA, Langer R, Martin I, Riesle J. Differential protein adsorption mediates attachment and gene expression of human articular chondrocytes. *Exp Cell Res* (**submitted**).

- [300] Mainil-Varlet P, Rieser F, Grogan S, Mueller W, Saager C, Jakob RP. Articular cartilage repair using a tissue-engineered cartilage-like implant: an animal study. *Osteo Cart* **2001**; 9 Suppl A: S6-15.
- [301] Malda J. *Cartilage Tissue Engineering: The Relevance of Oxygen*. PhD Thesis - University of Twente, Enschede, The Netherlands, **2003**; 224
- [302] Malda J, Kreijveld E, Temenoff JS, van Blitterswijk CA, Riesle J. Expansion of human nasal chondrocytes on macroporous microcarriers enhances redifferentiation. *Biomater* **2003**; 24(28): 5153-5161.
- [303] Malda J, Martens DE, Tramper J, van Blitterswijk CA, Riesle J. Cartilage tissue engineering: controversy in the effect of oxygen. *Crit Rev Biotechnol* **2003**; 23(3): 175-194.
- [304] Malda J, Rouwkema J, Martens DE, Le Comte EP, Kooy FK, Tramper J, van Blitterswijk CA, Riesle J. Oxygen gradients in tissue-engineered PEGT/PBT cartilaginous constructs: Measurement and modeling. *Biotechnol Bioeng* **2004**; 86(1): 9-18.
- [305] Malda J, van Blitterswijk CA, Grojec M, Martens DE, Tramper J, Riesle J. Expansion of bovine chondrocytes on microcarriers enhances redifferentiation. *Tissue Eng* **2003**; 9(5): 939-948.
- [306] Malda J, Woodfield TBF, van der Vloodt F, Kooy FK, Martens DE, Tramper J, van Blitterswijk CA, Riesle J. The effect of PEGT/PBT scaffold architecture on oxygen gradients in tissue engineered cartilagenous constructs. *Biomater* (**in press**).
- [307] Malda J, Woodfield TBF, van der Vloodt F, Wilson C, Martens DE, Tramper J, van Blitterswijk CA, Riesle J. The effect of PEGT/PBT scaffold architecture on the composition of tissue engineered cartilage. *Biomater* (**in press**).
- [308] Mallein-Gerin F, Ruggiero F, Garrone R. Proteoglycan core protein and type II collagen gene expressions are not correlated with cell shape changes during low density chondrocyte cultures. *Differentiation* **1990**; 43(3): 204-211.
- [309] Mallein-Gerin F, Ruggiero F, Quinn TM, Bard F, Grodzinsky AJ, Olsen BR, van der Rest M. Analysis of collagen synthesis and assembly in culture by immortalized mouse chondrocytes in the presence or absence of alpha 1(I)X collagen chains. *Exp Cell Res* **1995**; 219(1): 257-265.
- [310] Mandell I, Yoo J, Johnstone B. Gene delivery to mesenchymal cells. *Trans Orthop Res Soc* **1999**; 24: 112.
- [311] Mandl E, van der Veen S, Verhaar J, van Osch G. Serum-free medium supplemented with high concentration of FGF-2 for cell expansion culture of human ear chondrocytes promotes redifferentiation capacity. *Tissue Eng* **2002**; 8(4): 573-580.
- [312] Mankin H, Jennings L, Treadwell B, Trippel S. Growth factors and articular cartilage. *J Rheumatol Suppl* **1991**; 27: 66-67.
- [313] Mankin HJ, Mow VC, Buckwalter JA. Articular cartilage repair and osteoarthritis. In "Orthopaedic Basic Science: Biology and Biomechanics of the Musculoskeletal System." Buckwalter JA, Einhorn TA and Simon SR, (Ed), 2nd ed.; American Academy of Orthopaedic Surgeons: Rosemont, IL, **2000**; 471-488.
- [314] Mankin HJ, Mow VC, Buckwalter JA, Iannotti JP, Ratcliffe A. Articular cartilage structure, composition and function. In "Orthopaedic Basic Science: Biology and Biomechanics of the Musculoskeletal System." Buckwalter JA, Einhorn TA and Simon SR, (Ed), 2nd ed.; American Academy of Orthopaedic Surgeons: Rosemont, IL, **2000**; 443-470.
- [315] Maroudas N. Chemical and mechanical requirements for fibroblast adhesion. *Nature* **1973**; 244(5415): 353-354.
- [316] Martin I, Obradovic B, Treppo S, Grodzinsky AJ, Langer R, Freed LE, Vunjak-Novakovic G. Modulation of the mechanical properties of tissue engineered cartilage. *Biorheology* **2000**; 37(1-2): 141-147.
- [317] Martin I, Suetterlin R, Baschong W, Heberer M, Vunjak-Novakovic G, Freed LE. Enhanced cartilage tissue engineering by sequential exposure of chondrocytes to FGF-2 during 2D expansion and BMP-2 during 3D cultivation. *J Cell Biochem* **2001**; 83(1): 121-128.
- [318] Martin I, Vunjak-Novakovic G, Yang J, Langer R, Freed LE. Mammalian chondrocytes expanded in the presence of fibroblast growth factor 2 maintain the ability to differentiate and regenerate three-dimensional cartilaginous tissue. *Exp Cell Res* **1999**; 253(2): 681-688.
- [319] Mason J, Breitbart A, Barcia M, Porti D, Pergolizzi R, Grande D. Cartilage and bone regeneration using gene-enhanced tissue engineering. *Clin Orthop* **2000**; 379(Suppl): S171-178.
- [320] Mason J, Grande D, Barcia M, Grant R, Pergolizzi R, Breitbart A. Expression of human bone morphogenic protein 7 in primary rabbit periosteal cells: potential utility in gene therapy for osteochondral repair. *Gene Ther* **1998**; 5(8): 1098-1104.
- [321] Matsuda S, Ishinishi T, White SE, Whiteside LA. Patellofemoral joint after total knee arthroplasty. Effect on contact area and contact stress. *J Arthroplasty* **1997**; 12(7): 790-797.

- [322] Matthews LS, Goldstein SA, Malvitz TA, Katz BP, Kaufer H. Proximal tibial osteotomy. Factors that influence the duration of satisfactory function. *Clin Orthop* **1988**; 229: 193-200.
- [323] Mauck RL, Nicoll SB, Stark R, Ateshian GA. Joint-specific surface moulds for articular cartilage tissue engineering. *Trans Orthop Res Soc* **2002**; 27: 251.
- [324] Mauck RL, Seyhan SL, Jamieson KV, Ateshian GA, Hung CT. Synergistic effects of growth factors and dynamic loading for cartilage tissue engineering. *Trans Orthop Res Soc* **2002**; 27: 213.
- [325] Mauck RL, Soltz MA, Wang CC, Wong DD, Chao PH, Valhmu WB, Hung CT, Ateshian GA. Functional tissue engineering of articular cartilage through dynamic loading of chondrocyte-seeded agarose gels. *J Biomech Eng* **2000**; 122(3): 252-260.
- [326] Meijer G, van Dooren A, Gaillard M, Dalmeijer R, de Putter C, Koole R, van Blitterswijk C. Polyactive as a bone-filler in a beagle dog model. *Int J Oral Maxillofac Surg* **1996**; 25(3): 210-216.
- [327] Mendes SC, Bezemer J, Claase MB, Grijpma DW, Bellia G, Degli-Innocenti F, Reis RL, de Groot K, van Blitterswijk CA, de Bruijn JD. Evaluation of two biodegradable polymeric systems as substrates for bone tissue engineering. *Tissue Eng* **2003**; 9(Suppl 1): S91-101.
- [328] Mikos A, Bao Y, Cima L, Ingber D, Vacanti J, Langer R. Preparation of poly(glycolic acid) bonded fiber structures for cell attachment and transplantation. *J Biomed Mater Res* **1993**; 27(2): 183-189.
- [329] Mikos A, Sarakinos G, Leite S, Vacanti J, Langer R. Laminated three-dimensional biodegradable foams for use in tissue engineering. *Biomater* **1993**; 14(5): 323-330.
- [330] Millennium Research Group. "US Markets for Orthopaedic Biomaterials." Toronto, ON: Millennium Research Group Inc., www.mrg.net, 2002.
- [331] Minas T. The role of cartilage repair techniques, including chondrocyte transplantation, in focal chondral knee damage. *Instr Course Lect* **1999**; 48: 629-643.
- [332] Minas T, Nehrer S. Current concepts in the treatment of articular cartilage defects. *Orthopedics* **1997**; 20(6): 525-538.
- [333] Miot S, Woodfield TBF, Daniels AU, Suetterlin R, Peterschmitt I, Heberer M, van Blitterswijk CA, Riesle J, Martin I. The effect of scaffold composition and architecture on human nasal chondrocyte redifferentiation and cartilaginous matrix deposition capacity. *Biomater* (accepted).
- [334] Mironov V, Boland T, Trusk T, Forgacs G, Markwald RR. Organ printing: computer-aided jet-based 3D tissue engineering. *Trends Biotechnol* **2003**; 21(4): 157-161.
- [335] Miyamoto S, Takaoka K, Okada T, Yoshikawa H, Hashimoto J, Suzuki S, Ono K. Evaluation of polylactic acid homopolymers as carriers for bone morphogenetic protein. *Clin Orthop* **1992**; 278: 274-285.
- [336] Mizuno S, Glowacki J. Chondroinduction of human dermal fibroblasts by demineralized bone in three-dimensional culture. *Exp Cell Res* **1996**; 227(1): 89-97.
- [337] Mizuno S, Ushida T, Tateishi T, Glowacki J. Effects of physical stimulation on chondrogenesis in vitro. *Mater Sci Eng C* **1998**; 6: 301-306.
- [338] Mooney D, Baldwin D, Suh N, Vacanti J, Langer R. Novel approach to fabricate porous sponges of poly(D,L-lactic-co-glycolic acid) without the use of organic solvents. *Biomater* **1996**; 17(14): 1417-1422.
- [339] Mooney DJ, Mazzoni CL, Breuer C, McNamara K, Hern D, Vacanti JP, Langer R. Stabilized polyglycolic acid fibre-based tubes for tissue engineering. *Biomater* **1996**; 17(2): 115-124.
- [340] Mooney DJ, Park S, Kaufmann PM, Sano K, McNamara K, Vacanti JP, Langer R. Biodegradable sponges for hepatocyte transplantation. *J Biomed Mater Res* **1995**; 29(8): 959-965.
- [341] Morales TI, Woessner JF, Howell DS, Marsh JM, Le Maire WJ. A microassay for the direct demonstration of collagenolytic activity in Graafian follicles of the rat. *Biochim Biophys Acta* **1978**; 524(2): 428-434.
- [342] Moseley J, Wray N, Kuykendall D, Willis K, Landon G. Arthroscopic treatment of osteoarthritis of the knee: a prospective, randomised, placebo-controlled trial. *Am J Sports Med* **1996**; 26: 28-34.
- [343] Moses M, Sudhalter J, Langer R. Identification of an inhibitor of neovascularization from cartilage. *Science* **1990**; 248(4961): 1408-1410.
- [344] Mow VC, Guo XE. Mechano-electrochemical properties of articular cartilage: their inhomogeneities and anisotropies. *Annu Rev Biomed Eng* **2002**; 4: 175-209.
- [345] Mow VC, Holmes MH, Lai WM. Fluid transport and mechanical properties of articular cartilage: a review. *J Biomech* **1984**; 17(5): 377-394.
- [346] Mow VC, Wang CC. Some bioengineering considerations for tissue engineering of articular cartilage. *Clin Orthop* **1999**; 367(Suppl): S204-223.

- [347] Mueller SM, Schneider TO, Shortkroff S, Breinan HA, Spector M. alpha-smooth muscle actin and contractile behavior of bovine meniscus cells seeded in type I and type II collagen-GAG matrices. *J Biomed Mater Res* **1999**; 45(3): 157-166.
- [348] Muller R, Ruegsegger P. Micro-tomographic imaging for the nondestructive evaluation of trabecular bone architecture. *Stud Health Technol Inform* **1997**; 40: 61-79.
- [349] Murphy WL, Dennis RG, Kileny JL, Mooney DJ. Salt Fusion: An Approach to Improve Pore Interconnectivity within Tissue Engineering Scaffolds. *Tissue Eng* **2002**; 8(1): 43-52.
- [350] Myles CM, Rowe PJ, Walker CR, Nutton RW. Knee joint functional range of movement prior to and following total knee arthroplasty measured using flexible electrogoniometry. *Gait Posture* **2002**; 16(1): 46-54.
- [351] Nakao A, Nagaoka S, Mori Y. Hemocompatibility of hydrogel with polyethyleneoxide chains. *J Biomater Appl* **1987**; 2(2): 219-234.
- [352] Nam Y, Yoon J, Park T. A novel fabrication method of macroporous biodegradable polymer scaffolds using gas foaming salt as a porogen additive. *J Biomed Mater Res* **2000**; 53(1): 1-7.
- [353] Naumann A, Dennis J, Awadallah A, Carrino D, Mansour J, Kastenbauer E, Caplan A. Immunohistochemical and mechanical characterization of cartilage subtypes in rabbit. *J Histochem Cytochem* **2002**; 50(8): 1049-1058.
- [354] Nehrer S, Breinan HA, Ramappa A, Shortkroff S, Young G, Minas T, Sledge CB, Yannas IV, Spector M. Canine chondrocytes seeded in type I and type II collagen implants investigated in vitro. *J Biomed Mater Res* **1997**; 38(2): 95-104.
- [355] Nehrer S, Breinan HA, Ramappa A, Young G, Shortkroff S, Louie LK, Sledge CB, Yannas IV, Spector M. Matrix collagen type and pore size influence behaviour of seeded canine chondrocytes. *Biomater* **1997**; 18(11): 769-776.
- [356] Nehring D, Adamietz P, Meenen N, Pörtner R. Perfusion cultures and modeling of oxygen uptake with three-dimensional chondrocyte pellets. *Biotechnol Techn* **1999**; 13(701-706).
- [357] Nerem R, Sambanis A. Tissue engineering: from biology to a biological substitute. *Tissue Eng* **1995**; 1: 3-12.
- [358] Newman AP. Articular cartilage repair. *Am J Sports Med* **1998**; 26(2): 309-324.
- [359] Ng K, Wang CC, Guo XE, Ateshian GA, Hung CT. Characterization of inhomogeneous bi-layered chondrocyte-seeded agarose constructs of differing agarose concentrations. *Trans Orthop Res Soc* **2003**; 28: 960.
- [360] Niederauer GG, Slivka MA, Leatherbury NC, Korvick DL, Harroff HH, Ehler WC, Dunn CJ, Kieswetter K. Evaluation of multiphase implants for repair of focal osteochondral defects in goats. *Biomater* **2000**; 21(24): 2561-2574.
- [361] Nixon AJ, Brower-Toland BD, Bent SJ, Saxer RA, Wilke MJ, Robbins PD, Evans CH. Insulinlike growth factor-I gene therapy applications for cartilage repair. *Clin Orthop* **2000**; 379(Suppl): S201-213.
- [362] Nixon AJ, Haupt JL, Frisbie DD, Morissett SS, McIlwraith CW, Robbins PD, Ghivizzani S, Evans CH. Enhanced cartilage repair by gene-mediated combination of insulin-like growth factor-I/interleukin-1 receptor antagonist therapy. *Trans Orthop Res Soc* **2002**; 27: 276.
- [363] Obradovic B, Carrier RL, Vunjak-Novakovic G, Freed LE. Gas exchange is essential for bioreactor cultivation of tissue engineered cartilage. *Biotechnol Bioeng* **1999**; 63(2): 197-205.
- [364] Obradovic B, Martin I, Padera RF, Treppo S, Freed LE, Vunjak-Novakovic G. Integration of engineered cartilage. *J Orthop Res* **2001**; 19(6): 1089-1097.
- [365] Obradovic B, Meldon J, Freed L, Vunjak-Novakovic G. Glycosaminoglycan deposition in engineered cartilage: Experiments and mathematical model. *AIChE J* **2000**; 46: 1860-1871.
- [366] Odgaard A. Three-dimensional methods for quantification of cancellous bone architecture. *Bone* **1997**; 20(4): 315-328.
- [367] O'Driscoll S. The healing and regeneration of articular cartilage. *J Bone Joint Surg Am* **1998**; 80(12): 1795-1812.
- [368] O'Driscoll SW. Preclinical cartilage repair: current status and future perspectives. *Clin Orthop* **2001**; 391(Suppl): S397-401.
- [369] O'Driscoll SW, Fitzsimmons JS. The role of periosteum in cartilage repair. *Clin Orthop* **2001**; 391(Suppl): S190-207.
- [370] Oh SH, Kang SG, Kim ES, Cho SH, Lee JH. Fabrication and characterization of hydrophilic poly(lactic-co-glycolic acid)/poly(vinyl alcohol) blend cell scaffolds by melt-molding particulate-leaching method. *Biomater* **2003**; 24(22): 4011-4021.
- [371] Olde Riekerink M, Claase M, Engbers G, Grijpma D, Feijen J. Gas plasma etching of PEO/PBT segmented block copolymer films. *J Biomed Mater Res* **2003**; 65A(4): 417-428.

- [372] Oostra J, le Comte EP, van den Huevel JC, Tramper J, Rinzema A. Intra-particle oxygen diffusion limitation in solid-state fermentation. *Biotechnol Bioeng* **2001**; 75: 13-42.
- [373] Ostrander R, Goomer R, Tontz W, Khatod M, Harwood F, Maris T, Amiel D. Donor cell fate in tissue engineering for articular cartilage repair. *Clin Orthop* **2001**; 389: 228-237.
- [374] Palmer G, Evans C, Ghivizzani S, Spector M, Robbins P, Gouze J, Gouze E. Direct gene transfer to osteochondral defects. *Trans Orthop Res Soc* **2002**; 27: 292.
- [375] Papadaki M, Mahmood T, Gupta P, Claase MB, Grijpma DW, Riesle J, van Blitterswijk CA, Langer R. The different behaviors of skeletal muscle cells and chondrocytes on PEGT/PBT block copolymers are related to the surface properties of the substrate. *J Biomed Mater Res* **2001**; 54(1): 47-58.
- [376] Park S, Hung CT, Ateshian GA. Mechanical response of bovine articular cartilage under dynamic unconfined compression loading at physiological stress levels. *Osteo Cart* **2004**; 12(1): 65-73.
- [377] Park Y, Lutolf M, Hubbell J, Hunziker E, Wong M. A synthetic MMP-sensitive PEG-based hydrogel for cartilage repair. *Trans Orthop Res Soc* **2002**; 27: 296.
- [378] Parkkinen J, Lammi M, Inkinen R, Jortikka M, Tammi M, Virtanen I, Helminen H. Influence of short-term hydrostatic pressure on organisation of stress fibers in cultured chondrocytes. *J Orthop Res* **1995**; 13: 495-502.
- [379] Passaretti D, Silverman RP, Huang W, Kirchhoff CH, Ashiku S, Randolph MA, Yaremchuk MJ. Cultured chondrocytes produce injectable tissue-engineered cartilage in hydrogel polymer. *Tissue Eng* **2001**; 7(6): 805-815.
- [380] Pazzano D, Mercier KA, Moran JM, Fong SS, DiBiasio DD, Rulfs JX, Kohles SS, Bonassar LJ. Comparison of chondrogenesis in static and perfused bioreactor culture. *Biotechnol Prog* **2000**; 16(5): 893-896.
- [381] Pearce S, Hurtig M, Clarnette R, Kalra M, Cowan B, Miniaci A. An investigation of 2 techniques for optimizing joint surface congruency using multiple cylindrical osteochondral autografts. *Arthroscopy* **2001**; 17(1): 50-55.
- [382] Pei M, Seidel J, Vunjak-Novakovic G, Freed L. Growth factors for sequential cellular de- and re-differentiation in tissue engineering. *Biochem Biophys Res Commun* **2002**; 294(1): 149-154.
- [383] Pei M, Solchaga L, Seidel J, Zeng L, Vunjak-Novakovic G, Caplan A, Freed L. Bioreactors mediate the effectiveness of tissue engineering scaffolds. *FASEB J* **2002**; 16(12): 1691-1694.
- [384] Pennypacker JP, Hassell JR, Yamada KM, Pratt RM. The influence of an adhesive cell surface protein on chondrogenic expression in vitro. *Exp Cell Res* **1979**; 121(2): 411-415.
- [385] Pereira CS, Gomes ME, Reis RL, Cunha AM. Hard cellular materials in the human body: properties and production of foamed polymers for bone replacement. In "Foams, emulsions and cellular materials." Sapoc F and Rivier N, (Ed); Kluwer Press: Dordrecht, The Netherlands, **1997**.
- [386] Peter S, Miller S, Zhu G, Yasko A, Mikos A. In vivo degradation of a poly(propylene fumarate)/beta-tricalcium phosphate injectable composite scaffold. *J Biomed Mater Res* **1998**; 41(1): 1-7.
- [387] Peterson L, Brittberg M, Kiviranta I, Akerlund EL, Lindahl A. Autologous chondrocyte transplantation. Biomechanics and long-term durability. *Am J Sports Med* **2002**; 30(1): 2-12.
- [388] Peterson L, Minas T, Brittberg M, Nilsson A, Sjogren-Jansson E, Lindahl A. Two- to 9-year outcome after autologous chondrocyte transplantation of the knee. *Clin Orthop* **2000**; 374: 212-234.
- [389] Peterson LF, Fitzgerald RH, Jr., Johnson EW, Jr. Total joint arthroplasty. The knee. *Mayo Clin Proc* **1979**; 54(9): 564-569.
- [390] Pieper J, van der Kraan P, Hafmans T, Kamp J, Buma P, van Susante J, van den Berg W, Veerkamp J, van Kuppevelt T. Crosslinked type II collagen matrices: preparation, characterisation and potential for cartilage engineering. *Biomater* **2002**; 23(15): 3183-3192.
- [391] Pilliar RM. Powder metal-made orthopedic implants with porous surface for fixation by tissue ingrowth. *Clin Orthop* **1983**; 176: 42-51.
- [392] Poole AR, Kojima T, Yasuda T, Mwale F, Kobayashi M, Lavery S. Composition and structure of articular cartilage: a template for tissue repair. *Clin Orthop* **2001**; 391(Suppl): S26-33.
- [393] Porter N, Pilliar R, Grynblas M. Fabrication of porous calcium polyphosphate implants by solid freeform fabrication: a study of processing parameters and in vitro degradation characteristics. *J Biomed Mater Res* **2001**; 56(4): 504-515.
- [394] Potter K, Butler J, Horton W, Spencer R. Response of engineered cartilage tissue to biochemical agents as studied by proton magnetic resonance microscopy. *Arthritis Rheum* **2000**; 43(7): 1580-1590.
- [395] Pridie K. A method of resurfacing osteoarthritic joints. *J Bone Joint Surg Br* **1959**; 41: 618-619.

- [396] Puelacher WC, Mooney D, Langer R, Upton J, Vacanti JP, Vacanti CA. Design of nasoseptal cartilage replacements synthesized from biodegradable polymers and chondrocytes. *Biomater* **1994**; 15(10): 774-778.
- [397] Putnam A, Mooney D. Tissue engineering using synthetic extracellular matrices. *Nat Med* **1996**; 2(7): 824-826.
- [398] Qui W, Scully S. Extracellular collagens demonstrate a type specific influence on cytokine regulation of articular chondrocytes. *Trans Orthop Res Soc* **1996**; 21: 308.
- [399] Quinn TM, Grodzinsky AJ, Buschmann MD, Kim YJ, Hunziker EB. Mechanical compression alters proteoglycan deposition and matrix deformation around individual cells in cartilage explants. *J Cell Sci* **1998**; 111(Pt 5): 573-583.
- [400] Quintavalla J, Uziel-Fusi S, Yin J, Boehnlein E, Pastor G, Blancuzzi V, Singh H, Kraus K, O'Byrne E, Pellas T. Fluorescently labeled mesenchymal stem cells (MSCs) maintain multilineage potential and can be detected following implantation into articular cartilage defects. *Biomater* **2002**; 23(1): 109-119.
- [401] Radder AM, Davies JE, Leenders H, van Blitterswijk CA. Interfacial behavior of PEO/PBT copolymers (Polyactive) in a calvarial system: an in vitro study. *J Biomed Mater Res* **1994**; 28(2): 269-277.
- [402] Radder AM, Leenders H, van Blitterswijk CA. Interface reactions to PEO/PBT copolymers (Polyactive) after implantation in cortical bone. *J Biomed Mater Res* **1994**; 28(2): 141-151.
- [403] Radder AM, Leenders H, van Blitterswijk CA. Application of porous PEO/PBT copolymers for bone replacement. *J Biomed Mater Res* **1996**; 30(3): 341-351.
- [404] Radice M, Brun P, Cortivo R, Scapinelli R, Battaliard C, Abatangelo G. Hyaluronan-based biopolymers as delivery vehicles for bone-marrow-derived mesenchymal progenitors. *J Biomed Mater Res* **2000**; 50(2): 101-109.
- [405] Ragan PM, Chin VI, Hung HH, Masuda K, Thonar EJ, Amer EC, Grodzinsky AJ, Sandy JD. Chondrocyte extracellular matrix synthesis and turnover are influenced by static compression in a new alginate disk culture system. *Arch Biochem Biophys* **2000**; 383(2): 256-264.
- [406] Rahardjo YS, Weber FJ, Le Comte EP, Tramper J, Rinzema A. Contribution of aerial hyphae of *Aspergillus oryzae* to respiration in a model solid-state fermentation system. *Biotechnol Bioeng* **2002**; 78: 539-544.
- [407] Rahfoth B, Weisser J, Sternkopf F, Aigner T, von dMK, Brauer R. Transplantation of allograft chondrocytes embedded in agarose gel into cartilage defects of rabbits. *Osteo Cart* **1998**; 6(1): 50-65.
- [408] Rahman MS, Tsuchiya T. Enhancement of chondrogenic differentiation of human articular chondrocytes by biodegradable polymers. *Tissue Eng* **2001**; 7(6): 781-790.
- [409] Rajpurohit R, Koch CJ, Tao Z, Teixeira CM, Shapiro IM. Adaptation of chondrocytes to low oxygen tension: relationship between hypoxia and cellular metabolism. *J Cell Physiol* **1996**; 168(2): 424-432.
- [410] Ratcliffe A, Fryer PR, Hardingham TE. The distribution of aggregating proteoglycans in articular cartilage: comparison of quantitative immunoelectron microscopy with radioimmunoassay and biochemical analysis. *J Histochem Cytochem* **1984**; 32(2): 193-201.
- [411] Ratcliffe A, Niklason LE. Bioreactors and bioprocessing for tissue engineering. *Ann N Y Acad Sci* **2002**; 961: 210-215.
- [412] Revsbech NP, Ward MW. Oxygen microelectrode that is insensitive to medium chemical composition: Use in an acid microbial mat dominated by *Cyanidium caldarium*. *App Envir Microbiol* **1983**; 45(755-759).
- [413] Richardson TP, Peters MC, Ennett AB, Mooney DJ. Polymeric system for dual growth factor delivery. *Nat Biotechnol* **2001**; 19(11): 1029-1034.
- [414] Roberts S, Knight M, Lee D, Bader D. Mechanical compression influences intracellular Ca²⁺ signaling in chondrocytes seeded in agarose constructs. *J Appl Physiol* **2001**; 90(4): 1385-1391.
- [415] Rosenthal O, Bowie M, Wagoner G. Studies on the metabolism of articular cartilage. I. Respiration and glycolysis in relation to its age. *J Cell Comp Physiol* **1941**; 17: 221-233.
- [416] Rötter N, Aigner J, Naumann A, Planck H, Hammer C, Burmester G, Sittlinger M. Cartilage reconstruction in head and neck surgery: comparison of resorbable polymer scaffolds for tissue engineering of human septal cartilage. *J Biomed Mater Res* **1998**; 42(3): 347-356.
- [417] Rötter N, Bonassar LJ, Tobias G, Lebl M, Roy AK, Vacanti CA. Age dependence of cellular properties of human septal cartilage: implications for tissue engineering. *Arch Otolaryngol Head Neck Surg* **2001**; 127(10): 1248-1252.
- [418] Rowley JA, Mooney DJ. Alginate type and RGD density control myoblast phenotype. *J Biomed Mater Res* **2002**; 60(2): 217-223.
- [419] Rueggsegger P, Koller B, Muller R. A microtomographic system for the nondestructive evaluation of bone architecture. *Calcif Tissue Int* **1996**; 58(1): 24-29.

- [420] Sah RL, Kim YJ, Doong JY, Grodzinsky AJ, Plaas AH, Sandy JD. Biosynthetic response of cartilage explants to dynamic compression. *J Orthop Res* **1989**; 7(5): 619-636.
- [421] Sakkers RJ, Dalmeyer RA, de Wijn JR, van Blitterswijk CA. Use of bone-bonding hydrogel copolymers in bone: an in vitro and in vivo study of expanding PEO-PBT copolymers in goat femora. *J Biomed Mater Res* **2000**; 49(3): 312-318.
- [422] Sakkers RJB, de Wijn JR, Dalmeyer RAJ, Brand R, van Blitterswijk CA. Evaluation of copolymers of polyethylene oxide and poly-buthylene terephthalate (Polyactive®): mechanical behaviour. *J Mater Sci* **1998**; 9: 375-379.
- [423] Saltzman WM, Baldwin SP. Materials for protein delivery in tissue engineering. *Adv Drug Deliv Rev* **1998**; 33(1-2): 71-86.
- [424] Saris DB, Mukherjee N, Berglund LJ, Schultz FM, An KN, O'Driscoll SW. Dynamic pressure transmission through agarose gels. *Tissue Eng* **2000**; 6(5): 531-537.
- [425] Schaefer D, Martin I, Jundt G, Seidel J, Heberer M, Grodzinsky A, Bergin I, Vunjak-Novakovic G, Freed L. Tissue-engineered composites for the repair of large osteochondral defects. *Arthritis Rheum* **2002**; 46(9): 2524-2534.
- [426] Schaefer D, Martin I, Shastri P, Padera RF, Langer R, Freed LE, Vunjak-Novakovic G. In vitro generation of osteochondral composites. *Biomater* **2000**; 21(24): 2599-2606.
- [427] Schantz JT, Hutmacher DW, Lam CX, Brinkmann M, Wong KM, Lim TC, Chou N, Guldberg RE, Teoh SH. Repair of calvarial defects with customised tissue-engineered bone grafts II. Evaluation of cellular efficiency and efficacy in vivo. *Tissue Eng* **2003**; 9(Suppl 1): S127-139.
- [428] Schantz JT, Teoh SH, Lim TC, Endres M, Lam CX, Hutmacher DW. Repair of calvarial defects with customized tissue-engineered bone grafts I. Evaluation of osteogenesis in a three-dimensional culture system. *Tissue Eng* **2003**; 9(Suppl 1): S113-126.
- [429] Schinagl R, Gurskis D, Chen A, Sah R. Depth-dependent confined compression modulus of full-thickness bovine articular cartilage. *J Orthop Res* **1997**; 15(4): 499-506.
- [430] Schipani E, Ryan H, Didrickson S, Kobayashi T, Knight M, Johnson R. Hypoxia in cartilage: HIF-1alpha is essential for chondrocyte growth arrest and survival. *Genes Dev* **2001**; 15(21): 2865-2876.
- [431] Schugens C, Maquet V, Grandfils C, Jerome R, Teyssie P. Polylactide macroporous biodegradable implants for cell transplantation. II. Preparation of polylactide foams by liquid-liquid phase separation. *J Biomed Mater Res* **1996**; 30(4): 449-461.
- [432] Schulze-Tanzil G, De SP, Villegas CH, John T, Merker H, Scheid A, Shakibaei M. Redifferentiation of dedifferentiated human chondrocytes in high-density cultures. *Cell Tissue Res* **2002**; 308(3): 371-379.
- [433] Schwartz Z, Martin J, Dean D, Simpson J, Cochran D, Boyan B. Effect of titanium surface roughness on chondrocyte proliferation, matrix production, and differentiation depends on the state of cell maturation. *J Biomed Mater Res* **1996**; 30(2): 145-155.
- [434] Sechrist VF, Miao YJ, Niyibizi C, Westerhausen-Larson A, Matthew HW, Evans CH, Fu FH, Suh JK. GAG-augmented polysaccharide hydrogel: a novel biocompatible and biodegradable material to support chondrogenesis. *J Biomed Mater Res* **2000**; 49(4): 534-541.
- [435] Semenza GL. Regulation of mammalian O₂ homeostasis by hypoxia-inducible factor 1. *Annu Rev Cell Dev Biol* **1999**; 15: 551-578.
- [436] Shapiro F, Koide S, Glimcher M. Cell origin and differentiation in the repair of full-thickness defects of articular cartilage. *J Bone Joint Surg Am* **1993**; 75(4): 532-553.
- [437] Shapiro I, Tokuoka T, Silvertown S. In "Cartilage: Molecular aspects." Hall B and Newman S, (Ed); CRC Press: Boca Raton, **1991**; 97-130.
- [438] Sharma B, Williams CG, Kim TK, Malik A, Elisseeff JH. Multi-layered hydrogel constructs recreate zonal organization of articular cartilage. *Trans Orthop Res Soc* **2003**; 28: 948.
- [439] Shastri V, Martin I, Langer R. Macroporous polymer foams by hydrocarbon templating. *Proc Natl Acad Sci U S A* **2000**; 97(5): 1970-1975.
- [440] Sheridan MH, Shea LD, Peters MC, Mooney DJ. Bioabsorbable polymer scaffolds for tissue engineering capable of sustained growth factor delivery. *J Controlled Release* **2000**; 64(1-3): 91-102.
- [441] Sherwood JK, Riley SL, Palazzolo R, Brown SC, Monkhouse DC, Coates M, Griffith LG, Landeen LK, Ratcliffe A. A three-dimensional osteochondral composite scaffold for articular cartilage repair. *Biomater* **2002**; 23(24): 4739-4751.
- [442] Shikinami Y, Kawarada H. Potential application of a triaxial three-dimensional fabric (3-DF) as an implant. *Biomater* **1998**; 19(7-9): 617-635.
- [443] Singhvi R, Kumar A, Lopez GP, Stephanopoulos GN, Wang DI, Whitesides GM, Ingber DE. Engineering cell shape and function. *Science* **1994**; 264(5159): 696-698.

- [444] Sittinger M, Reitzel D, Dauner M, Hierlemann H, Hammer C, Kastenbauer E, Planck H, Burmester GR, Bujia J. Resorbable polyesters in cartilage engineering: affinity and biocompatibility of polymer fiber structures to chondrocytes. *J Biomed Mater Res* **1996**; 33(2): 57-63.
- [445] Slivka MA, Leatherbury NC, Kieswetter K, Niederauer GG. Porous, resorbable, fiber-reinforced scaffolds tailored for articular cartilage repair. *Tissue Eng* **2001**; 7(6): 767-780.
- [446] Smith RL, Donlon BS, Gupta MK, Mohtai M, Das P, Carter DR, Cooke J, Gibbons G, Hutchinson N, Schurman DJ. Effects of fluid-induced shear on articular chondrocyte morphology and metabolism in vitro. *J Orthop Res* **1995**; 13(6): 824-831.
- [447] Smith RL, Lin J, Trindade M, Shide J, Kajiyama G, Vu T, Hoffman A, van der Meulen M, Goodman S, Schurman D, Carter D. Time-dependant effects of intermittent hydrostatic pressure on articular chondrocyte type II collagen and aggrecan mRNA expression. *J Rehab Res Dev* **2000**; 37(2): 153-161.
- [448] Sodian R, Loebe M, Hein A, Martin D, Hoerstrup S, Potapov E, Hausmann H, Lueth T, Hetzer R. Application of stereolithography for scaffold fabrication for tissue engineered heart valves. *ASAIO J* **2002**; 48(1): 12-16.
- [449] Sohler J, Haan RE, de Groot K, Bezemer JM. A novel method to obtain protein release from porous polymer scaffolds: emulsion coating. *J Control Release* **2003**; 87(1-3): 57-68.
- [450] Solchaga L, Dennis J, Goldberg V, Caplan A. Hyaluronic acid-based polymers as cell carriers for tissue-engineered repair of bone and cartilage. *J Orthop Res* **1999**; 17(2): 205-213.
- [451] Solchaga L, Yoo J, Lundberg M, Dennis J, Huijbregtse B, Goldberg V, Caplan A. Hyaluronan-based polymers in the treatment of osteochondral defects. *J Orthop Res* **2000**; 18(5): 773-780.
- [452] Solchaga LA, Goldberg VM, Caplan AI. Cartilage regeneration using principles of tissue engineering. *Clin Orthop* **2001**; 391(Suppl): S161-170.
- [453] Solursh M, Meier S. Effects of cell density on the expression of differentiation by chick embryo chondrocytes. *J Exp Zool* **1974**; 187: 311-322.
- [454] Stading M, Langer R. Mechanical shear properties of cell-polymer cartilage constructs. *Tissue Eng* **1999**; 5(3): 241-250.
- [455] Stairmand JW, Holm S, Urban JP. Factors influencing oxygen concentration gradients in the intervertebral disc. A theoretical analysis. *Spine* **1991**; 16(4): 444-449.
- [456] Steadman J, Rodkey W, Singleton S, Briggs K. Microfracture technique for full thickness chondral defects: technique and clinical results. In "Operative techniques in orthopaedics. Treatment of chondral injuries." Fu F, Ed. 7, **1997**: 300-304.
- [457] Steadman JR, Rodkey W, Rodrigo JJ. Microfracture: Surgical Technique and Rehabilitation to Treat Chondral Defects. *Clin Orthop* **2001**; 391(Suppl): S362-369.
- [458] Steele J, Johnson G, McFarland C, Dalton B, Gengenbach T, Chatelier R, Underwood P, Griesser H. Roles of serum vitronectin and fibronectin in initial attachment of human vein endothelial cells and dermal fibroblasts on oxygen- and nitrogen-containing surfaces made by radiofrequency plasmas. *J Biomater Sci Polym Ed* **1994**; 6(6): 511-532.
- [459] Suh JK, Baek GH, Aroen A, Malin CM, Niyibizi C, Evans CH, Westerhausen-Larson A. Intermittent sub-ambient interstitial hydrostatic pressure as a potential mechanical stimulator for chondrocyte metabolism. *Osteo Cart* **1999**; 7(1): 71-80.
- [460] Sun W, Lal P. Recent development on computer aided tissue engineering - a review. *Comput Methods Programs Biomed* **2002**; 67(2): 85-103.
- [461] Sun W, Starly B, Darling A, Gomez C. Computer-aided tissue engineering: application to biomimetic modelling and design of tissue scaffolds. *Biotechnol Appl Biochem* **2004**; 39(Pt 1): 49-58.
- [462] Sun Y, Kandel R. Deep zone articular chondrocytes in vitro express genes that show specific changes with mineralization. *J Bone Miner Res* **1999**; 14(11): 1916-1925.
- [463] Svoboda K. Chondrocyte-matrix attachment complexes mediate survival and differentiation. *Microsc Res Tech* **1998**; 43(2): 111-122.
- [464] Tabata Y. Necessity of drug delivery systems for protein delivery in tissue engineering. In "Biomaterials and drug delivery toward the new millennium." Park KD, Ed.; Han Rim Won Publishing Co.: Seoul, Korea, **2000**; 531-544.
- [465] Tabata Y, Miyao M, Ozeki M, Ikada Y. Controlled release of vascular endothelial growth factor by use of collagen hydrogels. *J Biomater Sci Polym Ed* **2000**; 11(9): 915-930.
- [466] Taboas J, Maddox R, Krebsbach P, Hollister S. Indirect solid free form fabrication of local and global porous, biomimetic and composite 3D polymer-ceramic scaffolds. *Biomater* **2003**; 24(1): 181-194.
- [467] Takigawa M, Shirai E, Fukuo K, Tajima K, Mori Y, Suzuki F. Chondrocytes dedifferentiated by serial monolayer culture form cartilage nodules in nude mice. *Bone Miner* **1987**; 2(6): 449-462.

- [468] Tan KH, Chua CK, Leong KF, Cheah CM, Cheang P, Abu Bakar MS, Cha SW. Scaffold development using selective laser sintering of polyetheretherketone-hydroxyapatite biocomposite blends. *Biomater* **2003**; 24(18): 3115-3123.
- [469] Tay A. Yield, proliferation, post-expansion differentiation capacity and growth factor responsiveness of human, nasal and rib chondrocytes. *Tissue Eng (in press)*.
- [470] Temenoff JS, Athanasiou KA, Lebaron RG, Mikos AG. Effect of poly(ethylene glycol) molecular weight on tensile and swelling properties of oligo(poly(ethylene glycol) fumarate) hydrogels for cartilage tissue engineering. *J Biomed Mater Res* **2002**; 59(3): 429-437.
- [471] Temenoff JS, Mikos AG. Injectable biodegradable materials for orthopedic tissue engineering. *Biomater* **2000**; 21(23): 2405-2412.
- [472] Temenoff JS, Mikos AG. Review: tissue engineering for regeneration of articular cartilage. *Biomater* **2000**; 21(5): 431-440.
- [473] Terlingen JG, Brenneisen LM, Super HT, Pijpers AP, Hoffman AS, Feijen J. Introduction of amine groups on poly(ethylene) by plasma immobilization of a preadsorbed layer of decylamine hydrochloride. *J Biomater Sci Polym Ed* **1993**; 4(3): 165-181.
- [474] Thomson B, Smith M, Boyer S, Turner R, Kidd D, Riggs H, Dowthwaite G, Archer C. Coated biomaterials, zonal cell-seeding and cartilage tissue engineering. *Trans Orthop Res Soc* **2002**; 27: 477.
- [475] Treppo S, Koepf H, Quan EC, Cole AA, Kuettner KE, Grodzinsky AJ. Comparison of biomechanical and biochemical properties of cartilage from human knee and ankle pairs. *J Orthop Res* **2000**; 18(5): 739-748.
- [476] Uchida T, Yagi A, Oda Y, Nakada Y, Goto S. Instability of bovine insulin in poly(lactide-co-glycolide) (PLGA) microspheres. *Chem Pharm Bull (Tokyo)* **1996**; 44(1): 235-236.
- [477] Urban JP. Present perspectives on cartilage and chondrocyte mechanobiology. *Biorheology* **2000**; 37(1-2): 185-190.
- [478] Urist M. Biogenesis of bone: Calcium and phosphorus in the skeleton and blood in vertebrate evolution. In "Handbook of physiology." Greep R and Astwood E, (Ed): 7; Am. Physiol. Soc.: Washington, DC, **1976**; 183-213.
- [479] Uvehammer J, Karrholm J, Regner L, Carlsson L, Herberts P. Concave versus posterior-stabilized fibial joint surface in total knee arthroplasty: randomized evaluation of 47 knees. *J Arthroplasty* **2001**; 16(1): 25-32.
- [480] van Blitterswijk CA, van den Brink J, Leenders H, Bakker D. The effect of PEO ratio on degradation, calcification and bone-bonding of PEO/PBT copolymer (Polyactive). *Cells Mater* **1993**; 3(23): 23-36.
- [481] van de Weert M, van't Hof R, Hennink WE, Crommelin DJA. Stability of pharmaceutical proteins in particulate carriers. In "Peptide and protein drug delivery." Frokjaer S, Christrup L and Krogsgaard-Larsen P, (Ed); Alfred Benzon Symposium 43: Copenhagen, **1998**; 359-375.
- [482] van Osch G, Bos P, Duynstee M, Verwoerd-Verhoef H, Verhaar J. Does the superficial zone of articular cartilage contain progenitor cells? *Trans Orthop Res Soc* **2002**; 27: 381.
- [483] van Osch G, van der Veen S, Verwoerd-Verhoef H. In vitro redifferentiation of culture-expanded rabbit and human auricular chondrocytes for cartilage reconstruction. *Plast Reconstr Surg* **2001**; 107(2): 433-440.
- [484] van Susante J, Buma P, Homminga G, van den Berg W, Veth R. Chondrocyte-seeded hydroxyapatite for repair of large articular cartilage defects. A pilot study in the goat. *Biomater* **1998**; 19(24): 2367-2374.
- [485] van Susante J, Buma P, Schuman L, Homminga G, van den Berg W, Veth R. Resurfacing potential of heterologous chondrocytes suspended in fibrin glue in large full-thickness defects of femoral articular cartilage: an experimental study in the goat. *Biomater* **1999**; 20(13): 1167-1175.
- [486] van Susante J, Buma P, van Osch G, Versleyen D, van der Kraan P, van der Berg W, Homminga G. Culture of chondrocytes in alginate and collagen carrier gels. *Acta Orthop Scand* **1995**; 66(6): 549-556.
- [487] van Susante J, Pieper J, Buma P, van Kuppevelt T, van Beuningen H, van Der Kraan P, Veerkamp J, van den Berg W, Veth R. Linkage of chondroitin-sulfate to type I collagen scaffolds stimulates the bioactivity of seeded chondrocytes in vitro. *Biomater* **2001**; 22(17): 2359-2369.
- [488] Vloeberghs M, Hatfield F, Daemi F, Dickens P. Soft tissue rapid prototyping in neurosurgery. *Comput Aided Surg* **1998**; 3(2): 95-97.
- [489] von der Mark K, Gauss V, von der Mark H, Muller P. Relationship between cell shape and type of collagen synthesised as chondrocytes lose their cartilage phenotype in culture. *Nature* **1977**; 267(5611): 531-532.

- [490] von Rechenberg B, Akens MK, Nadler D, Bittmann P, Zlinszky K, Kutter A, Poole AR, Auer JA. Changes in subchondral bone in cartilage resurfacing—an experimental study in sheep using different types of osteochondral grafts. *Osteo Cart* **2003**; 11(4): 265-277.
- [491] Vozzi G. Microsyringe-Based Deposition of Two-Dimensional and Three-Dimensional Polymer Scaffolds with a Well-Defined Geometry for Application to Tissue Engineering. *Tissue Eng* **2002**; 8(6): 1089-1098.
- [492] Vozzi G, Flaim C, Ahluwalia A, Bhatia S. Fabrication of PLGA scaffolds using soft lithography and microsyringe deposition. *Biomater* **2003**; 24(14): 2533-2540.
- [493] Vunjak-Novakovic G, Freed L, Biron R, Langer R. Effects of mixing on tissue engineered cartilage. *AIChE J* **1996**; 42: 850-860.
- [494] Vunjak-Novakovic G, Martin I, Obradovic B, Treppo S, Grodzinsky AJ, Langer R, Freed LE. Bioreactor cultivation conditions modulate the composition and mechanical properties of tissue-engineered cartilage. *J Orthop Res* **1999**; 17(1): 130-138.
- [495] Vunjak-Novakovic G, Obradovic B, Martin I, Bursac P, Langer R, Freed L. Dynamic cell seeding of polymer scaffolds for cartilage tissue engineering. *Biotechnol Prog* **1998**; 14(2): 193-202.
- [496] Vunjak-Novakovic G, Obradovic B, Martin I, Freed L. Bioreactor studies of native and tissue engineered cartilage. *Biorheology* **2002**; 39(1,2): 259-268.
- [497] Wakitani S, Goto T, Pineda S, Young R, Mansour J, Caplan A, Goldberg V. Mesenchymal cell-based repair of large, full-thickness defects of articular cartilage. *J Bone Joint Surg Am* **1994**; 76(4): 579-592.
- [498] Wakitani S, Goto T, Young R, Mansour J, Goldberg V, Caplan A. Repair of large full-thickness articular cartilage defects with allograft articular chondrocytes embedded in a collagen gel. *Tissue Eng* **1998**; 4(4): 429-444.
- [499] Wakitani S, Imoto K, Yamamoto T, Saito M, Murata N, Yoneda M. Human autologous culture expanded bone marrow mesenchymal cell transplantation for repair of cartilage defects in osteoarthritic knees. *Osteo Cart* **2002**; 10(3): 199-206.
- [500] Wald H, Sarakinos G, Lyman M, Mikos A, Vacanti J, Langer R. Cell seeding in porous transplantation devices. *Biomater* **1993**; 14(4): 270-278.
- [501] Waldman S, Grynepas M, Pilliar R, Kandel R. The use of specific chondrocyte populations to modulate the properties of tissue-engineered cartilage. *J Orthop Res* **2003**; 21(1): 132-138.
- [502] Waldman SD, Sun YL, Grynepas MD, Pilliar RM, Kandel RA. The effect of regional subpopulations on the composition and load-bearing capacity of tissue-engineered cartilage. *Trans Soc Biomater* **2001**; 27: 244.
- [503] Wang CC, Hung CT, Mow VC. An analysis of the effects of depth-dependent aggregate modulus on articular cartilage stress-relaxation behavior in compression. *J Biomech* **2001**; 34(1): 75-84.
- [504] Wang HJ, Bertrand-De Haas M, Van Blitterswijk CA, Lamme EN. Engineering of a Dermal Equivalent: Seeding and Culturing Fibroblasts in PEGT/PBT Copolymer Scaffolds. *Tissue Eng* **2003**; 9(5): 909-917.
- [505] Watt F. Effect of seeding density on stability of the differentiated phenotype of pig articular chondrocytes in culture. *J Cell Sci* **1988**; 89(Pt 3): 373-378.
- [506] Weisl H. Intertrochanteric osteotomy for osteoarthritis. A long-term follow-up. *J Bone Joint Surg Br* **1980**; 62(1): 37-42.
- [507] West CM, Lanza R, Rosenbloom J, Lowe M, Holtzer H, Avdalic N. Fibronectin alters the phenotypic properties of cultured chick embryo chondroblasts. *Cell* **1979**; 17(3): 491-501.
- [508] Whang K, Goldstick TK, Healy KE. A biodegradable polymer scaffold for delivery of osteotropic factors. *Biomater* **2000**; 21(24): 2545-2551.
- [509] Whang K, Thomas CH, Healy KE, Nuber G. A novel method to fabricate bioabsorbable scaffolds. *Polymer* **1995**; 36: 837-842.
- [510] Whang K, Tsai DC, Nam EK, Aitken M, Sprague SM, Patel PK, Healy KE. Ectopic bone formation via rhBMP-2 delivery from porous bioabsorbable polymer scaffolds. *J Biomed Mater Res* **1998**; 42(4): 491-499.
- [511] Whitaker MJ, Quirk RA, Howdle SM, Shakesheff KM. Growth factor release from tissue engineering scaffolds. *J Pharm Pharmacol* **2001**; 53(11): 1427-1437.
- [512] Widmer M, Gupta P, Lu L, Meszlenyi R, Evans G, Brandt K, Savel T, Gurlek A, Patrick C, Mikos A. Manufacture of porous biodegradable polymer conduits by an extrusion process for guided tissue regeneration. *Biomater* **1998**; 19(21): 1945-1955.
- [513] Wilkins R, Browning J, Urban J. Chondrocyte regulation by mechanical load. *Biorheology* **2000**; 37(1-2): 67-74.

- [514] Wilson CE, de Bruijn JD, van Blitterswijk CA, Verbout AJ, Dhert WJ. Design and fabrication of standardized hydroxyapatite scaffolds with a defined macro-architecture by rapid prototyping for bone-tissue-engineering research. *J Biomed Mater Res* **2004**; 68A(1): 123-132.
- [515] Wintermantel E, Mayer J, Blum J, Eckert KL, Luscher P, Mathey M. Tissue engineering scaffolds using superstructures. *Biomater* **1996**; 17(2): 83-91.
- [516] Wong M, Wuethrich P, Egli P, Hunziker E. Zone-specific cell biosynthetic activity in mature bovine articular cartilage: a new method using confocal microscopic stereology and quantitative autoradiography. *J Orthop Res* **1996**; 14(3): 424-432.
- [517] Woodfield TBF, Bezemer JM, Pieper JS, van Blitterswijk CA, Riesle J. Scaffolds for tissue engineering of cartilage. *Crit Rev Eukaryot Gene Expr* **2002**; 12(3): 209-236.
- [518] Woodfield TBF, Mahmood T, Riesle J, van Blitterswijk CA. Enhanced Cell Attachment and Onset of Chondrogenesis on Glow Discharge Treated 2D and 3D PEGT/PBT Scaffolds. *Trans Orthop Res Soc* **2002**; 27: 473.
- [519] Woodfield TBF, Malda J, de Wijn J, Pétters F, Riesle J, van Blitterswijk CA. Design of porous scaffolds for cartilage tissue engineering using a three-dimensional fiber-deposition technique. *Biomater* **2004**; 25(18): 4149-4161.
- [520] Wu F, Dunkelmann N, Peterson A, Davisson T, de la Torre R, Jain D. Bioreactor Development for Tissue-Engineered Cartilage. *Ann NY Acad Sci* **1999**; 875(1): 405-404.
- [521] Xie Y, Yang ST, Kniss DA. Three-dimensional cell-scaffold constructs promote efficient gene transfection: Implications for cell-based gene therapy. *Tissue Eng* **2001**; 7(5): 585-598.
- [522] Xiong Z, Yan YN, Zhang RJ, Sun L. Fabrication of porous poly(L-lactic acid) scaffolds for bone tissue engineering via precise extrusion. *Scr Mater* **2001**; 45: 773-779.
- [523] Xu C, Oyajobi B, Frazer A, Kozaci L, Russell R, Hollander A. Effects of growth factors and interleukin-1 alpha on proteoglycan and type II collagen turnover in bovine nasal and articular chondrocyte pellet cultures. *Endocrinology* **1996**; 137(8): 3557-3565.
- [524] Yaeger P, Masi T, de Ortiz J, Binette F, Tubo R, McPherson J. Synergistic action of transforming growth factor-beta and insulin-like growth factor-I induces expression of type II collagen and aggrecan genes in adult human articular chondrocytes. *Exp Cell Res* **1997**; 237(2): 318-325.
- [525] Yamamoto M, Tabata Y, Ikada Y. Ectopic bone formation induced by biodegradable hydrogels incorporating bone morphogenetic protein. *J Biomater Sci Polym Ed* **1998**; 9(5): 439-458.
- [526] Yang S, Leong K, Du Z, Chua C. The design of scaffolds for use in tissue engineering. Part II. Rapid prototyping techniques. *Tissue Eng* **2002**; 8(1): 1-11.
- [527] Yang S, Leong KF, Du Z, Chua CK. The design of scaffolds for use in tissue engineering. Part I. Traditional factors. *Tissue Eng* **2001**; 7(6): 679-689.
- [528] Yates K, Mizuno S, Glowacki J. Early shifts in gene expression during chondroinduction of human dermal fibroblasts. *Exp Cell Res* **2001**; 265(2): 203-211.
- [529] Yoo JU, Mandell I, Angele P, Johnstone B. Chondrogenitor cells and gene therapy. *Clin Orthop* **2000**; 379(Suppl): S164-170.
- [530] Yoshimoto H, Shin YM, Terai H, Vacanti JP. A biodegradable nanofiber scaffold by electrospinning and its potential for bone tissue engineering. *Biomater* **2003**; 24(12): 2077-2082.
- [531] Yu H, Grynblas M, Kandel R. Composition of cartilagenous tissue with mineralized and non-mineralized zones formed in vitro. *Biomater* **1997**; 18(21): 1425-1431.
- [532] Yuan H, de Bruijn JD, Zhang X, van Blitterswijk CA, de Groot K. Bone induction by porous glass ceramic made from Bioglass (45S5). *J Biomed Mater Res* **2001**; 58(3): 270-276.
- [533] Zanetti NC, Solursh M. Effect of cell shape on cartilage differentiation. In "Cell shape: determinants, regulation and regulatory role." Stein WD and Bronner F, (Ed); Academic Press: New York, **1989**; 291-327.
- [534] Zein I, Huttmacher DW, Tan KC, Teoh SH. Fused deposition modeling of novel scaffold architectures for tissue engineering applications. *Biomater* **2002**; 23(4): 1169-1185.
- [535] Zellinger J, Sherwood J, Graham D, Mueller R, Griffith L. Effect of pore size and void fraction on cellular adhesion, proliferation, and matrix deposition. *Tissue Eng* **2001**; 7(5): 557-572.
- [536] Zhang R, Ma PX. Poly(alpha-hydroxy acids)/hydroxyapatite porous composites for bone-tissue engineering. I. Preparation and morphology. *J Biomed Mater Res* **1999**; 44(4): 446-455.
- [537] Zhang R, Ma PX. Porous poly(L-lactic acid)/apatite composites created by biomimetic process. *J Biomed Mater Res* **1999**; 45(4): 285-293.

Acknowledgements

First of all, I would like to thank my supervisors Prof. Dr. Clemens van Blitterswijk and Dr. Jens Riesle. I am grateful to you both for giving me the opportunity to pursue my PhD in The Netherlands in the combined academic and commercial environments of the University of Twente and IsoTis. I sincerely appreciate your time, guidance and feedback throughout my PhD studies. I have learned a lot and gained many positive experiences from my period in Bilthoven, experiences which will hopefully allow me to tackle even bigger challenges in the future. I look forward to continued partnerships and contact in the future.

To my fellow PhD students over the past 4 years: Jos, Clayton, Jeanine, Tahir, Aart, Moyo, Pamela, Jiaping, Jaiwei, Florence, Yuan, Sandra, Hongjun, Robert, Floor - a special thanks to you all for helping create such a vibrant and intellectually stimulating work environment. I particularly want to thank Jos for the great collaborations, conferences and adventure travels. It has been a pleasure sharing our friendship and PhD experiences together, and I look forward to sharing more adventures with you in New Zealand and Australia in the future. Also, Clayton for all the discussions and advice for all things mechanical and scaffold analysis related, as well as our new venture with PoroGen B.V. I look forward to continuing our partnership. Additional thanks go to Jan de Boer and the "new" PhD's, in particular Doreen for the great collaboration with the infamous rabbit study, and Lorenzo as my protégé in scaffold development and rapid prototyping. Best of luck to you all for your future studies. From the PhD group at the University of Twente, thanks also go to Menno Claase for scaffold processing and collaborative work.

To everyone in the Cartilage Group at IsoTis; Monika, Mireille, Roka, Ellen, Marion, Jacqueline and Carla - thank you very much with all the lab assistance, advice and support throughout my studies, as well as all the "gezelligheid" over coffee and "gevulde koekjes." I would also like to thank my students Matthijs and Natalie for all their hard work during their time at IsoTis.

In addition to the PhD and Cartilage groups at IsoTis, sincere thanks go to Joost de Wijn for all your assistance with the prototype 3D fibre deposition device as well as our stimulating discussions about scaffolds, biomaterials, processing and their porous architectures. I also would like to thank Jeroen Pieper and Jeroen Bezemer for all your help with the review paper, and our numerous discussions on scaffolds and PEGT/PBT co-polymers. Fabienne, your help with DSC and scaffold processing was greatly appreciated. Thanks also go to Mirella (the tennis ace) and Chantal for help with niggling histology questions. To all my colleagues, particularly the ones I car-pooled with (e.g. Michel, Clayton, Jos, Pamela), thank you for putting up with my perpetual lack of punctuality.

With regard to rapid prototyping techniques, thanks go to Rüdiger Landers (Freiberg University, DE) for advice in implementing the BioPlotter system, as well as Hendrik John (EnvisionTec GmbH, DE). Furthermore, thanks go to Andres Laib (Scanco Medical, CH) for assistance with micro-CT analysis.

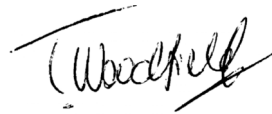
To collaborators in the European SCAFCART grant program, I thank you all for your critical comments and input. In particular I would like to acknowledge Dr. Ivan Martin and Sylvie Miot (University Hospital Basel, CH) for all your discussions, critical comments and collaborative work in a number of publications. Similar thanks are extended to Dr. Anthony Hollander, Trevor Sims (Bristol University, UK) and Dr. Paul Hatton (Sheffield University, UK).

To collaborators in the Dutch BTS grant program; Dr. Gerjo van Osch, Dr. Harrie Weinans, Erik Mandl, Jarno van de Breevaart Bravenboer (EMC, Rotterdam) and Dr. Roel Kuijer (MMC, Maastricht) – I very much appreciated your guidance and close collaboration throughout my PhD studies.

To my Swiss collaborators at University Hospital Zurich, Dr. Volker Wedler and Dr. Maria Schneller – I enjoyed the opportunity to work with you both on the rabbit study and appreciated my visits to your lab in Zurich as well as your kind hospitality. Many thanks and I look forward to continuing our fruitful partnership.

To the kiwi “whanau” in the UK; Carl, Tracey, Kent, Lynaire, Alex, Ed, Rob T, Meagan and Grant – many thanks for all the great European adventures. The active nature of all our skiing, mountain biking and climbing time-outs helped keep me sane throughout the PhD. Special thanks also go to my long time kiwi buddies, Chris, Andy, Nick and Matt for all the support along the way – kia kaha. I'm looking forward to hitting the hills in New Zealand with you boys soon.

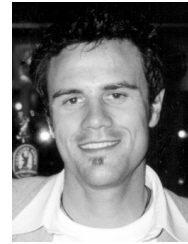
Finally, to my close “whanau” in New Zealand, a massive thanks go to my parents and my sister Sara (Dr. Woodfield #1) for all the love, support and motivation throughout both my Masters and PhD studies abroad - even from half a world away. A very special thanks goes to Amanda for all your patience, inspiration and understanding, especially towards the latter stages of the PhD. Your pick-me-ups and ability to make me laugh were greatly appreciated. As this life chapter comes to a close, I look forward to the start of new chapters and adventures.



“Well, it is a plea to those of you who are adventurous to keep fighting, not to be discouraged when you are frustrated by the unadventurous, and to remember that adventure in any form can act as a most appetising spice for the flavourless gruel of modern civilised existence. Search for worthy objectives for your adventures and then prosecute them with wisdom and judgement.”
[in *Hall & Ball – Kiwi Mountaineers*, Colin Monteath Ed, 1997]

Curriculum Vitae

Tim B.F. Woodfield was born on February 8th, 1975 in Dunedin, New Zealand. His early childhood was spent growing up in Adelaide (Australia), but his primary and secondary school education was based in Christchurch (New Zealand), where he later enrolled at the University of Canterbury in 1992. After obtaining a Bachelor of Engineering degree (Mechanical Engineering Honours) in 1996, he was awarded the J.R. Templin Travelling scholarship and spent 2 years completing a Masters of Applied Science degree at the University of Toronto (Canada) between



1997 and 1999. Based within the Institute of Biomaterials and Biomedical Engineering, and supervised by Prof. R.M. Pilliar, Dr. M. Grynopas and Dr. R. Kandel, his masters thesis was entitled "*Interfacial Shear Strength Criteria for Tissue-Engineered Cartilage Anchored to Porous Synthetic Scaffolds.*"

In January 2000, he accepted a PhD position at IsoTis S.A. (Bilthoven, The Netherlands) in collaboration with the Institute for Biomedical Technology (BMTI), University of Twente, (The Netherlands). The research was performed under the supervision of Prof. C.A. van Blitterswijk and Dr. J. Riesle, the results of which are described in this thesis entitled "*Cartilage Tissue Engineering: instructing cell-based tissue repair through scaffold design.*"

Currently he is a post-doc within the Institute for Biomedical Technology (BMTI), University of Twente and also holds a Scientific Collaborator position within the Executive Board of PoroGen B.V., a start-up biotech company established in The Netherlands in March 2004, focusing on rapid prototyping of novel porous biomaterials. In late 2004, he will return to New Zealand to take up a cross-appointment as a Research Fellow within the Centre for Bioengineering at the University of Canterbury (Christchurch) and Scientific Officer within the Department of Orthopaedics and Musculoskeletal Medicine at Christchurch Hospital.

Selected Colour Figures

Chapter 1

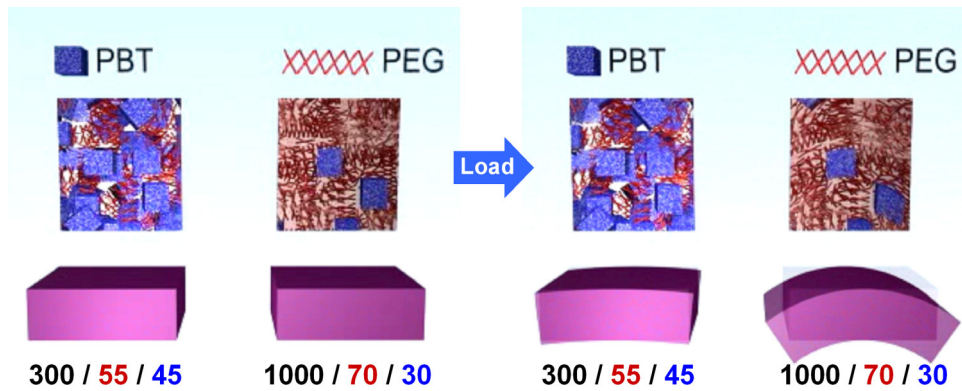


Figure 4 – Schematic representation of the distribution of amorphous PEGT and crystalline PBT blocks within PEGT/PBT biomaterials. By varying the PEG molecular weight, and the wt% ratio of PEGT to PBT, a range of mechanical properties can be achieved. Higher PEG MW and wt% PEGT content (i.e. 1000/70/30) results in a decrease in material stiffness.

Chapter 3

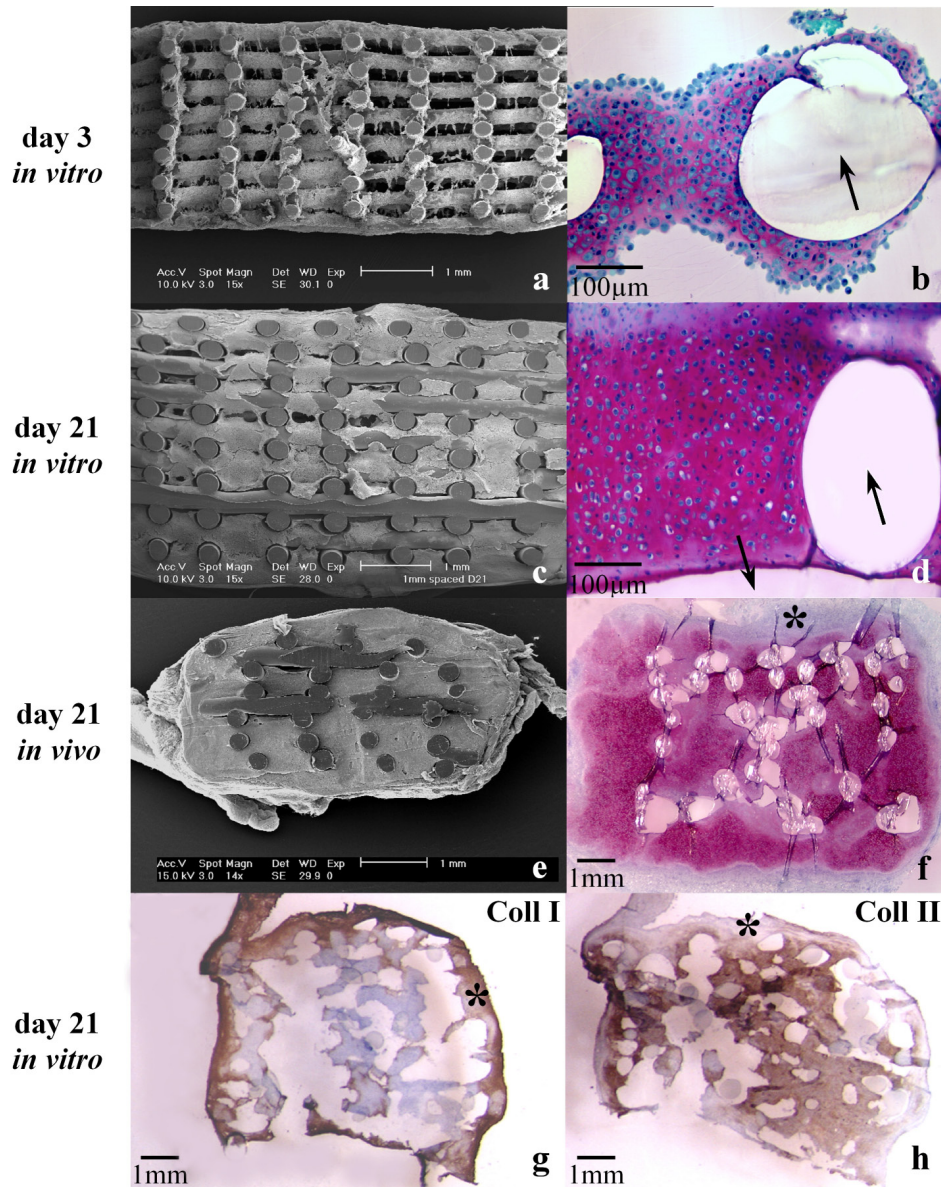


Figure 5 – SEM (A, C, E x 15), safranin-O stained (B, D, F), and collagen type-I and type-II immunohistochemistry sections (G, H) of 3D-deposited 300/55/45 scaffolds following (A, B) 3 days dynamic seeding of bovine articular chondrocytes; (C, D, G, H) 21 days dynamic culture in vitro ; (E, F) 21 days subcutaneous implantation in nude mice; (arrows indicate PEGT/PBT fibre, * indicates fibrous capsule).

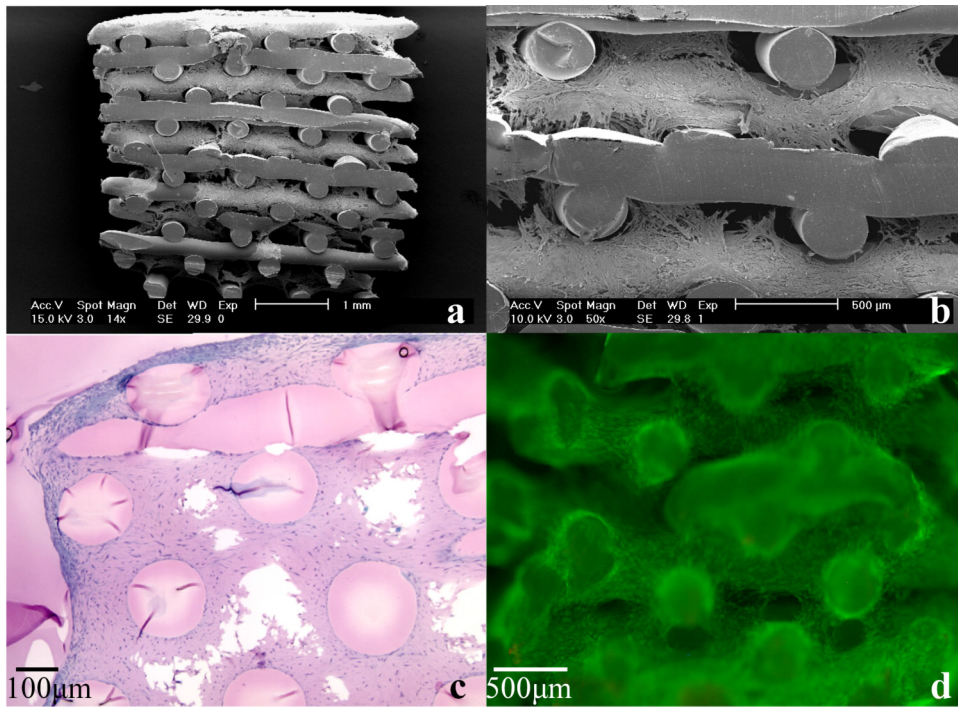


Figure 6 – SEM (A x 15, B x 50), safranin-O (C), and live/dead (D) sections showing attachment, proliferation and high percentage of live (green) expanded human articular chondrocytes throughout interconnecting pores on 3D-deposited 300/55/45 scaffolds following 5 days dynamic seeding.

Chapter 4

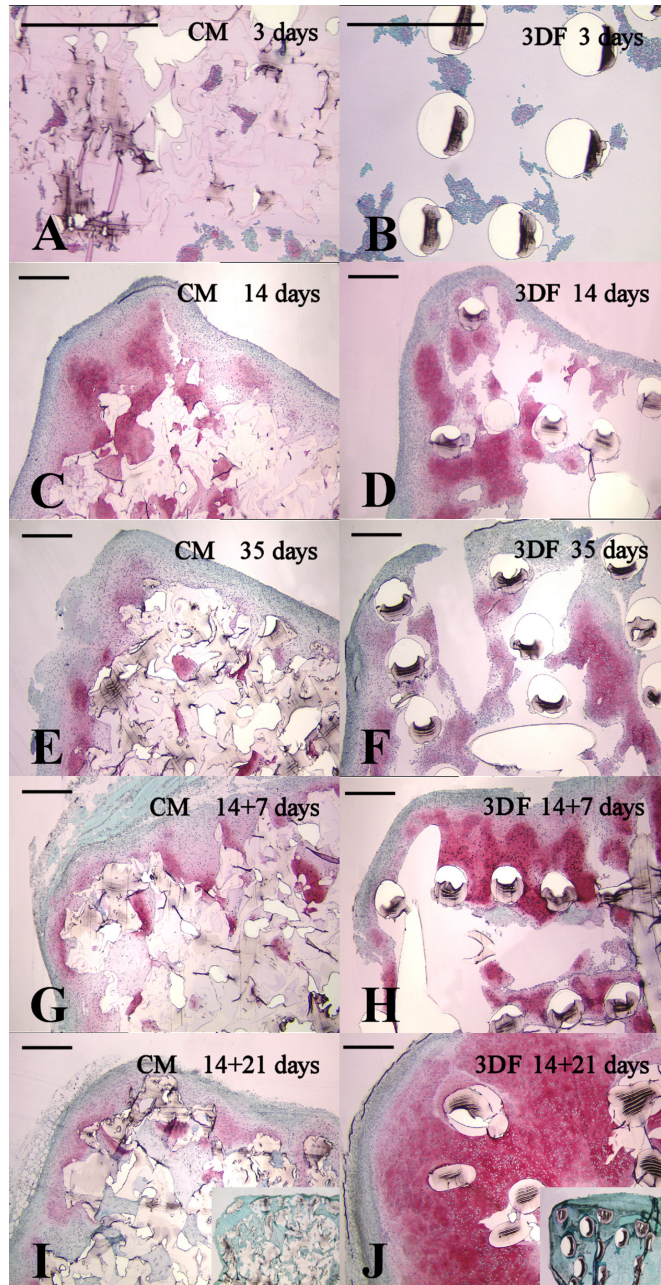


Figure 4 - Photomicrographs of safranin-O stained sections of CM (A, C, E, G, I) and 3DF (B, D, F, H, J) constructs cultured for 3 (A, B), 14 (C, D), 35 (E, F) days *in vitro* and 14 days *in vitro* and subsequently 7 (G, H) and 21 (I, J) days *in vivo*. Inset of I and J shows non-seeded controls. Scale bar represents 500 μm.

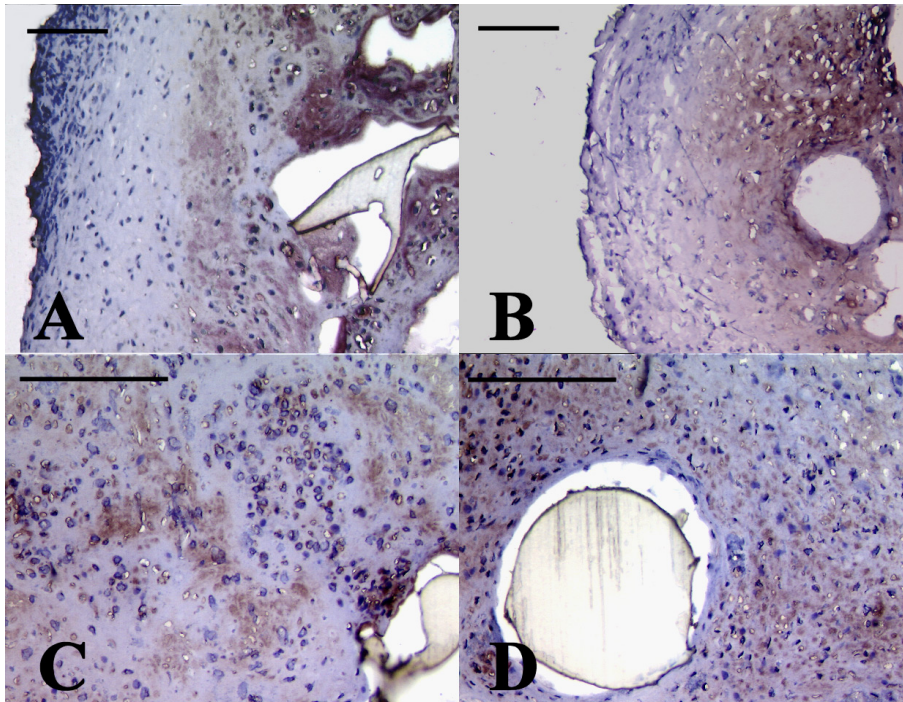


Figure 8 - Immunolocalization of collagen type II in the periphery (A, B) and centre (C, D) of CM (A, C) and 3DF (B, D) constructs cultured 14 days *in vitro* and, additionally, 21 days *in vivo*. Scale bar represents 150 μm . Collagen type II was localized mainly within the centre of the constructs.

Chapter 5

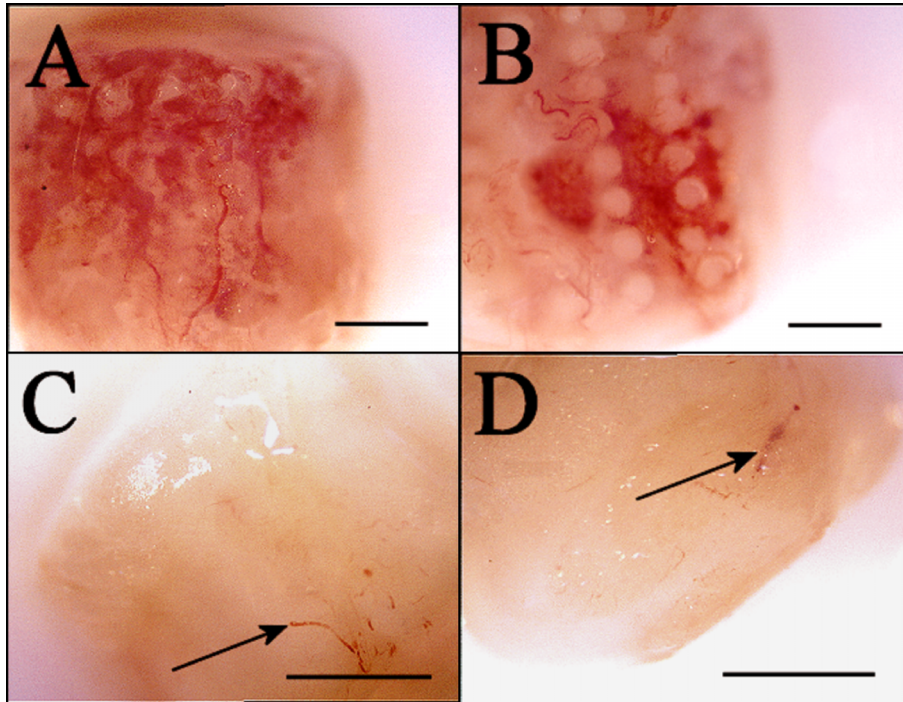


Figure 2 - Photomicrograph of CM (A, C) and 3D (B, D) constructs after 28 days in vivo containing no cells at time point of implantation (cross section) (A, B) and seeded with 3 million cells and pre-cultured cultured for 14 days in vitro (C, D). Arrow indicates superficial blood vessels. Scale bar represents 1 mm.

Chapter 6

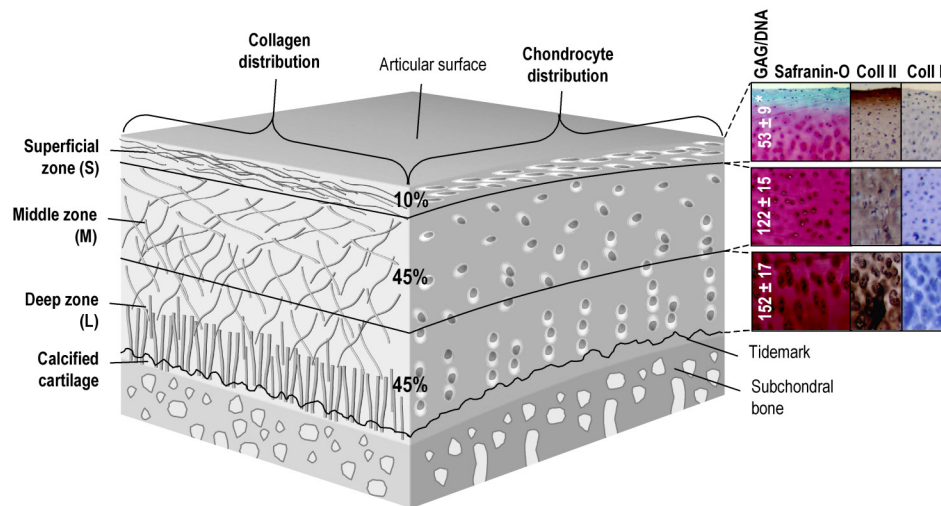


Figure 1 – Anisotropic distribution and orientation of collagen fibres (left face), chondrocytes (right face) and glycosaminoglycan (GAG) within the superficial (S, 10%), middle (M, 45%) and deep or lower (L, 45%) zones of articular cartilage. GAG/DNA content, and safranin-O staining for GAG and immunohistochemistry for collagen type II and type I are illustrated at right. The superficial (S) zone contains flattened chondrocytes and thin, densely packed collagen fibrils (Ø20 nm) oriented tangentially to the articular surface. The middle (M) zone contains larger, randomly oriented collagen fibres and chondrocytes have a more rounded appearance. The lower (L), or deep zone, consists of large, spherical chondrocytes aligned in a columnar fashion, and thicker collagen fibres (Ø120 nm) oriented perpendicular to the joint surface. A zone of calcified cartilage follows, whose thickness and intermediate stiffness modulate the transfer of forces through articular cartilage to subchondral bone (* indicates significant difference in GAG/DNA content; illustration adapted from Woodfield et al., [518] with permission from publisher).

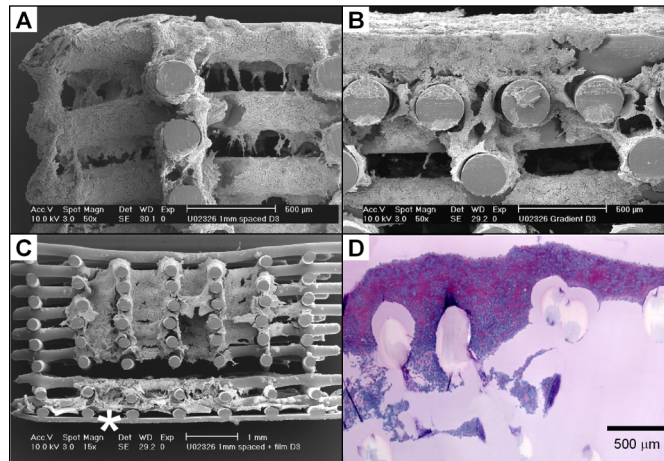


Figure 6 – SEM (A-C) and safranin-O stained sections (D) showing cell attachment and GAG staining on 1mm (A), Grad (B, D), 1mmF (C) scaffolds after 3 days seeding. Available fibre surfaces of spinner flask seeded 1mm and Grad scaffolds were near completely covered with a layer of chondrocytes (A, B). Statically seeded scaffolds (1mmF shown in C) contained more localized regions of high cell density (* indicates dense film).

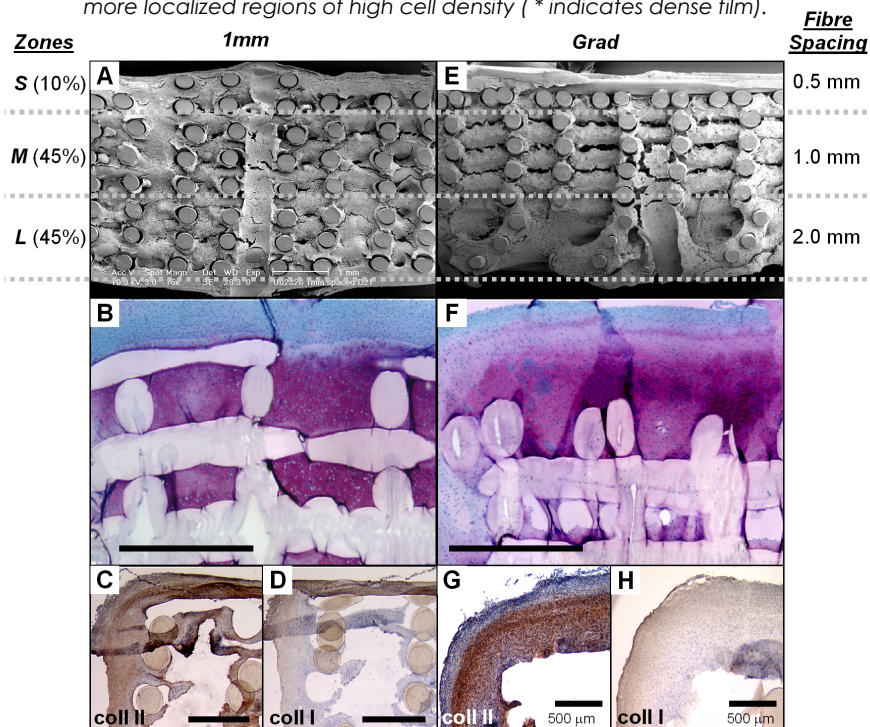


Figure 7 – SEM (A, E), safranin-O (B, F) and collagen type II (C, G) and type I (D, H) immunohistology sections showing extra cellular matrix (ECM) formation within 1mm (A-D) and Grad scaffolds (E-H) after 21 days dynamic culture. Regions corresponding to S, M and L zones are indicated on the left, with associated fibre spacing indicated on the right (scale bar = 1 mm unless otherwise stated).

Chapter 7

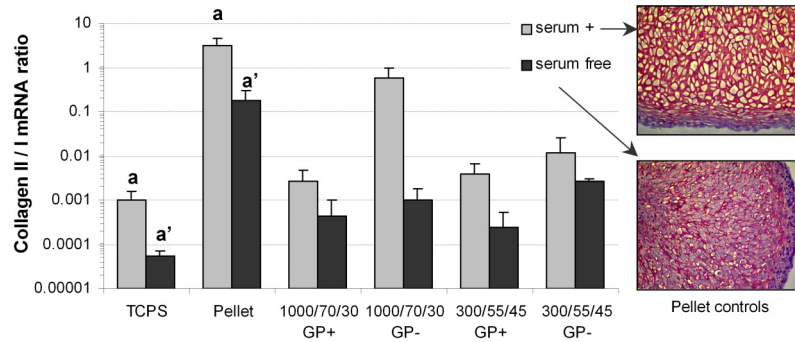


Figure 3 - Re-differentiation potential (collagen II/I mRNA ratio) of expanded (P2) human nasal chondrocytes on gas plasma treated (GP+) and untreated (GP-) substrates after 10 days culture in serum containing (S+) or serum free (SF) media. Negative control for re-differentiation = TCPS; positive control for re-differentiation = pellet. Inset pictures show positive safranin-O staining in pellet cultures in both S+ and SF media (x100). Significant difference between substrates denoted by: S+ media = a ; SF media = a'.

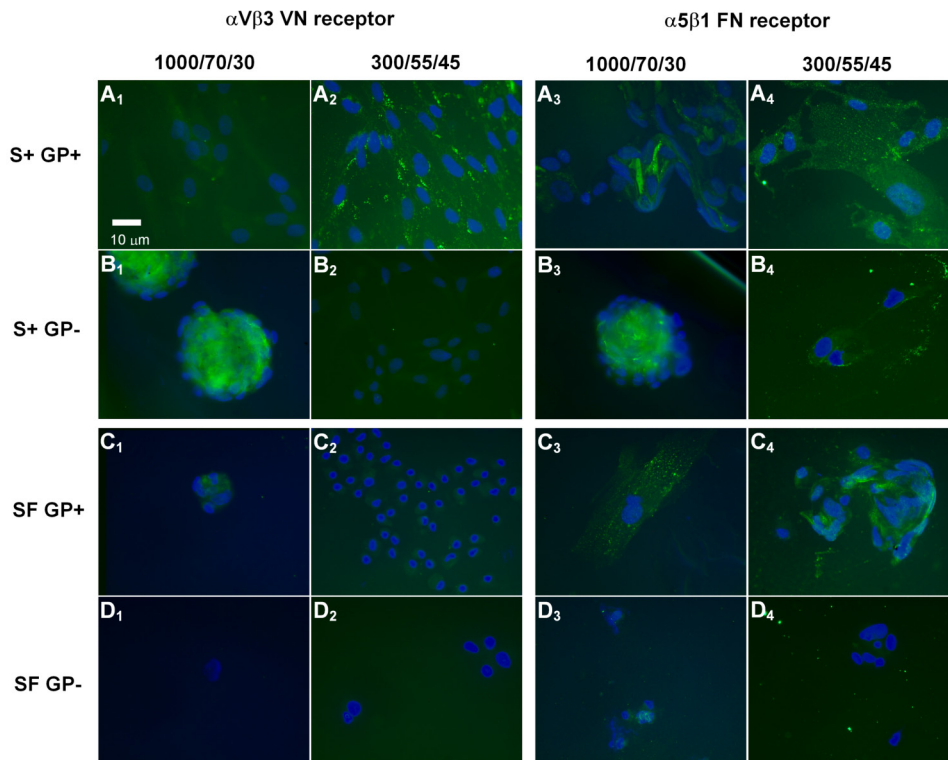


Figure 4 – Immunofluorescence images showing αVβ3 vitronectin (VN, A₁-D₂) and α5β1 fibronectin (FN, A₃-D₄) integrin intensity in expanded human nasal chondrocytes at day 10. Cells were plated on GP+ (A₁₋₄, C₁₋₄) and GP- films (B₁₋₄, D₁₋₄) with 1000/70/30 (A₁-D₁, A₃-D₃) and 300/55/45 compositions (A₂-D₂, A₄-D₄), and cultured in S+ (A₁-B₄) or SF media (C₁-D₄). Cell nuclei stained blue with DAPI.

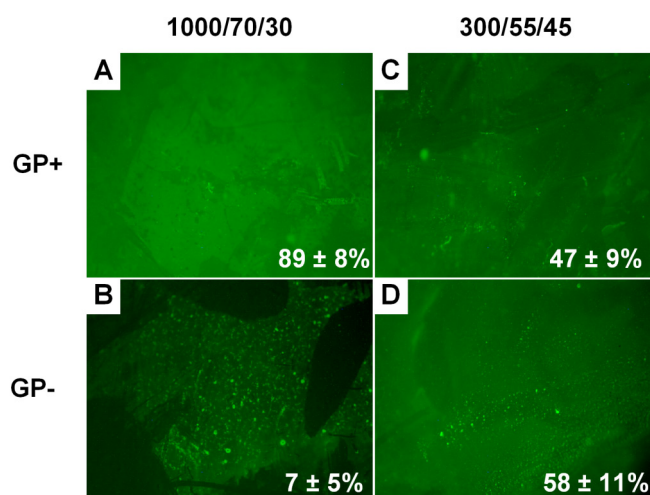


Figure 5 – Fluorescence images (x100) showing adsorption of FITC bovine serum albumin (BSA) GP+ (A, C) and GP- (B, D) films with 1000/70/30 (A, B) and 300/55/45 compositions (C, D). Image analysis was used to estimate the percentage intensity of FITC-BSA and are included in each image.

Chapter 8

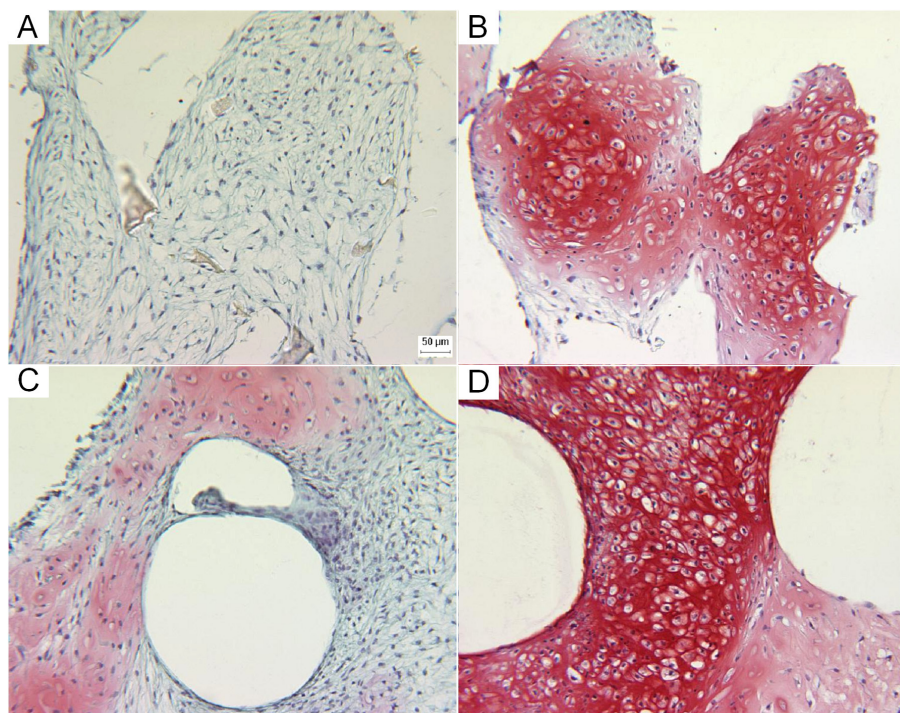


Figure 4 - Representative cross-sectional fields of constructs generated by 4 weeks culture of human nasal chondrocytes on CM 300/55/45 (A), CM 1000/70/30 (B), 3DF 300/55/45 (C), or 3DF 1000/70/30 (D) scaffolds. Histological sections were stained by Safranin-O. Scale bar = 50 µm.

Chapter 9

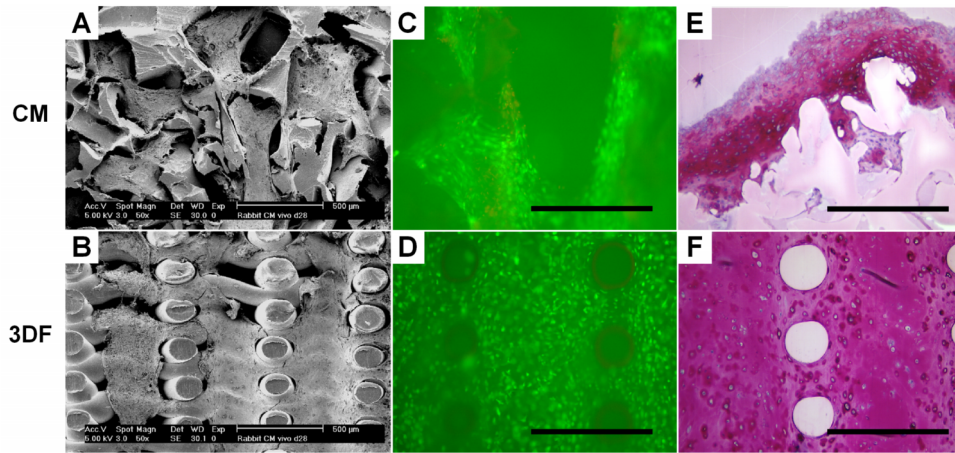


Figure 4 – Results from preliminary study in cylindrical CM (A, C, E) and 3DF (B, D, F) scaffolds illustrating tissue formation in SEM images (A, B) after 21 days in vitro culture and cell viability (C, D) and safranin-O staining (E, F) after 28 days subcutaneous implantation (scale bar = 500 µm).

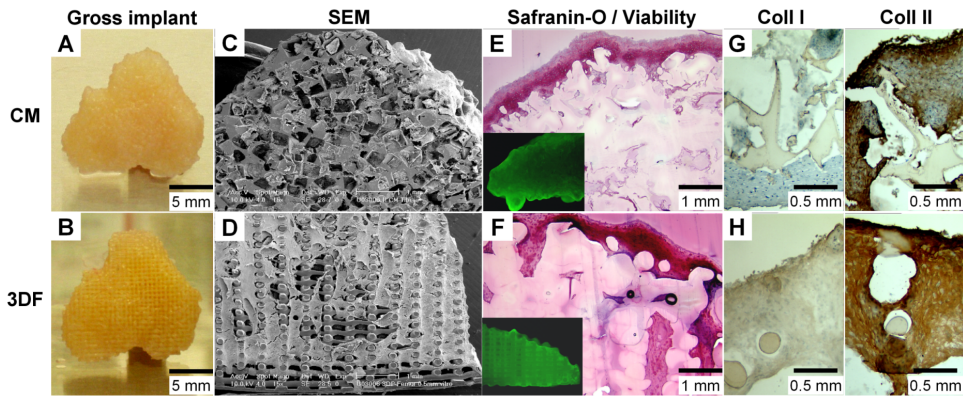


Figure 6 – Gross appearance of tissue-engineered tibial implants (A, B), and cross-sectional SEM (C, D), cell viability (inset) and safranin-O (E, F) and collagen type I/II immunostaining images (G, H) after 21 days in vitro culture. (A, C, E, G) CNC milled CM scaffold, (B, D, F, H) 3DF scaffold.

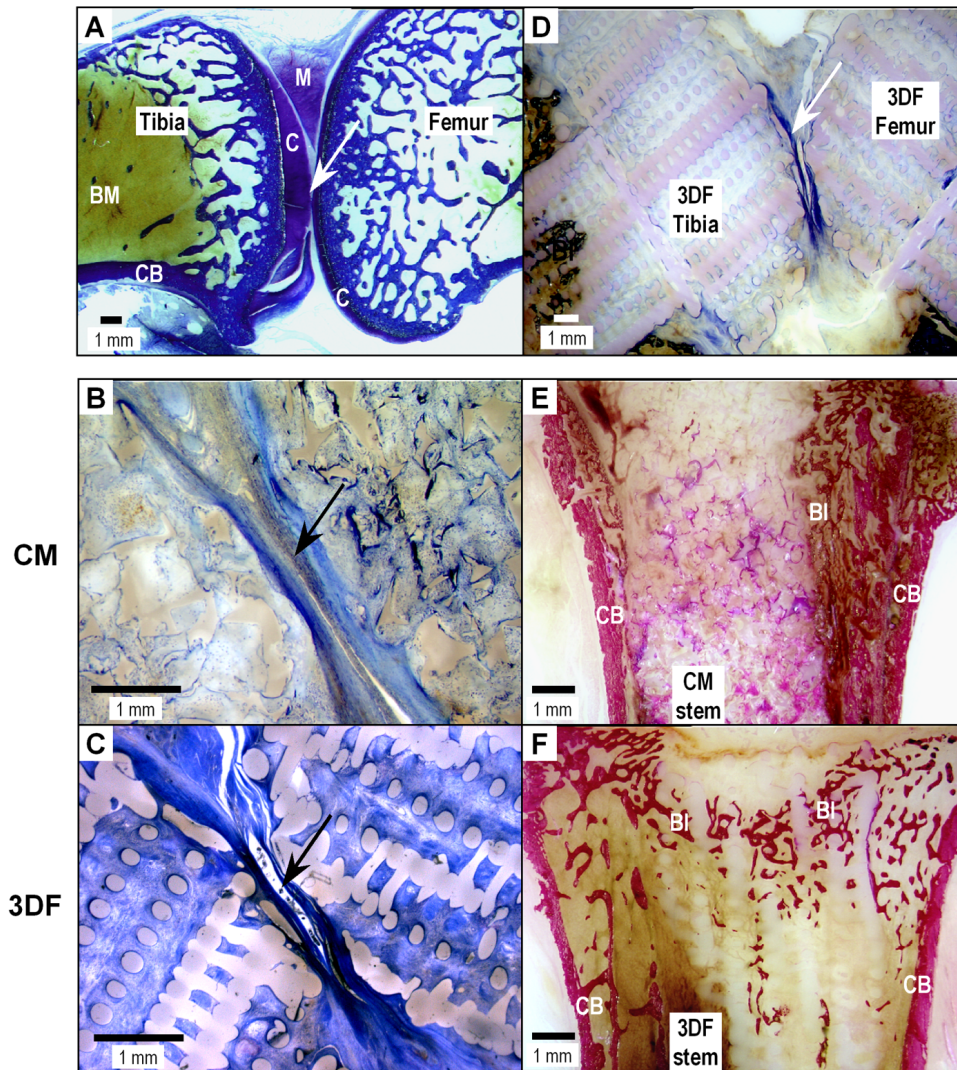


Figure 7 – Histological sections of control (A) and operated joints (B-F) at 6 week follow-up using anatomically-shaped CM (B, E) and 3DF implants (C, F). Example of 3DF femoral and tibial implants shown in D. Samples were stained with thionine (A-D) and basic fuchsin/methylene blue (E, F). Arrow indicates articulating surface; C = articular cartilage; M = meniscus; CB = cortical bone; BM = bone marrow; BI = bone in-growth.

Appendix A

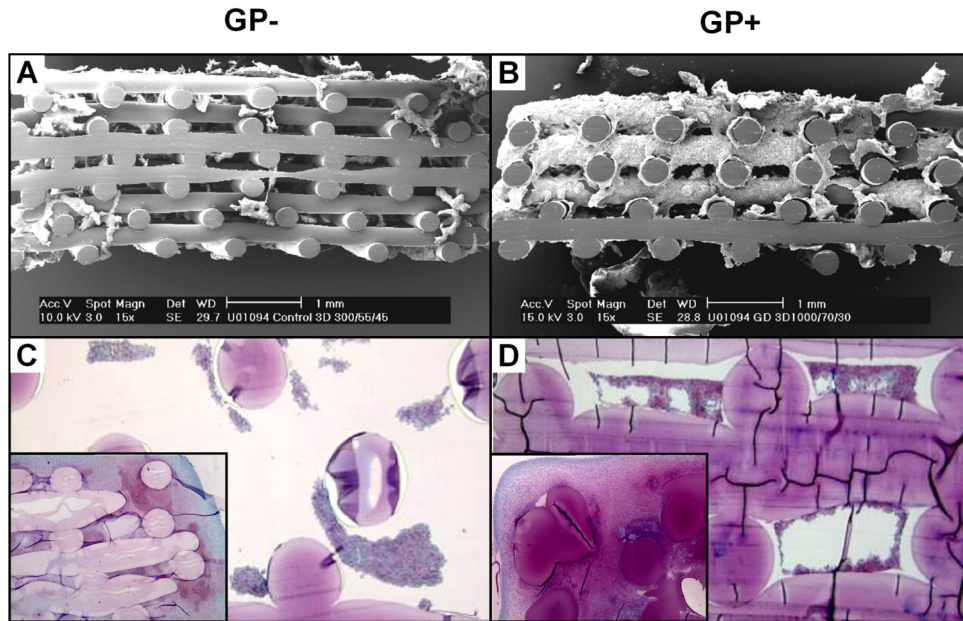


Figure A.2 – Day 3 (A) SEM x-section of untreated 3D 1000/70/30 (B) GP treated 3D 1000/70/30; (C) Saf-O untreated 3D 1000/70/30; (D) Saf-O GP treated 3D 1000/70/30 showing positive GAG formation. Inset (C, D) shows Saf-O staining at day 12.